Analysis of Concrete Deep Beams with Fibre Reinforced Polymer Reinforcements using Indeterminate Strut-and-Tie Method

by

Shuqing Liu

A thesis

presented to the University of Waterloo

in fulfilment of the

thesis requirement for the degree of

Master of Applied Science

in

Civil Engineering

Waterloo, Ontario, Canada, 2022

Author’s Declaration

I hereby declare that I am the sole author of this thesis. This is a true copy of the thesis, including any required final revisions, as accepted by my examiners.

I understand that my thesis may be made electronically available to the public.

Abstract

Fibre-reinforced polymer (FRP) bars have gained popularity in industry to reinforce concrete. They are noncorrosive, strong in tension, but they are less stiff than traditional steel bars and fail in a brittle manner. Therefore, the behaviour of concrete beams reinforced with FRP bars is different in many ways than the behaviour of traditional steel bars reinforced beams. Development of rational design provisions for these beams is essential for wide acceptance of FRP bars in industry and for safe designs of FRP reinforced concrete.

In order to develop these design principles, a good analysis model for such structural elements is needed. Strut-and-tie (ST) modelling is one accepted way to analyze reinforced concrete deep members, however the classical ST method was developed for steel reinforced concrete, where the ST method is based on steel yielding. Such ST method cannot be directly applied to FRP reinforced concrete.

Based on the work done by Krall (2014), the indeterminate strut-and-tie (IST) method developed initially for steel reinforced deep beams that does not assume steel yielding and includes the nonlinear behavior of concrete can predict good results for FRP reinforced deep beams.

In this thesis, the IST methodology for FRP reinforced concrete is developed and analyzed. Several aspects are studied to be the most essential features of IST method, which are the proposed geometries for the ST models, the softened concrete stress-strain relationships, the assumed heights of the compression nodes (h_C) and the softening factors for concrete struts (ζ).

Different ways to compute these features can affect the results predicted by the IST method, thus four ST models for deep beams with vertical reinforcement, four softened concrete stress-strain relationships, four approaches of h_C, and four approaches of softening factors are developed. Some of the approaches and models are modified from existing ones, and the others are newly proposed in this research.

The approaches and models are analyzed with specimens tested in different research programs having different reinforcement design, different beam sizes and different slenderness ratios, in order to find if the approaches and models can work properly with the IST method on different kinds of deep beams.

As a result, an improved IST method is proposed, which can predict accurate results and can capture how different factors affect the shear strengths. Although the selected combinations of the approaches and models for the features are slightly different for beams with and without vertical reinforcement, the proposed IST method is proved to work properly on all kinds of deep beams.

It is also found that the proposed IST method cannot properly predict the shear strength of FRP reinforced concrete slender beams, thus it shall only apply to find the shear strength of FRP reinforced concrete deep beams governed by arch action.

Acknowledgements

I would like to thank

- Professor Maria Anna Polak, my supervisor, who always provides advice and helps when I face problems, brainstorms with me for new ideas and being kind and patient with my research program.
- my fellow graduate students in Polak research group, Amin Izadi, Graeme Milligan, Patrick Michael Beaulieu, Ryan Barrage, Zahra Miri, who listen to my presentations and provide opinions and suggestions on my research. Special thanks to Zahra Miri, who always encourages me and gives me snacks when I feel stressful.
- Professor Trevor Hrynyk for holding the concrete graduate courses and explaining concrete behavior clearly and in detail.
- Martin Krall, who I only have talked through emails, for testing the deep beams with stirrups and developing the idea of applying IST method to FRP reinforced concrete deep beams.
- Professor Eugene Kim and Professor Juliane Mai for examining my thesis.
- my parents for assisting me and listening to my ideas.

Table of Contents

List of Figures

List of Tables

List of Symbols

The list of symbols used is presented here, though all symbols are identified in the text when it appears. Generally, the same symbol is used to define the same variable, with several exceptions to provide clarity under specific situations or to present the symbol used in the referenced research with same definition.

Symbol	**Unit**	**Definition**
A_{bar}	mm^2	Area of a rebar
A_{FT}	mm^2	Area of reinforcement in the tie
A_{Ff},	mm^2	Area of one flexural FRP bar
A_{Fv}	mm^2	Area of one vertical FRP bar
A_{FRP}	mm^2	Total area of flexural FRP bars
A_{si}	mm^2	Total area of distributed reinforcement crossing concrete strut
A_s	mm^2	Total area of flexural steel bars
a	mm	The length of the shear span
a/d	-	Shear span to depth ratio
a_i	degrees	Angle of reinforcement crossing a strut
b	mm	Beam width
b_s, w_s	mm	Strut width
c	mm	Depth of concrete in compression
d, d_{eff}	mm	Effective depths of beams, measured from the extreme compressive fibre to the centroid of tensile flexural bars.
d_{bar}	mm	Rebar diameter
E_c	GPa	Initial elastic modulus of concrete
E_f	GPa	Elastic modulus of flexural bars
E_{FRP}	GPA	Elastic modulus of flexural FRP bars
E_v	GPa	Elastic modulus of stirrups
f_c, f_{c2}	MPa	Concrete compressive stress
f_c'	MPa	Concrete compressive strength, tested from concrete cylinders
f_{ce}, f_{cu}	MPa	Limited strength (effective strength) of concrete compressive strut.
f_{c2max}	MPa	Compressive strength of concrete under biaxial loading
f_{Fu}	MPa	Ultimate strength of FRP bars
f_{fu}	MPa	Ultimate strength of FRP flexural bars
f_r	MPa	Concrete rupture strength in tension
f_t	MPa	Concrete tensile stress
$f_{vu,bent}$	MPa	Ultimate strength in bent sections of FRP stirrups
f_u	MPa	Ultimate strength of rebar
f_y	MPa	Yielding strength of steel bars
h	mm	Beam height
h_C	mm	Height of the nodes in compression side; the assumed compression height.
jd	mm	The length of the lever arm between the resultant tensile and compressive forces

s_i	mm	spacing in the i-th direction of reinforcement crossing a strut
s	mm	Stirrup spacing
α_1, β_1	-	Factors to transfer non-linear concrete compressive stress distribution into the equivalent stress block. α_1 is for the equivalent stress; β_1 is for the height of the stress block
β_s	-	Strut coefficient to calculate the effective strength of concrete strut
β_c, β_n, m	-	Modification factor to increase the strengths of struts or nodes for members with bearing plates not covering the full width
ε_0	-	Concrete compressive strain corresponding to concrete compressive strength
ε_1	-	Principal tensile strain in an element
ε_2	-	Principal compressive strain in an element
ε_x	-	Strain in x-direction of an element
ε_y	-	Strain in y-direction of an element
ε_c	-	Concrete compressive strain
ε_{cu}	-	Ultimate concrete compressive strain; concrete crushing strain
ε_F	-	Tensile strain in the tie bar located closest to the tension face of the beam
ε_r	-	Concrete rupture strain in tension corresponding to f_r
ε_s	-	Strain in the strut
ε_t	-	Concrete tensile strain
ε_{Top}	-	Concrete outmost compressive strain
θ_s, θ_{strut}	degrees	Smallest angle between the strut and the adjoining ties
γ_{xy}	-	Shear strain in an element
γ_c	kg/m^3	Density of concrete
ρ, ρ_f	-	Flexural reinforcement ratio
ζ	-	Softening factor applied to concrete stress-strain models to reduce the strengths of concrete struts

List of Abbreviations

The list of abbreviations used is presented here, though all abbreviations are identified in the text when it appears.

Abbreviations	**Definition**
ACI	American Concrete Institute
CSA	Canadian Standards Association
FEA	Finite element analysis
FRP	Fibre reinforced polymer
HSF model	Half section fanning model (proposed ISTM)
H1 model	Hognestad Parabola with only f_c' softened
H2 model	Hognestad Parabola with all factors related to f_c' softened
IST	Indeterminate strut-and-tie
ISTM	Statically indeterminate strut-and-tie model
Kr model	Indeterminate strut-and-tie model proposed by Krall (2014)
MCFT	Modified Compression Field Theory
RC	Reinforced concrete
ST	Strut-and-tie
STM	Strut-and-tie model
T1 model	Thorenfeldt et al. (1987) model with only f_c' softened
T2 model	Thorenfeldt et al. (1987) model with all factors related to f_c' softened
WSF model	Whole section fanning model (proposed ISTM)

1. Introduction

This chapter briefly introduces what this research focuses on, why it is important, and what are the objectives and scopes of this research.

1.1 Overview

Fibre reinforced polymer (FRP) is light-weight, non-corrosive, linear elastic, and brittle. Because FRP bars are light-weight and non-corrosive, they are gained popularity as reinforcement to concrete structures. However, because they are brittle and generally have lower stiffness, the design and analysis strategies of FRP reinforced concrete (RC) members are different from that of steel reinforced one. For example, FRP RC members prefer concrete failing at first, and the design cannot be based on reinforcement yielding.

Compared to research on FRP reinforced slender members, there are not enough research on how to analyze or design FRP reinforced deep members, and current codes and standards are also lack of information on how to analyze FRP reinforced deep beams.

Shear strength of deep members is governed by arch action, and it is generally analyzed with the strut-and-tie (ST) method, which is to model the deep beams as ST models (STMs) consisting concrete struts and reinforcement ties. In most cases, especially when the members are reinforced with both vertical and horizontal rebars, ST models are statically indeterminate; and the internal forces of such models are usually computed based on reinforcement yielding if the members are reinforced with steel bars. However, FRP bars cannot yield, and how to analyze indeterminate ST models (ISTMs) becomes a problem for FRP RC deep members.

Current research on FRP reinforced deep members mostly focus on beams without vertical reinforcement to find how to correctly soften the strength of a strut in a determinate ST model; and there is nearly no research work on how to analyze indeterminate ST models for deep beams with vertical reinforcement.

Current codes and standards do not provide enough information for engineers to design deep members reinforced by FRP bars. ACI 440.1R-15 (2015) does not have the section for ST method. CSA S806-12 (R2017) takes the equations used for steel reinforced deep members directly to FRP reinforced deep members, and it does not include any explanation on how to use it if the ST model is indeterminate.

Therefore, research must be done on ST method to make it available to design and analyze FRP RC deep members.

Krall (2014) adopted the indeterminate strut-and-tie (IST) method initially developed for steel reinforced deep members to FRP reinforced deep members, because IST method considers the concrete non-linear behavior and avoids the assumption of reinforcement yielding. It turned out to work nicely on FRP reinforced deep beams.

Hence, this research is based on the research done by Krall (2014) and focuses on developing the IST method into an even better method that can predict accurate shear strengths and can correctly capture the strength trends from other factors like slenderness, shear and flexural reinforcement ratios.

1.2 Background

Background information is provided in this section including the explanations of shear failure in deep beams and how these beams are different from slender beams; the properties of fibre reinforced polymer (FRP) bars and how they are different from steel bars; and the properties of concrete.

1.2.1 Shear Failure and Deep Beams

Beam sections are under shear if the moments are changing along the sections, and the existence of shear stresses leads to inclined principal stresses as shown in Figure 1.1 (from Fig. 6-3 by MacGregor and Wight (2011)). Because concrete is weak in tension, the principal tensile stresses can easily split these concrete elements, which causes inclined cracks in the shear span, and leads to shear failure if no vertical reinforcement are placed crossing these inclined cracks.

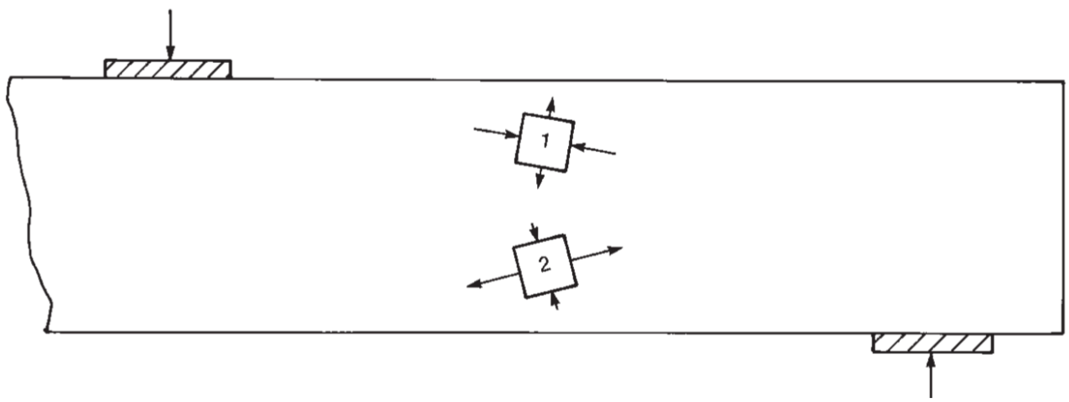

Figure 1.1: Principal stresses of elements in the shear span (MacGregor & Wight, 2011)

According to MacGregor and Wight (2011), shear resistance in concrete can be achieved by beam action and arch action, which are the first half and second half of the following equation

$$V = \frac{d(T)}{dx} jd + \frac{d(jd)}{dx} T \tag{1.1}$$

where T represents the resultant tensile force in the horizontal reinforcement; and jd is the length of the lever arm between resultant tensile and compressive forces.

The change in the lengths of the lever arms (jd) becomes negligible in beam sections away from supports, hence $d(jd)/dx$ can be assumed as zero, and the shear is resisted mainly by the beam action. Conversely, jd clearly varies with x at beam sections near supports or at other disturbed sections (regions around openings, regions with changing heights, etc.), and the arch action takes place as shown in Figure 1.2 (from Fig. 6-6 by MacGregor and Wight (2011)). The regions governed by the beam action are called as B-regions, while the regions governed by the arch action are called as D-regions.

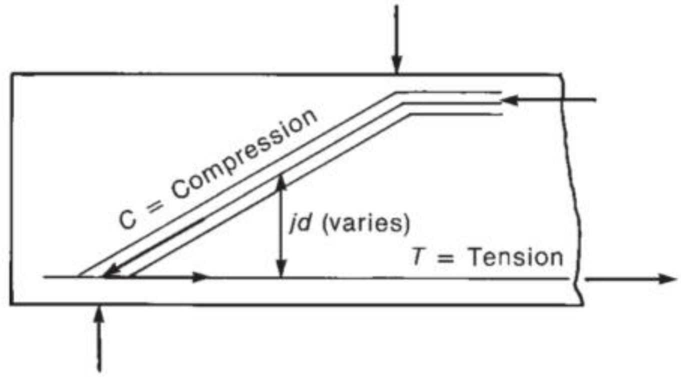

Figure 1.2: Arch action in a beam (MacGregor & Wight, 2011)

If vertical reinforcement is not placed, beam action reaches its maximum when inclined cracking appears, and B-regions fail. However, stresses in D-regions will go with the arch action path after inclined cracking formed, and higher shear strengths can be reached.

If a beam has a relatively long shear span, and the shear failure occurs in B-regions, it is a slender beam, and the design and analysis shall focus on the beam action. However, if a beam has a short shear span, and the arch action can occur in the entire span, it is seen as a deep beam, and the arch action governs the shear capacity.

MacGregor and Wight (2011) present how the arch action can increase the shear resistance of concrete with the pictures (from fig. 6-8 by MacGregor and Wight (2011)) organized in Figure 1.3.

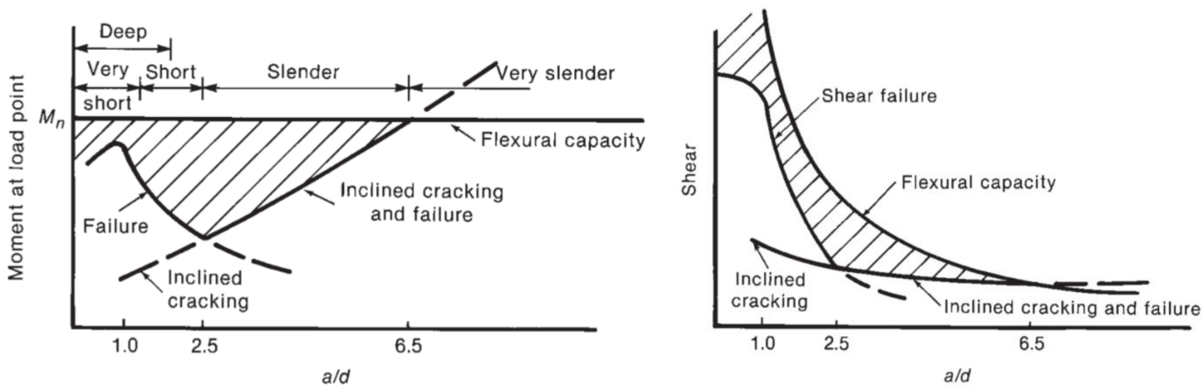

Figure 1.3: Shear strengths of beams with different a/d ratios (MacGregor & Wight, 2011)

According to Figure 1.3 (MacGregor & Wight, 2011), shear strength is governed by arch action for beams with shear span to depth (a/d) ratios smaller than 2.5, and the codes tend to categorize a beam as deep with a more conservative value. In ACI 318-19 (2019), deep beams is defined as those with clear span over depth (l_0/d) ratios smaller than 4 or a/d ratios smaller than 2.

Because sectional analysis developed specifically for beam action is not appropriate for deep beams, current codes (ACI 318-19, 2019; CSA A23.3-19, 2019) suggest using strut-and-tie (ST) method to analyze such members.

The main idea of ST method is to simplify the load paths in concrete into concrete struts. The load path of a deep beam under three point bending analyzed through a preliminary finite element analysis (FEA) in Smith (2009) is presented in Figure 1.4, and this can be modeled by the ST model shown in Figure 1.5.

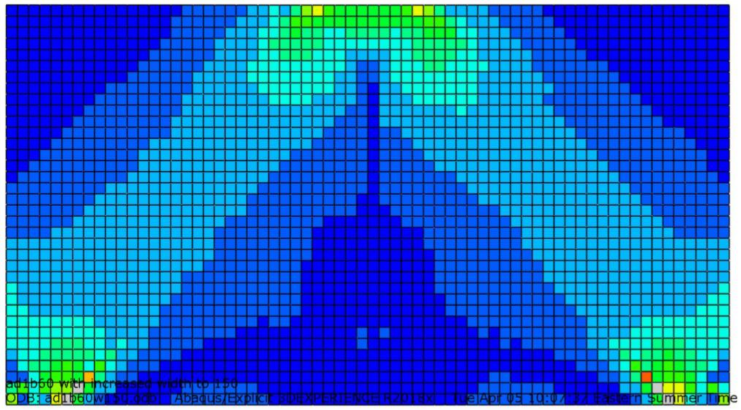

Figure 1.4: Mises stress distribution of a deep beam under three-point bending analyzed with Abaqus (Smith, 2009)

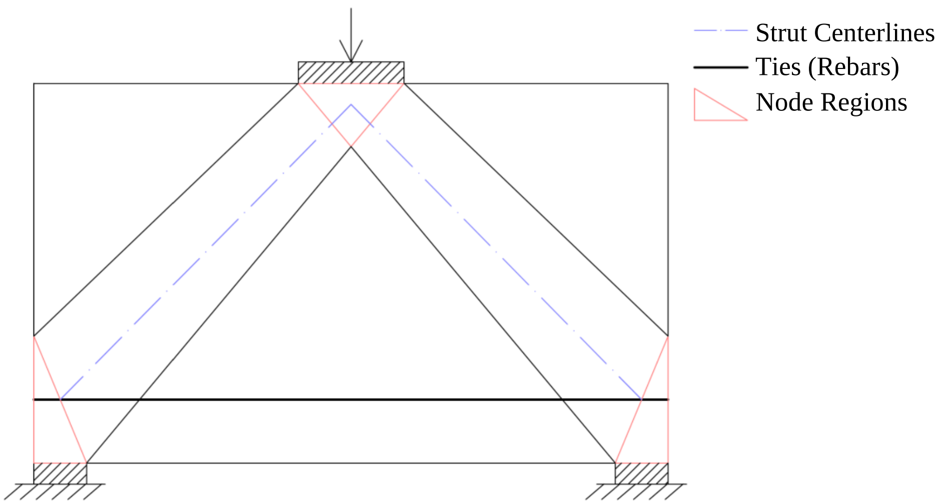

Figure 1.5: ST model for a deep beam under three-point bending

Analyzing a determinate ST model is simple, but if a statically indeterminate ST model is required, it becomes much more complicated to analyze it. The conventional ST method assumes the yielding of ties to simplify the analysis, which is to calculate the forces yielding the ties at first, and then computes other internal forces and the shear strengths based on the force equilibrium at nodes.

Conversely, indeterminate strut-and-tie (IST) method does not assume yielding of ties but solves the IST models based on the stiffness matrix that relates to the area, length, and elastic modulus of the members. As concrete behaves non-linearly, the elastic modulus of concrete struts changes under increasing loads, thus the analysis shall be done with incremental loadings.

Regardless of the accuracy of both methods at predicting shear strengths, assuming tie yielding makes the analysis much easier, while IST method can work with more detailed analysis and can be applied to beams reinforced by brittle rebars.

Because the strength of an FRP RC member relies on concrete, and reinforcement yielding cannot be assumed, it is impossible to use the conventional ST method to find the shear strength of an FRP reinforced deep beam requiring indeterminate ST models. CSA S806-12 (R2017) did not provide enough information on analyzing indeterminate ST models, and ACI 440.1R-15 (2015) did not even have the section for analyzing the shear strength of deep beams with ST method.

1.2.2 Fibre Reinforced Polymer Bars

FRP is a kind of non-corroding material that is linear-elastic and brittle when being stressed in the fibre direction. Common FRP bars used in the industry including aramid-fibre reinforced polymer bars (AFRP) bars, basalt-fibre reinforced polymer bars (BFRP) bars, carbon-fibre reinforced polymer (CFRP) bars and glass-fibre reinforced polymer (GFRP) bars.

Because of the low price of GFRP bars, it is the most commonly used to reinforce concrete, though it has a relatively low elastic modulus (E) that ranges from 35 to 51 GPa, while the elastic modulus of AFRP bars ranges from 41 to 125 GPa, of BFRP bars ranges from 50-65 GPa, of CFRP bars ranges from 120-580 GPa (Ahmed et al., 2020), and of conventional steel bars is around 200 GPa pre-yielding.

ACI 440R-07 (2007) presents the differences in tensile behaviors between FRP bars and steel bars with the stress-strain relationships shown in Figure 1.6 according to the data organized from Teng et al. (2002), Tamuzs et al. (1996) and Apinis et al. (1998).

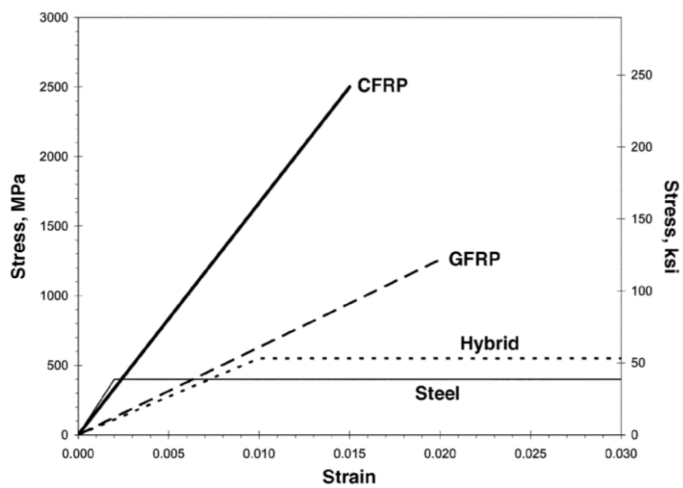

Figure 1.6: - Typical stress-strain curves for FRP products (Fig 1.5 in ACI 440R-07 (2007) based on data from Teng et al. (2002), Tamuzs et al. (1996) and Apinis et al. (1998))

FRP bars have some other differences compared to steel bars except for not yielding. Firstly, the ultimate strengths of FRP bars are larger than the yielding strength of steel bars. Secondly, the ultimate strain of FRP bars is smaller than that of steel bars. Thirdly, FRP bars are generally less stiff (having smaller E) than steel bars (except for some high strength CFRP bars, but those bars are seldomly used to reinforce concrete).

Due to the differences listed above, cracks are more likely to form under a lower load in an FRP RC member, and the tensile strain built in FRP RC sections are generally larger. Because cracks reduce the effective concrete area to take compressive forces, and larger tensile strains reduce concrete compressive strength, FRP RC members are worried to be weaker than steel reinforced ones. This concern was stated by Nehdi et al. (2008) specifically for FRP reinforced deep beams by saying that the efficiency of the concrete struts in ST models will likely be affected by the low axial stiffnesses of FRP bars.

1.2.3 Concrete

Concrete is week in tension but strong in compression, hence it is usually used to take compression forces. In compression, its stress-strain curve is like a parabola. In elastic range, its elastic modulus decreases with increasing stress and strain. In plastic range, the stress decreases with increasing strain till rupture. Its behavior is significantly affected by its strength as high strength concrete is more linear elastic but less ductile as shown in Figure 1.7 which is a part of Fig. 9 from Hognestad et al. (1955) based on the test data. Because FRP RC beams count on the ductility of concrete instead of reinforcement, how to calculate the elastic modulus of concrete and how to utilize its plastic behavior becomes important.

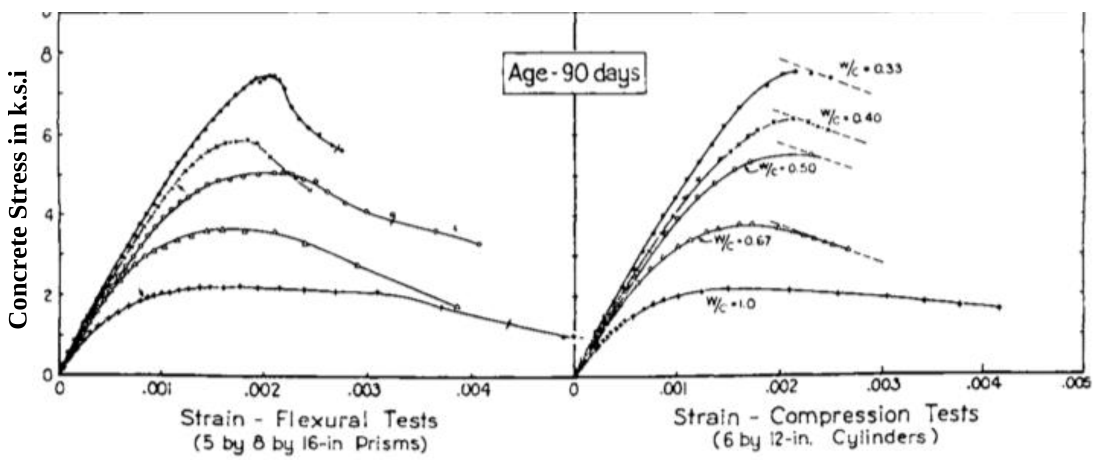

Figure 1.7: Concrete stress-strain relations (Hognestad et al., 1955)

Moreover, strength of concrete changes when it is loaded under biaxial or triaxial loading. Based on Kupfer et al. (1969), when concrete is loaded in biaxial pure compression, the compressive strength is increased; however if concrete is loaded in biaxial tension and compression, both the compressive and tensile strength are decreased. As the concrete inclined struts in ST models are always under biaxial tension and compression as shown in Figure 1.1, how to correctly alter the strength of these struts becomes another important problem to tackle.

1.3 Objectives and Scope

This research is aimed at developing IST method into a detailed methodology to construct and analyze ST models specifically for FRP RC deep beams with and without transverse reinforcement. The objectives are:

1. Finding reasonable model geometries to represent load paths in the beams
2. Finding how to correctly soften concrete stress-strain relationships for concrete struts
3. Suggesting the ways to find the sizes and softening factors for concrete struts
4. Applying the proposed models and methods to analyze tested beams to check their validity and limitations.

This research includes analysis of beams with different slenderness ratios, including those that are typical deep beams and those that can be considered as semi-deep beams; even slender beams are analyzed to check the limitation of the IST method. Both beams with and without vertical reinforcements are analyzed. Most of the analyzed beams are reinforced with GFRP bars, but some are reinforced with AFRP bars or CFRP bars.

All specimens introduced and analyzed in this research are tested in other research, and the detailed information of these beams will be specified in later chapters.

Although the proposed method shall be applicable for all deep regions like corbels and beams with opening or dapped ends, this research focuses on deep beams, hence no specific ST models for deep regions other than deep beams are produced and analyzed.

2. Literature Review

This chapter includes the reviewed literatures that help in improving the indeterminate strut-and-tie (IST) method to analyze FRP reinforced concrete (RC) deep beams, which includes those focusing on how to build and analyze indeterminate strut-and-tie (ST) models and those focusing on predicting the strength of concrete struts. Current codes and standards are also studied to know what the regulations are for designing and analyzing FRP RC deep beams.

2.1 IST method and Non-Linear analysis

IST method was firstly developed for steel RC deep beams to increase the accuracy of the results, as the results from a conventional ST method can be too conservative due to the assumption of steel yielding or the simplified load paths.

Research by Yun (2000)

In Yun (2000)'s paper, complicated indeterminate ST models with not only concrete struts and steel ties, but also concrete ties and steel struts were developed based on the principal stress flows to increase the accuracy of the ST method.

Yun (2000) didn't assume tie yielding during computing the internal forces of the indeterminate ST model, but used one-dimensional finite-element analysis (elastic analysis) to calculate the internal forces in the members based on their stiffnesses. Yun (2000) used finite element nonlinear analysis to evaluate the behavior and strength of structural concrete and to obtain accurate strut and tie forces. In Yun (2000)'s analysis of concrete struts, each strut was supposed to have its own stress-strain relationship, and the tangent modulus of elasticity of every strut under incremental external loads was used.

The sizes of struts and ties were designed based on the effective stresses that are decreased from the ultimate strengths, and the sizes were designed with steel yielding at first. The effective stresses of concrete members were determined based on another work done by Yun and Ramirez (1996) that established the method to obtain the effective stresses based on the experimental data from Kupfer et al. (1969).

Yun (2000) also analyzed the bearing capacity of nodal zones based on finite-element nonlinear analysis; and different shapes of nodal zones were tested under different conditions. Yun (2000)'s approach predicts much more accurate results (compared to strengths predicted through code provisions) though being quite complicated.

CAST Computing Program by Tjhin and Kuchma (2002)

Tjhin and Kuchma (2002) introduced a computing program CAST for building and analyzing ST models. The computing program is developed because even the simplest ST method requires doing the calculations repeatedly to find the proper ST geometry and the suitable reinforcement design for the interest member, and the process could be massive when multiple load cases are considered.

Tjhin and Kuchma (2002) pointed out that the conventional ST method could be confusing on determining the internal forces of statically indeterminate ST models. Although the *plastic truss method* (assuming all steel ties at yielding at failure) could be used, the results obtained with this method might be against the strain compatibility requirements and the limited ductility in concrete.

The methods suggested by Tjhin and Kuchma (2002) to solve this problem were from Anderheggen and and Schlaich (1990), which determine the forces in such a way that minimizes tie resistances corresponding to the minimum weight of steel ties (Tjhin & Kuchma, 2002). The methods considered strain compatibility while assumed steel yielding, and predicted results fall in between the elastic analysis and the *plastic truss method*.

Tjhin and Kuchma (2002) suggested these methods because the elastic analysis considering the non-linear behavior of concrete members could be too time-consuming and complicated. As the purpose of the program was to directly show whether the proposed ST model could take the required load, and to save the effort for engineers to design steel RC D-regions based on code provisions, analysis considering concrete nonlinear behavior was not needed.

The methods mentioned above are quite different. Yun (2000)'s work focused on establishing a more precise ST method taking the non-linear behavior of concrete into consideration. CAST (Tjhin & Kuchma, 2002) focused on making the ST method more straight-forward for engineers to save time on calculations while giving slightly better results than the *plastic truss method*.

Research by B. H. Kim and Yun (2011a, 2011b)

As the reinforcement of FRP RC deep regions cannot yield and the strength is relied on the concrete struts, process similar to Yun (2000)'s research could be adopted, which was done by Krall (2014). Krall (2014) specifically stated that the IST method was according to B. H. Kim and Yun (2011a, 2011b), which was similar to Yun (2000)'s research, but explained the steps more detailed in.

B. H. Kim and Yun (2011a, 2011b) did the research for steel RC deep beams and focused on the load distribution ratio between the ST and the truss load transfer mechanism. To find the distribution ratio, B. H. Kim and Yun (2011a, 2011b) analyzed 234 simply supported deep beams with IST method through steps similar to what Yun (2000) did, but the analysis was conducted with simpler ST models and omitted the complicated finite-element nonlinear analysis on the node regions.

B. H. Kim and Yun (2011a) suggested to use the softened Hognestad parabola according to Pang and Hsu (1995) for the stress-strain relationship of concrete, which were

$$f_c = \zeta f_c' \left[2\left(\frac{\varepsilon_c}{\zeta\varepsilon_0}\right) - \left(\frac{\varepsilon_c}{\zeta\varepsilon_0}\right)^2 \right] \text{ for } \frac{\varepsilon_c}{\zeta\varepsilon_0} \leq 1 \tag{2.1}$$

$$f_c = \zeta f_c' \left[1 - \left(\frac{\varepsilon_c/_{\zeta\varepsilon_0} - 1}{2/_{\zeta} - 1}\right)^2 \right] \text{ for } \frac{\varepsilon_c}{\zeta\varepsilon_0} > 1 \tag{2.2}$$

where ζ represents the softening factor; f_c is the concrete compressive stress at certain strain ε_c; f_c' is the tested concrete cylinder compressive strength; and ε_0 is the strain when the stress reaches its maximum, which is usually obtained from $2\, f_c'/E_c$.

This softening way reduced both the concrete strength (f_c') and its corresponding strain (ε_0) by the softening factor as shown in Figure 2.1 (from Figure 6. a) by B. H. Kim and Yun (2011a)), and the softening factors used by B. H. Kim and Yun (2011a) were directly from ACI 318M-08 (2008), which were equal to $0.85\beta_s$, and β_s was the strut coefficient equal to 1.0 for horizontal struts, 0.75 for inclined struts with vertical ties crossed and 0.6 for inclined struts without ties crossed (ACI 318M-08, 2008).

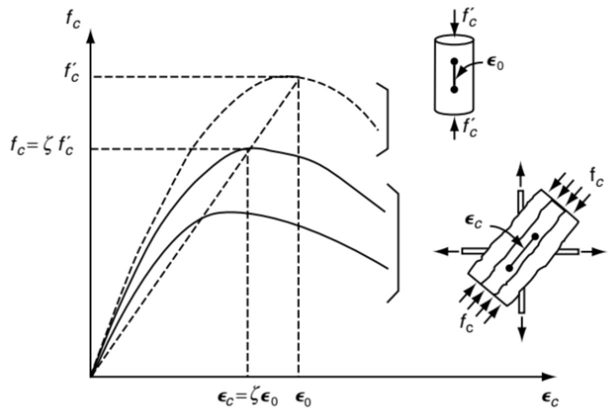

Figure 2.1: Strength reduction in concrete struts (B. H. Kim & Yun, 2011a)

This agrees with Hognestad (1951), as Hognestad (1951) believed that the ultimate strength of concrete members shall only be 0.85 of the cylinder strength, and ε_0 shall also be decreased by 0.85. However, Vecchio and Collins (1986) suggested to deduct the strengths while keeping ε_0 the same as shown in Figure 2.2 (from Fig. 11 a) by Vecchio and Collins (1986)), and they developed the Modified Compression Field Theory (MCFT) to soften the strength of concrete struts (which will be introduced later).

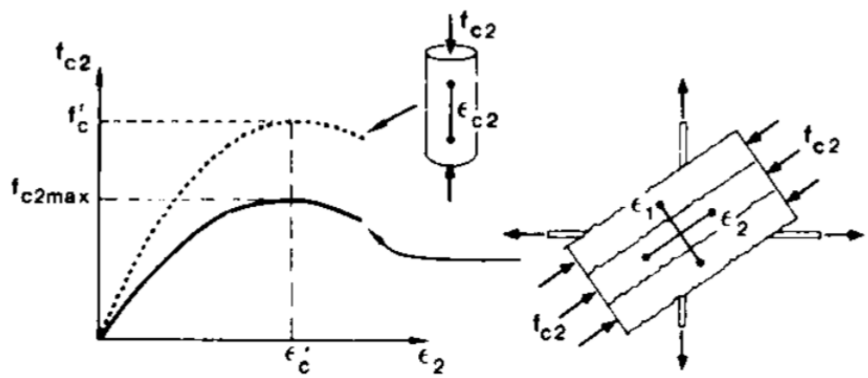

Figure 2.2: Stress-strain relationship for cracked concrete in compression (Vecchio & Collins, 1986)

B. H. Kim and Yun (2011a) also specified the method to obtain the sizes of the struts and the nodes. They used the force equilibrium at loading point assuming the ultimate state of ties and node regions to compute the height of the loading node, and then obtained the widths of the struts as the smaller one of the values calculated based on the sizes of the loading and supporting nodes. However, as this method assumes tie yielding and cannot be applied to FRP RC deep beams, Krall (2014) cooperated this method with strain compatibility to avoid the assumption of tie yielding, and kept the other steps as the same.

Research by Krall (Krall, 2014; Krall & Polak, 2019)

Krall and Polak (2019) casted and tested 12 simply supported FRP RC deep beams with same shear span to depth (a/d) ratio under three-point bending. Beams were casted with different horizontal and vertical reinforcement ratio, and 9 beams had stirrups placed.

Shear strengths of the beams were analyzed through IST method according to B. H. Kim and Yun (2011a) but with new ST models proposed specifically for deep beams with stirrups. The predicted strengths were compared with the tested strengths, which showed that the IST method can predict fairly good results.

However, the predicted strengths still contained problems. Firstly, the method overpredicts the strength of several beams; and secondly, the method cannot capture the increase in shear strength with smaller stirrup spacings.

As the purpose of Krall (2014)'s research was to check if the IST model could be used for FPR RC deep beams, the analysis was preliminary and some variables were not analyzed in detail, like the model geometries and the softening factors.

The ST models proposed and checked by Krall (2014) are as shown in Figure 2.3 (from Figure 6.1 in Krall (2014)'s work). Model type I was for beams without vertical ties, type II was the design model based on the model used by B. H. Kim and Yun (2011a), type III was the proposed model for beams with larger spacings, and type IV was the proposed model for beams with smaller stirrup spacings. Type II, III and IV models were all indeterminate and were for beams with stirrups. According to Krall (2014), the design model (type II model) did not work; and the other models were proven to work with the softening factors from the ACI 318 (-08, -14 versions).

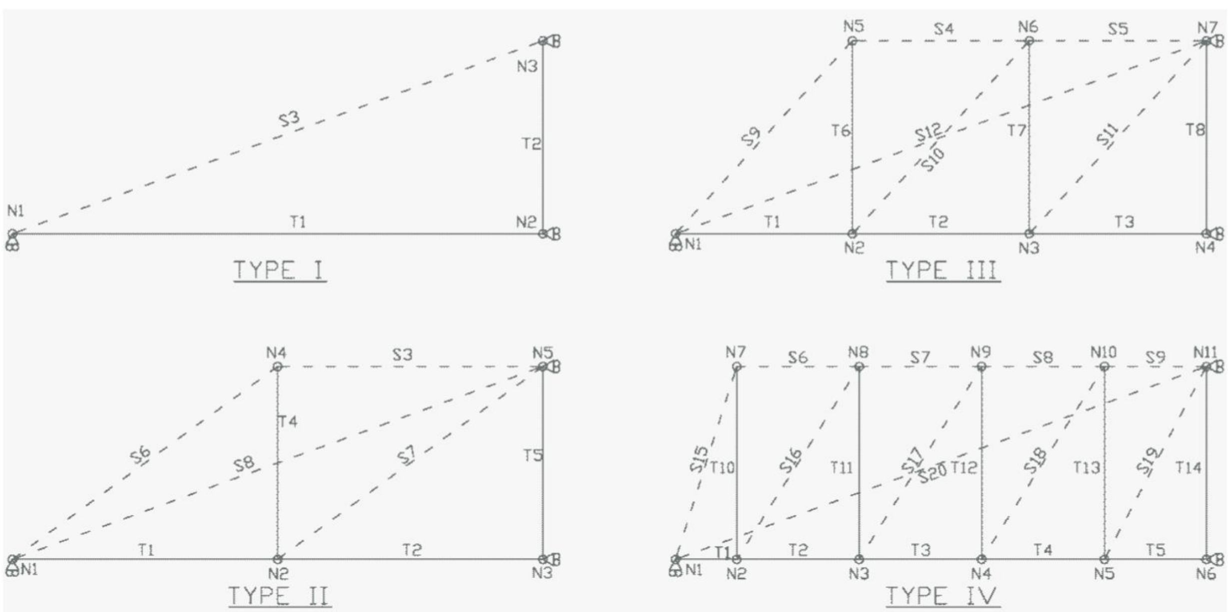

Figure 2.3: Strut-tie model types analyzed in Krall (2014)'s research (Krall, 2014)

Furthermore, Krall (2014) also included one more concrete stress-strain model by Thorenfeldt et al. (1987). Krall (2014) obtained the equations from MacGregor and Wight (2011), and modified them with the softening factor resulting in

$$f_c = \frac{\zeta f_c' n\left(\varepsilon_c/_{\zeta\varepsilon_0}\right)}{n-1+\left(\varepsilon_c/_{\zeta\varepsilon_0}\right)^{nk}} \tag{2.3}$$

where

$$n = 0.8 + \frac{\zeta f_c' \; [MPa]}{17} \tag{2.4}$$

$$k = \begin{cases} 1.0 & for \; \frac{\varepsilon_c}{\zeta \varepsilon_0} \leq 1 \\ 0.67 + \frac{\zeta f_c'[MPa]}{62} & for \; \frac{\varepsilon_c}{\zeta \varepsilon_0} > 1 \end{cases} \tag{2.5}$$

As listed in the equations, Krall (2014) applied the softening factor to all parameters calculated from f_c' including ε_0, n and k.

Based on the analysis, Krall (2014) made several important conclusions. Firstly, the IST method was most sensitive to the choice of softening factors. Secondly, the IST method was not very sensitive to the choice of the concrete material model as these models are mainly differentiated in the post-peak behaviour that is ignored in the IST method. Thirdly, the method was not very sensitive to the initial concrete elastic modulus. Lastly, the choice of the ST model geometries could affect the values and the trends of the results significantly.

Other than the research done by Krall (2014), there was no other research found on analyzing IST models for FRP RC deep beams. Current research on ST models for FRP RC deep beams are mainly for the determinate ones. They focus on the strength of the inclined struts and how the softening factors for these struts shall be different from them in steel reinforced beams, which will be discussed in the following section.

2.2 Inclined Strut Strengths and Softening Factors for FRP RC Deep Beams

As FRP RC deep beams rely on the strength of the concrete struts, it is important to correctly soften the strengths of these struts.

Research by Nehdi et al. (2008)

Nehdi et al. (2008) pointed out that FRP bars as reinforcement could affect the shear behavior of structural concrete members, such as the crack width, deflection, ultimate load capacity and stiffness of the members; and it might be due to the relativity low elastic modulus of some types of FRP bars (e.g., GFRP bars). Hence, Nehdi et al. (2008) casted and tested 8, 7, and 4 concrete short beams reinforced with CFRP, GFRP, and steel rebars in the longitudinal direction with shear span to depth (a/d) ratio between 1.5 to 2.5.

Based on the test data, Nehdi et al. (2008) observed that the factors influence the ultimate capacity and shear behavior of the beams are the a/d ratio, the axial stiffness of the flexural reinforcement and the effective depth. Hence, Nehdi et al. (2008) established the following equations for the strengths of inclined struts, which were modified from ACI 318 codes.

$$\beta_s = 0.68 - 0.012 \left(\frac{a}{d}\right)^4 \text{ for } \left(E_f \rho_f\right)^{1/3} \leq 10 \tag{2.6}$$

$$\beta_s = 0.75 - 0.01 \left(\frac{a}{d}\right)^4 \text{ for } \left(E_f \rho_f\right)^{1/3} > 10 \tag{2.7}$$

$$k = \max\left(\frac{250+d}{550}, \; 1.0\right) \tag{2.8}$$

$$f_{ce} = 0.85 k \beta_s f_c' \tag{2.9}$$

where f_{ce} is the effective strength of concrete strut; E_f is the elastic modulus of flexural reinforcement in GPa; and ρ_f is the flexural reinforcement ratio.

Research by D. J. Kim et al. (2014)

D. J. Kim et al. (2014) casted and tested FPR RC deep beams focusing on how FRP rebars could affect the shear strength by having lower elastic modulus. A total of 15 beams were tested by D. J. Kim et al. (2014), with 7 reinforced with AFRP bars, another 7 reinforced with CFRP bars and the last one reinforced with steel rebars. The test focused on the effect of slenderness ratio, elastic modulus, effective depth, and reinforcement ratio on the shear strength.

Beams tested by D. J. Kim et al. (2014) were organized so that there were always two beams cast with only one different feature while keeping all others the same.

D. J. Kim et al. (2014) noticed that all the features could affect the shear strength; but as it would be too complicated to include all the factors to change the softening factor, they categorized the beams into two groups based on the beam size, slenderness ratio, reinforcement ratio and rebar strength and assigned one softening factor to each group to decrease the strength of struts.

The test data from D. J. Kim et al. (2014) is really valuable, but the softening factor approach proposed by them was too simple and may not be able to reflect how shear strengths changed with other features.

Research by Dhahir et al. (2021)

To find what would be the most suitable softening factor of the strut strength for FRP RC deep beams, Dhahir et al. (2021) organized the test data from different research, and did a regression model on the actual softening factor of the tested beams. The value of softening factors derived was 0.25. However, this value only showed that the accuracy of the predicted results was most stable with this softening factor, but this softening factor could not reflect how the shear strengths could change with elastic modulus of FRP bars, beam sizes, reinforcement ratios and beam slenderness ratios.

Some specimens were analyzed in all research mentioned above through same softening factor approach (e.g., approach defined by ACI 318-08 (or -14)), but the predicted strengths presented in different research were different from each other, which was caused by constructing the ST models in slightly different ways. For example, Nehdi et al. (2008) and Dhahir et al. (2021) clearly mentioned that the widths of the struts were obtained from the nodes in the tension side only, while D. J. Kim et al. (2014) didn't specify it clearly but probably analyzed it as an average of the value obtained from nodes in both sides; and the assumed distance between the resultant compression and tension forces was expressed as 0.9d by Dhahir et al. (2021), while others didn't mention anything on this.

According to the research (Dhahir et al., 2021; D. J. Kim et al., 2014; Nehdi et al., 2008), CSA A23.3 codes generally predict the most conservative results, while ACI 318 codes may overestimate the strength but predict results close to the actual strength. However, the ACI approach used in these research referred to the older versions of ACI 318 codes, the factors were reduced in the most recent version, which will be introduced in later sections.

Cracked Strut-and-Tie Model by (Chen et al., 2018; Chen et al., 2020)

Chen et al. (2018) developed the cracking strut-and-tie model (CSTM) for analyzing the shear strength of deep beams that avoided to use the softening factor to obtain the strut strengths, and then modified the original model for steel RC deep beams to a model suitable for FRP RC deep beams (Chen et al., 2020).

In CSTM, the strut was divided into two portions: the cracked portion and the uncracked portion based on the differences between angles of the major crack and the inclined strut. The strengths of the cracked portion and the uncracked portion were analyzed differently. The uncracked portion was treated similarly to a horizontal strut, while the stress in the cracked portion were assumed to be taken by aggregate interlock, dowel action and horizontal web reinforcement.

According to Chen et al. (2018); Chen et al. (2020), the results predicted by CSTM were quire accurate for both steel and FRP RC deep beams, but the calculations in the CSTM were complicated as multiple factors shall be computed and iterative process was required. Moreover, CSTM was designed for deep beams without vertical reinforcement, and the analysis was assumed to perform under an ultimate stage.

Two-Parameter Kinematic Theory by Mihaylov et al. (2013)

Another method to predict the shear strength of deep beams is Two-Parameter Kinematic Theory (2PKT) by Mihaylov et al. (2013), which predicted the capacity without utilizing the ST models. This method used two degrees of freedom (DOFs) to describe the deformed shape of diagonally-cracked, point-loaded deep beams. The first DOF was based on the average strain in the bottom reinforcement, and the other one was based on the vertical displacement of the critical loading zone (CLZ) that was around the loading point connecting the upper and bottom portion divided by the critical crack. The deformation pattern, crack widths and shear strengths could be computed with these two DOFs, and the shear capacity was obtained from the shear forces resisted by the CLZ, the aggregate interlock, stirrups, and the dowel action.

Mihaylov et al. (2013) applied this method to 434 simply supported steel reinforced deep beams, and the average value of test to predicted shear strength ratios was 1.10 with a coefficient of variation of 13.7%, which was better than the conventional ST method according to Mihaylov et al. (2013). However, as the 2PKT method is totally different from the ST method, it cannot be included in this research.

Modified Compression Field Theory by Vecchio and Collins (1986)

The theory behind the formula to calculate the strut strength in CSA codes (CSA A23.3-19 (2019) and CSA S806-12 (R2017)) for steel and FRP reinforced beams is the Modified Compression Field Theory (MCFT) from Vecchio and Collins (1986). Vecchio and Collins (1986) tested 30 concrete specimens under biaxial loading, and found out that the principal compressive strength of a concrete member was related to its principal tensile strain, and Vecchio and Collins (1986) established the relationship with the Hognestad parabola as

$$f_{c2} = f_{c2max}\left[2\left(\frac{\varepsilon_c}{\varepsilon_0}\right) - \left(\frac{\varepsilon_c}{\varepsilon_0}\right)^2\right] \tag{2.10}$$

$$\frac{f_{c2max}}{f_c'} = \frac{1}{0.8 - 0.34\,{\varepsilon_1}/{\varepsilon_0}} \leq 1.0 \tag{2.11}$$

where f_{c2} is the concrete compressive stress; f_{c2max} is the compressive strength of a concrete member under biaxial loading; and ε_1 is the principal tensile strain of the member. Note that Vecchio and Collins (1986) required to include the positive sign for tensile strain and negative sign for compressive strain during using these equations.

2.3 Current Code Provisions

As mentioned before, current code provisions are not well developed to analyze the strength of FRP RC deep members.

ACI Codes (ACI 440, ACI 318)

There is no suggestion on how to calculate the shear strength of deep beams in ACI 440.1R-15 (2015) specifically for FRP RC members, and only the sectional method for slender beams was presented. Therefore, the ST method for FRP reinforced deep members can only follow the process developed for steel reinforced members in ACI 318-19 (2019).

ACI 318-19 (2019) provisions are developed for steel reinforced members. Therefore, the ACI ST method assumes reinforcement yielding, hence some clauses are not suitable for FRP reinforced deep members. For example, ACI 318-19 (2019) suggests to compute the strut width based on the supporting node with the height obtained from the location of the flexural bars. This may not affect the shear capacity of steel reinforced deep regions, as it only requires the stress built in the struts to be under its effective strength; but it makes the shear capacity of FRP reinforced deep beams directly related to the location of flexural bars hence shall not be used.

Furthermore, ACI 318-19 (2019) changes slightly from the previous versions. Previous versions of ACI 318 code (including the -08, -14 versions) calculated the effective strength f_{ce} of concrete struts as

$$f_{ce} = 0.85\beta_s f_c' \tag{2.12}$$

where β_s was the strut coefficient equal to 1.0 for horizontal struts, 0.75 for inclined struts crossed by enough vertical reinforcement, and 0.6 for inclined struts not crossed by vertical reinforcement.

Current version (ACI 318-19) changes the equation to

$$f_{ce} = 0.85\beta_s\beta_c f_c' \tag{2.13}$$

which includes an extra coefficient β_c used to increase the strengths of struts and nodes for members with bearing plates not covering the full width of the member, and the cases and values of β_s are slightly changed.

The change impacting the interest of this research is on β_s for inclined struts not crossed by vertical reinforcement. The value reduced from 0.6 to 0.4.

The equation for counting if there is enough vertical reinforcement crossing the struts is also changed. Previously, the minimum distributed reinforcement ratio was expressed as

$$\sum \frac{A_{si}}{b_s s_i} \sin a_i \geq 0.003 \tag{2.14}$$

where A_{si} was the total area of distributed reinforcement at spacing s_i in the i-th direction of reinforcement crossing a strut at an angle a_i, and b_s was the width of the strut.

But, ACI 318-19 (2019) changes that to

$$0.0025 / \sin^2 a_i \tag{2.15}$$

for reinforcement in one direction, and no less than 0.0025 in each direction for orthogonal grid. ACI 318-19 (2019) also requires the spacing of the distributed reinforcement not exceeding 12 in (304.8 mm) and a_i no less than 40 degrees.

ACI 318-19 (2019) similarly adds the extra factor β_c to the original $0.85\beta_n f_c'$ equation for the strength of node regions, but the value of β_n is not changed, which is 1.0 for nodes under pure compression, 0.8 for nodes anchoring one tie, and 0.6 anchoring two or more ties.

CSA Codes

CSA provides the clauses for analyzing the shear capacity of FRP RC deep regions with STMs in CSA S806-12 (R2017). CSA S806-12 (R2017) provides the following requirements to calculate the limited strut strength (f_{cu}).

$$f_{cu} = \frac{f_c'}{0.8+170\varepsilon_1} \leq 0.85 f_c' \tag{2.16}$$

$$\varepsilon_1 = \varepsilon_F + (\varepsilon_F + 0.002)\cot^2\theta_s \tag{2.17}$$

where θ_s is the smallest angle between the strut and the adjoining ties; ε_F is the tensile strain in the tie bar located closest to the tension face of the beam and inclined at θ_s to the strut. If the tensile strain in the tie changes as the tie crosses the width of the strut, θ_s may be taken as the strain in the tie at the centreline of the strut (CSA S806-12, R2017).

The equations are identical to the ones listed in CSA A23.3-19 (2019) for steel reinforced members, except that CSA A23.3-19 (2019) provides another equation by assuming the yielding strain of steel ties equal to 0.002,

$$f_{cu} = \frac{1}{1.14+0.68\cot^2\theta_s} \leq 0.85 f_c' \tag{2.18}$$

which cannot be applied to FRP reinforced members as FRP rebars cannot yield.

Because θ_s is 90 degrees for horizontal struts, these struts could have the maximum limited strength equal to $0.85 f_c'$, which agrees with ACI 318-19 (2019).

CSA S806-12 (R2017) multiplies 0.85, 0.75 and 0.65 to the cylinder strength (f_c') for the strengths of nodes under only compression, with one tie and with two or more ties. However, in CSA A23.3-19 (2019), as it is published later than CSA S806-12 (R2017), it includes the confinement modification factor (m) for members with bearing plates not covering the full width, which is same as β_c in ACI 318-19 (2019). However, CSA A23.3-19 (2019) does not add this factor to increase the strength of struts, and specifically mentioned that this factor shall be taken as 1.0 unless reinforcement capable of controlling cracking is provided.

As the strength of node regions is not extremely critical to ST method, this research consistently follows CSA S806-12 (R2017) for analyzing it.

CSA S806-12 (R2017) also regulates the maximum tensile force in ties not exceeding $0.65 A_{FT} f_{Fu}$, where A_{FT} is the area of reinforcement in the tie, and f_{Fu} is the ultimate strength of the FRP bars.

Moreover, this research uses CSA A23.3-19 (2019) for the initial elastic modulus of concrete during modelling the concrete behavior, which are

$$E_c = \left(3300\sqrt{f_c'} + 6900\right)\left(\frac{\gamma_c}{2300}\right)^{1.5} \text{ for } \gamma_c \text{ between 1500 to 2500 kg/m}^3 \quad (2.19)$$

where γ_c is the density of concrete; and

$$E_c = 4500\sqrt{f_c'} \text{ for } f_c' \text{ between 20 to 40 MPa} \quad (2.20)$$

3. Specimens

This chapter introduces the beams that are analyzed in this research. The Beams include specimens tested in different research with different flexural and shear reinforcement ratios, shear span to depth (a/d) ratios, reinforcement stiffnesses and beam sizes.

3.1 Beams tested by Krall (Krall, 2014; Krall & Polak, 2019)

Krall (2014) tested 12 GFRP RC deep beams with 9 beams having stirrups and 3 beams not having stirrups. Beams tested by Krall (2014) all had same a/d ratios equal to 2.5. Although this a/d ratio does not fall into the range set by ACI 318-19 (2019) for deep beams, MacGregor and Wight (2011) proved that beams with this a/d ratio still resist shear through arch action, hence shall be analyzed with ST models.

The beams were tested under three-point bending as shown in Figure 3.1 (Krall, 2014), and the details of the beams tested by Krall (2014) are organized in Table 3.1, where h is the beam height; b is the beam width; d is the effective depth; A_{Ff} is the area of one GFRP bar placed as flexural reinforcement; f_{fu} and E_f are the ultimate strength and elastic modulus of the flexural GFRP bars; ρ_f is the flexural reinforcement ratio; A_{Fv} is the area of one leg of the GFRP stirrups; $f_{vu,bent}$ is the ultimate strength of GFRP stirrups at bent sections that is smaller than the strength of the straight portions; E_v is the elastic modulus of the GFRP stirrups; and s is the spacing of the stirrups.

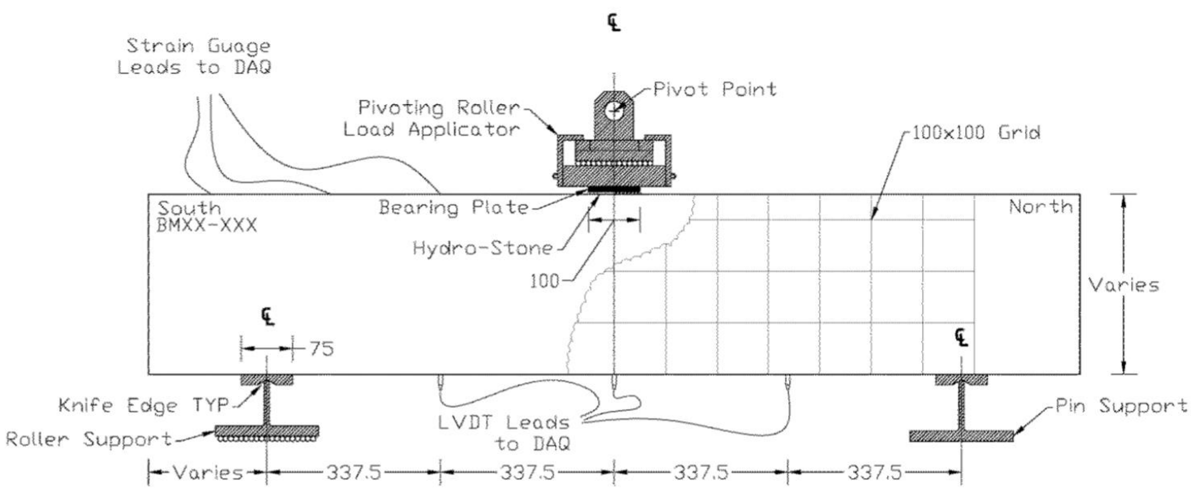

Figure 3.1: Test setup of beams tested by Krall (Krall, 2014)

Table 3.1: Details of beams tested by Krall (2014)

Specimens	h (mm)	b (mm)	d (mm)	Flexural Reinforcement					Shear Reinforcement			
				A_{Ff} (mm^2)	# of bars	f_{fu} (MPa)	E_f (GPa)	ρ_f (%)	A_{Fv} (mm^2)	$f_{vu,bent}$ (MPa)	E_v (GPa)	s (mm)
BM12-INF	350	200	270	113	12	1000	60	2.51	-	-	-	-
BM12-220	350	200	270	113	12	1000	60	2.51	113	700	50	220
BM12-150	350	200	270	113	12	1000	60	2.51	113	700	50	150
BM12-s230	350	230	270	113	12	1000	60	2.18	314	550	50	230
BM16-INF	345	200	270	201	6	1000	64	2.23	-	-	-	-
BM16-220	345	200	270	201	6	1000	64	2.23	113	700	50	220
BM16-150	345	200	270	201	6	1000	64	2.23	113	700	50	150
BM16-s230	345	230	270	201	6	1000	64	1.94	314	550	50	230
BM25-INF	330	200	270	491	2	1000	60	1.82	-	-	-	-
BM25-220	330	200	270	491	2	1000	60	1.82	113	700	50	220
BM25-150	330	200	270	491	2	1000	60	1.82	113	700	50	150
BM25-s230	330	230	270	491	2	1000	60	1.58	314	550	50	230

The names of the beams generally follow the form of BM "diameter of flexural bars" – "stirrup spacings", while "INF" stands for beams without stirrups, and "s" is for beams with larger stirrups. For example, BM25-s230 is for the beam with 25 mm flexural bars and larger stirrups at 230 mm spacings.

The designed strength of concrete was 45 MPa, and the average 28-day strength of the concrete cylinders was 47.3 MPa; the average density of the concrete cylinders was 2416.5 kg/m^3 (Krall, 2014).

Furthermore, the test results of the beams are organized in Table 3.2, and the typical failure patterns are presented in Figure 3.2 (Krall & Polak, 2019). The test of most beams went smoothly, but during the test of BM16-220, power blip occurred and caused a sudden load about 43 percent of the peak load applied to the beam, which resulted in a much lower failure load. Hence, this test result is excluded in further analyses.

Table 3.2: Test results of beams by Krall (2014)

Specimens	Failure Load (kN)	Failure Pattern
BM12-INF	163.1	Shear
BM12-220	382.4	Critical shear crack form firstly with crushing around loading point at failure
BM12-150	405.2	
BM12-s230	466.9	
BM16-INF	150.2	Shear
*BM16-220**	*309.3*	Critical shear crack form firstly with crushing around loading point at failure
BM16-150	416.5	
BM16-s230	450.8	
BM25-INF	125.1	Shear
BM25-220	360.1	Critical shear crack form firstly with crushing around loading point at failure
BM25-150	415.8	
BM25-s230	444	

* BM16-220 experienced an unexpected sudden load during the test.

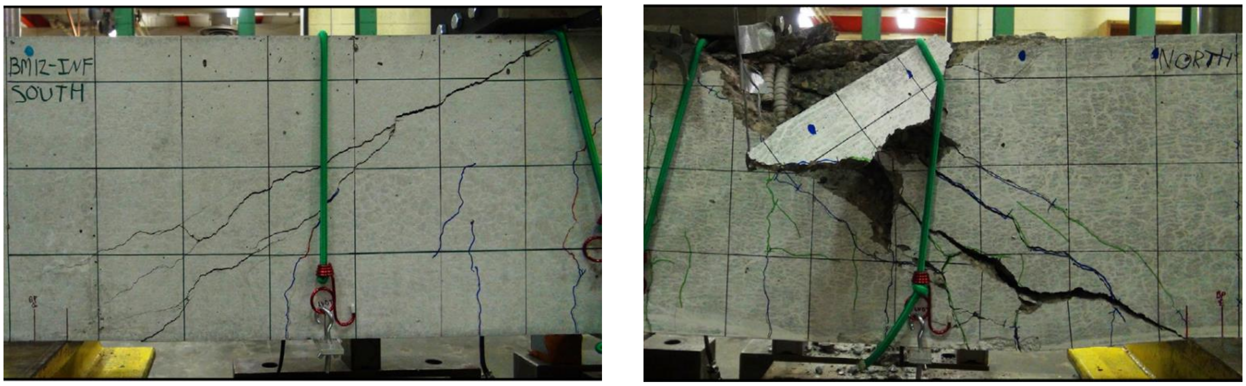

a) Critical shear crack only
b) Critical shear crack with concrete crushing

Figure 3.2: Typical crack patterns of beams tested by Krall (Krall & Polak, 2019)

Based on the test, the factors increasing the shear capacity include having smaller stirrup spacings and having larger stirrups, as the shear reinforcement ratio increases in both cases. Moreover, flexural reinforcement does not impact the shear strength significantly, but small flexural reinforcement ratio may decrease the shear capacity especially for beams with small vertical reinforcement.

3.2 Beams tested by D. J. Kim et al. (2014)

D. J. Kim et al. (2014) casted and tested 15 deep beams without vertical reinforcement. 7 of the beams were reinforced with AFRP bars, 7 others were reinforced with CFRP bars, and one more was reinforced with steel bars. The beams were tested under four-point bending as shown in Figure 3.3 (D. J. Kim et al., 2014).

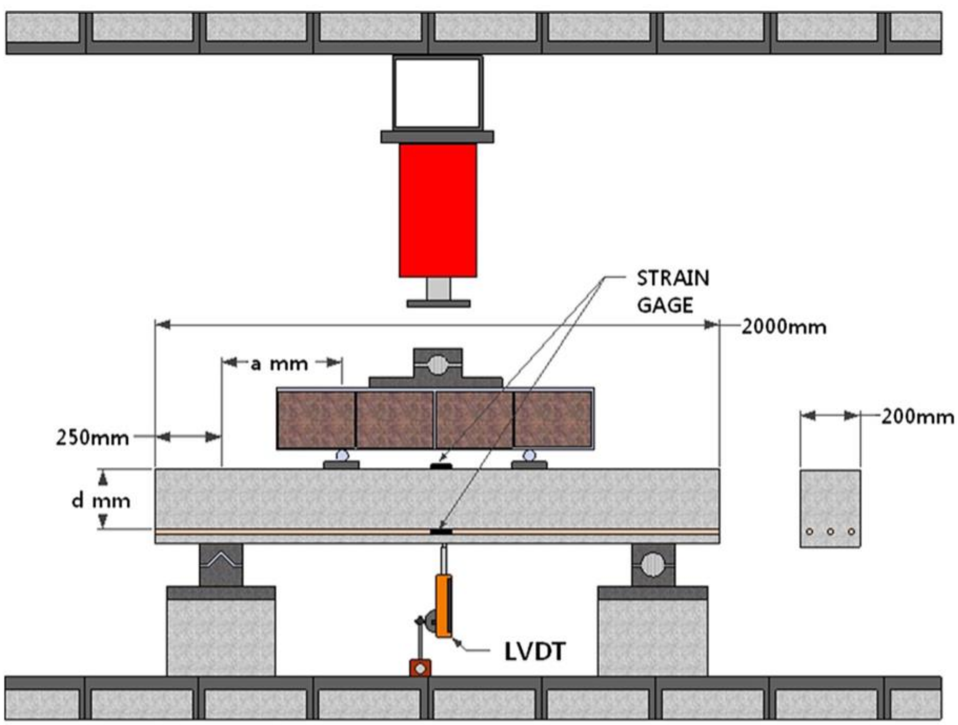

Figure 3.3: Test setup of beams tested by D. J. Kim et al. (2014)

The specimen details are organized in Table 3.3, where f_u is the ultimate strength of FRP bars and yielding strength of steel bars and d_{bar} is the bar diameter. The names of the beams were explained by D. J. Kim et al. (2014) in Figure 3.4 (from Fig.1 in D. J. Kim et al. (2014)).

Table 3.3: Details of beams tested by D. J. Kim et al. (2014)

Specimens	b (mm)	d (mm)	a/d	Reinforcement Details				
				ρ_f (%)	E_f (GPa)	f_{fu} (MPa)	d_{bar} (mm)	A_{Ff} (mm^2)
A3D9M-1.4	200	250	1.4	0.38	80.70	1827	9	63.62
A3D9M-1.7	200	250	1.7	0.38	80.70	1827	9	63.62
A3D9M-2.1	200	250	2.1	0.38	80.70	1827	9	63.62
A4D9M-1.7	200	250	1.7	0.51	80.70	1827	9	63.62
A5D9M-1.7	200	250	1.7	0.64	80.70	1827	9	63.62
A3D9S-1.7	200	190	1.7	0.50	80.70	1827	9	63.62
A5D9L-1.7	200	310	1.7	0.51	80.70	1827	9	63.62
C3D9M-1.4	200	250	1.4	0.38	120.21	1956	9	63.62
C3D9M-1.7	200	250	1.7	0.38	120.21	1956	9	63.62
C3D9M-2.1	200	250	2.1	0.38	120.21	1956	9	63.62
C4D9M-1.7	200	250	1.7	0.51	120.21	1956	9	63.62
C5D9M-1.7	200	250	1.7	0.64	120.21	1956	9	63.62
C3D9S-1.7	200	190	1.7	0.50	120.21	1956	9	63.62
C5D9L-1.7	200	310	1.7	0.51	120.21	1956	9	63.62
S4D10M-1.7	200	250	1.7	0.63	200	400	1.58	491

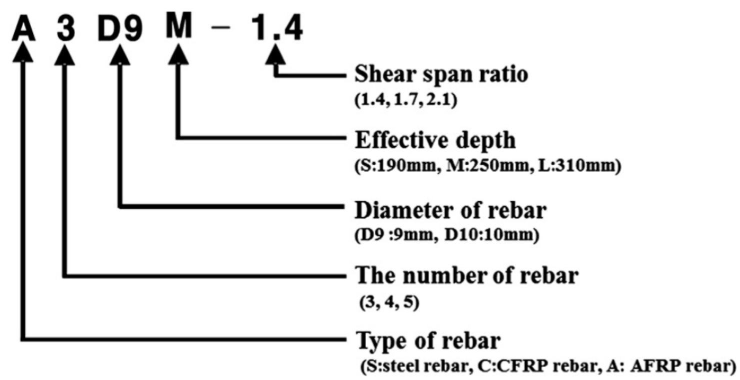

Figure 3.4: Notation to indicate the type of each specimen (D. J. Kim et al., 2014)

The test results are listed in Table 3.4, and the typical failure pattern is presented in Figure 3.5 (D. J. Kim et al., 2014). Two beams had different failure mode from others with significantly low failure load, which might be caused by uneven curing and compaction during the manufacturing process (D. J. Kim et al., 2014). Therefore, these two results are excluded during the analysis. Moreover, D. J. Kim et al. (2014) did not present the test result for the steel reinforced beam, and as this research is for FRP RC deep beams, that beam is not included in this research. Furthermore, the measured average compressive strength of concrete cylinders was 26.1 MPa.

Table 3.4: Test results of beams by D. J. Kim et al. (2014)

Specimens	Failure Load (kN)	Failure Mode
A3D9M-1.4	136.05	Shear-Compression
A3D9M-1.7	98.98	Shear-Compression
A3D9M-2.1	88.00	Shear-Compression
A4D9M-1.7	121	Shear-Compression
A5D9M-1.7	133.97	Shear-Compression
A3D9S-1.7	109.58	Shear-Compression
A5D9L-1.7	134.27	Shear-Compression
C3D9M-1.4	169.26	Shear-Compression
C3D9M-1.7	106.54	Shear-Compression
*C3D9M-2.1**	52.64	Shear-Tension
*C4D9M-1.7**	96.09	Shear-Tension
C5D9M-1.7	151.39	Shear-Compression
C3D9S-1.7	104.84	Shear-Compression
C5D9L-1.7	145.39	Shear-Compression

* Beams with relatively low failure load and different failure modes.

Figure 3.5: Typical failure pattern of beams tested by D. J. Kim et al. (2014)

Based on the results, factors benefitting the shear capacity of deep beams without shear reinforcement include smaller slenderness ratio, larger effective depth, larger flexural reinforcement ratio, and larger stiffness of flexural reinforcement. Hence, the improved IST method shall capture how these factors change the shear capacity.

3.3 Beams tested by Tedford (Tedford, 2019)

To verify if FRP RC slender beams governed by shear can also be analyzed with truss models, beams tested by Tedford (2019) are also analyzed.

Tedford (2019) casted and tested 10 slender beams reinforced with FRP bars. As truss models can only apply to slender beams with stirrups and shall be used to analyze shear strengths, four beams listed in Table 3.5 tested by Tedford (2019) are analyzed in this research, and the names of the specimens follow the same format as those by Krall (2014) (BM "a/d" – "stirrup spacing"). The beams were also tested under three-point bending, and the test setup is similar to Figure 3.1 by Krall (2014).

Table 3.5: Details of beams tested by Tedford (2019)

Specimens	d (mm)	a/d	Flexural Reinforcement					Shear Reinforcement			
			A_{Ff} (mm^2)	# of bars	f_{fu} (MPa)	E_f (GPa)	ρ_f (%)	A_{Fv} (mm^2)	$f_{vu,bent}$ (MPa)	E_v (GPa)	s (mm)
BM4.5-90	270	4.5	201	6	1000	64	2.23	78.5	560	45	90
BM4.5-150	270	4.5	201	6	1000	64	2.23	78.5	560	45	150
BM6.5-90	270	6.5	201	6	1000	64	2.23	78.5	560	45	90
BM6.5-150	270	6.5	201	6	1000	64	2.23	78.5	560	45	150

All beams have the same size with a height of 350 mm and a width of 200 mm, and the average 28-day cylinder compressive strength was measured as 50.2 MPa. Normal density concrete was used, and the test results of these beams are organized in Table 3.6.

Table 3.6: Test results of beams by Tedford (2019)

Specimens	Failure Load (kN)	Failure Mode
BM4.5-90	222.5	Shear
BM4.5-150	171.2	Shear
BM6.5-90*	145.6	Flexure
BM6.5-150	141.0	Shear

* Beam failed in flexure.

As shown in Table 3.6, BM6.5-90 failed in flexure, but not shear. However, to find out if the proposed method can capture the difference in the failure mode, this specimen is still included in this research.

Based on the test results, having more stirrups can increase the shear capacity, and more slender beams will have smaller shear strength even with the same shear and flexural reinforcement ratios.

4. Development of Strut-and-Tie Models

4.1 General Ideas

Strut-and-tie modelling is a method to simplify load transfer mechanism into strut-and-tie (ST) models with struts taking compressive forces and ties taking tensile forces. The properties and the failure criterion of the elements in the ST models shall be assigned in a proper way as they can affect the predicted results. The analysis of steel reinforced deep beams is based on steel yielding; thus, the material properties can be simplified. However, it cannot apply to FRP RC deep beams, as FRP bars cannot yield and such beams fail by crushing of concrete compressive struts, which makes it much more complicated to construct and analyze ST models, hence the details are described in this chapter.

4.2 Elements

ST models representing FRP reinforced deep beams consist of FRP ties taking tensile forces, concrete struts taking compressive forces and nodes connecting struts to other elements.

4.2.1 Ties

Ties are located where FRP bars are placed to take tensile forces. One tie represents all the bars taking one resultant tensile force. Each tie is at the centroid of the bars that it represents, and it has the summed area and the mechanics properties of those bars. Because FRP bars are linear-elastic and brittle, its elastic modulus is constant till rupture.

As beams analyzed in this research are all singly reinforced with same material, the properties of the ties are easy to define. Both vertical and horizontal ties shall be placed in the ST models for beams having shear reinforcement.

4.2.2 Struts

Struts are concrete blocks assumed to be the paths transferring compressive stresses. They are always simplified into lines like in the ST model in Figure 4.1 for calculations of internal forces, strains, etc.

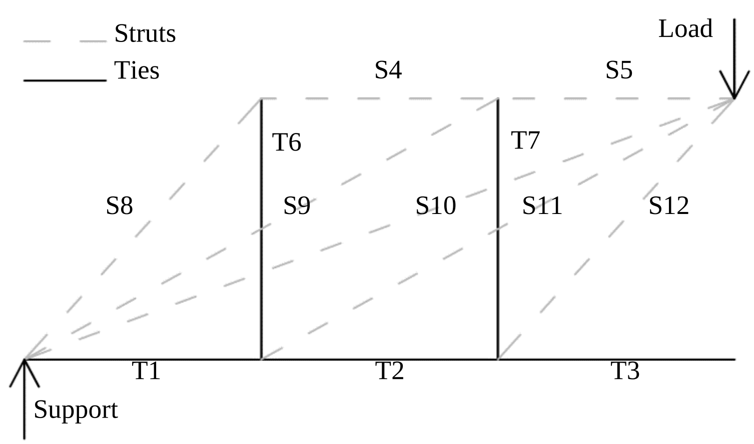

Figure 4.1: Example of an ST model

Unlike ties where the areas can be obtained directly from the rebars, the area of a strut is calculated from multiplying the beam width with the assumed strut width (w_s) that is unique for each strut. Because one strut connects to two nodes, the values obtained from those nodes are different. Take a beam without vertical reinforcement under three-point bending as an example, Figure 4.2 shows that

$$w_{sT} = h_T \cos\theta_{strut} + l_T \sin\theta_{strut} \tag{4.1}$$

$$w_{sC} = h_C \cos\theta_{strut} + l_C \sin\theta_{strut} \tag{4.2}$$

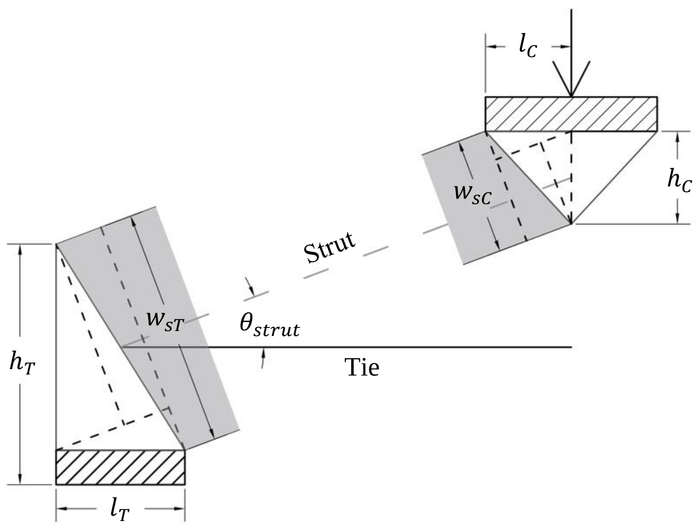

Figure 4.2: Example of calculating strut widths

where h_C, l_C, h_T, l_T are the horizontal and vertical sizes of the node regions that the strut is connected to, and θ_{strut} is the incline of the strut as shown in Figure 4.2.

ACI 318-19 (2019) allows to use w_{sT} (which can be calculated more easily based on the reinforcement design and is generally the larger one) as the strut width for steel reinforced beams, because shear capacity of those beams does not relate directly to the strength of concrete struts. However, w_s directly relates to the predicted shear capacity of FRP reinforced beams as concrete crushing is preferred, hence both w_{sT} and w_{sC} shall be considered.

In some research (Eom & Park, 2010; Mohamed et al., 2020), w_s is taken as the average value of w_{sT} and w_{sC}; and in some other research (B. H. Kim & Yun, 2011a; Krall, 2014), w_s is taken as the smaller of w_{sT} and w_{sC}. In this research, w_s is taken as the smaller of w_{sT} and w_{sC} to be conservative. Horizontal struts only connect to nodes in the compression side, hence w_s are equal to h_C.

Another important property of the struts is the elastic modulus. Concrete is not linear under compression, and elastic modulus decreases with increased applied loads. This study uses tangential modulus consistent with the iterative process. Therefore, the elastic modulus can be the derivative from stress-strain curve at the interest points.

4.2.3 Node Regions

Nodes are the points where struts and ties connect to each other. Because concrete struts have relatively large areas, nodes become node regions for connecting struts to other members or external forces. Node regions can be in different shapes, and the most common shape is triangle, which is also the shape used in this research for making the construction of nodes simple. The dimensions of node regions depend on the forces and members that meet at the nodes.

As shown in Figure 4.2, the heights of all nodes in the tension side are equal to h_T, while the heights of all nodes in the compression side are equal to h_C. h_T is based on the flexural bars, which is equal to the height of the bearing plate if there is one, or twice the distance between the centroid of flexural reinforcement and the outmost concrete tensile fibre.

There is no determined way to calculate h_C for FRP RC deep beams based on current codes and standards, and no research is found specifically on how to obtain it. In this research, it is called the assumed compression height and will be further discussed and analyzed in following chapters, as it is a key feature in the IST method.

The base of the loading and supporting nodes shall be determined based on the widths of the bearing plates or columns, as the compression fan (the name for having multiple struts with different angles connected to one node) connects to them; and the base of other nodes can be determined by assuming the inclined faces of the nodes perpendicular to the centerlines of the inclined strut connected to it, which are

$$l_T = h_T \tan\theta_{strut} \tag{4.3}$$

$$l_C = h_C \tan\theta_{strut} \tag{4.4}$$

With the heights and bases determined, the sizes of the inclined faces of the nodes can be easily obtained.

4.3 Failure Modes

The shear strength of a deep beam is achieved when members of the ST models reach the defined failure including the rupture of ties and the crushing of concrete struts and node regions. As indeterminate ST (IST) models can still be stable after the failure of one member, the load causes the system to fail is generally larger than the load failing the first member.

4.3.1 Tie Rupture

Tie rupture occurs when the stress calculated in any of the ties reaching its ultimate strength. The strengths of the ties representing stirrups are taken as the strength at the bent sections instead of the strengths in the straight portions, as the bent sections are weaker (with less strength).

As tie rupture is brittle and shall be avoided in the design, a factor can be applied to the ultimate strength ensuring that ties will not be near rupture at the system failure. However, for research perspective, this kind of safety factor shall not be included in the analysis.

4.3.2 Strut Crushing

Concrete crushing is the preferred failure for FRP RC beams as it is more ductile than tie rupture. Because FRP RC members need to utilize the ductility of concrete, the failure of concrete strut is assumed to occur when strain reaches ε_0 (the strain corresponds to the compressive strength of concrete), but not ε_{cu} (the crushing strain). As this research uses tangential elastic modulus, strut crushing can also be defined to occur when the elastic modulus reaches zero.

However, as IST models may require multiple members to fail, and the negative stiffnesses can cause errors during the calculation of internal forces, the elastic modulus of a "crushed" strut cannot still be the derivative of the post-peak stress-strain curve. As a failed strut in an IST model shall be a zero-force member, and the force shall be distributed to other members, the elastic modulus of a failed strut can be set to a small number to make the internal force distributed to it close to zero. In this research, the remained elastic modulus of a failed strut is set to 1% of it original elastic modulus at zero strain according to Krall (2014).

4.3.3 Node Crushing

Node crushing is also caused by concrete crushing. However, as it is generally caused by concentrated loads and can be avoided simply by increasing the area to spread out the loads (for example, increasing the sizes of the load bearing plates), it shall also be avoided.

The node crushing criteria are based on CSA S806-12 (R2017), which is to apply the reduction factors of 0.85, 0.75 and 0.65 to concrete strengths (f_c') depending on how many ties connect to this node (0.85 if the node is under pure compression, 0.75 if one tie connects it, and 0.65 if two or more ties connect to it) (CSA S806-12, R2017).

4.3.4 System Failure and Preferred Failure Mode

The failure of a statically determinate ST model occurs when any member of the model fails, which is straightforward; and the failure of the inclined strut indicates the shear failure mode of the beam.

However, the failure of an IST model happens when enough members failed leading the model unstable. As tie rupture and node crushing are the undesirable failure modes, analysis shall be stopped and the changes in reinforcement ratios, beam widths or the node sizes shall be made if they occur prior to the failure of the struts.

System failure can be categorized into three types, failure of only inclined struts (shear failure), failure of horizontal struts (flexural failure) and failure of both kinds of struts (combined).

Failure of inclined struts is the most straight forward type. The failure mode of this type is shear failure, and the strength predicted through this failure type is the shear strength.

The combined failure mode usually follows a pattern with multiple members failing after the failure of one member, and the failed members include both horizontal and inclined struts. This happens because the alternative load paths can neither take the load failing the first load path. This failure type also predicts that the beam will fail in shear, and the predicted strength is the shear strength, no matter if the first failed element is horizontal or inclined strut.

Moreover, if the IST model is predicted to fail in the combined way, the actual failure pattern of the deep beam is more likely to have both critical shear cracks and concrete crushed, especially when the first failed member is predicted to be a horizontal strut. Sometimes, node crushing occurs simultaneously with the failure of multiple struts leading to a system failure, which can also be defined as the combined failure type. It always occurs in some IST model types for beams with relatively small spacings between vertical reinforcement, as the shear strengths of those beams are relatively closer to their flexural strengths.

In contrast, IST models are not designed to predict the flexural failure as the predicted results can be affected by the location and the number of ties, which is not true. Hence, all failed struts being horizontal can only indicate that the beam is governed by flexural failure, but the predicted load is not the flexural strength of the beam, and a further flexural analysis is required.

The IST models in Figure 4.3 under same load (P) are analyzed to show how the predicted flexural strength can be affected by the ties. The force equilibriums in x and y directions for the models in Figure 4.3 can be organized into equations listed below by assuming the stirrups are placed at x_1, x_2 to x_n from support.

$$S_{10y} + S_{11y} + S_{12y} = P \quad \text{for y-direction in a)} \tag{4.5}$$

$$S_5 + S_{10y}\frac{a}{jd} + S_{11y}\frac{a-x_1}{jd} + S_{12y}\frac{a-x_2}{jd} = P\frac{a}{jd} \quad \text{for x-direction in a)} \tag{4.6}$$

$$S_{14y} + S_{15y} + S_{16y} + S_{17y} = P \quad \text{for y-direction in b)} \tag{4.7}$$

$$S_7 + S_{14y}\frac{a}{jd} + S_{15y}\frac{a-x_1}{jd} + S_{16y}\frac{a-x_2}{jd} + S_{17y}\frac{a-x_3}{jd} = P\frac{a}{jd} \quad \text{for x-direction in b)} \tag{4.8}$$

where S_n is the force in S_n; a is the length of the shear span; and jd is the length of the lever arm between resultant compressive and tensile forces.

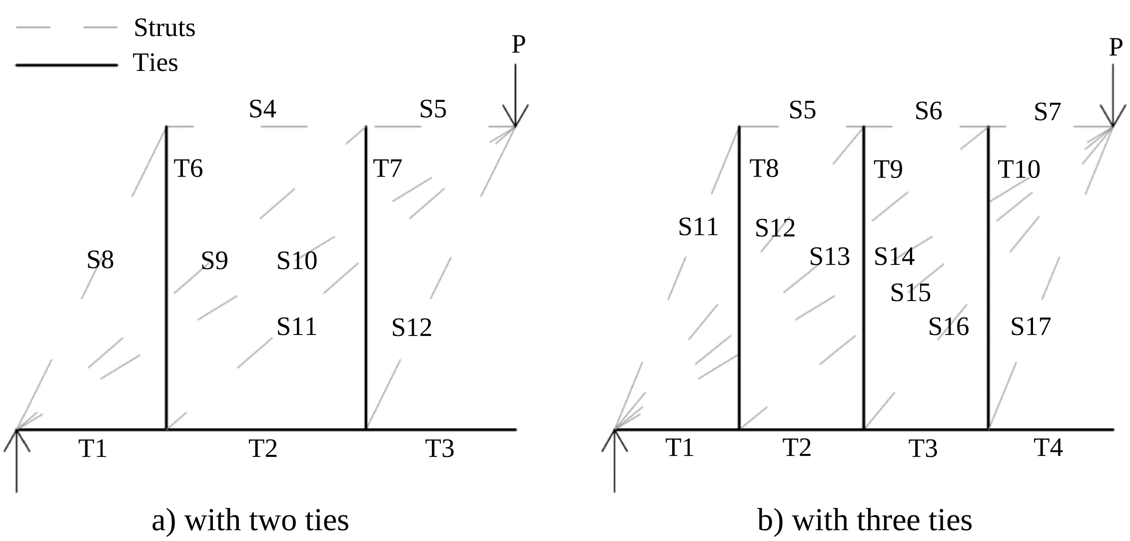

Figure 4.3: IST models with different stirrup spacings

The following equations can be computed by multiplying the y-direction equations with a/jd, and then subtracting them by the x-direction equations

$$S_5 = S_{11y}\frac{x_1}{jd} + S_{12y}\frac{x_2}{jd} \quad \text{in a)} \tag{4.9}$$

$$S_7 = S_{15y}\frac{x_1}{jd} + S_{16y}\frac{x_2}{jd} + S_{17y}\frac{x_3}{jd} \quad \text{in b)} \tag{4.10}$$

Therefore, it is nearly impossible to have S_5 and S_7 be the same, even if stirrups equally divide the shear span with each strut afford same amount of P in y-direction, which makes

$$S_5 = \frac{P}{3}\frac{a}{3jd} + \frac{P}{3}\frac{2a}{3jd} = \frac{Pa}{3jd} \quad \text{in a)} \tag{4.11}$$

$$S_7 = \frac{P}{4}\frac{a}{4jd} + \frac{P}{4}\frac{2a}{4jd} + \frac{P}{4}\frac{3a}{4jd} = \frac{3Pa}{8jd} \quad \text{in b)} \tag{4.12}$$

It is only possible when there is no force taken by the strut connecting the support and the loading point (S10 and S14 in Figure 4.3 a) and b)) with stirrups equally dividing the shear span and each stirrup taking the same amount of force. Furthermore, even with same numbers of stirrups, forces taken by S_5 and S_7 will be different when the locations of these stirrups are changed.

Therefore, when an IST model shows failure of only horizontal struts, it only indicates that the beam will be failed in flexure, and a further flexural analysis is required to determine the flexural strength. However, the analysis of the flexural strength of deep beams is not included in this research as this research focuses on the shear strength.

4.4 Analysis Process

Iterative analysis is done through following incremental loading steps and is organized as a flow chart in Figure 4.4.

1. Before applying loads to the model, the geometry of the model and the sizes of the members shall be determined based on the size of the beam and the arrangement of the longitudinal and vertical reinforcement.
2. In each load step, the forces, stresses, and strains of members are calculated based on the stiffness matrix that is according to the areas, lengths, and elastic moduli of the members.
    - The elastic modulus of a tie is constant
    - The elastic modulus of a strut changes in each load step, and the elastic modulus used in this step is calculated based on the strains obtained from last step.
    - If it is the initial step, the elastic moduli of concrete struts are based on zero strain.
3. After the forces, stresses and strains are obtained. The failure of each member shall be checked.
    - The stresses of ties are compared with their strengths to find if they are ruptured.
    - The failure of a struts is checked based on its elastic modulus calculated from newly obtained strain.
    - To find if a node region is crushed, a resultant force exerted on the node can be calculated based on the x and y components of all forces exerted on this node; and the stress of this node can be computed and compared with its strength according to its type.
4. Based on the check on the strength of the members, the following actions can be made:

- If no member is failed in this step, the next increased load can be applied to the model.
- If bar rupture or node crushing happens in this step, the process shall be stopped as unwanted failure occurs, and the design shall be changed to increase the reinforcement ratio or the node region size.
- If any strut is failed in this step, the number or name of that strut shall be recorded along with the load failing it, and the elastic modulus of the failed strut in all following steps is set to 1% of its initial elastic modulus.

5. The analysis ends when the model becomes unstable with enough struts failing. Based on the types of the failed struts, the failure type of the system can be determined.
   - If the failure type is shear failure or combined failure, the system failing load is the beam's shear strength, and the failure mode of the beam is shear failure.
   - If the flexural failure type is observed, the failure mode of the beams is flexural failure, and the strength of the beam shall be further evaluated based on the flexural analysis.

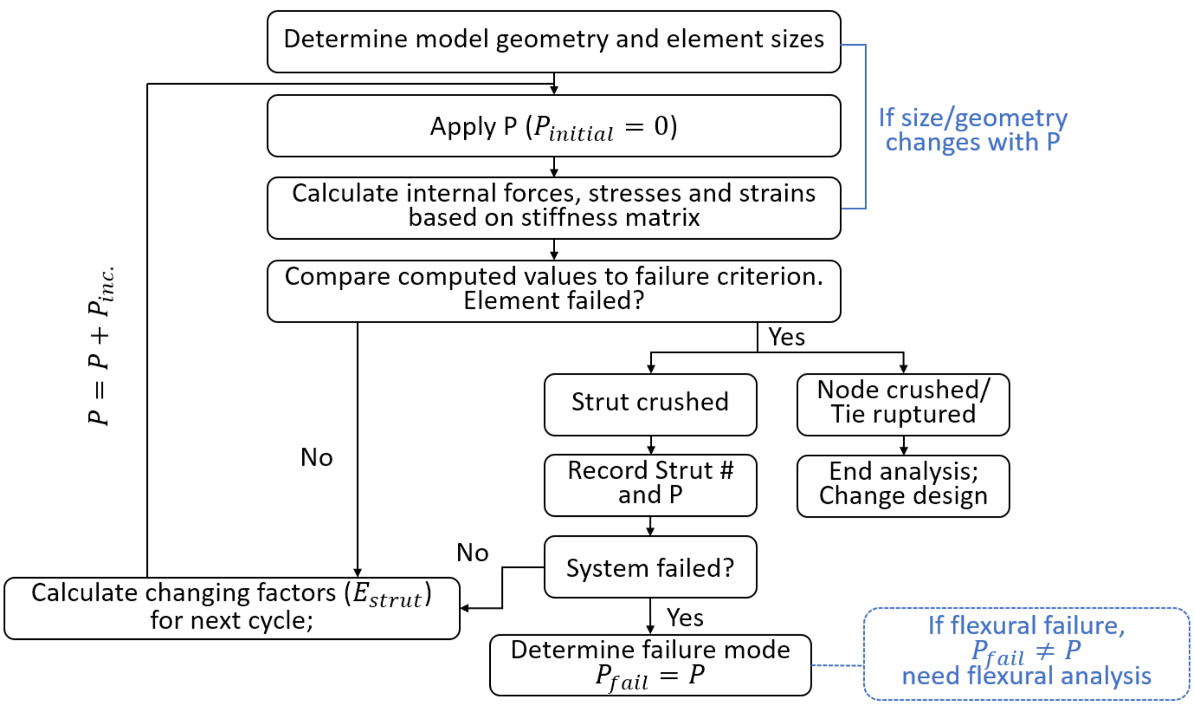

Figure 4.4: Flow chart of the overall analysis process

5. Features of Indeterminate Strut-and-Tie Method

As the design logic for FRP and steel RC deep beams is quite different, the approaches of several features that work for steel RC deep beams do not work appropriately for FRP RC deep beams (like softening factors). Hence, this chapter introduces these factors that are essential to the IST method with their existing and proposed approaches, which are analyzed and compared in later chapters to determine the ones that are suitable.

5.1 Proposed Strut-and-Tie Models

The structure of an ST model is used to represent the load transfer path in the deep beams and affects the predicted results.

Models analyzed in this research are presented in this section. The models are single-shear-span models as the specimens are symmetric, and one zero-force tie is located under the loading point for the convenience in constructing the models in computing programme. Dashed lines in models are for the struts while the thicker continued lines are for the ties.

5.1.1 STM for Deep Beams without Vertical Reinforcement

deep beams without vertical reinforcement are always analyzed with the model geometry presented in Figure 5.1. It is determinate and has a main strut connecting the loading and supporting points. The numbering system is also shown in Figure 5.1.

Because it only has one load path, the failure of this model occurs when S2 is failed.

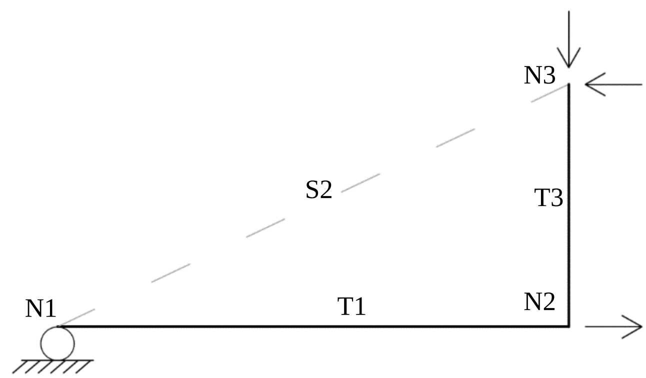

Figure 5.1: STM for beams without vertical reinforcement

5.1.2 STM for Deep Beams with Vertical Reinforcement

ST models to analyze deep beams with vertical reinforcement are generally indeterminate, and there are different types of IST models. This research includes the models used by Krall (2014), by B. H. Kim and Yun (2011a, 2011b) (which was also the design model used by Krall (2014)) and two proposed models.

During the construction of the models, the stirrups too close to the supports (those located inside the supporting node region) are excluded as they cannot help in transferring the loads.

5.1.2.1 Kr Model according to Krall (2014)

The models proposed by Krall (2014) place ties at the exact locations stirrups designed, with one main strut connecting the loading and supporting nodes and multiple struts in between the ties as shown in Figure 5.2. This model is called "Kr model" in this research, and the numbering system is included in Figure 5.2.

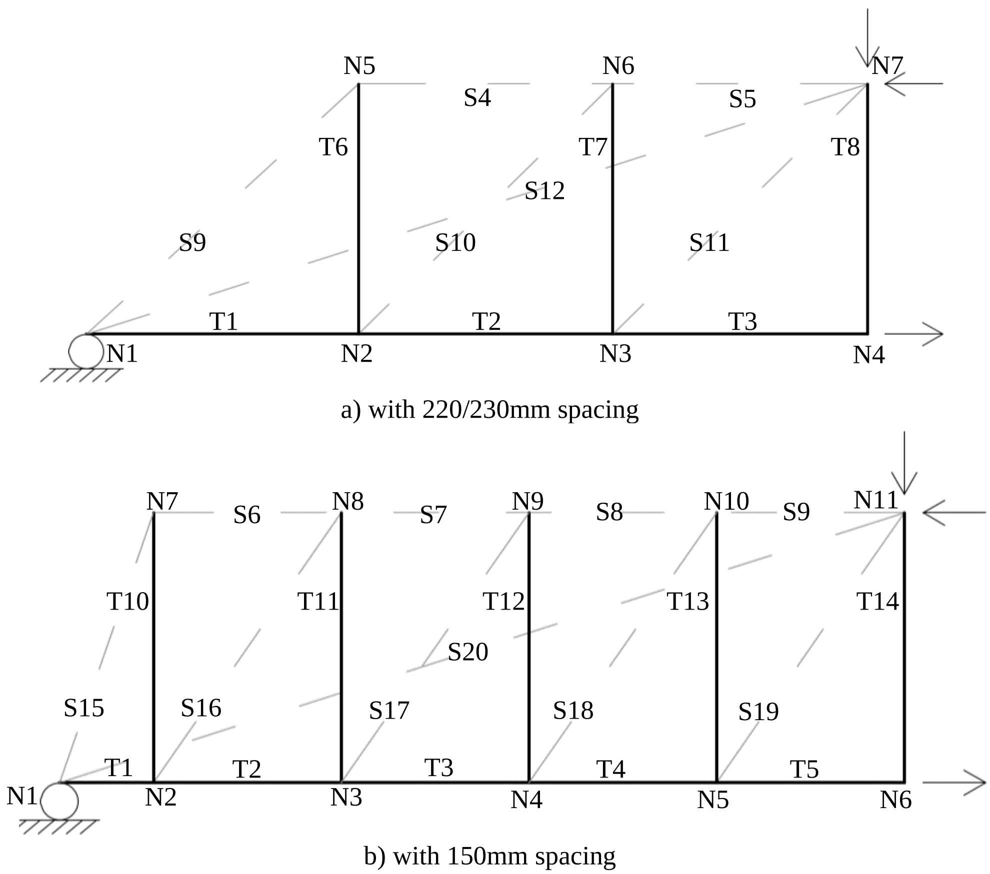

Figure 5.2: Kr model (Krall, 2014) for beams with stirrups

As there are two load paths included in this type of model, the system failure of Kr models occurs when failure occurs in the main strut (S12 and S20 in Figure 5.2 a) and b)) and any other strut.

5.1.2.2 Design Model according to B. H. Kim and Yun (2011a, 2011b)

The model used by B. H. Kim and Yun (2011a, 2011b) is presented in Figure 5.3 with the numbering system. This model is also the one typically used in the industry for designing steel RC deep beams with vertical reinforcement, because it is easy to construct and analyze by consolidating all stirrups into one tie. In this research, it is called "design model".

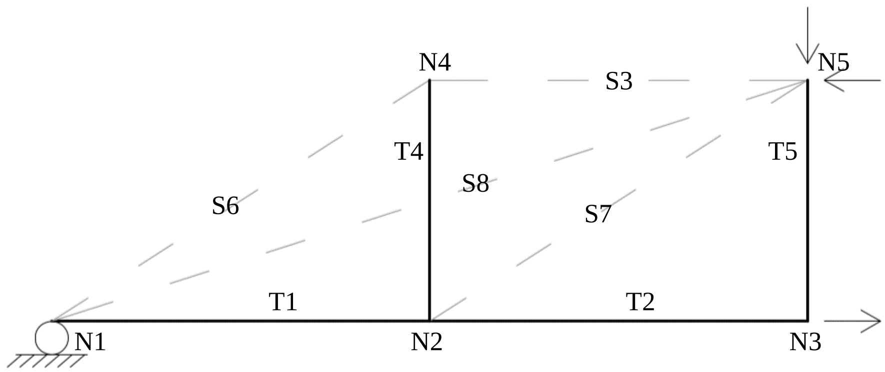

Figure 5.3: Design model for beams with stirrups

This model also has two load paths; thus, the system failure occurs when S8 and any other strut fail.

5.1.2.3 Two Proposed Models (WSF Model and HSF Model)

As will be shown later, Kr model has an issue of overpredicting the results and not capturing the increase in strength with smaller stirrup spacings; two models are proposed in this research to improve the performance of IST modelling. The proposed models are based on the idea of having compression fan in deep sections.

Compression fan is constructed for the whole deep beam in the first proposed model type as shown in Figure 5.4, hence this model type is called "WSF model" (whole section fanning model) in this research.

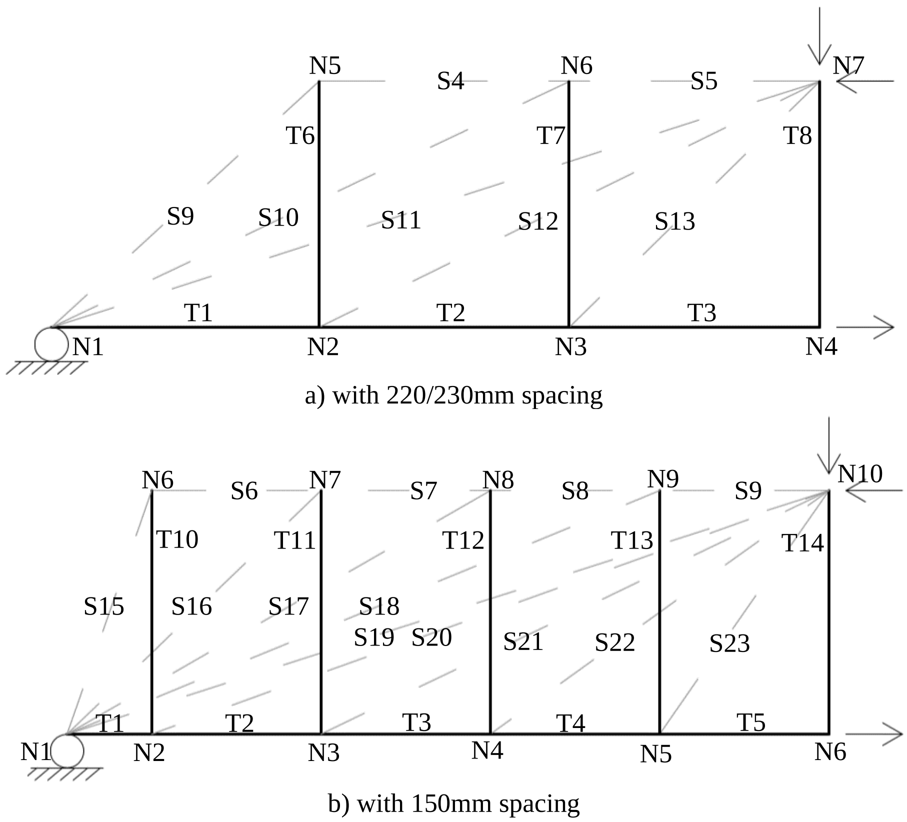

Figure 5.4: WSF model for beams with stirrups

In WSF models, the number of load paths is equal to the number of vertical ties, and the load paths other than the one governed by the main strut connecting the loading and supporting nodes (S11 and S19 in Figure 5.4 a) and b)) consist of the inclined struts connected to the same vertical tie. The system failure occurs when all the load paths are failed, and the failure of a load path occurs when any inclined strut in that load path is failed or when any node in that load path cannot be in equilibrium. Note that the failure of horizontal struts next to loading nodes (S5 and S9 in Figure 5.4 a) and b)) can cause the failure of all other load paths except for the one governed by that main strut.

Because the specimens tested by Krall (2014) were not very deep, another model type with compression fan extended to $2.0d$ is proposed and is presented in Figure 5.5. As about half of the ST model is constructed as compression fan, it is called “HSF model” (half section fanning model) in this research.

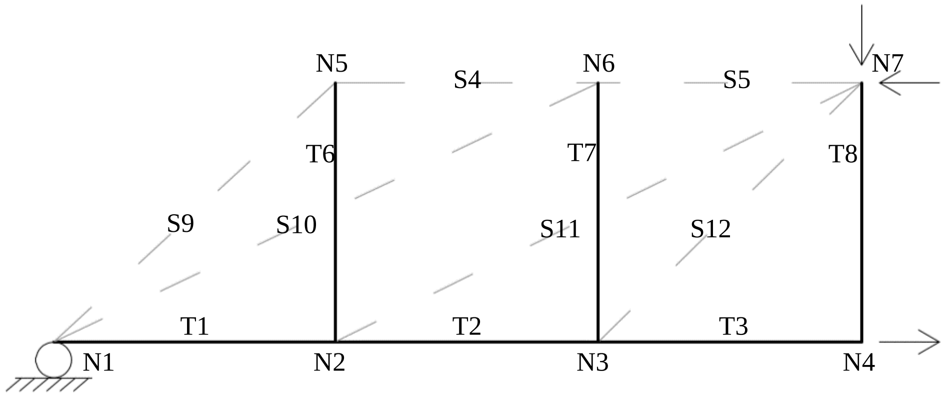

a) with 220/230mm spacing

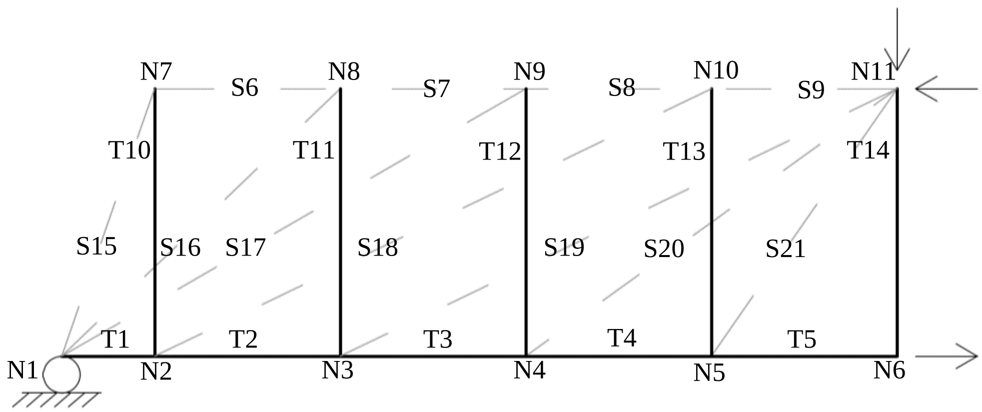

b) with 150mm spacing

Figure 5.5: HSF model for beams with stirrups

The load paths of the HSF model also consist of the inclined struts connected to the same vertical tie, and the system failure occurs when all load paths are failed. HSF model has less load paths compared to WSF model, and there is no strut connecting the supporting and the loading nodes.

5.2 Concrete Stress – Strain Relationships

As FRP RC deep beams rely on the strength of concrete, and the key elements of ST models are the concrete struts, the concrete stress-strain relationship shall be important to the analysis. Although Krall (2014) concluded that the IST method was not sensitive to the choice of concrete stress-strain models, it is still considered as an essential feature in this research, because the pre-peak elastic modulus of concrete could change dramatically if the softening factors are applied in different ways.

As mentioned before, Krall (2014) and B. H. Kim and Yun (2011a, 2011b) applied the softening factor (ζ) to not only the compressive strength (f_c') but also the corresponding strain (ε_0), hence the pre-peak softened stress-strain relationships and elasticity-strain relationships based on the Hognestad parabola and the model by Thorenfeldt et al. (1987) are as shown in Equation (5.1) to (5.2) and Equation (5.3) to (5.4).

$$f_c = \zeta f_c' \left[2\left(\frac{\varepsilon_c}{\zeta\varepsilon_0}\right) - \left(\frac{\varepsilon_c}{\zeta\varepsilon_0}\right)^2 \right] \tag{5.1}$$

$$E = \frac{2\cdot f_c'}{\varepsilon_0}\left(1 - \frac{\varepsilon_c}{\zeta\varepsilon_0}\right) \tag{5.2}$$

where ε_0 can be calculated from $2f_c'/E_c$; and E_c is concrete initial elastic modulus and is calculated based on CSA A23.3-19 (2019) in this research;

$$f_c = \frac{n\cdot\zeta f_c'\left(\varepsilon_c/\zeta\varepsilon_0\right)}{n-1+\left(\varepsilon_c/\zeta\varepsilon_0\right)^{nk}} \tag{5.3}$$

$$E = \frac{n\cdot f_c'/\varepsilon_0}{n-1+\left(\varepsilon_c/\zeta\varepsilon_0\right)^{nk}}\left[1 - \frac{nk\left(\varepsilon_c/\zeta\varepsilon_0\right)^{nk}}{n-1+\left(\varepsilon_c/\zeta\varepsilon_0\right)^{nk}}\right] \tag{5.4}$$

where ε_0 can be calculated from $n\,f_c'/[E_c(n-1)]$; and n and k are parameters for the model by Thorenfeldt et al. (1987). k is equal to 1.0, and n can be obtained from $0.8 + \zeta f_c'\ [MPa]/17$ for pre-peak relationships. Note that n is also softened according to Krall (2014), as it is also a factor obtained from f_c'.

However, only the strength was suggested to be reduced in the Modified Compression Field Theory (MCFT) developed by Vecchio and Collins (1986), and the softened Hognestad parabola and the model by Thorenfeldt et al. (1987) become

$$f_c = \zeta f_c' \left[2\left(\frac{\varepsilon_c}{\varepsilon_0}\right) - \left(\frac{\varepsilon_c}{\varepsilon_0}\right)^2 \right] \tag{5.5}$$

$$E = \frac{2\cdot\zeta f_c'}{\varepsilon_0}\left(1 - \frac{\varepsilon_c}{\varepsilon_0}\right) \tag{5.6}$$

$$f_c = \frac{n\cdot\zeta f_c'\left(\varepsilon_c/\varepsilon_0\right)}{n-1+\left(\varepsilon_c/\varepsilon_0\right)^{nk}} \tag{5.7}$$

$$E = \frac{n\cdot\zeta f_c'/\varepsilon_0}{n-1+\left(\varepsilon_c/\varepsilon_0\right)^{nk}}\left[1 - \frac{nk\left(\varepsilon_c/\varepsilon_0\right)^{nk}}{n-1+\left(\varepsilon_c/\varepsilon_0\right)^{nk}}\right] \tag{5.8}$$

where Equation (5.5), (5.6) are for Hognestad parabola, and Equation (5.7), (5.8) are for the model by Thorenfeldt et al. (1987); and n is calculated as $0.8 + f_c'\ [MPa]/17$, which is not softened.

In this research, the softened Hognestad parabola and Thorenfeldt et al. (1987) model with only the strength reduced are called “H1 model” and “T1 models” respectively, and the models will softening all of the factors calculated from the strength are called “H2 model” and “T2 models” respectively.

The differences in elastic modulus of the models can be found in Figure 5.6 under constant softening factor equal to 0.6375 (the factor from ACI 318-19 (2019) for beams with vertical reinforcement).

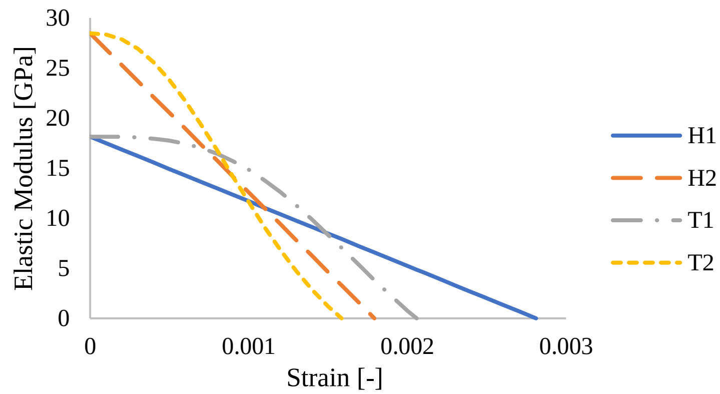

Figure 5.6: Elastic modulus versus strain with different models

It is clear that the initial elastic modulus at zero strain is different if the softening factors are applied in different ways, and the curves from different models are quite different. When the strain is small, the predicted elastic modulus from T2 model tends to be larger than that of H2 model than that of T1 model than that of H1 model; but the strain corresponding to the zero elastic modulus predicted by T2 is smaller than that by H2 than by T1 than by H1.

It is difficult to tell which model will reduce the shear strength the most by only looking at the elastic modulus to strain curves, as different struts are under different stresses, and the relationship between elastic modulus and force distribution is too complicated to determine. Therefore, only the analysed results of the specimens can verify if the models are suitable, and if the shear strength is sensitive to the choice of the softened stress-strain relationships.

5.3 Assumed Concrete Compression Height

As mentioned before, the assumed concrete compression height (h_c) determines the struts' widths and affects the predicted shear strengths. However, there is no determined way to calculate it, and it is computed in different ways in different research and are related to different beam parameters.

5.3.1 Based on Strain Compatibility

Krall (2014) suggested to obtain h_c from strain compatibility with the assumption of concrete top fibre reaches ultimate strain (ε_{cu} of 0.0035) and linear strain distribution as shown in Figure 5.7.

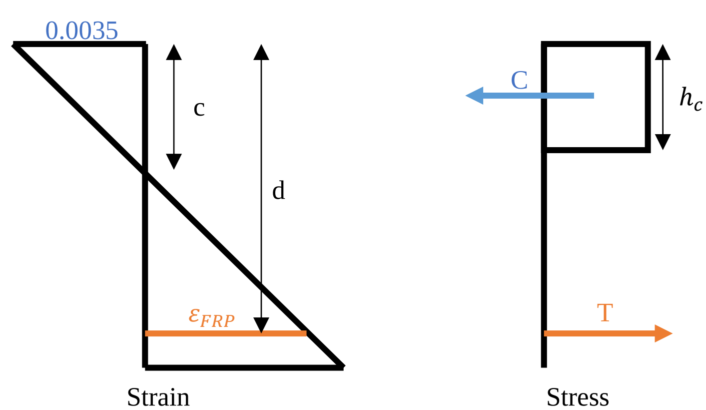

Figure 5.7: Assumed strain distribution and resultant forces

Therefore, the following relationship can be established.

$$\alpha_1 f_c' \beta_1 cb = A_{FRP} E_{FRP} (d - c) \frac{0.0035}{c} \tag{5.9}$$

where f_c' is the concrete cylinder compressive strength; $\alpha_1$and β_1 are the factors suggested in CSA A23.3-19 (2019) for concrete equivalent stress block with concrete reaching ultimate strain of 0.0035 ($\alpha_1 = 0.85 - 0.0015 f_c'$; $\beta_1 = 0.97 - 0.0025 f_c'$); A_{FRP} is the total area of the longitudinal FRP bars; E_{FRP} is the elastic modulus of the FRP bars; d is the effective depth; and c is the only unknown labelled in Figure 5.7.

Therefore, c can be computed, and h_C can also be obtained.

$$c = \frac{-0.0035 A_{FRP} E_{FRP} + \sqrt{(0.0035 A_{FRP} E_{FRP})^2 - 4(\alpha_1 f_c' \beta_1 b)(0.0035 A_{FRP} E_{FRP} d)}}{2(\alpha_1 f_c' \beta_1 b)} \tag{5.10}$$

$$h_C = \beta_1 c \tag{5.11}$$

However, there are several problems of this approach. Firstly, the assumption of plane section remaining plane (linear strain distribution) does not hold true for deep beams. Secondly, the assumption of top fibre reaching ε_{cu} is for beams failing in flexure, but the top fibre of concrete may not reach the ultimate strain when the beam is failed in shear.

h_C calculated based on this approach are organized in Table 5.1, which clearly shows the influence of elastic modulus and ratio of flexural reinforcement (E_f and ρ_f) on the value of h_C.

Table 5.1: h_C of specimens based on strain compatibility

Specimens	ρ_f (%)	E_f (GPa)	h_C (mm)
BM12-INF	2.51	60	76.89
BM12-220	2.51	60	76.89
BM12-150	2.51	60	76.89
BM12-s230	2.18	60	72.68
BM16-INF	2.23	64	75.03
BM16-220	2.23	64	75.03
BM16-150	2.23	64	75.03
BM16-s230	1.94	64	71.15
BM25-INF	1.82	60	67.42
BM25-220	1.82	60	67.42
BM25-150	1.82	60	67.42
BM25-s230	1.58	60	63.28
A3D9M-1.4	0.38	80.70	52.7
A3D9M-1.7	0.38	80.70	52.7
A3D9M-2.1	0.38	80.70	52.7
A4D9M-1.7	0.51	80.70	59.76
A5D9M-1.7	0.64	80.70	65.75
A3D9S-1.7	0.50	80.70	45.15
A3D9L-1.7	0.51	80.70	74.35
C3D9M-1.4	0.38	120.21	62.68
C3D9M-1.7	0.38	120.21	62.68
C3D9M-2.1	0.38	120.21	62.68
C4D9M-1.7	0.51	120.21	70.79
C5D9M-1.7	0.64	120.21	77.62
C3D9S-1.7	0.50	120.21	53.5
C3D9L-1.7	0.51	120.21	88.07
BM4.5-90	2.23	64	74.00
BM4.5-150	2.23	64	74.00
BM6.5-90	2.23	64	74.00
BM6.5-150	2.23	64	74.00

5.3.2 Based on Force Equilibrium

The approach of h_C usually found in IST modelling of steel RC deep beams is based on the force equilibrium, which is to assume that the resultant compressive force at ultimate state makes the stress in the concrete equivalent stress block reaching $0.85f_c'$, and the resultant tensile force at ultimate state makes flexural bars yielding. Hence, based on the force equilibrium,

$$h_c = \frac{A_s f_y}{0.85 f_c' b} \tag{5.12}$$

where A_s is the total area of steel flexural bars; f_y is the yielding strength of steel bars; and b is beam width.

However, FRP bars do not yield; hence, an assumed strength at ultimate state shall be proposed to adopt this approach. As CSA S806-12 (R2017) regulated the stress in FRP bars shall not exceed 65% of its ultimate strength, this approach can be modified to

$$h_c = \frac{0.65 A_{FRP} f_u}{0.85 f_c' b} \tag{5.13}$$

where A_{FRP} is the total area of flexural FRP bars; and f_u is the strength of these flexural bars.

Therefore, h_C based on this approach can be easily computed, and Table 5.2 organized h_C through this approach. The value of h_C also changes with the flexural reinforcement area; but the values obtained from this approach are quite large and are extremely sensitive to the flexural reinforcement compared to the values obtained based on strain compatibility. The predicted values being relatively large may be due to that the stresses in flexural rebars are generally smaller than the regulated 65% of its ultimate strength.

Table 5.2: h_C of specimens based on force equilibrium

Specimens	ρ_f (%)	E_f (GPa)	h_C (mm)
BM12-INF	2.51	60	109.61
BM12-220	2.51	60	109.61
BM12-150	2.51	60	109.61
BM12-s230	2.18	60	85.78
BM16-INF	2.23	64	97.49
BM16-220	2.23	64	97.49
BM16-150	2.23	64	97.49
BM16-s230	1.94	64	76.29
BM25-INF	1.82	60	79.38
BM25-220	1.82	60	79.38
BM25-150	1.82	60	79.38
BM25-s230	1.58	60	62.12
A3D9M-1.4	0.38	80.70	51.08
A3D9M-1.7	0.38	80.70	51.08
A3D9M-2.1	0.38	80.70	51.08
A4D9M-1.7	0.51	80.70	68.11
A5D9M-1.7	0.64	80.70	85.13
A3D9S-1.7	0.50	80.70	51.08
A3D9L-1.7	0.51	80.70	85.13
C3D9M-1.4	0.38	120.21	54.68
C3D9M-1.7	0.38	120.21	54.68
C3D9M-2.1	0.38	120.21	54.68
C4D9M-1.7	0.51	120.21	72.91
C5D9M-1.7	0.64	120.21	91.14
C3D9S-1.7	0.50	120.21	54.68
C3D9L-1.7	0.51	120.21	91.14
BM4.5-90	2.23	64	91.67
BM4.5-150	2.23	64	91.67
BM6.5-90	2.23	64	91.67
BM6.5-150	2.23	64	91.67

5.3.3 FEA Analysis

Because the results from methods mentioned above are quite different from each other, and the assumption of the previous methods may not agree with the behavior of FRP RC deep beams at peak loads, a preliminary finite element analysis (FEA) is conducted in Abaqus (Smith, 2009) to find out the values of h_C in beams with different beam designs having different parameters including different slenderness ratios, beam dimensions, and reinforcement ratios.

At first, the pinned boundary conditions (BCs) are applied on all three directions to the supporting areas with the load (set as increasing displacement at the loading direction) applied to the loading area. Under this kind of boundary conditions, the analyzed crack pattern and stress distribution diagram do not change when the beam design is changed, which reflects that such model cannot reflect the beam behavior. Therefore, the boundary conditions of the supporting area used by Stoner and Polak (2020) are referred, which is to restrain the lines parallel to x-axis in x-direction and to restrain the lines parallel to y-axis in y-direction with the coordinate system as shown in Figure 5.8, which leads to much better results similar to the ones presented by Stoner and Polak (2020).

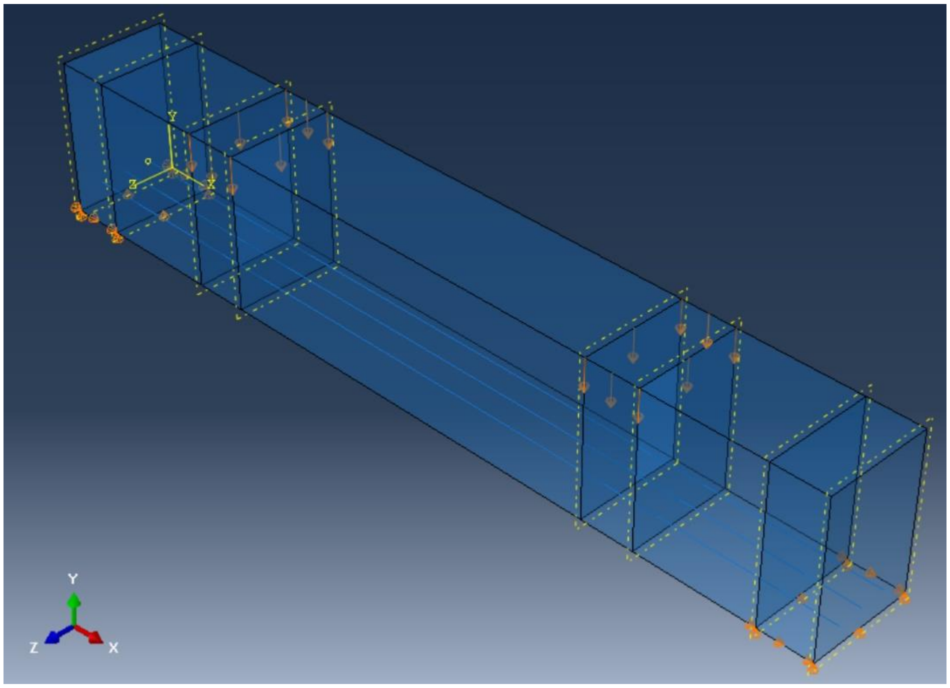

Figure 5.8: Coordinate system and BCs for FEA from Abaqus (Smith, 2009)

Because this is a preliminary analysis, the material parameters are not studied in detail and the reinforcements are embedded into the concrete region without considering the bond-slip. As the mesh sizes depend on the beam sizes, and different concrete stress-strain models are used, they will be specified after the analyzed specimens are introduced.

Moreover, because the FEA in this research focuses on how h_C is affected by the parameters of beam design (e.g., beam dimensions, reinforcement ratios), the analysis is conducted on mostly imaginary beams, and the models can only be briefly validated through checking the crack patterns and the load-displacement curves. A detailed and thorough FEA cannot be performed on h_C limited to the scope of this research, thus this can be a good topic for future study.

The general process to compute h_C goes as:

1. Suitable loads (increasing displacements) are applied at loading points, which can lead to plateau appearing in loading versus displacement plot.
2. The stresses in the x-direction (S11 from Abaqus (Smith, 2009), based on the coordinate system presented in Figure 5.8) of each element under the loading point (usually at the mid span) are obtained from Abaqus (Smith, 2009).
3. The load step that failure occurred is found based on the load-displacement plot and the analyzed crack pattern.
4. h_C is computed as twice the distance from the centroid of the compressive stress curve to concrete top along the height of the beam at the failure step.

The distribution of the stresses in x-direction (S11 from Abaqus (Smith, 2009) on the cross section of a beam under the loading point is presented in Figure 5.9, where negative values are for stresses in compression and positive values are for stresses in tension. Moreover, because loads are applied to the full width of the beams, the stresses in the elements under the loading point and at the same height (the stresses in the elements on the same row in Figure 5.9) are almost the same, thus the elements labelled in red in Figure 5.9 are selected to find the stress along the beam height at failure.

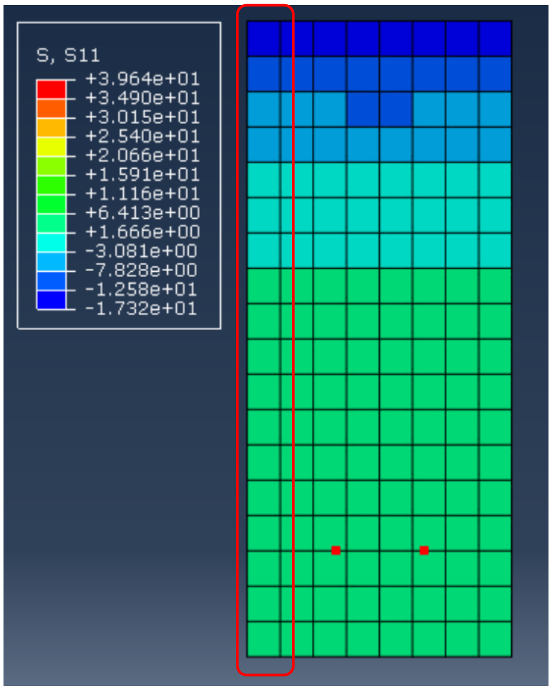

Figure 5.9: Stress profile along beam height

Figure 5.10 shows an example graph of stress along the beam height at failure. Continuous lines label out the elements and show the stress exerted on each element, while dash lines connect the stresses in the elements into a stress profile. Based on the stress profile, h_c can be calculated as twice the distance from concrete top to the centroid of the compression part, thus

$$h_c = 2\frac{\sum y_i \sigma_{xi} \Delta_i}{\sum \sigma_{xi} \Delta_i} \tag{5.14}$$

where y_i is the distance in y-direction from the beam top to the centerline of i-th element; σ_{xi} is the stress in x-direction exerted on that element; Δ_i is the size of the element; and only elements in compression are included.

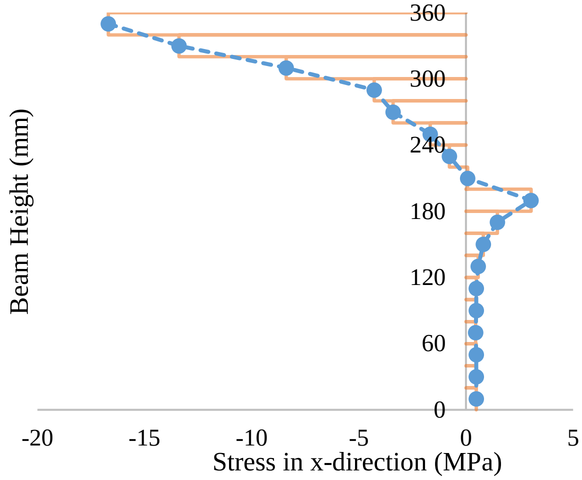

Figure 5.10: Stress profile along beam height

Firstly, the following beams with features listed in Table 5.3 are analyzed, where a/d is the shear span to depth ratio, A_{bar} is the area of one rebar, and ρ_f is the longitudinal reinforcement ratio. Most of the beams are imaginary beams with several beams from Krall (2014).

Table 5.3: First set of beams analyzed with FEA

Name	Height (mm)	Width (mm)	Depth (mm)	a/d	# of bars	A_{bar} (mm^2)	ρ_f (%)
ad1	360	60	-	-	0	-	-
ad1b60	360	60	300	1	2	491	5.46
ad1b60-h	360	60	300	1	2	200	2.22
ad1b60-d	360	60	300	1	2	1000	11.11
ad1b60-3000	360	60	300	1	2	3000	33.33
ad1b60w150	360	150	300	1	2	491	2.18
ad1b100	400	60	300	1	2	491	5.46
ad1b100-d	400	60	300	1	2	1000	11.11
ad1.5b60	360	60	300	1.5	2	491	5.46
ad1.5b60-h	360	60	300	1.5	2	200	2.22
ad1.5b60-d	360	60	300	1.5	2	1000	11.11
ad1.5b60w150	360	150	300	1.5	2	491	2.18
ad2b60	360	60	300	2	2	491	5.46
ad2.5b60	360	60	300	2.5	2	491	5.46
ad2.5b60-d	360	60	300	2.5	2	1000	11.11
ad3b60	360	60	300	3	2	491	5.46
ad4b60	360	60	300	4	2	491	5.46
BM25-INF	330	200	270	2.5	2	491	1.82
BM25-220	330	200	270	2.5	2	491	1.82
BM25-150	330	200	270	2.5	2	491	1.82

It is assumed that these imaginary beams use the same material as BM25 beams from Krall (2014) (for material properties), and the concrete models used for these beams are the modified Hognestad parabola suggested by Stoner and Polak (2020) for compressive behavior and exponential tension model in the following equations with n equal to 0.4 for tensile behavior of concrete.

$$f_c = f'_c\left[2\left(\frac{\varepsilon_c}{\varepsilon_0}\right) - \left(\frac{\varepsilon_c}{\varepsilon_0}\right)^2\right] \text{ for } \frac{\varepsilon_c}{\varepsilon_0} \leq 1 \tag{5.15}$$

$$f_c = f'_c\left[1 - \left(\frac{\varepsilon_c/\varepsilon_0 - 1}{2}\right)^2\right] \text{ for } \frac{\varepsilon_c}{\varepsilon_0} > 1 \tag{5.16}$$

$$f_t = E_c\varepsilon_t \text{ for } \frac{\varepsilon_t}{\varepsilon_r} \leq 1 \tag{5.17}$$

$$f_t = f_r\left(\frac{\varepsilon_r}{\varepsilon_t}\right)^n \text{ for } \frac{\varepsilon_t}{\varepsilon_r} > 1 \tag{5.18}$$

where f_t is concrete tensile stress at tensile strain ε_t; f_r is the rupture strength of concrete equal to $0.6\sqrt{f'_c}$; and ε_r is the rupture strain equal to f_r/E_c. The symbols used in compressive model are the same as those in previous equations for concrete compressive models, and E_c is assumed to be same for concrete in compression and in tension.

Compared to using the same equation for pre- and post-peak compressive behavior, the modified Hognestad parabola increase the post-peak capacity of concrete as shown in Figure 5.11 (for concrete with cylinder strength of 40 MPa).

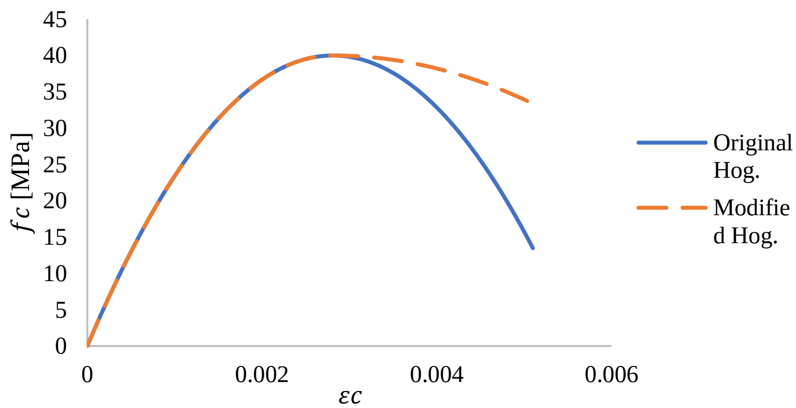

Figure 5.11: Compressive stress-strain curves of original and modified Hognestad parabola

The exponential tension model is commonly used to model the concrete post-peak tensile behavior, and the factor n controls the post-peak capacity. The post peak capacity increases when the value of n decreases as shown in Figure 5.12 with n equal to 0.4 and 1.0.

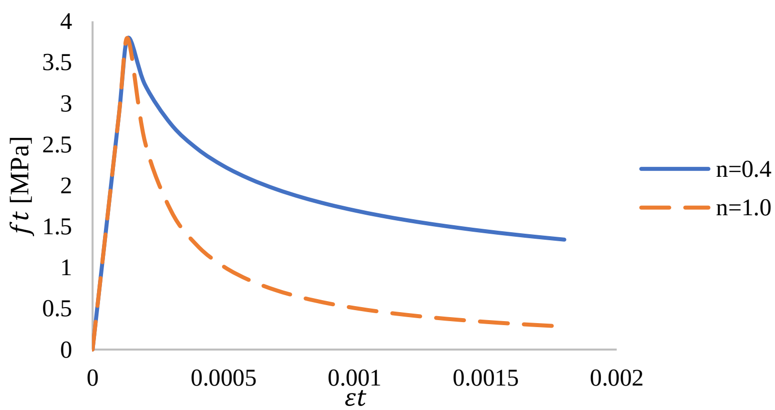

Figure 5.12: Exponential tension model with different n

Based on the sizes of these beams, the values of h_C obtained with the mesh size of 20 mm and 10 mm are not that different, hence 20 mm C3D8R (8-node linear brick, reduced integration, hourglass control) elements (Smith, 2009) are used for the analysis, and the results are organized in Table 5.4, where h is the beam height, d is the effective depth and ρ_f is the longitudinal reinforcement ratio.

Table 5.4: Results of beams analyzed with first set of concrete models

Name	h_c (mm)	h_c/h	h_c/d	ρ_f (%)
ad1	37.95	0.1054	-	-
ad1b60	71.94	0.1998	0.2398	5.46
ad1b60-h	46.64	0.1296	0.1555	2.22
ad1b60-d	71.42	0.1984	0.2381	11.11
ad1b60-3000	79.62	0.2212	0.2654	33.33
ad1b60w150	62.27	0.1730	0.2076	2.18
ad1b100	67.12	0.1678	0.2237	5.46
ad1b100-d	66.89	0.1672	0.2230	11.11
ad1.5b60	48.95	0.1360	0.1632	5.46
ad1.5b60-h	43.81	0.1217	0.1460	2.22
ad1.5b60-d	48.91	0.1358	0.1630	11.11
ad1.5b60w150	48.34	0.1343	0.1611	2.18
ad2b60	51.92	0.1442	0.1731	5.46
ad2.5b60	60.70	0.1686	0.2023	5.46
ad2.5b60-d	62.11	0.1725	0.2070	11.11
ad3b60	84.61	0.2350	0.2820	5.46
ad4b60	89.31	0.2481	0.2977	5.46
BM25-INF	53.90	0.1633	0.1996	1.82
BM25-220	53.40	0.1618	0.1978	1.82
BM25-150	51.25	0.1553	0.1898	1.82
Average of deep beams	-	0.16	0.20	

The results showed that firstly, h_C is affected by the flexural reinforcement ratio, but the influence is limited; secondly, h_C relates more closely to depth but not height according to specimens ad1b60, ad1b60-d, ad1b100 and ad1b100-d; thirdly, slender beams tend to have larger h_C than deep beams; and lastly, with the first set of material models, h_C ranges from 0.15d to 0.25d for deep beams, and the average value is about 0.2d.

It is interesting to find that the average value of 0.2d agrees with the effective shear depth value of 0.9d suggested by CSA A23.3-19 (2019), which is used to assume the distance between resultant tensile and compressive forces for beams under shear.

To verify the findings and to test how h_C changes when the post-peak behaviour is modelled differently. Most of the beams are analyzed again with the original Hognestad parabola for the post-peak behavior of concrete in compression and the exponential tension model having n equal to 1.0, and the results are organized in Table 5.5.

Table 5.5: Results of beams analyzed with second set of concrete models

Name	h_c (mm)	h_c/h	h_c/d	ρ_f (%)
ad1	36.91	0.1025	-	-
ad1b60	66.14	0.1837	0.2205	5.46
ad1b60-h	41.61	0.1156	0.1387	2.22
ad1b60-d	77.27	0.2146	0.2576	11.11
ad1b60-3000	92.36	0.2566	0.3079	33.33
ad1b60w150	49.19	0.1367	0.1640	2.18
ad1.5b60	45.80	0.1272	0.1527	5.46
ad2b60	47.80	0.1328	0.1593	5.46
ad2.5b60	54.07	0.1502	0.1802	5.46
ad2.5b60-d	53.02	0.1473	0.1767	11.11
ad3b60	59.19	0.1644	0.1973	5.46
ad4b60	58.30	0.1619	0.1943	5.46
BM25-INF	50.06	0.1517	0.1854	1.82
BM25-220	59.03	0.1789	0.2186	1.82
BM25-150	56.99	0.1727	0.2111	1.82
Average of deep beams	-	0.16	0.20	

The results show that the influence from both the flexural and vertical reinforcement becomes slightly larger with this set of concrete models; the influence from slenderness is not as obvious as previously; and the value of h_c ranges similarly from 0.13d to 0.3d and the average h_c value for deep beams is also around 0.2d.

Furthermore, to find if h_c/d values can be still inside a similar range for beams with different heights and material properties, the following beams in Table 5.6 based on the specimens tested by D. J. Kim et al. (2014) are also analyzed along with some of the previously mentioned beams.

Table 5.6: Beams based on specimens by D. J. Kim et al. (2014) analyzed with FEA

Name	Height (mm)	Width (mm)	Depth (mm)	a/d	# of bars	A_{bar} (mm^2)	ρ_f (%)
A3D9M1.4	285	200	250	1.4	3	63.62	0.38
A3D9M1.7	285	200	250	1.7	3	63.62	0.38
A3D9M2.1	285	200	250	2.1	3	63.62	0.38
A4D9M1.7	285	200	250	1.7	4	63.62	0.51
A5D9M1.7	285	200	250	1.7	5	63.62	0.64
A3D9S1.7	225	200	190	1.7	3	63.62	0.50
A5D9L1.7	345	200	310	1.7	5	63.62	0.51
A3D9M1.3	285	200	250	3	3	63.62	0.38
A3D9M1.5	285	200	250	3	3	63.62	0.38
A3D9M1.6	285	200	250	3	3	63.62	0.38
A3D9M1.4d	285	200	250	1.4	3	491	2.95

As the size of these beams are smaller, mesh size is reduced to 10 mm to ensure the accuracy of the analyzed results. Moreover, to find what will happen to the results if only the tension exponential model has decreased post-peak capacity with n equal to 1.0 while use the modified Hognestad parabola for compression post-peak behavior, the beams are analyzed with this third set of material models, and the results are organized in Table 5.7.

Table 5.7: Results of beams analyzed with third set of concrete models

Name	h_c (mm)	h_c/h	h_c/d	ρ_f (%)
ad1	32.83	0.0912	-	-
ad1b60	62.33	0.1731	0.2078	5.46
ad1b60-h	45.46	0.1263	0.1515	2.22
ad1b60-d	70.85	0.1968	0.2362	11.11
ad1b60-3000	92.40	0.2567	0.3080	33.33
ad1b60w150	44.77	0.1244	0.1492	2.18
ad1.5b60	46.61	0.1295	0.1554	5.46
ad2b60	46.10	0.1280	0.1537	5.46
ad2.5b60	51.28	0.1425	0.1709	5.46
ad2.5b60-d	55.23	0.1534	0.1841	11.11
ad3b60	52.86	0.1468	0.1762	5.46
ad4b60	57.72	0.1603	0.1924	5.46
BM25-INF	48.69	0.1475	0.1803	1.82
BM25-220	47.90	0.1451	0.1774	1.82
BM25-150	47.43	0.1437	0.1757	1.82
A3D9M1.4	30.78	0.1080	0.1231	0.38
A3D9M1.7	33.34	0.1170	0.1334	0.38
A3D9M2.1	42.87	0.1504	0.1715	0.38
A4D9M1.7	33.51	0.1176	0.1340	0.51
A5D9M1.7	37.77	0.1325	0.1511	0.64
A3D9S1.7	26.61	0.1183	0.1400	0.50
A5D9L1.7	44.54	0.1291	0.1437	0.51
A3D9M1.3	34.63	0.1215	0.1385	0.38
A3D9M1.5	34.25	0.1202	0.1370	0.38
A3D9M1.6	33.11	0.1162	0.1325	0.38
A3D9M1.4d	77.06	0.2704	0.3082	2.95
Average of deep beams	-	0.14	0.17	

h_c ranges similarly from 0.13d to 0.3d, and the average value of h_c/d slightly decreases to 0.17 but is still close to 0.2. The decrease in the average value is mainly from the new specimens based on beams tested by D. J. Kim et al. (2014), which were casted with lower strength concrete and much lower reinforcement ratios.

Because the analysis is preliminary, most of the beams are imaginary beams without test data to verify the behavior, and the trends are not clear, thus it is difficult to find the relationships between h_c and the parameters of beam design (e.g., beam dimensions, reinforcement ratios). However, as the value of h_c always fall into the range of 0.13d to 0.3d, and the average value is always around 0.2d, it may be a good guess to always obtain h_c as 0.2d for analysis.

Computing h_c as 0.2d does not give precise value of h_c for beams with different design, but this guess is neither a bad guess based on the analyzed range of h_c (0.13d to 0.3d) and shall not give values much different from the real situation. This approach slightly overestimates h_c of beams that are deeper and do not have stirrups, and it gives conservative values when the beams are slenderer and have stirrups.

Moreover, the value of 0.2d is always more conservative than the two other approaches introduced previously based on strain compatibility and force equilibrium as shown in Table 5.8.

Table 5.8: h_C equal to 0.2d of specimens

Specimens	d (mm)	h_C (mm)
BM12-INF	270	54.00
BM12-220	270	54.00
BM12-150	270	54.00
BM12-s230	270	54.00
BM16-INF	270	54.00
BM16-220	270	54.00
BM16-150	270	54.00
BM16-s230	270	54.00
BM25-INF	270	54.00
BM25-220	270	54.00
BM25-150	270	54.00
BM25-s230	270	54.00
A3D9M-1.4	250	50.00
A3D9M-1.7	250	50.00
A3D9M-2.1	250	50.00
A4D9M-1.7	250	50.00
A5D9M-1.7	250	50.00
A3D9S-1.7	190	38.00
A3D9L-1.7	310	62.00
C3D9M-1.4	250	50.00
C3D9M-1.7	250	50.00
C3D9M-2.1	250	50.00
C4D9M-1.7	250	50.00
C5D9M-1.7	250	50.00
C3D9S-1.7	190	38.00
C3D9L-1.7	310	62.00
BM4.5-90	270	54.00
BM4.5-150	270	54.00
BM6.5-90	270	54.00
BM6.5-150	270	54.00

5.3.4 New Approach

Although assuming h_c equal to 0.2d is simple to use and more conservative than the other two approaches, it cannot capture how the parameters of beam design (e.g., beam dimensions, reinforcement ratios) affect the value of h_c, hence a further analysis of h_c is conducted to propose a new approach.

Based on the FEA done previously, the strain profile of beams with different loading conditions are obtained. The pre-crack strain profile is presented in Figure 5.13 for deep beams under three-point bending, four-point bending and uniformly distributed load (UDL) and slender beams. The profiles are similar to the ones suggested by Abdel-Nasser et al. (2017). It is only that Figure 5.13 shows similar proposed strain profile of deep beams under three-point bending and four-point bending, but Abdel-Nasser et al. (2017) suggested that the strain profile of deep beams under four-point bending is similar to that under UDL.

Hence, if linear strain profile is assumed for deep beams under three-point and four-point bending, the value of h_c is over-estimated; but this assumption is safe for deep beams under UDL. Moreover, if the linear strain distribution is only assumed to the section under compression, the estimated value would be closer to the actual value. Furthermore, the strain in the top fibre of concrete is far smaller than the ultimate strain.

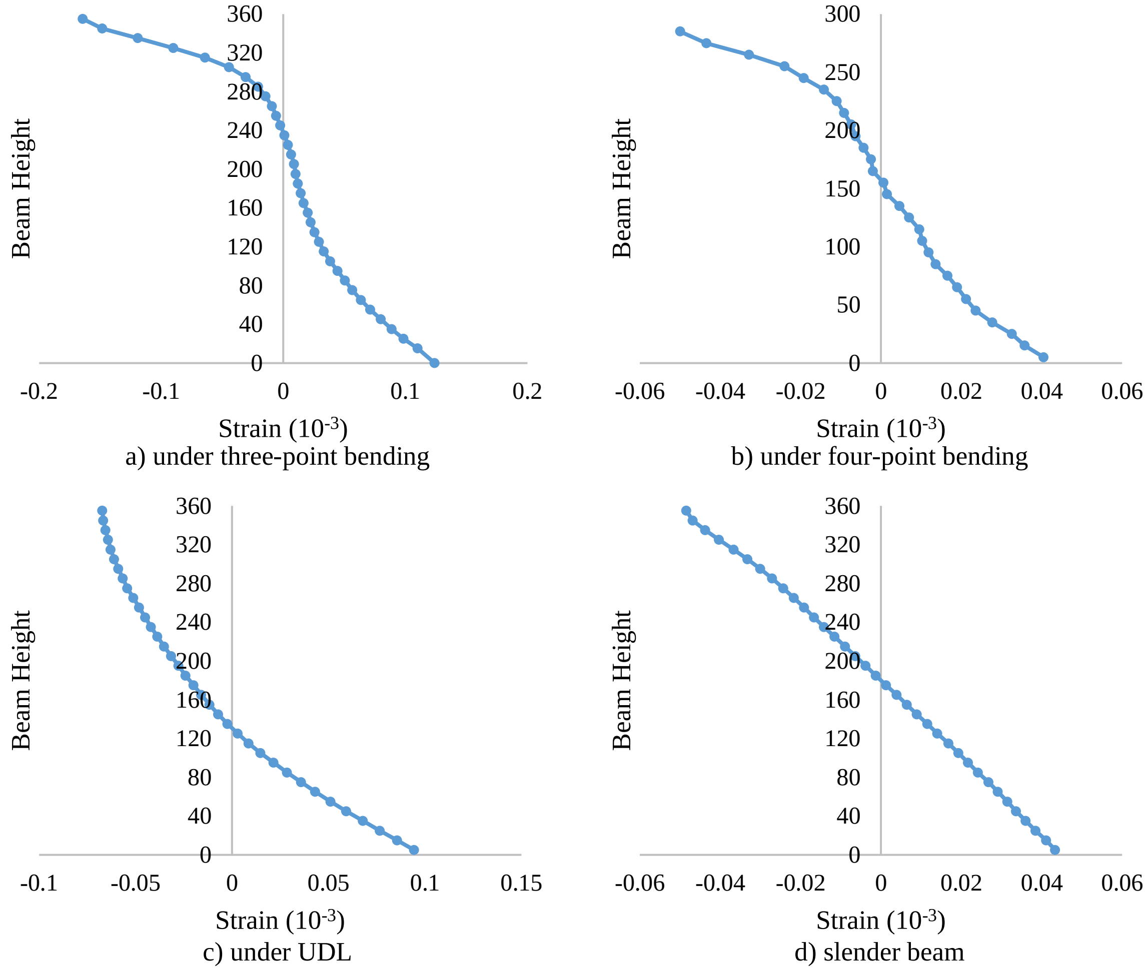

Figure 5.13: Pre-crack strain profile

If the beams are cracked, the strain profiles at crack near loading point for deep beams under one-point load are presented in Figure 5.14; the strain profiles for deep beams under two-point load are presented in Figure 5.15.

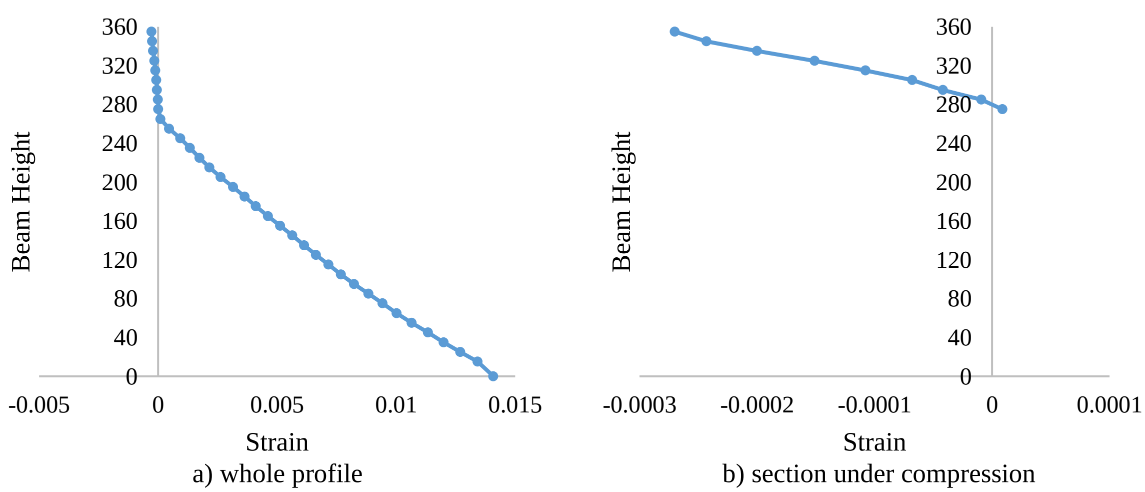

Figure 5.14: Strain profile at crack for deep beams under three-point bending

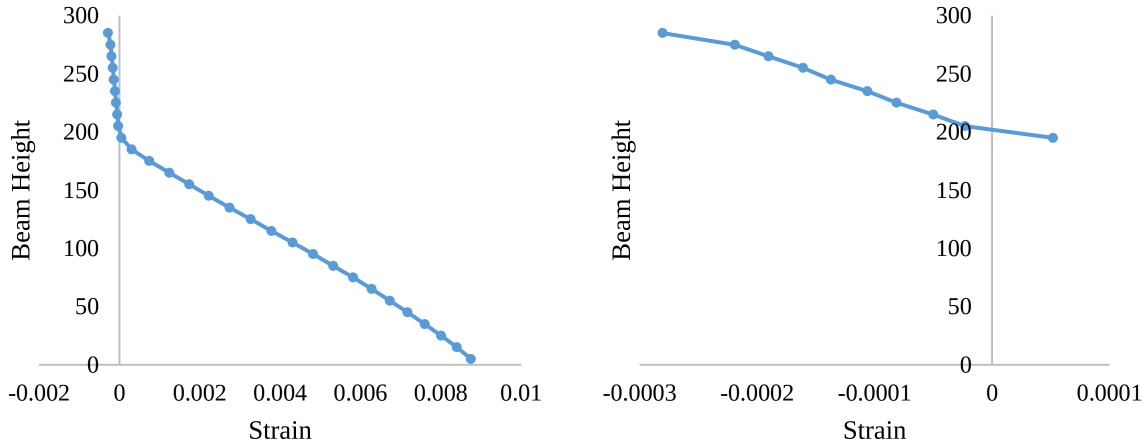

a) whole profile b) section under compression

Figure 5.15: Strain profile at crack for deep beams under four-point bending

Based on the analyzed strain profile for cracked beams, the strain profile at compression section is much closer to linear distribution compared to uncracked beams, and the whole strain profile is like a combination of two straight lines, one shows the strain distribution of uncracked section, and the other one shows the crack opening.

Moreover, Figure 5.16 presents the strain profile not at the crack of a cracked deep beam, which shows a nearly linear strain distribution of uncracked section, but the cracked section almost loses the ability to take the tensile force.

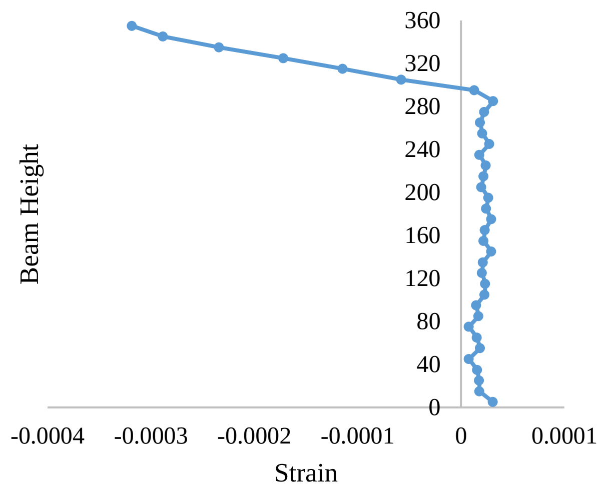

Figure 5.16: Strain profile not at crack for cracked deep beams

Therefore, a linear strain distribution in the compression part is assumed for both uncracked and cracked beams as shown in Figure 5.17, and the strain distribution can be expressed as

$$\varepsilon(x) = \frac{\varepsilon_{Top}}{c} x \tag{5.19}$$

where ε_{Top} is the strain of the concrete top fibre, or the outmost compressive fibre; c is the depth of concrete in compression; and x is the distance from neutral axis (N. A.) as shown in Figure 5.17.

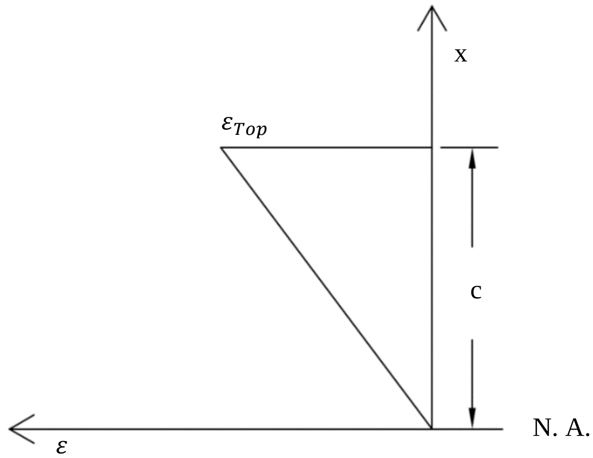

Figure 5.17: Assumed strain profile

With Hognestad parabola modelling the concrete compressive stress-strain relationship, and by setting an unknown factor k equal to ε_{Top}/c, the relationship between concrete compressive stress (f_c) and x is developed as

$$f_c(x) = \frac{2f_c'}{\varepsilon_0}kx - \frac{f_c'}{\varepsilon_0{}^2}k^2x^2 \tag{5.20}$$

As the total compression force (R_C) is equal to the integral of Equation (5.20) times the beam width (b), the following equation can be obtained

$$\frac{R_C}{b} = \int_0^c f_c(x) = \frac{f_c'}{\varepsilon_0}kc^2 - \frac{f_c'}{3\varepsilon_0{}^2}k^2c^3 = \frac{f_c'}{\varepsilon_0}\varepsilon_{Top}c - \frac{f_c'}{3\varepsilon_0{}^2}\varepsilon_{Top}{}^2c \tag{5.21}$$

Meanwhile, based on force equilibrium as shown in Figure 5.18,

$$Pa = R_C(jd) \tag{5.22}$$

where a is the length of the shear span; P is the applied load; and jd is the distance between the resultant forces, which is equal to $d - h_c/2$.

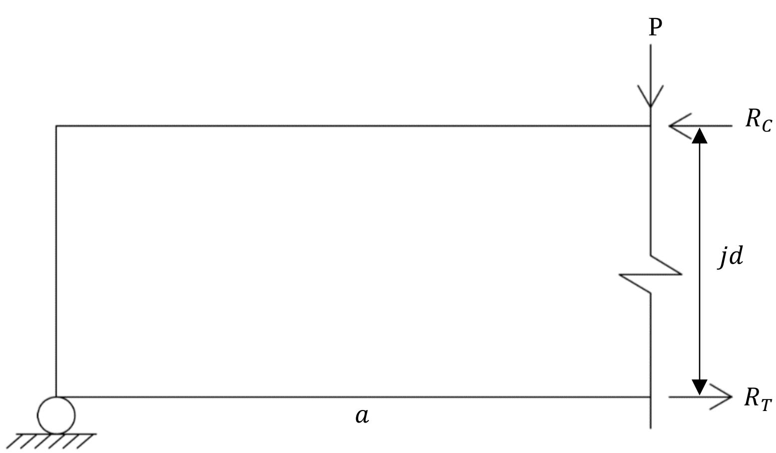

Figure 5.18: Forces exerted on shear span

the following relationship is established by combining the two equations related to R_C

$$\frac{f_c'}{\varepsilon_0}\varepsilon_{Top}c - \frac{f_c'}{3{\varepsilon_0}^2}{\varepsilon_{Top}}^2 c = \frac{Pa}{jd\cdot b} \tag{5.23}$$

which can be rearranged into

$${\varepsilon_{Top}}^2 - 3\varepsilon_0\varepsilon_{Top} + \frac{3P\cdot a\cdot {\varepsilon_0}^2}{jd\cdot b\cdot f_c'\cdot c} = 0 \tag{5.24}$$

However, there are two unknowns, ε_{Top} and c in this equation; hence, one of the unknowns shall be solved with another equation. As c is related to the location of neutral axis, it can be solved with the following equations for uncracked and cracked concrete sections.

$$c = \frac{h\cdot b\cdot {}^{h}/_{2} + A_{FRP}\cdot d}{h\cdot b + (n-1)A_{FRP}} \text{ when beam is uncracked} \tag{5.25}$$

$$c = \left(\sqrt{(\rho n)^2 + 2\rho n} - \rho n\right)d \text{ when beam is fully cracked} \tag{5.26}$$

where h is the height of the beam; b is the width of the beam; d is the effective depth of the beam; A_{FRP} is the total area of the flexural FRP bars; ρ is the flexural reinforcement ratio; and n is equal to E_{FRP}/E_c to count the difference in the elastic modulus of FRP bars and concrete.

Because it is hard to define the transition zone between beams being uncracked and fully cracked, it is conservatively assumed that beam is fully cracked after the strain in FRP flexural bars reaching the concrete rupture tensile strain.

Therefore, ε_{Top} can be calculated after c is computed.

$$\varepsilon_{Top} = \frac{3\varepsilon_0 - \sqrt{(3\varepsilon_0)^2 - \frac{12P\cdot a\cdot {\varepsilon_0}^2}{jd\cdot b\cdot f_c'\cdot c}}}{2} \le 1.5\varepsilon_0 \tag{5.27}$$

Because c is conservatively computed, and the post-peak behavior of concrete is modeled with the original Hognestad parabola which decreases fast, the value inside the square root may become negative if the shear strength is close to the flexural strength. Hence, the value inside the square root is assumed to be zero when it is computed as negative, which gives a maximum limit of ε_{Top} equal to $1.5\varepsilon_0$.

Furthermore, the centroid of the stress distribution from neutral axis can be computed with the assumed strain distribution and the relationship between concrete compressive stress (f_c) and x presented in Equation (5.20)

$$\overline{y}_{fromN.A.} = \frac{\int_0^c f_c\cdot x(x)}{\int_0^c f_c(x)} \tag{5.28}$$

where

$$\int_0^c f_c\cdot x(x) = \frac{2f_c'}{3\varepsilon_0}kc^3 - \frac{f_c'}{4{\varepsilon_0}^2}k^2c^4 = \frac{2f_c'}{3\varepsilon_0}\varepsilon_{Top}c^2 - \frac{f_c'}{4{\varepsilon_0}^2}{\varepsilon_{Top}}^2c^2 \tag{5.29}$$

As the integral of $f_c(x)$ has been computed in Equation (5.21),

$$\overline{y}_{from\_N.A.} = \frac{\int_0^c f_c\cdot x(x)}{\int_0^c f_c(x)} = \frac{\frac{2f_c'}{3\varepsilon_0}\varepsilon_{Top}c^2 - \frac{f_c'}{4{\varepsilon_0}^2}{\varepsilon_{Top}}^2c^2}{\frac{f_c'}{\varepsilon_0}\varepsilon_{Top}c - \frac{f_c'}{3{\varepsilon_0}^2}{\varepsilon_{Top}}^2c} = \frac{8\varepsilon_0c - 3\varepsilon_{Top}c}{12\varepsilon_0 - 4\varepsilon_{Top}} \tag{5.30}$$

Because h_c is twice the distance from concrete top to the centroid, it can be computed with

$$h_c = 2\left(c - \bar{y}_{from\_N.A.}\right) = \frac{4\varepsilon_0 - \varepsilon_{Top}}{6\varepsilon_0 - 2\varepsilon_{Top}} c \tag{5.31}$$

Moreover, the maximum value of h_c would be $\frac{5}{6}c$ that is around 0.833c with the maximum value of ε_{Top} mentioned previously.

This approach of h_c can only be used if the applied load is known, which would be the case with a known design load or with incremental loading like the IST method. Hence, h_c cannot be pre-determined and changes when the specimens are analyzed in different ways.

5.4 Softening Factors

According to Krall (2014), the predicted results from ST method are most sensitive to the softening factors applied to the struts, and most of the research on predicting the shear strength of FRP RC deep beams without vertical reinforcement focusing on establishing this factor. Hence, this research analyzed the specimens with three existing approaches (two are modified for IST method and for deep beams with vertical reinforcement) and one proposed approach to find the approaches suitable for the IST method.

5.4.1 ACI Approach

The softening factors suggested by (ACI 318-19, 2019) is straightforward. As all the specimens have bearing plates extended to the full beam widths, the softening factors from ACI approach (ζ_{ACI}) are simply 0.6375 (obtained from 0.85 times 0.75) for beams with stirrups; 0.34 (obtained from 0.85 times 0.4) for beams without stirrups; and 0.85 for horizontal struts (which are boundary struts classified by (ACI 318-19, 2019)).

5.4.2 Modified Nehdi et al. (2008)'s Approach

As mentioned in literature review, Nehdi et al. (2008) tested multiple deep beams without stirrups with a/d between 1.5 to 2.5, and established following equations for softening factors of inclined struts based on the previous versions of ACI code provision.

$$\beta_s = 0.68 - 0.012\left(\frac{a}{d}\right)^4 \quad \text{for} \quad \left(E_f \rho_f\right)^{1/3} \leq 10 \tag{5.32}$$

$$\beta_s = 0.75 - 0.01\left(\frac{a}{d}\right)^4 \quad \text{for} \quad \left(E_f \rho_f\right)^{1/3} > 10 \tag{5.33}$$

$$k = \max\left(\frac{250+d}{550},\ 1.0\right) \tag{5.34}$$

$$f_{ce} = 0.85 k \beta_s f_c' \tag{5.35}$$

where f_{ce} is the reduced effective strength of concrete strut; E_f is the elastic modulus of flexural reinforcement in GPa; ρ_f is the flexural reinforcement ratio.

However, there are limitations of this approach, and shall be modified to fit the IST method.

Firstly, as the a/d ratios of beams tested by Nehdi et al. (2008) are in the range of 1.5 to 2.5, the a/d value in the equations shall be limited with a maximum of 2.5 and a minimum of 1.5; hence, the values shall be decreased or increased to 2.5 or 1.5 for specimens with a/d ratios outside the range.

Secondly, the equations are developed for beams without vertical reinforcement, and are analyzed through ST models with only one type of inclined strut. However, IST models contain multiple inclined struts with different angles. If the equations are directly applied to all inclined struts, the results would have poor accuracy as it is way too conservative. As a/d is approximately equal to the cotangent of the angle of the inclined strut in the ST models for deep beams without stirrups, the approach is modified into

$$\beta_s = 0.68 - 0.012(\cot\theta_s)^4 \text{ for } \left(E_f\rho_f\right)^{1/3} \leq 10 \tag{5.36}$$

$$\beta_s = 0.75 - 0.01(\cot\theta_s)^4 \text{ for } \left(E_f\rho_f\right)^{1/3} > 10 \tag{5.37}$$

$$k = \max\left(\frac{250+d}{550},\ 1.0\right) \tag{5.38}$$

$$\zeta_{Nd} = 0.85k\beta_s \tag{5.39}$$

where θ_s is the angle of the inclined strut from the flexural rebars measured counter-clockwise; and ζ_{Nd} represents the softening factor obtained from the modified Nehdi et al. (2008)'s Approach. ζ_{Nd} is equal to 0.85 for horizontal struts.

5.4.3 Modified CSA Approach

According to CSA S806-12 (R2017),

$$f_{cu} = \frac{f_c'}{0.8+170\varepsilon_1} \leq 0.85f_c' \tag{5.40}$$

$$\varepsilon_1 = \varepsilon_F + (\varepsilon_F + 0.002)\cot^2\theta_s \tag{5.41}$$

where f_{cu} is the limited strength of concretes struts; θ_s is the smallest angle between the strut and the adjoining ties; ε_F is the tensile strain in the tie bar located closest to the tension face of the beam and inclined at θ_s to the strut. If the tensile strain in the tie changes as the tie crosses the width of the strut, θ_s may be taken as the strain in the tie at the centreline of the strut (CSA S806-12, R2017).

With the Modified Compression Field Theory (MCFT) by Vecchio and Collins (1986) shown below, Equation (5.40) is found to be the same as MCFT assuming ε_0 as (-)0.002.

$$\frac{f_{c2max}}{f_c'} = \frac{1}{0.8-0.34^{\varepsilon_1}/\varepsilon_0} \leq 1.0 \tag{5.42}$$

where f_{c2max} is the compressive strength of a concrete member under biaxial loading; ε_1 is the principal tensile strain of the member in positive; and ε_0 is the compressive strain in negative corresponding to compressive strength f_c'.

Moreover, Equation (5.41) is actually developed from Mohr's circle as presented in Figure 5.19 with ε_1 as the principal tensile strain; ε_2 as the principal compressive strain; ε_x as the strain in x-direction; ε_y as the strain in y-direction; γ_{xy} as the shear strain; and θ as the orientation of the stress element.

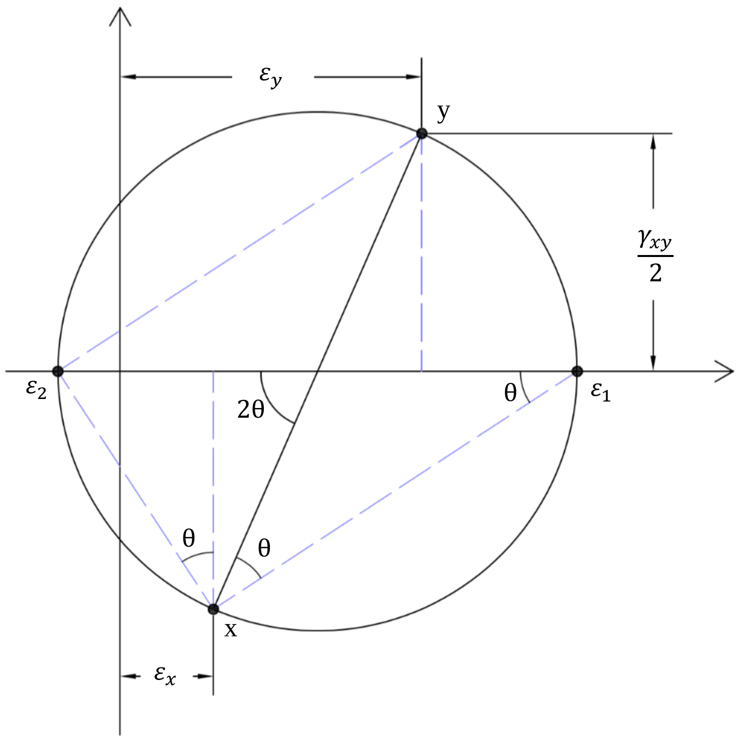

Figure 5.19: Typical Mohr's circle

Based on different triangles in the Mohr's circle, the following relationships can be obtained.

$$\tan\theta = \frac{\gamma_{xy}/2}{\varepsilon_1 - \varepsilon_x} \tag{5.43}$$

$$\tan\theta = \frac{\varepsilon_x - \varepsilon_2}{\gamma_{xy}/2} \tag{5.44}$$

By combining these two equations,

$$\tan\theta = \frac{\varepsilon_x - \varepsilon_2}{(\tan\theta)(\varepsilon_1 - \varepsilon_x)} \tag{5.45}$$

Hence,

$$\varepsilon_1 = \frac{\varepsilon_x - \varepsilon_2}{\tan^2\theta} + \varepsilon_x = \varepsilon_x + (\varepsilon_x - \varepsilon_2)\cot^2\theta \tag{5.46}$$

and Equation (5.41) from CSA S806-12 (R2017) is developed from Equation (5.46) of Mohr's circle by assuming ε_2 equal to (-)0.002, and ε_x equal to ε_F.

Because strains can be calculated inside each iteration of IST method, there is no need to assume the value of ε_2 in the struts; and ε_0 can be calculated based on the concrete models; the CSA approach is modified into

$$\zeta_{CSA} = \frac{1}{0.8 - 0.34\,\varepsilon_1/\varepsilon_0} \leq 0.85 \tag{5.47}$$

$$\varepsilon_1 = \varepsilon_f + \left(\varepsilon_f - \varepsilon_s\right)\cot^2\theta_s \tag{5.48}$$

where ζ_{CSA} is for the softening factor obtained from CSA approach; ε_0 is based on the concrete stress-strain relationship and is in negative; ε_f is the maximum tensile strain in the flexural FRP ties inside the projection of the interest strut; and ε_s is the compressive strain in the interest strut in negative.

5.4.4 Proposed Approach Based on MCFT

The modified CSA approach has one problem of not reflecting the confinement from vertical reinforcement properly, which makes the approach quite conservative; hence a new approach is proposed to count the influence from the stirrups.

CSA S806-12 (R2017) used Equation (5.41) because the vertical strain cannot be obtained if an analysis with iterative process (like IST method) is not used; but if the vertical strain can be computed, ε_1 can be computed simply as

$$\varepsilon_1 = \varepsilon_x + \varepsilon_y - \varepsilon_2 \tag{5.49}$$

Therefore, a new method can be proposed with

$$\zeta_{new} = \frac{1}{0.8 - 0.34^{\varepsilon_1}/_{\varepsilon_0}} \leq 0.85 \tag{5.50}$$

$$\varepsilon_1 = \varepsilon_f + \varepsilon_v - \varepsilon_s \tag{5.51}$$

where ζ_{new} is the softening factor obtained from the proposed approach; ε_0 is based on the concrete stress-strain relationship in negative; ε_s is the compressive strain in the interest strut in negative; and ε_f and ε_v are the strain in the flexural and vertical FRP ties inside the projection of the interest strut.

however, ε_f is not simply the maximum strain of the flexural ties in this approach. ε_f and ε_v values are treated as a whole, and the combination of ε_f and ε_v having the maximum value is used to calculate ε_1 of the interest strut.

Take the HSF model shown in Figure 5.20 as an example, the value of strain in T1 plus strain in T6 is compared with the value of strain in T2 plus strain in T7, and the larger value is used as $\varepsilon_f + \varepsilon_v$ for computing the softening factor of S10.

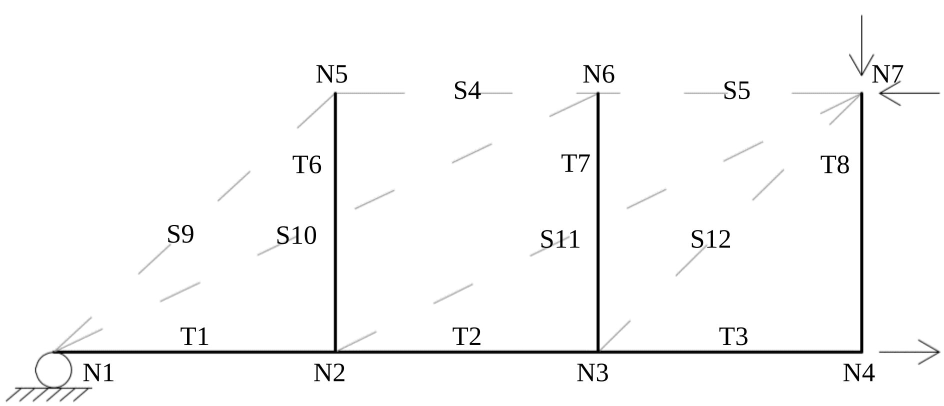

Figure 5.20: HSF model for beams with stirrups

Furthermore, because there are no vertical ties in ST models for beams without stirrups, the shear capacity will be overpredicted if ε_v is simply assumed to be zero; hence multiple imaginary ties with nearly no stiffness can be placed to find the strain in the y-direction.

The beam can be modeled to have the ST model with a main strut at the front and the truss model with the imaginary ties behind, in order to find the strain in the y-direction, which is close to the Kr model, except that the shear strength shall be calculated as

$$P_{predict} = C_{strut@failure} \sin\theta_s \tag{5.52}$$

where $P_{predict}$ is the predicted shear strength; $C_{strut@failure}$ is the force taken by the main strut at failure; and θ_s is the incline of the main strut.

As the stiffnesses of the stirrups are set to a value close to zero, there is nearly no difference between $P_{predict}$ and the failure load, which can be neglected in most cases.

The influence of the number of the imaginary ties and if this approach can predict accurate results is unknown at this point, hence this approach shall be tested by the specimens.

6. Analyses and Results

This chapter presents the analyzed results on the specimens described in Chapter 3 through IST method described in Chapter 4 with the approaches and models of the features mentioned in Chapter 5. Through the analyses, the validity of the method is checked, the suitable approaches and models are suggested, and the limitation of this method is tested.

All analyses in this research are conducted with incremental loadings of 10 newtons, and the results presented are rounded to the nearest kilonewtons for beam with stirrups and to the nearest 0.1 kilonewtons for beams without stirrups, as the strengths of beams without stirrups are much smaller.

6.1 Verification of the IST Method used by Krall (2014)

As the IST method for FRP RC deep beams was initially adopted and checked by Krall (2014), the predicted strengths are firstly checked through the same approaches used by Krall (2014) to verify the IST method.

Because Krall (2014) analyzed the specimens with softening factors based on old versions of ACI codes, and ACI 318-19 (2019) changed the factor for beams without vertical reinforcement, the specimens analyzed for the verification are the beams with stirrups tested by Krall (2014).

The results are presented in Table 6.1 with the predicted strengths by Krall (2014) through using the H2 model for concrete stress-strain relationship, Kr model for IST structure, h_C based on strain compatibility, and ACI approach for softening factors.

Table 6.1: Test results of beams by Krall (2014)

Specimens	P_{test} (kN)	$P_{pred.}$ (kN)	P_{Krall} (kN)
BM12-220	382.4	411	391
BM12-150	405.2	296	295
BM12-s230	466.9	469	484
*BM16-220**	*309.3*	412	395
BM16-150	416.5	295	286
BM16-s230	450.8	455	451
BM25-220	360.1	427	406
BM25-150	415.8	296	285
BM25-s230	444	383	395

Although there are small differences between the results predicted in this research and those done by Krall (2014), which may be caused by using different initial concrete elastic modulus and having different incremental loadings, the results prove that this IST method is applicable to find the shear strengths of FRP RC deep beams, as most of the predicted results are close to the tested results, especially for those with larger spacing.

The results also show the problems of the method used by Krall (2014) include overestimating the strengths, and not capturing the shear strength increase with smaller stirrup spacings, which are also why different approaches for the essential features are developed in Chapter 5.

Therefore, the new models and approaches need to be analyzed, and the improved IST method for FRP RC deep beams shall be proposed.

6.2 Analyses on Deep Beams with Stirrups

This chapter introduces the analyses done on deep beams with stirrups, which are the 9 specimens tested by Krall (2014), and presents the results obtained through different models and approaches of the essential features to exclude the ones not suitable and to find out which ones work best with the IST method.

6.2.1 Preliminary Analysis on Concretes Stress-Strain Relationships

Based on the models and approaches developed, there could be 256 ways to analyze one specimen with stirrups. Hence, to analyze the specimens with less variables, a throughout analysis on concrete stress-strain models is firstly done to find if the IST method is sensitive to the concrete stress-strain relationship, and if there is any concrete model inappropriate to use with this method.

The results are presented in Table 6.2 with h_C constantly equal to 0.2d to control the number of variables.

Table 6.2: Comparison of concrete stress-strain models

Model Type	Specimen	Averaged values with different ζ approaches			
		$\frac{P_{H1}}{P_{H2}}$	$\frac{P_{H2}}{P_{H2}}$	$\frac{P_{T1}}{P_{H2}}$	$\frac{P_{T2}}{P_{H2}}$
Kr model	BM12-220	1.12	1	1.21	1.10
	BM12-150	1.03	1	1.22	1.17
	BM12-s230	1.02	1	1.23	1.12
	BM16-220	1.12	1	1.21	1.10
	BM16-150	1.03	1	1.22	1.16
	BM16-s230	1.01	1	1.22	1.11
	BM25-220	1.11	1	1.18	1.07
	BM25-150	1.03	1	1.22	1.16
	BM25-s230	1.03	1	1.22	1.11
	Average	**1.05**	**1.00**	**1.22**	**1.12**
WSF model	BM12-220	0.99	1	1.06	0.99
	BM12-150	1.03	1	1.13	1.07
	BM12-s230	1.04	1	1.13	0.99
	BM16-220	0.99	1	1.07	0.99
	BM16-150	1.04	1	1.14	1.06
	BM16-s230	1.05	1	1.14	0.99
	BM25-220	1.01	1	1.11	1.01
	BM25-150	1.05	1	1.19	1.06
	BM25-s230	1.09	1	1.18	0.99
	Average	**1.03**	**1.00**	**1.13**	**1.02**
HSF model	BM12-220	0.99	1	1.15	1.05
	BM12-150	1.00	1	1.21	1.13
	BM12-s230	0.99	1	1.14	1.04
	BM16-220	1.00	1	1.15	1.04
	BM16-150	1.00	1	1.21	1.13
	BM16-s230	1.00	1	1.14	1.03
	BM25-220	1.00	1	1.15	1.04
	BM25-150	1.00	1	1.21	1.13
	BM25-s230	1.01	1	1.15	1.02
	Average	**1.00**	**1.00**	**1.17**	**1.07**

Design model	BM12-220	0.98	1	1.15	1.04
	BM12-150	0.99	1	1.14	1.03
	BM12-s230	1.00	1	1.15	1.02
	BM16-220	0.98	1	1.15	1.04
	BM16-150	0.99	1	1.14	1.02
	BM16-s230	1.01	1	1.15	1.02
	BM25-220	0.98	1	1.14	1.02
	BM25-150	1.02	1	1.16	1.02
	BM25-s230	1.03	1	1.17	1.01
	Average	**1.00**	**1.00**	**1.15**	**1.02**
	Total Average	**1.02**	**1.00**	**1.16**	**1.06**

Based on the analysis, the only outliner is T1 model, which is the one modelling the concrete behavior through Thorenfeldt et al. (1987) model with only the compressive strength reduced. As it predicts results generally 10% larger than the other models, this model is considered as inappropriate.

Moreover, softening all factors calculated from concrete compressive strength (f_c', ε_0, n, k) seems to be better than just softening the strength, as the difference between H2 and T2 models is much less than the difference between H1 and T1 models.

In order to limit the numbers of variables, H2 model as the most conservative model is chosen to use for the analyses on other features; and H1, T2 models are used to verify the proposed method after the proper approaches of other features are determined.

6.2.2 General Results for Different Approaches and Models

As four IST model types, four approaches for h_c and another four approaches for softening factors need to be analyzed, it is better to find the general suitability of the approaches with the ratios between predicted and test strengths, and the predicted failure modes, which are presented in Table 6.3 to Table 6.6.

The tables also include the average differences between the ratios to indicate the accuracy of that combination of approaches, and the standard deviations of the ratios to show if the accuracy is stable and if the predicted results generally follow a similar trend with the test results. Moreover, the overestimated results and unwanted predicted failure mode are labelled out in bold.

Table 6.3: Results with h_C based on strain compatibility

Model Type	Specimen	$P_{predict}/P_{test}$ with ζ_{ACI}	ζ_{Nc}	ζ_{CSA}	ζ_{New}	**Predicted Failure Mode with ζ_{ACI}	ζ_{Nc}	ζ_{CSA}	ζ_{New}
Kr model	BM12-220	**1.08**	0.85	0.80	0.76	Combined	Combined	Shear	Shear
	BM12-150	0.73	0.72	0.72	0.72	Combined	Combined	Combined	Combined
	BM12-s230	**1.01**	0.96	0.68	**1.01**	Combined	Combined	Shear	Combined
	*BM16-220**	*1.33*	*1.03*	*0.97*	*0.93*	Combined	Combined	Shear	Shear
	BM16-150	0.71	0.68	0.68	0.68	Combined	Combined	Combined	Combined
	BM16-s230	**1.01**	0.97	0.69	**1.01**	Combined	Combined	Shear	Combined
	BM25-220	**1.18**	0.81	0.73	0.78	Combined	Combined	Shear	Shear
	BM25-150	0.71	0.62	0.62	0.62	Combined	Combined	Combined	Combined
	BM25-s230	0.86	0.79	0.62	0.87	Combined	Combined	Shear	Combined
	Avg. Diff.	0.16	0.20	0.31	0.20				
	Std. Dev.	0.18	0.12	0.06	0.14				
WSF model	BM12-220	**1.25**	**1.21**	0.70	**1.02**	**Node Failure**	Shear	Shear	Shear
	BM12-150	**1.06**	**1.06**	0.78	**1.07**	**Flexure**	Combined	Shear	Combined
	BM12-s230	1.00	0.91	0.55	0.88	Combined	Shear	Shear	Shear
	*BM16-220**	*1.53*	*1.46*	*0.84*	*1.22*	Shear	Shear	Shear	Shear
	BM16-150	0.99	1.00	0.73	1.00	**Flexure**	Combined	Shear	Combined
	BM16-s230	1.00	0.91	0.55	0.88	Combined	Shear	Shear	Shear
	BM25-220	**1.16**	**1.09**	0.60	0.89	Combined	Shear	Shear	Shear
	BM25-150	0.84	0.84	0.62	0.84	**Flexure**	Combined	Shear	Combined
	BM25-s230	0.86	0.66	0.46	0.74	Combined	Shear	Shear	Shear
	Avg. Diff.	0.10	0.13	0.38	0.11				
	Std. Dev.	0.14	0.17	0.10	0.11				
HSF model	BM12-220	**1.08**	1.00	0.63	0.86	**Bar Failure**	Shear	Shear	Shear
	BM12-150	0.99	0.99	0.77	0.98	Combined	Combined	Shear	Combined
	BM12-s230	0.99	0.89	0.55	0.87	Combined	Shear	Shear	Shear
	*BM16-220**	*1.31*	*1.21*	*0.76*	*1.04*	Combined	Shear	Shear	Shear
	BM16-150	0.94	0.94	0.73	0.94	Combined	Combined	Shear	Combined
	BM16-s230	**1.01**	0.90	0.55	0.88	Combined	Shear	Shear	Shear
	BM25-220	**1.03**	0.96	0.57	0.80	Combined	Shear	Shear	Shear
	BM25-150	0.85	0.85	0.65	0.85	Combined	Combined	Shear	Combined
	BM25-s230	0.92	0.70	0.48	0.78	Combined	Shear	Shear	Shear
	Avg. Diff.	0.05	0.10	0.38	0.13				
	Std. Dev.	0.07	0.10	0.10	0.07				
Design model	BM12-220	**1.11**	0.98	0.64	0.89	Shear	Shear	Shear	Shear
	BM12-150	0.94	0.86	0.58	0.87	Shear	Shear	Shear	Shear
	BM12-s230	0.87	0.80	0.52	0.80	Shear	Shear	Shear	Shear
	*BM16-220**	*1.34*	*1.20*	*0.77*	*1.06*	Shear	Shear	Shear	Shear
	BM16-150	0.89	0.82	0.54	0.83	Shear	Shear	Shear	Shear
	BM16-s230	0.87	0.81	0.53	0.81	Shear	Shear	Shear	Shear
	BM25-220	1.00	0.91	0.57	0.79	Shear	Shear	Shear	Shear
	BM25-150	0.77	0.72	0.46	0.72	Shear	Shear	Shear	Shear
	BM25-s230	0.75	0.61	0.45	0.69	Shear	Shear	Shear	Shear
	Avg. Diff.	0.13	0.18	0.46	0.20				
	Std. Dev.	0.12	0.11	0.06	0.07				

* Note that test result of BM16-220 contains error, hence the specimen excluded for calculating averages and deviations.

** All beams failed in shear during test; both shear failure mode and combined failure mode predict shear failure.

Table 6.4: Results with h_C based on force equilibrium

Model Type	Specimen	$P_{predict}/P_{test}$ with ζ_{ACI}	ζ_{Nc}	ζ_{CSA}	ζ_{New}	**Predicted Failure Mode with ζ_{ACI}	ζ_{Nc}	ζ_{CSA}	ζ_{New}
Kr model	BM12-220	**1.48**	**1.13**	0.86	0.91	**Bar Failure**	Combined	Shear	Shear
	BM12-150	0.97	0.95	0.95	0.95	Combined	Combined	Combined	Combined
	BM12-s230	**1.11**	**1.08**	0.70	**1.05**	Combined	Combined	Shear	Shear
	*BM16-220**	*1.68*	*1.27*	*1.02*	*1.06*	**Bar Failure**	Combined	Shear	Shear
	BM16-150	0.87	0.85	0.85	0.85	Combined	Combined	Combined	Combined
	BM16-s230	**1.05**	**1.02**	0.70	**1.04**	Combined	Combined	Shear	Shear
	BM25-220	**1.35**	0.92	0.76	0.85	**Node Failure**	Combined	Shear	Shear
	BM25-150	0.81	0.72	0.72	0.72	Combined	Combined	Combined	Combined
	BM25-s230	0.85	0.78	0.61	0.86	Combined	Combined	Shear	Combined
	Avg. Diff.	0.19	0.13	0.23	0.12				
	Std. Dev.	0.24	0.15	0.11	0.11				
WSF model	BM12-220	**1.54**	**1.32**	0.72	**1.08**	**Node Failure**	Shear	Shear	Shear
	BM12-150	**1.24**	**1.26**	0.78	**1.27**	**Flexure**	Combined	Shear	Combined
	BM12-s230	**1.09**	0.94	0.56	0.90	Combined	Shear	Shear	Shear
	*BM16-220**	*1.77*	*1.58*	*0.86*	*1.28*	**Node Failure**	Shear	Shear	Shear
	BM16-150	**1.13**	**1.14**	0.74	**1.15**	**Flexure**	Combined	Shear	Combined
	BM16-s230	**1.04**	0.93	0.56	0.89	Combined	Shear	Shear	Shear
	BM25-220	**1.27**	1.16	0.62	0.94	**Bar Failure**	Shear	Shear	Shear
	BM25-150	0.91	0.92	0.63	0.92	**Flexure**	Combined	Shear	Combined
	BM25-s230	0.85	0.66	0.46	0.74	Combined	Shear	Shear	Shear
	Avg. Diff.	0.19	0.18	0.37	0.14				
	Std. Dev.	0.22	0.22	0.11	0.17				
HSF model	BM12-220	**1.42**	**1.17**	0.68	0.98	**Bar Failure**	Shear	Shear	Shear
	BM12-150	**1.29**	**1.29**	0.82	**1.24**	**Bar Failure**	**Bar Failure**	Shear	Combined
	BM12-s230	**1.13**	0.97	0.57	0.93	Combined	Shear	Shear	Shear
	*BM16-220**	*1.61*	*1.39*	*0.81*	*1.15*	**Bar Failure**	Shear	Shear	Shear
	BM16-150	**1.15**	**1.15**	0.77	**1.15**	Combined	Combined	Shear	Combined
	BM16-s230	**1.07**	0.94	0.57	0.90	Combined	Shear	Shear	Shear
	BM25-220	**1.17**	**1.06**	0.59	0.86	**Bar Failure**	Shear	Shear	Shear
	BM25-150	0.97	0.97	0.68	0.97	Combined	Combined	Shear	Combined
	BM25-s230	0.91	0.70	0.48	0.77	Combined	Shear	Shear	Shear
	Avg. Diff.	0.17	0.14	0.35	0.12				
	Std. Dev.	0.16	0.18	0.11	0.15				
Design model	BM12-220	**1.24**	**1.13**	0.85	0.98	Shear	Shear	Shear	Shear
	BM12-150	**1.03**	0.95	0.58	0.93	Shear	Shear	Shear	Shear
	BM12-s230	0.90	0.83	0.53	0.82	Shear	Shear	Shear	Shear
	*BM16-220**	*1.46*	*1.33*	*0.79*	*1.15*	Shear	Shear	Shear	Shear
	BM16-150	0.95	0.88	0.55	0.87	Shear	Shear	Shear	Shear
	BM16-s230	0.89	0.82	0.53	0.81	Shear	Shear	Shear	Shear
	BM25-220	**1.07**	0.99	0.58	0.84	Shear	Shear	Shear	Shear
	BM25-150	0.83	0.77	0.47	0.73	Shear	Shear	Shear	Shear
	BM25-s230	0.74	0.61	0.45	0.69	Shear	Shear	Shear	Shear
	Avg. Diff.	0.13	0.16	0.43	0.17				
	Std. Dev.	0.16	0.16	0.12	0.10				

* Note that test result of BM16-220 contains error, hence the specimen excluded for calculating averages and deviations.

** All beams fail in shear during test; both shear failure mode and combined failure mode predict shear failure.

Table 6.5: Results with h_C equal to 0.2d

Model Type	Specimen	$P_{predict}/P_{test}$ with ζ_{ACI}	ζ_{Nc}	ζ_{CSA}	ζ_{New}	**Predicted Failure Mode with ζ_{ACI}	ζ_{Nc}	ζ_{CSA}	ζ_{New}
Kr model	BM12-220	0.83	0.63	0.63	0.65	Combined	Combined	Combined	Combined
	BM12-150	0.57	0.53	0.53	0.53	Combined	Combined	Combined	Combined
	BM12-s230	0.82	0.73	0.59	0.81	Combined	Combined	Combined	Combined
	*BM16-220**	*1.04*	*0.77*	*0.77*	*0.81*	Combined	Combined	Combined	Shear
	BM16-150	0.56	0.51	0.51	0.51	Combined	Combined	Combined	Combined
	BM16-s230	0.83	0.77	0.61	0.83	Combined	Combined	Combined	Combined
	BM25-220	0.99	0.66	0.66	0.71	Combined	Combined	Combined	Shear
	BM25-150	0.61	0.51	0.51	0.51	Combined	Combined	Combined	Combined
	BM25-s230	0.77	0.66	0.60	0.78	Combined	Combined	Shear	Combined
	Avg. Diff.	0.25	0.37	0.42	0.33				
	Std. Dev.	0.15	0.10	0.06	0.14				
WSF model	BM12-220	**1.04**	0.97	0.63	0.91	Combined	Shear	Shear	Shear
	BM12-150	0.95	0.85	0.74	0.86	Combined	Combined	Shear	Combined
	BM12-s230	0.84	0.82	0.52	0.82	Combined	Shear	Shear	Shear
	*BM16-220**	*1.27*	*1.20*	*0.76*	*1.11*	Combined	Shear	Shear	Shear
	BM16-150	0.93	0.82	0.69	0.82	Combined	Combined	Shear	Combined
	BM16-s230	0.85	0.83	0.53	0.83	Combined	Shear	Shear	Shear
	BM25-220	1.00	0.99	0.57	0.84	Combined	Shear	Shear	Shear
	BM25-150	0.73	0.74	0.60	0.75	**Flexure**	Combined	Shear	Combined
	BM25-s230	0.78	0.63	0.45	0.72	Combined	Shear	Shear	Shear
	Avg. Diff.	0.12	0.17	0.41	0.18				
	Std. Dev.	0.11	0.12	0.09	0.06				
HSF model	BM12-220	0.81	0.80	0.56	0.74	Combined	Shear	Shear	Shear
	BM12-150	0.73	0.73	0.70	0.73	Combined	Combined	Shear	Combined
	BM12-s230	0.78	0.75	0.50	0.77	Combined	Shear	Shear	Shear
	*BM16-220**	*1.00*	*0.99*	*0.68*	*0.90*	Combined	Shear	Shear	Shear
	BM16-150	0.71	0.71	0.67	0.71	Combined	Combined	Shear	Combined
	BM16-s230	0.81	0.77	0.51	0.78	Combined	Shear	Shear	Shear
	BM25-220	0.85	0.83	0.52	0.73	Combined	Shear	Shear	Shear
	BM25-150	0.71	0.71	0.61	0.71	Combined	Combined	Shear	Combined
	BM25-s230	0.81	0.64	0.46	0.73	Combined	Shear	Shear	Shear
	Avg. Diff.	0.22	0.26	0.43	0.26				
	Std. Dev.	0.05	0.06	0.09	0.03				
Design model	BM12-220	0.88	0.74	0.57	0.76	Shear	Shear	Shear	Shear
	BM12-150	0.75	0.68	0.55	0.75	Shear	Shear	Shear	Shear
	BM12-s230	0.71	0.65	0.51	0.72	Shear	Shear	Shear	Shear
	*BM16-220**	*1.07*	*0.92*	*0.70*	*0.93*	Shear	Shear	Shear	Shear
	BM16-150	0.72	0.66	0.52	0.71	Shear	Shear	Shear	Shear
	BM16-s230	0.72	0.67	0.51	0.73	Shear	Shear	Shear	Shear
	BM25-220	0.85	0.77	0.55	0.72	Shear	Shear	Shear	Shear
	BM25-150	0.67	0.62	0.47	0.65	Shear	Shear	Shear	Shear
	BM25-s230	0.67	0.55	0.45	0.67	Shear	Shear	Shear	Shear
	Avg. Diff.	0.25	0.33	0.48	0.29				
	Std. Dev.	0.08	0.07	0.04	0.04				

* Note that test result of BM16-220 contains error, hence the specimen excluded for calculating averages and deviations.

** All beams fail in shear during test; both shear failure mode and combined failure mode predict shear failure.

Table 6.6: Results with new h_C approach proposed in this research

Model Type	Specimen	$P_{predict}/P_{test}$ with ζ_{ACI}	ζ_{Nc}	ζ_{CSA}	ζ_{New}	**Predicted Failure Mode with ζ_{ACI}	ζ_{Nc}	ζ_{CSA}	ζ_{New}
Kr model	BM12-220	0.89	0.59	0.59	0.64	Combined	Combined	Combined	Combined
	BM12-150	0.55	0.49	0.49	0.51	Combined	Combined	Combined	Combined
	BM12-s230	0.84	0.69	0.53	0.83	Combined	Combined	Combined	Combined
	*BM16-220**	1.10	0.72	0.72	0.78	Combined	Combined	Combined	Combined
	BM16-150	0.54	0.47	0.47	0.49	Combined	Combined	Combined	Combined
	BM16-s230	0.84	0.72	0.54	0.84	Combined	Combined	Combined	Combined
	BM25-220	0.96	0.55	0.55	0.66	Combined	Combined	Combined	Shear
	BM25-150	0.54	0.42	0.42	0.46	Combined	Combined	Combined	Combined
	BM25-s230	0.68	0.50	0.49	0.68	Combined	Combined	Combined	Combined
	Avg. Diff.	0.27	0.44	0.49	0.36				
	Std. Dev.	0.17	0.11	0.05	0.15				
WSF model	BM12-220	**1.09**	**1.04**	0.62	0.94	**Node Failure**	Shear	Shear	Shear
	BM12-150	**1.01**	0.91	0.74	0.91	Combined	Combined	Shear	Combined
	BM12-s230	0.86	0.83	0.51	0.83	Combined	Shear	Shear	Shear
	*BM16-220**	1.34	1.26	0.74	1.13	**Node Failure**	Shear	Shear	Shear
	BM16-150	0.98	0.86	0.69	0.86	Combined	Combined	Shear	Combined
	BM16-s230	0.86	0.83	0.51	0.83	Combined	Shear	Shear	Shear
	BM25-220	0.97	0.97	0.54	0.83	Combined	Shear	Shear	Shear
	BM25-150	0.71	0.72	0.59	0.74	**Flexure**	Combined	Shear	Combined
	BM25-s230	0.73	0.58	0.42	0.69	Combined	Shear	Shear	Shear
	Avg. Diff.	0.12	0.17	0.42	0.17				
	Std. Dev.	0.14	0.14	0.10	0.08				
HSF model	BM12-220	0.87	0.85	0.55	0.73	Combined	Shear	Shear	Shear
	BM12-150	0.73	0.73	0.70	0.73	Combined	Combined	Combined	Combined
	BM12-s230	0.80	0.73	0.48	0.78	Combined	Shear	Shear	Shear
	*BM16-220**	1.06	1.04	0.66	0.88	Combined	Shear	Shear	Shear
	BM16-150	0.70	0.70	0.66	0.70	Combined	Combined	Combined	Combined
	BM16-s230	0.81	0.74	0.48	0.79	Combined	Shear	Shear	Shear
	BM25-220	0.77	0.78	0.48	0.68	Combined	Shear	Shear	Shear
	BM25-150	0.62	0.62	0.58	0.62	Combined	Combined	Shear	Combined
	BM25-s230	0.74	0.55	0.42	0.67	Combined	Shear	Shear	Shear
	Avg. Diff.	0.24	0.29	0.46	0.29				
	Std. Dev.	0.08	0.09	0.10	0.06				
Design model	BM12-220	0.95	0.73	0.56	0.76	Shear	Shear	Shear	Shear
	BM12-150	0.81	0.67	0.55	0.75	Shear	Shear	Shear	Shear
	BM12-s230	0.67	0.61	0.50	0.70	Shear	Shear	Shear	Shear
	*BM16-220**	1.13	0.89	0.68	0.91	Shear	Shear	Shear	Shear
	BM16-150	0.72	0.63	0.52	0.71	Shear	Shear	Shear	Shear
	BM16-s230	0.67	0.61	0.51	0.70	Shear	Shear	Shear	Shear
	BM25-220	0.83	0.68	0.53	0.67	Shear	Shear	Shear	Shear
	BM25-150	0.60	0.54	0.45	0.60	Shear	Shear	Shear	Shear
	BM25-s230	0.57	0.45	0.44	0.59	Shear	Shear	Shear	Shear
	Avg. Diff.	0.27	0.39	0.49	0.32				
	Std. Dev.	0.13	0.09	0.04	0.06				

* Note that test result of BM16-220 contains error, hence the specimen excluded for calculating averages and deviations.

** All beams fail in shear during test; both shear failure mode and combined failure mode predict shear failure.

Several approaches can be discarded according to the results. Firstly, the h_C approach based on force equilibrium overpredicts the strengths of some specimens while falsely predicting their failure modes, especially when it is combined with the ζ_{ACI} approach. According to Table 6.4, this h_C approach can only work with ζ_{CSA} approach regardless the choice of models to avoid overestimating, but the accuracy is poor. The only way to have it predicting good results is to use it with the design model and the new ζ approach, but other h_C approaches also work well with those approaches and are with smaller standard deviations. This approach especially does not work well with BM12 series, as it predicts h_C too large for these specimens, which shows that this approach is too sensitive to the flexural reinforcement area and cannot correctly predict h_C, hence shall be discarded and shall not be used with the IST method.

Secondly, the ζ_{ACI} approach also predicts unconservative results and the false failure modes, even with h_C approach other than the one based on force equilibrium mentioned above. The problem of this method is that it cannot sufficiently reduce the strength of the inclined struts, which makes the predicted strength of the inclined struts much higher than what it should be and leads to an unwanted failure mode with overpredicted strengths. Therefore, ζ_{ACI} approach is excluded for further analyses on deep beams with stirrups, but it will be included for analyses on deep beams without stirrups as it suggests different values for them.

6.2.3 Trends of the Predicted Strengths

Another problem observed in the IST method used by Krall (2014) is not capturing the strength increase with smaller stirrup spacings. To use the IST method for analyzing and designing FRP RC deep beams with stirrups, it must be able to predict the correct trends of having larger shear strength with smaller stirrup spacings and larger stirrup areas. Hence, the detailed analysis on the trends of the strengths is conducted.

The predicted shear strengths with the tested strengths and the predicted failure modes are organized in Table 6.7 to Table 6.9 to analyze the trends of the predicted results.

Table 6.7: Shear strengths with h_c based on strain compatibility

Model Type	Specimen	P_{test} (kN)	$P_{predict}$ (kN) with			**Predicted Failure Mode with		
			ζ_{Nc}	ζ_{CSA}	ζ_{New}	ζ_{Nc}	ζ_{CSA}	ζ_{New}
Kr model	BM12-220	382.4	325	306	292	Combined	Shear	Shear
	BM12-150	405.2	291	291	291	Combined	Combined	Combined
	BM12-s230	466.9	446	317	469	Combined	Shear	Combined
	*BM16-220**	*309.3*	319	299	289	Combined	Shear	Shear
	BM16-150	416.5	285	285	285	Combined	Combined	Combined
	BM16-s230	450.8	438	310	456	Combined	Shear	Combined
	BM25-220	360.1	290	264	283	Combined	Shear	Shear
	BM25-150	415.8	259	259	259	Combined	Combined	Combined
	BM25-s230	444	352	276	387	Combined	Shear	Combined
WSF model	BM12-220	382.4	462	267	389	Shear	Shear	Shear
	BM12-150	405.2	431	314	433	Combined	Shear	Combined
	BM12-s230	466.9	423	258	410	Shear	Shear	Shear
	*BM16-220**	*309.3*	451	258	378	Shear	Shear	Shear
	BM16-150	416.5	417	305	418	Combined	Shear	Combined
	BM16-s230	450.8	411	249	396	Shear	Shear	Shear
	BM25-220	360.1	394	217	321	Shear	Shear	Shear
	BM25-150	415.8	350	258	351	Combined	Shear	Combined
	BM25-s230	444	293	206	330	Shear	Shear	Shear
HSF model	BM12-220	382.4	382	242	328	Shear	Shear	Shear
	BM12-150	405.2	399	312	399	Combined	Shear	Combined
	BM12-s230	466.9	415	257	406	Shear	Shear	Shear
	*BM16-220**	*309.3*	376	235	322	Shear	Shear	Shear
	BM16-150	416.5	391	305	390	Combined	Shear	Combined
	BM16-s230	450.8	408	250	396	Shear	Shear	Shear
	BM25-220	360.1	346	204	290	Shear	Shear	Shear
	BM25-150	415.8	354	272	354	Combined	Shear	Combined
	BM25-s230	444	312	214	345	Shear	Shear	Shear
Design model	BM12-220	382.4	376	244	339	Shear	Shear	Shear
	BM12-150	405.2	350	234	354	Shear	Shear	Shear
	BM12-s230	466.9	374	244	375	Shear	Shear	Shear
	*BM16-220**	*309.3*	370	238	329	Shear	Shear	Shear
	BM16-150	416.5	343	227	344	Shear	Shear	Shear
	BM16-s230	450.8	364	237	363	Shear	Shear	Shear
	BM25-220	360.1	329	206	285	Shear	Shear	Shear
	BM25-150	415.8	298	193	298	Shear	Shear	Shear
	BM25-s230	444	272	201	307	Shear	Shear	Shear

* Note that test result of BM16-220 contains error, hence is not compared with others.

** All beams fail in shear during test; both shear failure mode and combined failure mode predict shear failure.

Table 6.8: Shear strengths with h_C equal to 0.2d

Model Type	Specimen	P_{test} (kN)	$P_{predict}$ (kN) with ζ_{Nc}	ζ_{CSA}	ζ_{New}	**Predicted Failure Mode with ζ_{Nc}	ζ_{CSA}	ζ_{New}
Kr model	BM12-220	382.4	239	239	249	Combined	Shear	Shear
	BM12-150	405.2	213	213	213	Combined	Combined	Combined
	BM12-s230	466.9	342	277	379	Combined	Shear	Combined
	*BM16-220**	*309.3*	239	239	249	Combined	Shear	Shear
	BM16-150	416.5	213	213	213	Combined	Combined	Combined
	BM16-s230	450.8	348	276	374	Combined	Shear	Combined
	BM25-220	360.1	239	239	255	Combined	Shear	Shear
	BM25-150	415.8	213	213	213	Combined	Combined	Combined
	BM25-s230	444	294	264	345	Combined	Shear	Combined
WSF model	BM12-220	382.4	371	240	350	Shear	Shear	Shear
	BM12-150	405.2	346	298	347	Combined	Shear	Combined
	BM12-s230	466.9	382	245	384	Shear	Shear	Shear
	*BM16-220**	*309.3*	372	235	342	Shear	Shear	Shear
	BM16-150	416.5	340	289	341	Combined	Shear	Combined
	BM16-s230	450.8	374	237	373	Shear	Shear	Shear
	BM25-220	360.1	356	206	302	Shear	Shear	Shear
	BM25-150	415.8	307	251	313	Combined	Shear	Combined
	BM25-s230	444	280	201	319	Shear	Shear	Shear
HSF model	BM12-220	382.4	306	215	281	Shear	Shear	Shear
	BM12-150	405.2	297	283	297	Combined	Shear	Combined
	BM12-s230	466.9	348	234	359	Shear	Shear	Shear
	*BM16-220**	*309.3*	306	211	279	Shear	Shear	Shear
	BM16-150	416.5	296	279	296	Combined	Shear	Combined
	BM16-s230	450.8	347	229	353	Shear	Shear	Shear
	BM25-220	360.1	300	189	263	Shear	Shear	Shear
	BM25-150	415.8	294	256	294	Combined	Shear	Combined
	BM25-s230	444	285	204	323	Shear	Shear	Shear
Design model	BM12-220	382.4	284	218	292	Shear	Shear	Shear
	BM12-150	405.2	277	224	303	Shear	Shear	Shear
	BM12-s230	466.9	304	238	335	Shear	Shear	Shear
	*BM16-220**	*309.3*	285	216	287	Shear	Shear	Shear
	BM16-150	416.5	274	218	297	Shear	Shear	Shear
	BM16-s230	450.8	300	232	328	Shear	Shear	Shear
	BM25-220	360.1	279	199	260	Shear	Shear	Shear
	BM25-150	415.8	256	194	269	Shear	Shear	Shear
	BM25-s230	444	245	200	296	Shear	Shear	Shear

* Note that test result of BM16-220 contains error, hence is not compared with others.
** All beams fail in shear during test; both shear failure mode and combined failure mode predict shear failure.

Table 6.9: Shear strengths with new h_C approach proposed in this research

Model Type	Specimen	P_{test} (kN)	$P_{predict}$ (kN) with			**Predicted Failure Mode with		
			ζ_{Nc}	ζ_{CSA}	ζ_{New}	ζ_{Nc}	ζ_{CSA}	ζ_{New}
Kr model	BM12-220	382.4	279	212	291	Combined	Shear	Shear
	BM12-150	405.2	270	221	306	Combined	Combined	Combined
	BM12-s230	466.9	283	235	325	Combined	Shear	Combined
	*BM16-220**	*309.3*	275	209	283	Combined	Shear	Shear
	BM16-150	416.5	263	216	295	Combined	Combined	Combined
	BM16-s230	450.8	274	228	314	Combined	Shear	Combined
	BM25-220	360.1	245	190	241	Combined	Shear	Shear
	BM25-150	415.8	225	187	249	Combined	Combined	Combined
	BM25-s230	444	202	196	264	Combined	Shear	Combined
WSF model	BM12-220	382.4	397	236	361	Shear	Shear	Shear
	BM12-150	405.2	369	298	369	Combined	Shear	Combined
	BM12-s230	466.9	387	237	387	Shear	Shear	Shear
	*BM16-220**	*309.3*	391	229	351	Shear	Shear	Shear
	BM16-150	416.5	357	288	357	Combined	Shear	Combined
	BM16-s230	450.8	376	229	374	Shear	Shear	Shear
	BM25-220	360.1	348	194	298	Shear	Shear	Shear
	BM25-150	415.8	298	244	306	Combined	Shear	Combined
	BM25-s230	444	257	189	307	Shear	Shear	Shear
HSF model	BM12-220	382.4	326	209	279	Shear	Shear	Shear
	BM12-150	405.2	297	282	297	Combined	Shear	Combined
	BM12-s230	466.9	343	223	364	Shear	Shear	Shear
	*BM16-220**	*309.3*	320	203	273	Shear	Shear	Shear
	BM16-150	416.5	290	275	290	Combined	Shear	Combined
	BM16-s230	450.8	335	217	355	Shear	Shear	Shear
	BM25-220	360.1	279	174	244	Shear	Shear	Shear
	BM25-150	415.8	257	243	257	Combined	Shear	Combined
	BM25-s230	444	246	185	299	Shear	Shear	Shear
Design model	BM12-220	382.4	279	212	291	Shear	Shear	Shear
	BM12-150	405.2	270	221	306	Shear	Shear	Shear
	BM12-s230	466.9	283	235	325	Shear	Shear	Shear
	*BM16-220**	*309.3*	275	209	283	Shear	Shear	Shear
	BM16-150	416.5	263	216	295	Shear	Shear	Shear
	BM16-s230	450.8	274	228	314	Shear	Shear	Shear
	BM25-220	360.1	245	190	241	Shear	Shear	Shear
	BM25-150	415.8	225	187	249	Shear	Shear	Shear
	BM25-s230	444	202	196	264	Shear	Shear	Shear

* Note that test result of BM16-220 contains error, hence is not compared with others.
** All beams fail in shear during test; both shear failure mode and combined failure mode predict shear failure.

Based on the tested and predicted strengths, it is found that no matter which model and approach is used with Kr model, the increase in shear strengths from having smaller stirrup spacings is never captured though it can capture the increase in shear strengths by having larger stirrups. The decrease in shear strength predicted with Kr model by having smaller stirrup spacings can be seen clearly with the plots organized in Figure 6.1.

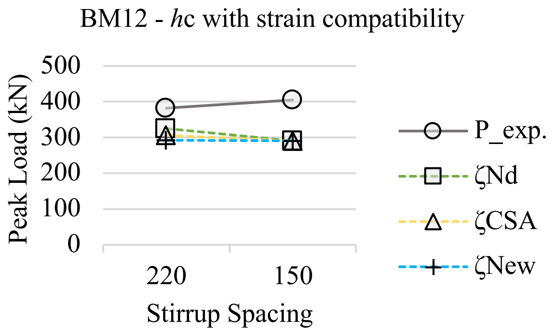
BM12 - hc with strain compatibility
Peak Load (kN)
500
400
300
200
100
0
220
150
Stirrup Spacing
P_exp.
ζNd
ζCSA
ζNew

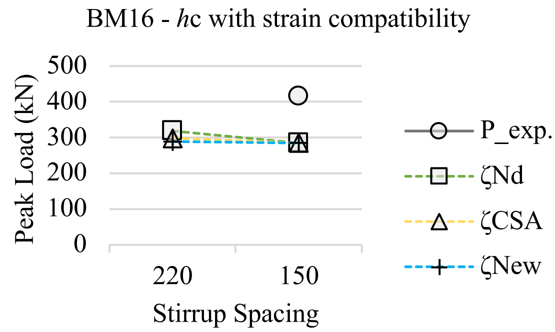
BM16 - hc with strain compatibility
Peak Load (kN)
500
400
300
200
100
0
220
150
Stirrup Spacing
P_exp.
ζNd
ζCSA
ζNew

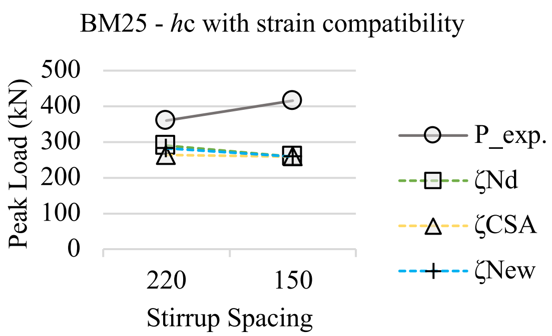
BM25 - hc with strain compatibility
Peak Load (kN)
500
400
300
200
100
0
220
150
Stirrup Spacing
P_exp.
ζNd
ζCSA
ζNew

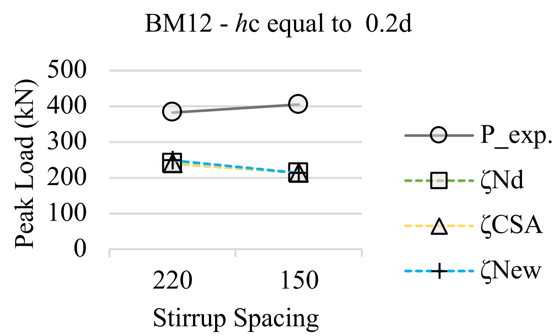
BM12 - hc equal to 0.2d
Peak Load (kN)
500
400
300
200
100
0
220
150
Stirrup Spacing
P_exp.
ζNd
ζCSA
ζNew

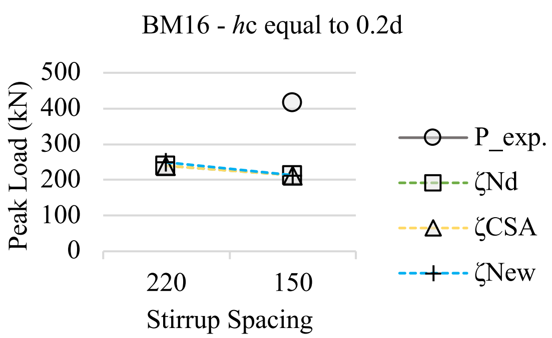
BM16 - hc equal to 0.2d
Peak Load (kN)
500
400
300
200
100
0
220
150
Stirrup Spacing
P_exp.
ζNd
ζCSA
ζNew

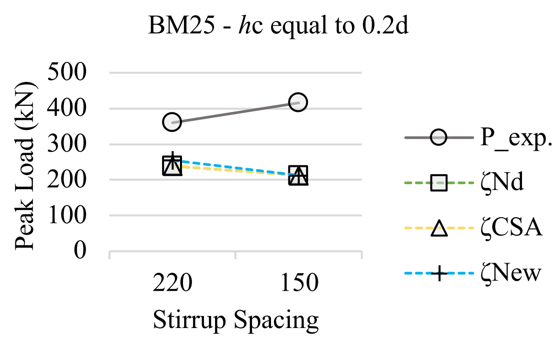
BM25 - hc equal to 0.2d
Peak Load (kN)
500
400
300
200
100
0
220
150
Stirrup Spacing
P_exp.
ζNd
ζCSA
ζNew

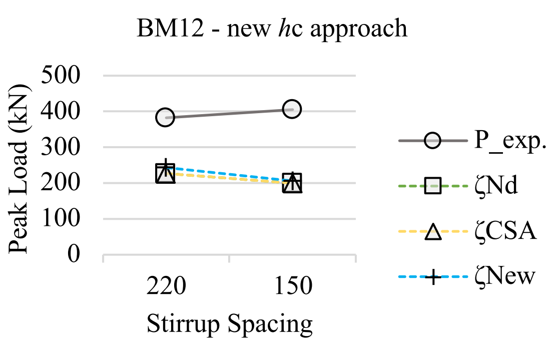
BM12 - new hc approach
Peak Load (kN)
500
400
300
200
100
0
220
150
Stirrup Spacing
P_exp.
ζNd
ζCSA
ζNew

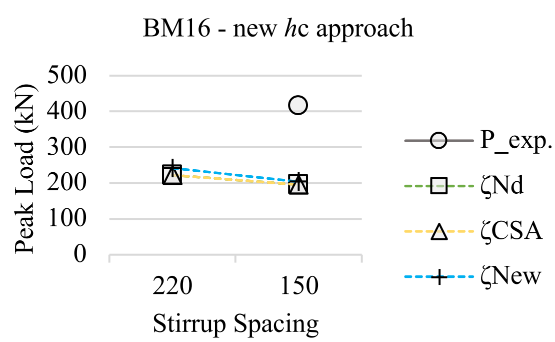
BM16 - new hc approach
Peak Load (kN)
500
400
300
200
100
0
220
150
Stirrup Spacing
P_exp.
ζNd
ζCSA
ζNew

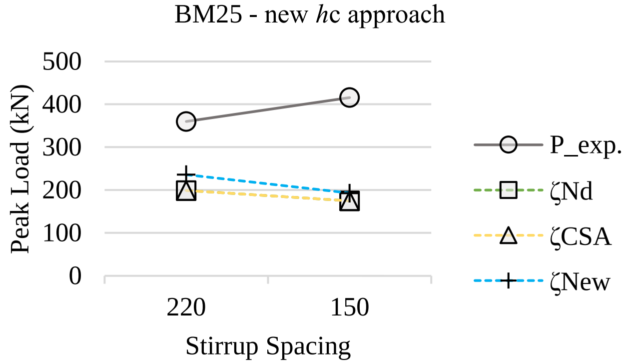

Figure 6.1: Trends of shear strengths predicted by Kr model

This may be caused by that the applied load is only taken by the y-component of the main strut and one stirrup in Kr model, while all the other stirrups do not contribute on affording the applied load but work as transferring the loads. Hence, even the beam is designed with more stirrups, these extra stirrups cannot take any more loads in the Kr model, but increase the load exerted on the horizontal struts with these extra members and decreased spacings, which as a result, decrease the analyzed failure load.

Therefore, Kr model shall not be sued with IST method, as it cannot correctly model the load transfer mechanism in the deep beams.

Furthermore, the combinations that can correctly show the increase in strengths with smaller stirrup spacings or having larger stirrups for all specimens are organized in Table 6.10.

Table 6.10: Results from approaches predicting correct trends

with h_C based on strain compatibility									
	P_{test} (kN)	$P_{predict}$ (kN) with				$P_{predict}/P_{test}$ with			
		WSF	HSF		Design	WSF	HSF		Design
Specimens		ζ_{CSA}	ζ_{CSA}	ζ_{New}	ζ_{New}	ζ_{CSA}	ζ_{CSA}	ζ_{New}	ζ_{New}
BM12-220	382.4	267	242	328	339	0.70	0.63	0.86	0.89
BM12-150	405.2	314	312	399	354	0.78	0.77	0.98	0.87
BM12-s230	466.9	258	257	406	375	0.55	0.55	0.87	0.80
*BM16-220**	*309.3*	258	235	322	329				
BM16-150	416.5	305	305	390	344	0.73	0.73	0.94	0.83
BM16-s230	450.8	249	250	396	363	0.55	0.55	0.88	0.81
BM25-220	360.1	217	204	290	285	0.60	0.57	0.80	0.79
BM25-150	415.8	258	272	354	298	0.62	0.65	0.85	0.72
BM25-s230	444	206	214	345	307	0.46	0.48	0.78	0.69
					Average Difference	0.38	0.38	0.13	0.20
					Standard Deviation	0.10	0.10	0.07	0.07

with h_C equal to 0.2d							
	P_{test} (kN)	$P_{predict}$ (kN) with			$P_{predict}/P_{test}$ with		
		HSF		Design	HSF		Design
Specimens		ζ_{CSA}	ζ_{New}	ζ_{New}	ζ_{CSA}	ζ_{New}	ζ_{New}
BM12-220	382.4	215	281	292	0.56	0.74	0.76
BM12-150	405.2	283	297	303	0.70	0.73	0.75
BM12-s230	466.9	234	359	335	0.50	0.77	0.72
*BM16-220**	*309.3*	211	279	287			
BM16-150	416.5	279	296	297	0.67	0.71	0.71
BM16-s230	450.8	229	353	328	0.51	0.78	0.73
BM25-220	360.1	189	263	260	0.52	0.73	0.72
BM25-150	415.8	256	294	269	0.61	0.71	0.65
BM25-s230	444	204	323	296	0.46	0.73	0.67
				Average Difference	0.43	0.26	0.29
				Standard Deviation	0.09	0.03	0.04

with the new h_C approach									
	P_{test} (kN)	$P_{predict}$ (kN) with				$P_{predict}/P_{test}$ with			
		WSF	HSF		Design	WSF	HSF		Design
Specimens		ζ_{New}	ζ_{CSA}	ζ_{New}	ζ_{New}	ζ_{New}	ζ_{CSA}	ζ_{New}	ζ_{New}
BM12-220	382.4	361	209	279	291	0.94	0.55	0.73	0.76
BM12-150	405.2	369	282	297	306	0.91	0.70	0.73	0.75
BM12-s230	466.9	387	223	364	325	0.83	0.48	0.78	0.70
*BM16-220**	*309.3*	351	203	273	283				
BM16-150	416.5	357	275	290	295	0.86	0.66	0.70	0.71
BM16-s230	450.8	374	217	355	314	0.83	0.48	0.79	0.70
BM25-220	360.1	298	174	244	241	0.83	0.48	0.68	0.67
BM25-150	415.8	306	243	257	249	0.74	0.58	0.62	0.60
BM25-s230	444	307	185	299	264	0.69	0.42	0.67	0.59
					Average Difference	0.17	0.46	0.29	0.32
					Standard Deviation	0.08	0.10	0.06	0.06

* Note that test result of BM16-220 contains error, hence is not compared with others.

The results show that:

1. The closest results are predicted by analyzing the beams through HSF models with h_C based on strain compatibility and ζ_{new} to soften struts.
2. The predicted results following the nearest trend with the test results are analyzed by HSF model with h_C equal to 0.2d and ζ_{new} to soften struts.
3. The approaches constantly capture the influence from stirrups are the HSF model with ζ_{new} to soften struts and Design model with ζ_{new} to soften struts.

Because the design model and the h_C approach equal to 0.2d can be analyzed without a detailed reinforcement design, they can be used to initially design the beams though the accuracy of the results predicted by this combination is not as good as the combination with HSF model and h_C based on strain compatibility.

Based on the results, the improved IST method for FRP RC deep beams with vertical reinforcement can be proposed.

For designing such beams, h_C can be preliminary calculated as 0.2d, and the design model with ζ_{new} can be used to find the suitable flexural and vertical reinforcement ratio. After the reinforcement design is determined, the design can be re-analyzed by HSF model with ζ_{new} and h_C based on strain compatibility.

6.2.4 Verification of the Proposed Method with Other Concrete Models

The proposed method for designing and analyzing FRP RC deep beams are analyzed again with H1 and T2 concrete models to check if the proposed method will work with other concrete stress-strain relationships, and the results are presented in Table 6.11 and Table 6.12.

Table 6.11: Verification of HSF model with ζ_{new}

with h_C based on strain compatibility							
	P_{test} (kN)	$P_{predict}$ (kN) with			$P_{predict}/P_{test}$ with		
Specimens		H_1	H_2	T_2	H_1	H_2	T_2
BM12-220	382.4	328	328	327	0.86	0.86	0.86
BM12-150	405.2	396	399	433	0.98	0.98	**1.07**
BM12-s230	466.9	409	406	409	0.88	0.87	0.88
*BM16-220**	*309.3*	322	322	320			
BM16-150	416.5	388	390	424	0.93	0.94	**1.02**
BM16-s230	450.8	400	396	399	0.89	0.88	0.88
BM25-220	360.1	293	290	288	0.81	0.80	0.80
BM25-150	415.8	353	354	379	0.85	0.85	0.91
BM25-s230	444	353	345	346	0.80	0.78	0.78
				Average Difference	0.13	0.13	0.12
				Standard Deviation	0.06	0.07	0.10

with h_C equal to 0.2d							
	P_{test} (kN)	$P_{predict}$ (kN) with			$P_{predict}/P_{test}$ with		
Specimens		H_1	H_2	T_2	H_1	H_2	T_2
BM12-220	382.4	282	281	284	0.74	0.74	0.74
BM12-150	405.2	295	297	352	0.73	0.73	0.87
BM12-s230	466.9	359	359	365	0.77	0.77	0.78
*BM16-220**	*309.3*	280	279	280	0.90	0.90	0.91
BM16-150	416.5	295	296	352	0.71	0.71	0.84
BM16-s230	450.8	355	353	358	0.79	0.78	0.80
BM25-220	360.1	266	263	263	0.74	0.73	0.73
BM25-150	415.8	293	294	347	0.70	0.71	0.84
BM25-s230	444	330	323	326	0.74	0.73	0.73
				Average Difference	0.26	0.26	0.21
				Standard Deviation	0.03	0.03	0.05

* Note that test result of BM16-220 contains error, hence is not compared with others.

Table 6.12: Verification of the design model with ζ_{new}

with h_C based on strain compatibility							
	P_{test}	$P_{predict}$ (kN) with			$P_{predict}/P_{test}$ with		
Specimens	(kN)	H_1	H_2	T_2	H_1	H_2	T_2
BM12-220	382.4	337	339	342	0.88	0.89	0.89
BM12-150	405.2	364	354	361	0.90	0.87	0.89
BM12-s230	466.9	390	375	384	0.84	0.80	0.82
*BM16-220**	*309.3*	329	329	332			
BM16-150	416.5	355	344	351	0.85	0.83	0.84
BM16-s230	450.8	378	363	371	0.84	0.81	0.82
BM25-220	360.1	290	285	287	0.81	0.79	0.80
BM25-150	415.8	311	298	303	0.75	0.72	0.73
BM25-s230	444	323	307	312	0.73	0.69	0.70
				Average Difference	0.18	0.20	0.19
				Standard Deviation	0.06	0.07	0.07

with h_C equal to 0.2d							
	P_{test}	$P_{predict}$ (kN) with			$P_{predict}/P_{test}$ with		
Specimens	(kN)	H_1	H_2	T_2	H_1	H_2	T_2
BM12-220	382.4	287	292	301	0.75	0.76	0.79
BM12-150	405.2	307	303	315	0.76	0.75	0.78
BM12-s230	466.9	343	335	347	0.73	0.72	0.74
*BM16-220**	*309.3*	283	287	295	0.92	0.93	0.96
BM16-150	416.5	302	297	308	0.73	0.71	0.74
BM16-s230	450.8	337	328	340	0.75	0.73	0.76
BM25-220	360.1	263	260	265	0.73	0.72	0.74
BM25-150	415.8	278	269	277	0.67	0.65	0.67
BM25-s230	444	308	296	308	0.69	0.67	0.69
				Average Difference	0.27	0.29	0.26
				Standard Deviation	0.03	0.04	0.04

* Note that test result of BM16-220 contains error, hence is not compared with others.

The proposed method works well with other two concrete stress-strain model. It is only that T2 model may overpredict the shear strength with HSF model for specimens with tight stirrup spacings, and the method works better with the two models softened from Hognestad parabola.

In conclusion, to initially design a FRP RC deep beam:

- h_C can be preliminary assumed as 0.2d,
- analysis can be performed on the design model (ST geometry),
- struts can be modelled with Hognestad parabola softened by ζ_{new}.

After the reinforcement design is determined, the design can be re-analyzed by:

- h_C based on strain compatibility,
- HSF model to represent the load paths,
- Hognestad parabola softened by ζ_{new}.

Although it is recommended to model the concrete behavior with softened Hognestad parabola based on the results, this may be due to that the specimens analyzed in this research are all constructed with normal-density, normal-strength concrete, which is what Hognestad parabola is designed for.

However, if the concrete used is not with normal-density or normal-strength and shall not be analyzed with Hognestad parabola, other models like the model by Thorenfeldt et al. (1987) shall be used. Because T2 model predicts correct trends and with generally conservative results, the proposed method shall work properly with other concrete models as long as the softening factors, ζ_{new} are applied correctly to all factors related to compressive strength, like ε_0, and the factor n of the Thorenfeldt et al. (1987) model.

6.3 Analyses on Deep Beams without Stirrups

There is one statically determinate ST model to analyze deep beams without stirrups, and all approaches of other features are analyzed again for these specimens, except that the h_C approach based on force equilibrium is excluded as it is too sensitive to the flexural reinforcement.

Specimens analyzed in this section includes the 3 specimens from Krall (2014), and 14 specimens from D. J. Kim et al. (2014). As the strengths of these specimens are much lower than those of the deep beams with vertical reinforcement, the results in this section are rounded to 0.1 kilonewtons.

Based on the analyzed result, the proper approaches and models are found, and the IST method specifically for deep beams without stirrups is proposed.

6.3.1 Analysis on the Details of ζ_{new} approach with specimens tested by Krall (2014)

How to apply ζ_{new} to deep beams without stirrups shall be determined before analyzing and comparing the approaches. As mentioned in Chapter 5, this approach requires imaginary ties with nearly no stiffness to find the strain in y-direction; hence, analysis is conducted to find the relationship between the numbers of imaginary stirrups and the predicted strengths on specimens tested by Krall (2014) , and the results are presented in Figure 6.2 with H2 concrete model and h_C equal to 0.2d.

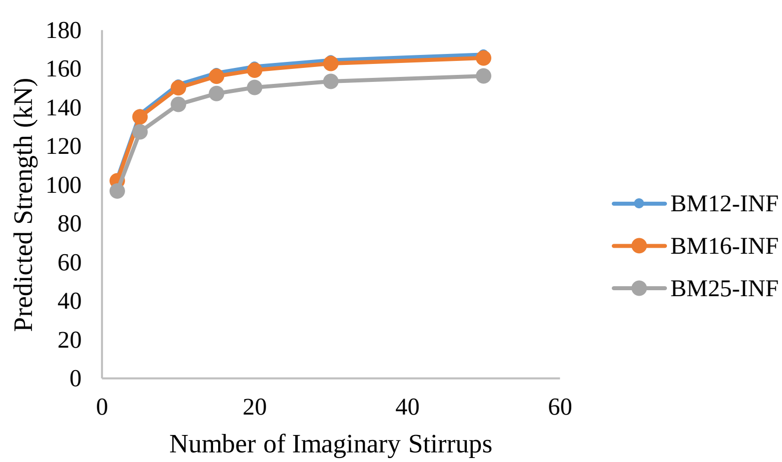

Figure 6.2: ζ_{new} approach with different numbers of imaginary ties

It is clear that the curves converge with increased imaginary ties, which proves that using the imaginary ties to predict the vertical strain is similar to conducting a simplified finite element analysis for the vertical strain. Hence, to save the analysis time and to be slightly more conservative, it is decided to consistently use 5 imaginary ties for the ζ_{new} approach, which is as shown in Figure 6.3.

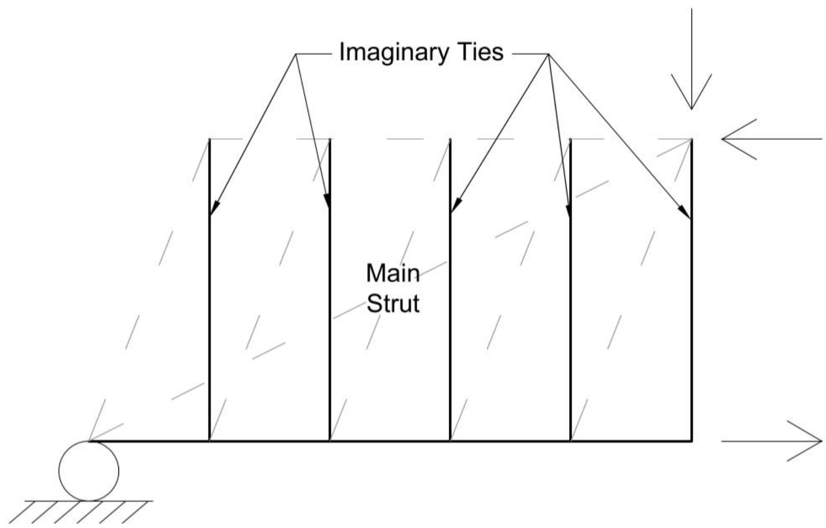

Figure 6.3: Proposed STM for ζ_{new} approach with 5 imaginary ties

Moreover, as the zero-force tie under the loading point is counted, the minimum number of imaginary ties is two but not one.

6.3.2 Analyzed Results with Different Approaches

The H2 concrete stress-strain relationship is firstly used to determine which combination of the approaches works best with the method. As the analyzed failure mode can only be shear failure, the predicted strengths along with the ratios between the predicted and tested strengths are presented in Table 6.13. The average differences of the ratios are computed to determine the accuracy, and the standard deviations are computed to check if the predicted results follow a similar trend with the test results, and if the accuracy is stable.

Table 6.13: Results for FRP RC deep beams without stirrups

with h_C based on strain compatibility

Specimens	P_{test} (kN)	$P_{predict}$ (kN) with				$P_{predict}/P_{test}$ with			
		ζ_{ACI}	ζ_{Nd}	ζ_{CSA}	ζ_{New}	ζ_{ACI}	ζ_{Nd}	ζ_{CSA}	ζ_{New}
BM12-INF	163.1	93.3	83.9	90.7	159.1	0.57	0.51	0.56	0.98
BM16-INF	150.2	91.8	82.5	88.6	155.6	0.61	0.55	0.59	**1.04**
BM25-INF	125.1	85.7	77.0	78.5	139.6	0.68	0.62	0.63	**1.12**
					Average Difference	0.38	0.44	0.41	0.06
					Standard Deviation	0.06	0.05	0.04	0.07
A3D9M-1.4	136.05	94.4	143.3	86.8	128.5	0.69	**1.05**	0.64	0.94
A3D9M-1.7	98.98	77.5	101.3	62.8	101.8	0.78	**1.02**	0.63	**1.03**
A3D9M-2.1	88	61.4	48.5	43.1	77.0	0.70	0.55	0.49	0.87
A4D9M-1.7	121	81.3	104.2	71.4	114.8	0.67	0.86	0.59	0.95
A5D9M-1.7	133.97	84.5	106.3	78.6	125.6	0.63	0.79	0.59	0.94
A3D9S-1.7	109.58	70.8	90.8	58.6	95.1	0.65	0.83	0.53	0.87
A5D9L-1.7	134.27	91.9	117.7	83.9	134.0	0.68	0.88	0.62	1.00
C3D9M-1.4	169.26	100.3	150.6	103.1	151.1	0.59	0.89	0.61	0.89
C3D9M-1.7	106.54	82.9	105.3	74.9	120.1	0.78	0.99	0.70	**1.13**
*C3D9M-2.1**	*52.64*	66.2	46.6	51.6	91.1				
*C4D9M-1.7**	*96.09*	87.1	107.8	84.6	134.6				
C5D9M-1.7	151.39	90.5	109.3	92.7	146.5	0.60	0.72	0.61	0.97
C3D9S-1.7	104.84	74.8	92.7	69.0	110.9	0.71	0.88	0.66	**1.06**
C5D9L-1.7	145.39	99.4	122.9	99.9	157.8	0.68	0.85	0.69	**1.09**
					Average Difference	0.32	0.15	0.39	0.07
					Standard Deviation	0.06	0.14	0.06	0.08

with h_C equal to 0.2d

Specimens	P_{test} (kN)	$P_{predict}$ (kN) with				$P_{predict}/P_{test}$ with			
		ζ_{ACI}	ζ_{Nd}	ζ_{CSA}	ζ_{New}	ζ_{ACI}	ζ_{Nd}	ζ_{CSA}	ζ_{New}
BM12-INF	163.1	74.3	66.7	81.9	136.6	0.46	0.41	0.50	0.84
BM16-INF	150.2	74.3	66.7	80.6	135.1	0.49	0.44	0.54	0.90
BM25-INF	125.1	74.3	66.7	73.8	127.4	0.59	0.53	0.59	**1.02**
					Average Difference	0.49	0.54	0.46	0.09
					Standard Deviation	0.07	0.06	0.04	0.09
A3D9M-1.4	136.05	92.7	141.2	86.4	127.4	0.68	**1.04**	0.64	0.94
A3D9M-1.7	98.98	76.0	100.1	62.5	100.8	0.77	**1.01**	0.63	**1.02**
A3D9M-2.1	88	60.1	48.8	42.8	76.2	0.68	0.55	0.49	0.87
A4D9M-1.7	121	76.0	100.1	70.2	111.0	0.63	0.83	0.58	0.92
A5D9M-1.7	133.97	76.0	100.1	76.5	118.9	0.57	0.75	0.57	0.89
A3D9S-1.7	109.58	67.2	88.5	58.1	93.0	0.61	0.81	0.53	0.85
A5D9L-1.7	134.27	84.8	111.7	81.8	128.4	0.63	0.83	0.61	0.96
C3D9M-1.4	169.26	92.7	141.2	101.0	145.1	0.55	0.83	0.60	0.86
C3D9M-1.7	106.54	76.0	100.1	73.3	114.9	0.71	0.94	0.69	**1.08**
*C3D9M-2.1**	*52.64*	60.1	48.8	50.3	86.9				
*C4D9M-1.7**	*96.09*	76.0	100.1	81.7	125.2				
C5D9M-1.7	151.39	76.0	100.1	88.5	133.0	0.50	0.66	0.58	0.88
C3D9S-1.7	104.84	67.2	88.5	67.9	105.5	0.64	0.84	0.65	**1.01**
C5D9L-1.7	145.39	84.8	111.7	95.0	144.2	0.58	0.77	0.65	0.99
					Average Difference	0.37	0.19	0.40	0.08
					Standard Deviation	0.07	0.14	0.06	0.07

with the new h_C approach

Specimens	P_{test} (kN)	$P_{predict}$ (kN) with				$P_{predict}/P_{test}$ with			
		ζ_{ACI}	ζ_{Nd}	ζ_{CSA}	ζ_{New}	ζ_{ACI}	ζ_{Nd}	ζ_{CSA}	ζ_{New}
BM12-INF	163.1	74.3	66.7	81.9	130.6	0.46	0.41	0.50	0.80
BM16-INF	150.2	74.3	66.7	80.6	128.0	0.49	0.44	0.54	0.85
BM25-INF	125.1	74.3	66.7	73.8	115.1	0.59	0.53	0.59	0.92
				Average Difference		0.49	0.54	0.46	0.14
				Standard Deviation		0.07	0.06	0.04	0.06
A3D9M-1.4	136.05	77.7	120.8	81.8	116.4	0.57	0.89	0.60	0.86
A3D9M-1.7	98.98	62.1	86.5	58.6	91.0	0.63	0.87	0.59	0.92
A3D9M-2.1	88	47.7	46.6	39.6	67.6	0.54	0.53	0.45	0.77
A4D9M-1.7	121	64.2	88.8	66.3	101.5	0.53	0.73	0.55	0.84
A5D9M-1.7	133.97	66.0	90.7	72.9	110.2	0.49	0.68	0.54	0.82
A3D9S-1.7	109.58	58.9	81.5	56.3	87.4	0.54	0.74	0.51	0.80
A5D9L-1.7	134.27	69.5	96.2	75.8	114.7	0.52	0.72	0.56	0.85
C3D9M-1.4	169.26	80.9	125.7	96.6	134.9	0.48	0.74	0.57	0.80
C3D9M-1.7	106.54	65.1	89.8	69.5	105.8	0.61	0.84	0.65	0.99
*C3D9M-2.1**	*52.64*	50.4	47.7	47.3	79.0				
*C4D9M-1.7**	*96.09*	67.5	92.3	78.3	117.3				
C5D9M-1.7	151.39	69.6	94.4	85.7	126.8	0.46	0.62	0.57	0.84
C3D9S-1.7	104.84	61.2	83.7	66.3	100.8	0.58	0.80	0.63	0.96
C5D9L-1.7	145.39	73.9	101.0	89.8	132.9	0.51	0.69	0.62	0.91
				Average Difference		0.46	0.26	0.43	0.14
				Standard Deviation		0.05	0.10	0.05	0.07

* Note that test results of these specimens contain error, hence are not compared with others.

Firstly, both ζ_{ACI} and ζ_{Nd} cannot predict the increase in shear strength from having stiffer flexural bars without h_C capturing that feature, hence these two approaches shall not be used with h_C equal to 0.2d, as h_C equal to 0.2d is neither related to the stiffness of the rebars.

Secondly, though ζ_{ACI} and ζ_{CSA} can capture the influence on the shear capacity from other features, the predicted results are too conservative, which may be good for code provisions, but makes them less accurate than other approaches.

Thirdly, both ζ_{Nd} and ζ_{New} predict accurate results but overestimate the shear strengths of several beams with h_C based on strain compatibility or equal to 0.2. Among these two approaches, ζ_{New} predicts better results, as it predicts closer results with more stable accuracies.

Therefore, the proposed method is to analyze and design FRP RC deep beams without vertical reinforcement with the new h_C approach and ζ_{New}.

6.3.3 Verification of the Proposed Method with Other Concrete Models

As the proposed method is developed, it is analyzed against different concrete models to check the validity, and the results are organized in Table 6.14.

Table 6.14: Results of the proposed method with different concrete models

Specimens	P_{test} (kN)	$P_{predict}$ (kN) with			$P_{predict}/P_{test}$ with		
		H_1	H_2	T_2	H_1	H_2	T_2
BM12-INF	163.1	120.4	130.6	146.0	0.74	0.80	0.90
BM16-INF	150.2	118.0	128.0	142.8	0.79	0.85	0.95
BM25-INF	125.1	106.1	115.1	126.8	0.85	0.92	**1.01**
			Average Difference		0.21	0.14	0.06
			Standard Deviation		0.06	0.06	0.06
A3D9M-1.4	136.05	111.1	116.4	108.7	0.82	0.86	0.80
A3D9M-1.7	98.98	86.2	91.0	84.6	0.87	0.92	0.85
A3D9M-2.1	88	63.5	67.6	62.6	0.72	0.77	0.71
A4D9M-1.7	121	96.1	101.5	95.7	0.79	0.84	0.79
A5D9M-1.7	133.97	104.3	110.2	105.0	0.78	0.82	0.78
A3D9S-1.7	109.58	82.8	87.4	81.5	0.76	0.80	0.74
A5D9L-1.7	134.27	108.6	114.7	109.1	0.81	0.85	0.81
C3D9M-1.4	169.26	128.5	134.9	128.4	0.76	0.80	0.76
C3D9M-1.7	106.54	100.1	105.8	100.3	0.94	0.99	0.94
*C3D9M-2.1**	*52.64*	73.9	79.0	74.4			
*C4D9M-1.7**	*96.09*	111.0	117.3	112.7			
C5D9M-1.7	151.39	119.9	126.8	123.0	0.79	0.84	0.81
C3D9S-1.7	104.84	95.4	100.8	95.8	0.91	0.96	0.91
C5D9L-1.7	145.39	125.8	132.9	132.9	0.87	0.91	0.91
			Average Difference		0.18	0.14	0.18
			Standard Deviation		0.07	0.07	0.07

* Note that test results of these specimens contain error, hence are not compared with others.

The predicted strengths are similar to each other, and H2 model and T2 could be slightly more accurate. It proves that the proposed method is able to work and works well with different stress-strain relationships. Hence, if a specific concrete model is required, it is safe to use that concrete model as long as it is properly softened.

The only outliner is BM25-INF analyzed with T2 model, as the strength is slightly overpredicted. However, it is only overpredicted about two kilonewtons, hence can be ignored.

In a conclusion, to design or analyze a FRP RC deep beam without vertical reinforcement, it is recommended

- to use the new approach to calculate h_C inside each iteration,
- and to use ζ_{New} with five imaginary ties having nearly no stiffness to find the strain in vertical direction.

Moreover, the number of imaginary ties can be reduced to two if more conservative results are wanted.

6.4 Analyses of Slender Beams

Selected beams bested by Tedford (2019) are also analyzed to verify if the IST method for FRP RC deep beams can be applied to truss models for FRP RC slender beams. Similarly, concrete is modeled with H2 model to limit the numbers of variables.

The truss models for slender beams generally have compression fans located at supports and loading points extended out to a certain distance as shown in Figure 6.4.

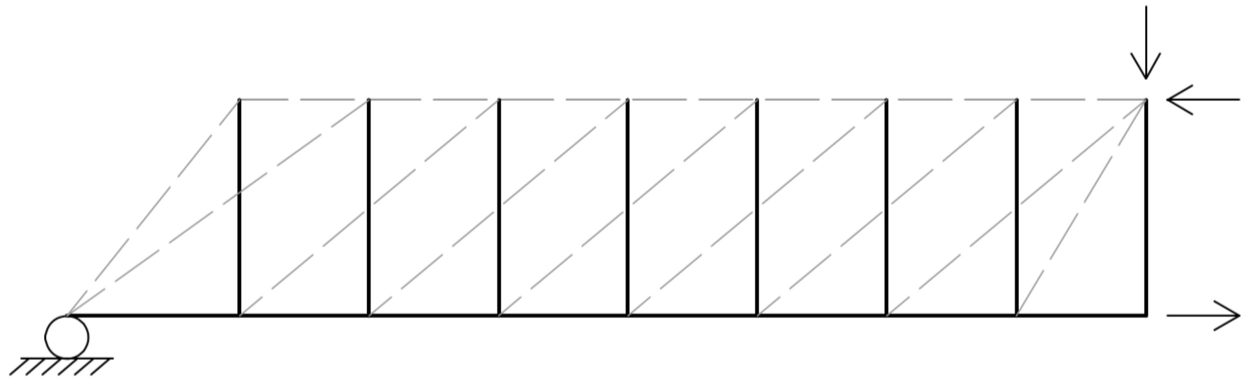

Figure 6.4: Typical truss model for slender beams with compression fans

Analyzing shear strengths of steel RC slender beams with truss models is to find how many ties are connected to the loading or supporting point by the compression fans. Therefore, the focus of a truss model is to determine how far the compression fan can be extended to, as it determines the number of stirrups can be utilized to take the shear force. If a beam is designed with large stirrup spacings, the compression fan might disappear as shown in Figure 6.5, and the shear strength is equal to the yielding force of one vertical tie.

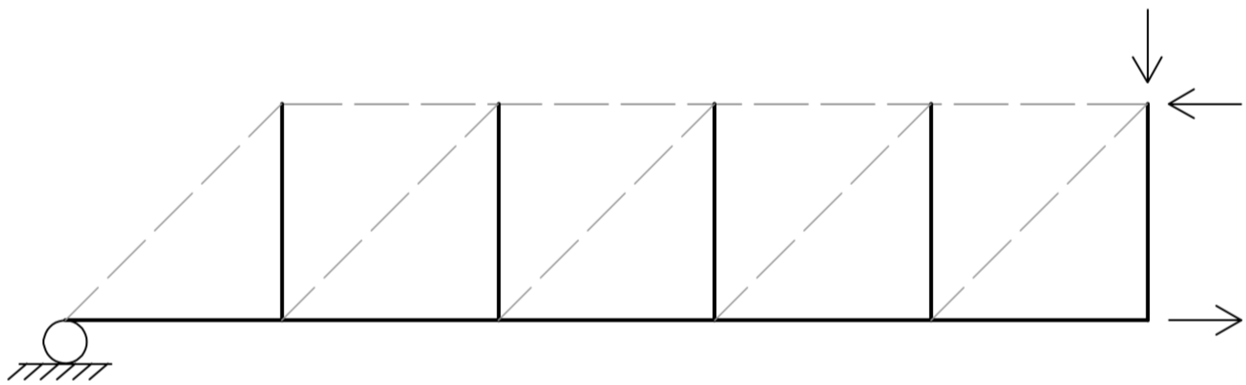

Figure 6.5: Typical truss model for slender beams without compression fans

However, reinforcement in FRP RC beams cannot yield, and the strength shall be governed by concrete crushing. Hence, the truss models can only be analyzed with the IST method. If the inclined struts are failed, it is predicted to fail in shear; if the horizontal struts are failed, it is predicted to fail in flexure.

How far should the compression fan extended to could also be important to FRP RC slender beams, as it defines the angles of the inclined struts and the number of struts utilized to take the applied force, which could still affect the predicted results.

Thus, truss models with compression fans extended to 2d and 0.9d from supports and loading points are constructed and analyzed. The value of 2d is from the maximum a/d value regulated by ACI 318-19 (2019) for deep beams, while the value of 0.9d is the generally govern value for the effective shear depth (d_v) from CSA A23.3-19 (2019), and CSA A23.3-19 (2019) defined that the region inside d_v from supports could be considered as deep regions inside slender beams in sectional shear analysis.

The results analyzed from these two truss models are presented in Table 6.15.

Table 6.15: Results for slender beams

Compression fan extended to 2d											
h_c approach	Specimens	P_{test} (kN)	$P_{predict}$ (kN) with				Predicted Failure Mode				Actual Failure
			ζ_{ACI}	ζ_{Nd}	ζ_{CSA}	ζ_{New}	ζ_{ACI}	ζ_{Nd}	ζ_{CSA}	ζ_{New}	
Based on Strain Compatibility	BM4.5-90	222.5	157.1	157.1	157.1	157.1	Flexure	Flexure	Flexure	Flexure	Shear
	BM4.5-150	171.2	162.5	162.5	162.5	162.5	Flexure	Flexure	Flexure	Flexure	Shear
	BM6.5-90	145.6	99.5	99.5	99.5	99.5	Flexure	Flexure	Flexure	Flexure	Flexure
	BM6.5-150	141.0	101.8	101.8	101.8	101.8	Flexure	Flexure	Flexure	Flexure	Shear
Equal to 0.2d	BM4.5-90	222.5	120.1	120.1	120.1	120.1	Flexure	Flexure	Flexure	Flexure	Shear
	BM4.5-150	171.2	124.1	124.1	124.1	124.1	Flexure	Flexure	Flexure	Flexure	Shear
	BM6.5-90	145.6	76.0	76.0	76.0	76.0	Flexure	Flexure	Flexure	Flexure	Flexure
	BM6.5-150	141.0	77.7	77.7	77.7	77.7	Flexure	Flexure	Flexure	Flexure	Shear
New Approach	BM4.5-90	222.5	109.0	109.0	109.0	109.0	Flexure	Flexure	Flexure	Flexure	Shear
	BM4.5-150	171.2	112.9	112.9	112.9	112.9	Flexure	Flexure	Flexure	Flexure	Shear
	BM6.5-90	145.6	68.5	68.5	68.5	68.5	Flexure	Flexure	Flexure	Flexure	Flexure
	BM6.5-150	141.0	70.1	70.1	70.1	70.1	Flexure	Flexure	Flexure	Flexure	Shear
Compression fan extended to 0.9d											
h_c approach	Specimens	P_{test} (kN)	$P_{predict}$ (kN) with				Predicted Failure Mode				Actual Failure
			ζ_{ACI}	ζ_{Nd}	ζ_{CSA}	ζ_{New}	ζ_{ACI}	ζ_{Nd}	ζ_{CSA}	ζ_{New}	
Based on Strain Compatibility	BM4.5-90	222.5	137.1	137.1	137.1	137.1	Flexure	Flexure	Flexure	Flexure	Shear
	BM4.5-150	171.2	139.0	139.0	139.0	139.0	Flexure	Flexure	Flexure	Flexure	Shear
	BM6.5-90	145.6	91.5	91.5	91.5	91.5	Flexure	Flexure	Flexure	Flexure	Flexure
	BM6.5-150	141.0	92.3	92.3	92.3	92.3	Flexure	Flexure	Flexure	Flexure	Shear
Equal to 0.2d	BM4.5-90	222.5	104.4	104.4	104.4	104.4	Flexure	Flexure	Flexure	Flexure	Shear
	BM4.5-150	171.2	105.9	105.9	105.9	105.9	Flexure	Flexure	Flexure	Flexure	Shear
	BM6.5-90	145.6	69.7	69.7	69.7	69.7	Flexure	Flexure	Flexure	Flexure	Flexure
	BM6.5-150	141.0	70.4	70.4	70.4	70.4	Flexure	Flexure	Flexure	Flexure	Shear
New Approach	BM4.5-90	222.5	93.8	93.8	93.8	93.8	Flexure	Flexure	Flexure	Flexure	Shear
	BM4.5-150	171.2	95.2	95.2	95.2	95.2	Flexure	Flexure	Flexure	Flexure	Shear
	BM6.5-90	145.6	62.5	62.5	62.5	62.5	Flexure	Flexure	Flexure	Flexure	Flexure
	BM6.5-150	141.0	63.1	63.1	63.1	63.1	Flexure	Flexure	Flexure	Flexure	Shear

Although the results prove that the compression fan influences the results, they also prove that FRP RC slender beams shall not be analyzed with truss models through IST method. The results show too many problems, and the only thing that the models can capture is the decrease in strengths by having more slender beams.

The problems shown by the results include:

1. The method cannot predict the correct failure mode. No matter which approach is chosen, the beams are predicted to fail in flexure, but most of the beams failed in shear according to Tedford (2019) (except for BM6.5-90 that was filed in flexure). The flexural failure mode also causes all softening factor approaches predicting identical results as the approaches are mainly different for the inclined struts.
2. It cannot capture the increase in shear strength with smaller stirrup spacings. Even if the predicted strength is treated as the reinforcement contribution to the shear strength, it shall capture the increase in shear strengths when more stirrups are placed.
3. Most of the predicted results are not close to the tested strengths especially for beams with a/d ratio equal to 6.5.

Therefore, the IST method shall only be used to find the shear strength of FRP RC deep beams, which is to find the shear strength by arch action, and it is not suitable for FRP RC slender beams. There may be a way to properly utilize the truss models, but as the main purpose of this research is to predict the shear strength of deep beams with IST method, it is not further developed in this work.

7. Conclusions and Recommendations

7.1 Conclusions and Proposed IST Method

Conclusions on IST model types for FRP RC deep beams with vertical reinforcement:

- Kr model works well at capturing the increase in shear strength with lager stirrups but fails to capture the increase in shear strength with smaller stirrup spacings (or more stirrups); which may be caused by only connecting one stirrup to the loading/supporting nodes leading to inefficient load paths.
- Design model commonly used to design steel RC deep beams with vertical reinforcement works well on FRP RC deep beams. Though it predicts slightly more conservative results, the trend of the strengths can be well reflected with the proposed new softening factor (ζ) approach.
- Both proposed IST model types work well, WSF model works best with the new h_C and the new softening factor approach, while HSF model works best with the h_C approach based on strain compatibility and the new softening factor approach.
- HSF model is considered to be slightly better than WSF model, as it can work with all three h_C approach (excluding the inappropriate h_C approach based on force equilibrium) and both ζ_{CSA} and ζ_{new}, and its best combination predicts slightly better results than the best combination of WSF model.

Conclusions on concrete stress-strain modelling:

- Stress-strain relationships shall be softened with ζ applied to all factors calculated from the concrete compressive strength.
- Based on the specimens analyzed in this test, stress-strain models softened from Hognestad parabola are slightly better than those softened from the model by Thorenfeldt et al. (1987). However, the difference is small and the model by Thorenfeldt et al. (1987) may be better if the specimens are not casted with normal-strength, normal-density concrete, as Hognestad parabola is not suitable for some concrete types.

Conclusions on the assumed concrete compression height (h_C):

- Although the approach based on force equilibrium is suggested for steel FRP RC deep beams, it shall not be applied to FRP RC deep beams, as it is too sensitive to flexural reinforcement and is possible to predict extremely high or extremely low h_C.
- All the other three approaches work well, and the IST method is not extremely sensitive to h_C. However, ζ_{ACI} and ζ_{Nd} shall not be used with h_C equal to 0.2d to predict the strength of deep beams without stirrups, as these softening approaches cannot reflect the changes in the stiffnesses of the flexural reinforcement.
- h_C equal to 0.2d can be used as a preliminary assumption as it is simple and can be obtained without a developed reinforcement design.
- h_C based on strain equilibrium works better with more slender beams with stirrups as the shear strength of those beams are closer to the flexural strength, and the assumptions used in this h_C approach is actually for flexural failure.

- The new h_C approach works better with more deep beams without stirrups, and generally predicts more conservative results than the other two approaches.

Conclusions on Softening factor approaches:

- ζ_{ACI} is not suggested for FRP RC deep beams with vertical reinforcement, as it cannot efficiently soften the strength of the inclined struts, which makes it predict false failure mode with overestimated strengths.
- ζ_{Nd} works good for some specimens under certain conditions but is not generally good. It may because that this approach does not relate to enough factors, thus cannot capture how strut strengths shall change under different loads during the analysis.
- ζ_{CSA} works well at predicting the trends, but generally being too conservative for FRP RC deep beams both with and without vertical reinforcement.
- The new strut coefficient included in ζ_{ACI} for deep beams without vertical reinforcement makes this method too conservative for such beams. It may be even more conservative than ζ_{CSA} in some cases.
- ζ_{New} works really well for specimens both with and without vertical reinforcement. It captures the factors influencing the strengths properly while predicting accurate and generally conservative results.

Proposed IST method:

- To design deep beams with vertical reinforcement, it is recommended to preliminary assume h_C as 0.2d, to use the concrete models with all factors related to f_c' softened by ζ_{new} to model behavior of concretes struts, and to analyze with the design model, which makes it easier to try different vertical and flexural reinforcement ratios and bar stiffnesses for the beam design. After the reinforcement design is developed, the design can be re-analyzed by HSF model with the same softened concrete model and h_C based on strain compatibility.
- The design and analysis process of deep beams without vertical reinforcement is the same. It is recommended to use the new approach to calculate h_C inside each iteration, and to soften the concrete by ζ_{New} (in the proper way mentioned above). The ζ_{New} approach can be reached with a simple truss model having imaginary ties with nearly no stiffness placed behind the ST model to calculate the strain in the y-direction, and the recommended number of the imaginary ties is five. If a more conservative result is wanted, the number of imaginary ties can be reduced to two (the minimum value). If a simpler method is required, h_C can be changed to be equal to 0.2d, and the number of imaginary ties shall be decreased to two.
- Furthermore, the IST method is only applicable to calculate the shear strength governed by arch action. Hence, it shall not be applied to analyze truss models for slender beams. Although it is possible to use the ST method analyzing truss models for steel RC slender beams to find the reinforcement contribution, the IST method does not focus on the reinforcement contribution, thus cannot analyze the truss models for FRP RC slender beams properly.

7.2 Recommendations

- More deep beams with stirrups shall be tested and analyzed through the proposed method to verify the method.
- How to use the proposed method to other deep regions can be analyzed, and tests can be done to find if the proposed method is only good to deep beams or is good to all deep regions.
- The new h_C approach can be further developed to include a better model for post-peak relationship or to analyze the semi-cracked concrete beams in a better way, thus this approach will not be limited to a specific range of deep beams.
- A more detailed and throughout finite element analysis on h_C can be conducted to find how h_C exactly changes with different factors, and how the strain profiles of deep beams are influenced by slenderness ratios, applied load cases, etc. if a throughout new method can be produced for h_C, the IST method could be further improved.
- Although the current IST method focuses on the strut strengths cannot be applied to slender beams, there may be a way to alter this method to focus on the reinforcement contribution, which may lead to a new method for predicting the shear strengths of slender beams.

References

Abdel-Nasser, A. G., Sharaf, T. A., Ibrahim, H. M., & Abdel-Galil, E. Y. (2017). Analysis of Reinforced Concrete Deep Beams Using Nonlinear Strain Model. *Port Said Engineering Research Journal, 21*(2), 231-240.

ACI 318-19. (2019). *Building Code Requirements for Structural Concrete*. Farmington Hills: American Concrete Institute.

ACI 318M-08. (2008). *Building Code Requirements for Structural Concrete*. Farmington Hills: American Concrete Institute.

ACI 440.1R-15. (2015). *Guide for the Design and Construction of Structural Con-crete Reinforced with Fiber-Reinforced Polymer (FRP) Bars*. Farmington Hills: American Concrete Institute.

ACI 440R-07. (2007). *Report on Fiber-Reinforced Plymer (FRP) Reinforcement for Concrete Structures*. Farmington Hills: American Concrete Institute.

Ahmed, A., Guo, S., Zhang, Z., Shi, C., & Zhu, D. (2020). A review on durability of fiber reinforced polymer (FRP) bars reinforced seawater sea sand concrete. *Construction and Building Materials, 256*.

Anderheggen, E., & and Schlaich, M. (1990). *Computer Aided Design of Reinforced Concrete Structures using the Truss Model Approach.* Paper presented at the Proceedings of the Second International Conference on Computer Aided Analysis and Design of Concrete Structures, Zell am See, Austria.

Apinis, R., Modniks, J., Tamuzs, V., & Tepfers, R. (1998). *Ductility of Hybrid Fiber Composite Reinforcement FRP for Concrete.* Paper presented at the 8th European Conference on Composite Materials (ECCM8), Naples.

Chen, H., Yi, W.-J., & Hwang, H.-J. (2018). Cracking strut-and-tie model for shear strength evaluation of reinforced concrete deep beams. *Engineering Structures, 163*, 396-408. doi:10.1016/j.engstruct.2018.02.077

Chen, H., Yi, W.-J., Ma, Z. J., & Hwang, H.-J. (2020). Modeling of shear mechanisms and strength of concrete deep beams reinforced with FRP bars. *Composite Structures, 234*. doi:10.1016/j.compstruct.2019.111715

CSA A23.3-19. (2019). *Design of Concrete Structure*. Toronto: CSA Group.

CSA S806-12. (R2017). *Design and Construction of Building Structure with Fibre-Reinforced Polymers.* Mississauga: Canadian Standards Association.

Dhahir, M. K., Ammash, H. K., Nadir, W., & Nasr, M. S. (2021). An efficiency factor for the bottle shaped concrete strut in deep beams reinforced with longitudinal FRPs bars. *Material Today: Proceedings, 42*, 2050-2057.

Eom, T.-S., & Park, H.-G. (2010). Secant Stiffness Method for Inelastic Design of Strut-and-Tie Model. *ACI STRUCTURAL JOURNAL, 107*(6), 689-698.

Hognestad, E. (1951). *A Study of Combined Bending and Axial Load in Reinforced Concrete Members*. Urbana: University of Illinois.

Hognestad, E., Hanson, N. W., & McHenry, D. (1955). Concrete Stress Distribution in Ultimate Strength Design. *Journal of the American Concrete Institute, 27*(4), 455-479.

Kim, B. H., & Yun, Y. M. (2011a). An Indeterminate Strut-Tie Model and Load Distribution Ratio for RC Deep Beams - (I) Model & Load Distribution Ratio. *Advances in Structural Engineering, 14*(6), 1031-1041.

Kim, B. H., & Yun, Y. M. (2011b). An Indeterminate Strut-Tie Model and Load Distribution Ratio for RC Deep Beams - (II) Validity Evaluation. *Advances in Structural Engineering, 14*(6), 1043-1057.

Kim, D. J., Lee, J., & Lee, Y. H. (2014). Effectiveness factor of strut-and-tie model for concrete deep beams reinforced with FRP rebars. *Composites: Par B, 56*, 117-125.

Krall, M. (2014). *Tests on concrete beams with GFRP flexural and shear re-inforcements & analysis method for indeterminate strut-and-tie models with brittle reinforcements.* (Master’s thesis). University of Waterloo, Waterloo.

Krall, M., & Polak, M. A. (2019). Concrete beams with different arrangements of GFRP flexural and shear reinforcement. *Engineering Structures, 198*.

Kupfer, H., Hilsdorf, H. K., & Rusch, H. (1969). Behavior of Concrete under Biaxial Stresses. *ACI Journal Proceedings, 66*(8), 656-666.

MacGregor, J. G., & Wight, J. K. (2011). *Reinforced Concrete Mechanics and Design (6th)*. New Jersey: Pearson Education, Inc.

Mihaylov, B. I., Bentz, E. C., & Collins, M. P. (2013). Two-Parameter Kinematic Theory for Shear Behavior of Deep Beams. *ACI STRUCTURAL JOURNAL, 110*(3), 447-455.

Mohamed, A. M., Mahmoud, K., & El-Salakawy, E. F. (2020). Behavior of Simply Supported and Continuous Concrete Deep Beams Reinforced with GFRP Bars. *Journal of Composites for Construction, 24*(4). doi:10.1061/(ASCE) CC.1943-5614.0001039

Nehdi, M., Omeman, Z., & El-Chabib, H. (2008). Optimal efficiency factor in strut-and-tie model for FRP-reinforced concrete short beams with (1.5<a/d<2.5). *Materials and Structures, 41*, 1713-1727. doi:10.1617/s11527-008-9359-9

Pang, X. B., & Hsu, T. T. C. (1995). Behavior of Reinforced Concrete Membrane Elements in Shear. *ACI STRUCTURAL JOURNAL, 92*(6), 665-677.

Smith, M. (2009). *Abaqus/Standard User's Manual, Version 6.9.*: Dassault Systèmes Simulia Corp.

Stoner, J. G., & Polak, M. A. (2020). Finite element modelling of GFRP reinforced concrete beams. *Computers and Concrete, 25*(4). doi:10.12989/cac.2020.25.4.000

Tamuzs, V., Apinis, R., Vilks, U., Modniks, J., & Tepfers, R. (1996). *Ductility of Hybrid Fiber Composite Reinforcement FRP for Concrete.* Paper presented at the First International Conference on Composites in Infrastructure, Tucson, Arizona.

Tedford, T. (2019). *Experimental Investigation of the Shear Behaviour of Slender Concrete Beams Reinforced with GFRP.* (Master's thesis). University of Waterloo, Waterloo.

Teng, J. G., Chen, J. F., Smith, S. T., & Lam, L. (2002). *FRP: Strengthed RC Structures*: Wiley.

Thorenfeldt, E., Tomaszewics, A., & Jensen, J. J. (1987). *Mechanical properties of high strength concrete and application in design.* Paper presented at the Proceedings of the Symposium on Utilization of High Strength Concrete.

Tjhin, T. N., & Kuchma, D. A. (2002). Computer-Based Tools for Design by Strut-and-Tie

Method: Advances and Challenges. *ACI STRUCTURAL JOURNAL, 99*(5), 586-594.

Vecchio, F. J., & Collins, M. P. (1986). The Modified Compression-Field Theory for Reinforced Concrete Elements Subjected to Shear. *ACI Journal, 83*(2), 219-231.

Yun, Y. M. (2000). Nonlinear Strut-Tie Model Approach for Structural Concrete. *ACI STRUCTURAL JOURNAL, 97*(4), 581-590.

Yun, Y. M., & Ramirez, J. A. (1996). Srength of Struts and Nodes in Strut-Tie Model. *Journal of Structural Engineering, 122*(1), 20-29.

Appendices

A: MATLAB Code

For beams tested by Krall (2014) and Tedford (2019)

```
clc, clear all, close all, format short
%% Initial Inputs
% Beams
Beam1 = [12.22,16.22,25.22;
         12.15,16.15,25.15;
         112,  116,  125;
         45.09, 45.15,  45;
         65.09, 65.15,  65];
Beam1 = [Beam1(1:3,:)];%,Beam1(1:3,2),Beam1(1:3,3)];
% ST Model
Model_num1 = [1,3,4,6]; %[1Krall, 2no_stir, 3whole_deep, 4half_deep, 5slender,
6design]
% Softening Factor
sfModel1= [1,2.1,3,3.2]; lim = 0; %lim is only for 3, input 0 or 0.4
                        %2.1 based on theta, 2.2 based on a/d, 2.3 based on s/d;
                        % 3 based on theta, 3.1 based on s/d
                        % 3.2 new method based on ex ey
% Assumed Concrete Properties
mode = [1,1.1,2.1]; % Put 1 for Hognestad; 2 for Thorenfeldt; .1 for all factors
reduced

%% Figure on/off
fi=1;
fid=0;
fisf=0;
fiE=0;
Ti=0; Tn=1;
%% Models
for im = 1%:numel(Model_num1)
Model_num = Model_num1(im);
for ib = 1:numel(Beam1)
Beam = Beam1(ib);
INF = 0; INFd1 = 5;
for inf = 1%:numel(INFd1)
    INFd = INFd1(inf);
for isf = 4%:numel(sfModel1)
    sfModel = sfModel1(isf);
for iss = 1:numel(mode)
    model = mode(iss);

if Model_num==2 && sfModel==1
    sfModel=1.1;
end


Name = [Beam,Model_num,sfModel,model,INF,INFd];
fprintf('\n------------\nBM-%g, ST# %g, SF# %g, M %g, INF %g, INFd %g',Name)

%% Inputs
[Area_flex,E_flex,bar_c,Area_stirrup,E_stirrup,f_FRP_cu,f_cc,L_full,h_full,d_eff,...
    s_stirrup,bearing_s,bearing_P,z,P_exp,fflex,h_Cf,gamma_c,f_FRP_v] =
Input_MK(Beam,INF,INFd);
%d_eff=270;
%h_Ci = h_Cf;
%h_Ci = 0.65*f_FRP_cu*Area_flex/(0.85*f_cc*z);
```

```
h_Ci = 0.2*d_eff;
aaa = 1;

if Model_num == 2
    s_stirrup=L_full;
end

if Model_num == 6
    n_effstir= floor((L_full-bearing_s/2)/s_stirrup);
    Area_stirrup = Area_stirrup*n_effstir;
end

[e,n,nodes,conn,e_s_pris,e_s_bottle,e_s,e_b_flex,e_b_stirrup,e_b,...
    nodes_defined,defined_dimensions,nodes_nocheck,nodes_C,Rstrut_C,nodes_T,...
    Rstrut_T,nodes_load,ndof,fixed_dofs,fixed_u,free_dofs,dof_load,h_T,a]...
    = Model(Model_num,h_Ci,bar_c,L_full,s_stirrup,bearing_s,bearing_P,d_eff);


%% Plot Original truss------------------------------------------------------------
if fi==1
%figure(11);
%figure('Name',"MODEL")
for i = 1:e
    element_x(i,:)=nodes(1,[conn(i,1),conn(i,2)]);
    element_y(i,:)=nodes(2,[conn(i,1),conn(i,2)]);
    locx=max(element_x(i,:))-s_stirrup/2; locy=max(element_y(i,:));
    lxx = min(element_x(i,:))+(max(element_x(i,:))-min(element_x(i,:)))*2/3;
    if ismember(i,e_b_flex)
    plot(element_x(i,:),element_y(i,:),'k-')
    if i==1
        text(max(element_x(i,:))/2, locy+7, num2str(i))
    else
        text(locx, locy+7, num2str(i))
    end
    elseif ismember(i,e_b_stirrup)
    plot(element_x(i,:),element_y(i,:),'k-')
    text(max(element_x(i,:))-15, locy/2, num2str(i))
    elseif ismember(i,e_s_pris)
    plot(element_x(i,:),element_y(i,:),'r--')
    text(locx, locy+7, num2str(i))
    elseif ismember(i,e_s_bottle)
        plot(element_x(i,:),element_y(i,:),'r--')
        if max(element_x(i,:))-min(element_x(i,:))==L_full
        text(max(element_x(i,:))*3/4-10, locy*3/4, num2str(i))
        else
            text(lxx, locy*2/3, num2str(i))
        end
    end
    hold on
end
for i = 1:n
    txt= sprintf('N%d',i);
    text(nodes(1,i),nodes(2,i),txt)
end
end

%% element geometries
[theta, Nodalzone, Area, Length] = Geometry(e,n,conn, nodes,...
    nodes_defined,defined_dimensions,h_Ci,nodes_C,Rstrut_C,h_T,nodes_T,...
    Rstrut_T,e_b_flex,e_b_stirrup,e_s_pris,Area_flex,Area_stirrup,z);


%% Analysis
```

```
% Initial Parameters
P_in = 0; %N initial applied load set to be 0
P_inc = -10; %N add 10N applied load every loop
strain_c = zeros(1,e); % initial strain set to be 0
P_max = -600E3; % N to define maximum number of loops
[E_origi,strain0,aabb,Ec] = Elasticity(e,e_b_flex,E_flex,e_b_stirrup,E_stirrup,...
    e_s_bottle,strain_c,e_s_pris,model,f_cc,L_full,d_eff,theta,sfModel,lim,...
    a,conn,fflex,s_stirrup,gamma_c);

% Checks
% strut check
E_check = 0.01*E_origi;
% system check
Uns_check_1 = e-2*n+4;
Uns_check_2 = size(find(conn(:,2)==n),1);
Unstable_check = min(Uns_check_1);%,Uns_check_2);
if INF ==1
Unstable_check = 1;
end
% nodalzone check
lim_CCC = 0.85*f_cc; lim_CCT = 0.75*f_cc; lim_CTT = 0.65*f_cc;
% FRP check
lim_FRP(e_b) = f_FRP_cu;
lim_FRP(e_b_stirrup) = f_FRP_v;

% Iterative IST Analysis
[d,r,stress,strain,f_internal,E_end,Ebs,strain0_end,sfb,P_fail,h_C]...
    =ISTAnalysis(P_max,P_in,P_inc,h_Ci,nodes_nocheck,E_origi,E_flex,...
    E_stirrup,model,f_cc,E_check,lim_CCC,lim_CCT,lim_CTT,lim_FRP,INF,...
    Model_num,bar_c,bearing_s,bearing_P,Unstable_check,z,P_exp,L_full,...
    d_eff,sfModel,lim,a,fflex,s_stirrup,Area_flex,Area_stirrup,gamma_c,aaa,h_full);

%% Plot softening factor
if ismember(sfModel,[3,3.1,3.2]) && fisf==1
figure('Name',num2str(sfModel));
for ii = 1:size(e_s_bottle,2)
Px=0:P_inc:P_fail*2;
sfy=sfb(:,ii);
plot(-Px/1000,sfy')
Leg{ii}=sprintf('S%d',e_s_bottle(ii));
end
legend(Leg','Location','southwest')
xlabel('P(kN)')
ylabel('Soften Factors')
hold on
end
SoftenF_end=sfb(end-10,:);
softenF_end_E = SoftenF_end(end);

%% Plot Elasticity change
if fiE==1
figure('Name',"Elasticity")
for ii = 1:size(e_s_bottle,2)
Px=0:P_inc:P_fail*2;
Eis=Ebs(:,ii)/1000;
plot(-Px/1000,Eis')
Leg{ii}=sprintf('S%d',e_s_bottle(ii));
end
legend(Leg','Location','southwest')
xlabel('P(kN)')
ylabel('Elasticity(GPa)')
hold on
end
```

```
%% Plot Deformed Shape
if fid ==1
for i3 =1:n
    dx(i3)=d(i3*2-1);
    dy(i3)=d(i3*2);
end
nodes_new(1,:) = nodes(1,:)+dx;
nodes_new(2,:) = nodes(2,:)+dy;

figure(11);
for i3 = 1:e
    element_x(i3,:)=nodes_new(1,[conn(i3,1),conn(i3,2)]);
    element_y(i3,:)=nodes_new(2,[conn(i3,1),conn(i3,2)]);
    if ismember(i3,e_b)
    plot(element_x(i3,:),element_y(i3,:),'b-')
    elseif ismember(i3,e_s)
    plot(element_x(i3,:),element_y(i3,:),'g--')
    end
    hold on
end
dx=[]; dy=[]; nodes_new=[];
end
StrengthV = -P_fail*2/1000;
if Ti==1
T(Tn,:) = table(Model_num, Beam, sfModel, model,StrengthV);
Tn=Tn+1;
writetable(T,'ShearStrength.xlsx','sheet',5)
end

h_C;
%Ebs(end,:)
%stress
%f_internal
%strain
end
end
end
end
end
%% ----------------------------------------------------------------------------
```

With Inputs:

```
function[Area_flex,E_flex,bar_c,Area_stirrup,E_stirrup,f_FRP_cu,f_cc,L_full,h_full,...
    d_eff,s_stirrup,bearing_s,bearing_P,z,P_exp,fflex,h_Cf,gamma_c,f_FRP_v] =
Input_MK(Beam,INF,INFd)
% known element properties (areas, elasticities, strengths)
%% For all beams
% Concrete
f_cc = 47.3; %MPa peak compressive strength of concrete
gamma_c = 2416.5; %kg/m3 concrete density
strain_cr = 0.0035; % crushing strain of concrete
alpha1 = 0.85-0.0015*f_cc; beta1 = 0.97-0.0025*f_cc; % ahlpha1 beta1
% Bearing Plates
bearing_s = 75; bearing_P = 50; %mm beraing plate widths

%Beam = 45.15; INF = 0;

%% For z=200 beams
if Beam < 100
z = 200; %mm beam width
L_full = 675; %mm beam geometries & spacing
```

```
% Stirrups
Area_stirrup = 2*113.1; %mm2 Area of bars
E_stirrup = 50*1000; %MPa elasticity of stirrups
% for FRP
f_FRP_cu = 1000; %MPa ultimate FRP strength
f_FRP_v = 700; %MPa ultimate FRP strength at bent

if INF==1
Area_stirrup = 2*113.1; %mm2 Area of bars
E_stirrup = 2.2; %MPa elasticity of stirrups
end
Beam2 = 0;
if floor(Beam)==45 || floor(Beam)==65
    f_cc = 50.3;
    L_full = 270*floor(Beam)/10;
    f_FRP_v = 560; %MPa ultimate FRP strength at bent
    Beam2 = Beam;
    Beam = Beam-(floor(Beam)-16);
end

%% BM Inputs
% BM12
if floor(Beam) == 12
% Flexural bars
ly_bar = 3; % Define # layers of bars
A_bar = [113,113,113]; h_bar = [47.7,80.1,112.5]; n_bar = [4,4,4]; % for bar layouts
Area_flex = sum(A_bar.*n_bar); % mm2 Area of bars
E_flex = 60*1000; %MPa elasticity of flexural bars
% Beam Height
h_full = 350; %mm
% Experimental Result
P_exp1 = [382.4,405.2,163.1]; % kN applied load from experiment.
%-----------------------------------------------------------------------------
% BM16
elseif floor(Beam) == 16
% Flexural bars
ly_bar = 2; % Define # layers of bars
A_bar = [201,201]; h_bar = [47+9.6,87+9.6]; n_bar = [3,3]; % for bar layouts
Area_flex = sum(A_bar.*n_bar); % mm2 Area of bars
E_flex = 64*1000; %MPa elasticity of flexural bars
% Beam Height
h_full = 345; %mm
% Experimental Result
P_exp1 = [309.34,416.5,150.2]; % kN applied load from experiment.
%-----------------------------------------------------------------------------
% BM25
elseif floor(Beam) == 25
% Flexural bars
ly_bar = 1; % Define # layers of bars
A_bar = [491]; h_bar = [37.9+22.2]; n_bar = [2]; % for bar layouts
Area_flex = sum(A_bar.*n_bar); % mm2 Area of bars
E_flex = 60*1000; %MPa elasticity of flexural bars
% Beam Height
h_full = 330; %mm
% Experimental Result
P_exp1 = [360.1,415.8,125.1]; % kN applied load from experiment.
end

if floor(Beam2)==45
h_full = 350;
P_exp1 = [222.5;171.2;108];
elseif floor(Beam2)==65
h_full = 350;
```

```matlab
P_exp1 = [145.6,141.0];
end


%% Spacings
BeamS = round(Beam-floor(Beam),2);
if BeamS == 0.22
    s_stirrup = 220; P_exp = P_exp1(1);
elseif BeamS == 0.15
    s_stirrup = 150; P_exp = P_exp1(2);
elseif BeamS == 0.09
    s_stirrup = 90; P_exp = P_exp1(1);
end

end

%% For stiffer stirrup beams
if Beam>=100
z = 230; %mm beam width
L_full = 675; %mm beam geometries & spacing
% Stirrups
Area_stirrup = 2*314.2; %mm2 Area of bars
E_stirrup = 50*1000; %MPa elasticity of stirrups
% for FRP
f_FRP_cu = 900; %MPa ultimate FRP strength
f_FRP_v = 550; %MPa ultimate FRP strength at bent
%% BM Inputs
% BM12
if Beam == 112
% Flexural bars
ly_bar = 3; % Define # layers of bars
A_bar = [113,113,113]; h_bar = [62.7,95.1,127.5]; n_bar = [4,4,4]; % for bar layouts
Area_flex = sum(A_bar.*n_bar); % mm2 Area of bars
E_flex = 60*1000; %MPa elasticity of flexural bars
% Beam Height
h_full = 365; %mm
% Experimental Result
P_exp = 466.9; % kN applied load from experiment.
%--------------------------------------------------------------------------------
% BM16
elseif Beam == 116
% Flexural bars
ly_bar = 3; % Define # layers of bars
A_bar = [201,201,201]; h_bar = [56.5,74.4,111.6]; n_bar = [1,2,3]; % for bar layouts
Area_flex = sum(A_bar.*n_bar); % mm2 Area of bars
E_flex = 64*1000; %MPa elasticity of flexural bars
% Beam Height
h_full = 360; %mm
% Experimental Result
P_exp = 450.8; % kN applied load from experiment.
%--------------------------------------------------------------------------------
% BM25
elseif Beam == 125
% Flexural bars
ly_bar = 1; % Define # layers of bars
A_bar = [491]; h_bar = [30+25+22.5]; n_bar = [2]; % for bar layouts
Area_flex = sum(A_bar.*n_bar); % mm2 Area of bars
E_flex = 60*1000; %MPa elasticity of flexural bars
% Beam Height
h_full = 345; %mm
% Experimental Result
P_exp = 444; % kN applied load from experiment.
end
```

```
%% Spacings
s_stirrup = 230;
end

%% Computed Values
% Geometries
for i = 1:ly_bar
    Ah_bar(i) = A_bar(i)*n_bar(i)*h_bar(i);
end
bar_c = sum(Ah_bar)/Area_flex; %mm location of center of flexural bars
d_eff = h_full-bar_c; % effective depth
if INF==1
    s_stirrup = L_full/INFd; P_exp = P_exp1(3);
end
% Flexural Reinf.
rou_f = Area_flex/(z*d_eff);
fflex = rou_f*E_flex;
% Compute c (stress strain block when strain_c reaches strain_cu)
aa = alpha1*f_cc*beta1*z;
bb = E_flex*Area_flex*strain_cr;
cc = -bb*d_eff;
h_Cf = (-bb+sqrt(bb^2-4*aa*cc))/(2*aa);
h_Cf = beta1*h_Cf;

end
```

For beams tested by D. J. Kim et al. (2014)

```
clc, clear all, close all, format short
%% Initial Inputs
% Beams
Beam1 = [1:7;11:17;21:27];
Beam1 = [Beam1(1,:),Beam1(2,:)];
%Beam1 = Beam1(16);
% ST Model
Model_num1 = [1]; %[1Krall, 2no_stir, 3whole_deep, 4half_deep, 5slender]
% Softening Factor
sfModel1= [1,2.1,3,3.2]; lim = 0; %lim is only for 3, input 0 or 0.4
                        %2.1 based on theta, 2.2 based on L/d, 2.3 based on s/d;
                        % 3 based on theta, 3.01 modified for elasticities
                        % 3.1 based on s/d, 3.2 based on ex ey
% Assumed Concrete Properties
mode = [1,1.1,2.1]; % Put 1 for Hognestad; 2 for Thorenfeldt; 3 for Feentra

%% Figure on/off
fi=0;
fid=0;
fisf=0;

%% Models
for ib = 1:numel(Beam1)
Beam = Beam1(ib); INF = 1; INFd1 = [5];
for im = 1
Model_num = Model_num1(im);
for isf = 4
sfModel = sfModel1(isf);
if Model_num==2 && sfModel==1
    sfModel=1.1;
end
for iss = 1:numel(mode)
    model = mode(iss);
for inf = 1%numel(INFd1)
    INFd = INFd1(inf);


Name = [Beam,Model_num,sfModel,model,INF,INFd];
fprintf('\n------------\nBM-%g, ST# %g, SF# %g, M %g, INF %g, INFd %g',Name)

%% Inputs
[Area_flex,E_flex,bar_c,Area_stirrup,E_stirrup,f_FRP_cu,f_cc,L_full,h_full,d_eff,...
    s_stirrup,bearing_s,bearing_P,z,P_exp,fflex,h_Cf,gamma_c] =
Input_Kim(Beam,INF,INFd);
%h_Ci = h_Cf;
%h_Ci = 0.65*f_FRP_cu*Area_flex/(0.85*f_cc*z);
h_Ci = 0.2*d_eff;
aaa = 1;

[e,n,nodes,conn,e_s_pris,e_s_bottle,e_s,e_b_flex,e_b_stirrup,e_b,...
    nodes_defined,defined_dimensions,nodes_nocheck,nodes_C,Rstrut_C,nodes_T,...
    Rstrut_T,nodes_load,ndof,fixed_dofs,fixed_u,free_dofs,dof_load,h_T,a]...
    = Model(Model_num,h_Ci,bar_c,L_full,s_stirrup,bearing_s,bearing_P,d_eff);


%% Plot Original truss------------------------------------------------------------
if fi ==1
figure(1);
for i = 1:e
    element_x(i,:)=nodes(1,[conn(i,1),conn(i,2)]);
    element_y(i,:)=nodes(2,[conn(i,1),conn(i,2)]);
```

```
    locx=max(element_x(i,:))-s_stirrup/2; locy=max(element_y(i,:));
    lxx = min(element_x(i,:))+(max(element_x(i,:))-min(element_x(i,:)))*2/3;
    if ismember(i,e_b_flex)
    plot(element_x(i,:),element_y(i,:),'k-')
    if i==1
        text(max(element_x(i,:))/2, locy+7, num2str(i))
    else
        text(locx, locy+7, num2str(i))
    end
    elseif ismember(i,e_b_stirrup)
    plot(element_x(i,:),element_y(i,:),'k-')
    text(max(element_x(i,:))-15, locy/2, num2str(i))
    elseif ismember(i,e_s_pris)
    plot(element_x(i,:),element_y(i,:),'r--')
    text(locx, locy+7, num2str(i))
    elseif ismember(i,e_s_bottle)
        plot(element_x(i,:),element_y(i,:),'r--')
        if max(element_x(i,:))-min(element_x(i,:))==L_full
        text(max(element_x(i,:))*3/4-10, locy*3/4, num2str(i))
        else
            text(lxx, locy*2/3, num2str(i))
        end
    end
    hold on
end
for i = 1:n
    txt= sprintf('N%d',i);
    text(nodes(1,i),nodes(2,i),txt)
end
end

%% element geometries
[theta, Nodalzone, Area, Length] = Geometry(e,n,conn, nodes,...
    nodes_defined,defined_dimensions,h_Ci,nodes_C,Rstrut_C,h_T,nodes_T,...
    Rstrut_T,e_b_flex,e_b_stirrup,e_s_pris,Area_flex,Area_stirrup,z);

%% Analysis
% Initial Parameters
P_in = 0; %N initial applied load set to be 0
P_inc = -10; %N add 10N applied load every loop
strain_c = zeros(1,e); % initial strain set to be 0
P_max = -500E3; % N to define maximum number of loops
[E_origi,strain0,aabb,Ec] = Elasticity(e,e_b_flex,E_flex,e_b_stirrup,E_stirrup,...
    e_s_bottle,strain_c,e_s_pris,model,f_cc,L_full,d_eff,theta,sfModel,lim,...
    a,conn,fflex,s_stirrup,gamma_c);

% Checks
% strut check
E_check = 0.01*E_origi;
% system check
Uns_check_1 = e-2*n+4;
Uns_check_2 = size(find(conn(:,2)==n),1);
if Uns_check_2>1
    Uns_check_2=Uns_check_2-1;
end
Unstable_check = min(Uns_check_1);%,Uns_check_2);
if INF ==1
Unstable_check = 1;
end
% nodalzone check
lim_CCC = 0.85*f_cc; lim_CCT = 0.75*f_cc; lim_CTT = 0.65*f_cc;
% FRP check
lim_FRP = f_FRP_cu;
```

```
% Iterative IST Analysis
[d,r,stress,strain,f_internal,E_end,Ebs,strain0_end,sfb,P_fail,h_C]...
    =ISTAnalysis(P_max,P_in,P_inc,h_Ci,nodes_nocheck,E_origi,E_flex,...
    E_stirrup,model,f_cc,E_check,lim_CCC,lim_CCT,lim_CTT,lim_FRP,INF,...
    Model_num,bar_c,bearing_s,bearing_P,Unstable_check,z,P_exp,L_full,...
    d_eff,sfModel,lim,a,fflex,s_stirrup,Area_flex,Area_stirrup,gamma_c,aaa,h_full);

%% Plot softening factor
if ismember(sfModel,[3,3.1,3.2]) && fisf==1
figure('Name',num2str(sfModel));
for ii = 1:size(e_s_bottle,2)
Px=0:P_inc:P_fail*2;
sfy=sfb(:,ii);
plot(-Px/1000,sfy')
Leg{ii}=sprintf('S%d',e_s_bottle(ii));
end
legend(Leg','Location','southwest')
xlabel('P(kN)')
ylabel('Soften Factors')
hold on
end
SoftenF_end=sfb(end-10,:);
softenF_end_E = SoftenF_end(end)

%% Plot Deformed Shape
if fid ==1
for ii =1:n
    dx(ii)=d(ii*2-1);
    dy(ii)=d(ii*2);
end
nodes_new(1,:) = nodes(1,:)+dx;
nodes_new(2,:) = nodes(2,:)+dy;

figure(1);
for ii = 1:e
    element_x(ii,:)=nodes_new(1,[conn(ii,1),conn(ii,2)]);
    element_y(ii,:)=nodes_new(2,[conn(ii,1),conn(ii,2)]);
    if ismember(ii,e_b)
    plot(element_x(ii,:),element_y(ii,:),'b-')
    elseif ismember(ii,e_s)
    plot(element_x(ii,:),element_y(ii,:),'g--')
    end
    hold on
end
dx=[]; dy=[]; nodes_new=[];
end
close all
h_C
%f_internal
end
end
end
end
end
f_internal;
strain;
%% -----------------------------------------------------------------------
```

With Inputs

```
function[Area_flex,E_flex,bar_c,Area_stirrup,E_stirrup,f_FRP_cu,f_cc,L_full,h_full,...
    d_eff,s_stirrup,bearing_s,bearing_P,z,P_exp,fflex,h_Ci,gamma_c] =
Input_Kim(Beam,INF,INFd)
% known element properties (areas, elasticities, strengths)
%Beam = 350
%INF = 1; INFd = 70;
%% For all beams
% Beam
z=200;
bar_c=45;
% Imaginary Stirrups
if INF==1
Area_stirrup = 400; %mm2 Area of bars
E_stirrup = 1; %MPa elasticity of stirrups
else
Area_stirrup = 400; %mm2 Area of bars
E_stirrup = 1; %MPa elasticity of stirrups
end
% Reinf.
Abar = 63.62; %mm^2 per AFRP/CFRP bar
% Concrete
f_cc = 26.1; %MPa peak compressive strength of concrete
gamma_c = 0; %kg/m3 concrete density not specified
strain_cr = 0.0035; % crushing strain of concrete
% Bearing Plates
bearing_s = 100; bearing_P = 100; %mm beraing plate widths
% Beam
d_eff = [250,250,250,250,250,190,310];
ad = [1.4,1.7,2.1,1.7,1.7,1.7,1.7]; %mm beam geometries & spacing
% Reinf.
Nbar = [3,3,3,4,5,3,5];

%% Variables
if Beam < 10
%% For AFRP
E_flex = 80697; %MPa elasticity of flexural bars
f_FRP_cu = 1826.9; %MPa ultimate FRP strength
% Experimental Result
P_exp1 = [136.05,98.98,88,121,133.97,109.58,134.27]; %kN failure load from lab.
iND = Beam;
% different ones
Area_flex = Abar*Nbar(iND);
L_full = d_eff(iND)*ad(iND);
P_exp = P_exp1(iND);
d_eff = d_eff(iND);

elseif Beam < 20
%% For CFRP
E_flex = 120214; %MPa elasticity of flexural bars
f_FRP_cu = 1955.8; %MPa ultimate FRP strength
% Experimental Result
P_exp1 = [169.58,106.54,52.64,96.09,151.39,104.84,145.39]; %kN failure load from lab.
iND = Beam-10;
% different ones
Area_flex = Abar*Nbar(iND);
L_full = d_eff(iND)*ad(iND);
P_exp = P_exp1(iND);
d_eff = d_eff(iND);

else
```

```
%% For Steel Reinforced
E_flex = 200000; %MPa elasticity of flexural bars
f_FRP_cu = 40000; %MPa ultimate FRP strength
% Experimental Result
P_exp1 = [169.58,106.54,52.64,96.09,151.39,104.84,145.39]; %kN failure load from lab.
iND = Beam-20;
% different ones
Area_flex = Abar*Nbar(iND);
L_full = d_eff(iND)*ad(iND);
P_exp = P_exp1(iND);
d_eff = d_eff(iND);
end

%% Computed Values
% Geometries
h_full = d_eff+bar_c; %mm
% Spacings
if INF==1
    s_stirrup = L_full/INFd;
else
    s_stirrup = L_full;
end
% Flexural Reinf.
rou_f = Area_flex/(z*d_eff);
fflex = rou_f*E_flex;
% Compute c (stress strain block when strain_c reaches strain_cu)
alpha1 = 0.85-0.0015*f_cc; beta1 = 0.97-0.0025*f_cc; % ahlpha1 beta1
aa = alpha1*f_cc*beta1*z;
bb = E_flex*Area_flex*strain_cr;
cc = -bb*d_eff;
h_Ci = (-bb+sqrt(bb^2-4*aa*cc))/(2*aa);

end
 %% ----------------------------------------------------------------------
```

With Functions:

```
function [E,strain0,sf_bottle,Ec] =
Elasticity(e,e_b_flex,E_flex,e_b_stirrup,E_stirrup,...
    e_s_bottle,strain_c,e_s_pris,model,f_cc,L_full,d_eff,theta,sfModel,lim,...
    a,conn,fflex,s_stirrup,gamma_c)

if gamma_c == 0
Ec = 4500*sqrt(f_cc);
else
Ec = (3300*sqrt(f_cc)+6900)*(gamma_c/2300)^1.5; % initial concrete elasticity
end

E = zeros(1,e);

% softening factor

[sf_bottle,sf_pris] = FSoften(sfModel,L_full,d_eff,e_s_bottle,...
    e_s_pris,theta,lim,strain_c,f_cc,Ec,a,conn,fflex,s_stirrup,E_flex);

for i = 1:e

if ismember(i,e_b_flex)==1
            E(i) = E_flex;
elseif ismember(i,e_b_stirrup)==1
            E(i) = E_stirrup;

elseif floor(model)==1
        if ismember(i,e_s_bottle)==1
            sf = sf_bottle(i);
        elseif ismember(i,e_s_pris)==1
            sf = sf_pris(i);
        end
        f_cp = sf*f_cc;
        strain0 = 2*f_cc/Ec;
        if model==floor(model)
            k_b = strain_c(i)/strain0;
            if k_b <=1
                E(i)=2*f_cp/strain0*(1-k_b); %strain0 stays as the same
            else
                E(i) =Ec-2*Ec^2/(4*f_cp)*strain_c(i);
            end
        elseif model-floor(model)<0.2
            k_b = strain_c(i)/strain0/sf;
            if k_b <=1
                E(i)=2*f_cc/strain0*(1-k_b); %strain0 moves to left with f'c
            else
                E(i) =Ec-2*Ec^2/(4*f_cp)*strain_c(i);
            end
        end


elseif floor(model)==2
        if ismember(i,e_s_bottle)==1
            sf = sf_bottle(i);
        elseif ismember(i,e_s_pris)==1
            sf = sf_pris(i);
        end
        f_cp = sf*f_cc;
        if model==floor(model)
        n = 0.8+ f_cc/17;
        strain0 = f_cc/Ec*n/(n-1);
```

```
        a_a = strain_c(i)/strain0;
        a_b = f_cp*n/strain0;
        elseif (model-floor(model))<0.2
        n = 0.8+ f_cp/17;
        strain0 = f_cc/Ec*n/(n-1);
        a_a = strain_c(i)/strain0/sf;
        a_b = f_cc*n/strain0;
        end
            if a_a<=1
                k = 1;
            else
                k = 0.67+ f_cc/62;
            end
        b_b = n-1;
        c_b = a_a^(n*k);
        E(i) = a_b/(b_b+c_b)*(1-(n*k*c_b)/(b_b+c_b));


elseif floor(model)==3
    if ismember(i,e_s_bottle)==1
            sf = sf_bottle(i);
        elseif ismember(i,e_s_pris)==1
            sf = sf_pris(i);
    end
    f_cp = sf*f_cc;
    e03 = f_cc/(3*Ec);
    strain0 = 5*e03;
    E(i) = 4*f_cp/(3*(strain0-e03)^2)*(strain0-strain_c(i));

end

end

end
%% -----------------------------------------------------------------------




%% -----------------------------------------------------------------------
function [d,r,strain,stress,f_internal]=FEASystem(ndof,e,conn,theta,Area,E,Length,...
    dof_load,fixed_dofs,free_dofs,fixed_u,P)
%% Stiffness Matricx
K = zeros(ndof,ndof);
for i = 1:e
    k_conn = conn(i,:);
    enodes = [2*k_conn(1)-1, 2*k_conn(1), 2*k_conn(2)-1, 2*k_conn(2)];
    c = cosd(theta(i));
    s = sind(theta(i));
    f_K = Area(i)*E(i)/Length(i);
    % Local Stiffness matrices
    Ke = f_K*[c^2, c*s, -c^2, -c*s;
              c*s, s^2, -c*s, -s^2;
              -c^2, -c*s, c^2, c*s;
              -c*s, -s^2, c*s, s^2];
    % Tranfer to Global system
    K(enodes,enodes) = K(enodes,enodes)+Ke;
end

K_EE = K(fixed_dofs,fixed_dofs); %for K_EE
K_EF = K(fixed_dofs,free_dofs); % K_EF
K_FF = K(free_dofs,free_dofs); % K_FF
```

```
%% Load matrix
f = zeros(ndof,1);
f(dof_load) = P;
f_F = f(free_dofs); % known external forces on the free nodes

%% Displacemnt matrix
d = zeros(ndof,1);
d(fixed_dofs) = fixed_u;
dE = d(fixed_dofs);

%% Compute unknowns (displacements and reactions)
dF = (K_FF)\(f_F-K_EF'*dE); % compute the unknown displacements

f_E = K_EE*dE+K_EF*dF; % Force at the fixed end
r = f_E-f(fixed_dofs); % Reaction at the fixed end

d(fixed_dofs) = dE; % Transfer d_E to d matrix
d(free_dofs) = dF; % Transfer d_F to d matrix


%% Compute strain stress and internal forces
strain = zeros(e,1);
for i = 1:e
    s_conn = conn(i,:);
    enodes = [2*s_conn(1)-1, 2*s_conn(1), 2*s_conn(2)-1, 2*s_conn(2)];
    c = cosd(theta(i));
    s = sind(theta(i));
    strain_e = [-c, -s, c, s]*d(enodes)/Length(i);
    strain(i) = strain_e;
end

stress = zeros(e,1);
for i = 1:e
    stress(i) = E(i)*strain(i);
end

f_internal = zeros(e,1);
for i = 1:e
    f_internal(i) = stress(i)*Area(i);
end

end
%% ------------------------------------------------------------------------
```

```
%% ------------------------------------------------------------------------
function [sf_bottle,sf_pris] = FSoften(sfModel,L_full,d_eff,e_s_bottle,...
    e_s_pris,theta,lim,strain_c,f_cc,Ec,a,conn,fflex,s_stirrup,E_flex)

if sfModel ==0
    sf_bottle(e_s_bottle) = 1;
    sf_pris(e_s_pris) = 1;

elseif sfModel ==1
    sf_bottle(e_s_bottle) = 0.85*0.75;
    sf_pris(e_s_pris) = 0.85;
```

```
elseif sfModel ==1.1
    sf_bottle(e_s_bottle) = 0.85*0.4;
    sf_pris(e_s_pris) = 0.85;

elseif sfModel ==2.1
    sf_pris(e_s_pris) = 0.85;
    for i = e_s_bottle
        aod = 1/(tand(theta(i)));
        if aod < 1.5
            aod = 1.5;
        elseif aod > 2.5
            aod = 2.5;
        end
    if fflex^(1/3)<=10
        sf_bottle(i) = 0.68-0.012*aod^4;
    else
        sf_bottle(i) = 0.75-0.01*aod^4;
    end
        sf_bottle(i)=0.85*sf_bottle(i);
    end

elseif sfModel ==2.2
    sf_pris(e_s_pris) = 0.85;
    aod = L_full/d_eff;
    if aod < 1.5
       aod = 1.5;
    elseif aod > 2.5
       aod = 2.5;
    end
    if fflex^(1/3)<=10
        sf_a = 0.68-0.012*aod^4;
    else
        sf_a = 0.75-0.01*aod^4;
    end
    sf_bottle(e_s_bottle)=0.85*sf_a;

elseif sfModel ==2.3
    sf_pris(e_s_pris) = 0.85;
    aod = s_stirrup/d_eff;
    if aod < 1.5
       aod = 1.5;
    elseif aod > 2.5
       aod = 2.5;
    end
    if fflex^(1/3)<=10
        sf_a = 0.68-0.012*aod^4;
    else
        sf_a = 0.75-0.01*aod^4;
    end
    sf_bottle(e_s_bottle)=0.85*sf_a;

elseif sfModel ==3
    sf_pris(e_s_pris) = 0.85;
    s0 = -2*f_cc/Ec;
    strain = -strain_c;
    for i = e_s_bottle
        if strain(i) == 0
            sf = 0.85;
        else
        ex = strain(conn(i,2)-a-1);
        e2 = strain(i);
        e1 = ex+(ex-e2)/(tand(theta(i)))^2;
```

```
        sf = 1/(0.8-0.34*e1/s0);
        end
        if sf>0.85
            sf=0.85;
        end
        if sf<lim
           sf=lim;
        end
        sf_bottle(i)=sf;
    end

elseif sfModel ==3.01
    sf_pris(e_s_pris) = 0.85;
    s0 = -2*f_cc/Ec;
    strain = -strain_c;
    for i = e_s_bottle
        if strain(i) == 0
            sf = 0.85;
        else
        ex = strain(conn(i,2)-a-1);
        %ex = E_flex/200000*ex;
        e2 = strain(i);
        e1 = ex+(ex-e2)/(tand(theta(i)))^2;
        e1 = E_flex/200000*e1;
        sf = 1/(0.8-0.34*e1/s0);
        end
        if sf>0.85
            sf=0.85;
        end
        if sf<lim
           sf=lim;
        end
        sf_bottle(i)=sf;
     end

elseif sfModel ==3.1
    sf_pris(e_s_pris) = 0.85;
    s0 = -2*f_cc/Ec;
    strain = -strain_c;
    for i = e_s_bottle
        if strain(i) == 0
            sf = 0.85;
        else
        ex = strain(conn(i,2)-a-1);
        e2 = strain(i);
        e1 = ex+(ex-e2)/(d_eff/s_stirrup)^2;
        sf = 1/(0.8-0.34*e1/s0);
        end
        if sf>0.85
            sf=0.85;
        end
        if sf<lim
           sf=lim;
        end
        sf_bottle(i)=sf;
    end

elseif sfModel ==3.2
    sf_pris(e_s_pris) = 0.85;
    s0 = -2*f_cc/Ec;
    strain = -strain_c;
    for i = e_s_bottle
        if strain(i) == 0
```

```
            sf = 0.85;
        else
        sizey=max(size((conn(i,1)+a+1):conn(i,2)));
        for ii = 1:sizey
            ey = strain(conn(i,2)+a-2+ii-sizey);
            ex = strain(conn(i,1)+ii-1);
            exey(ii)=ex+ey;
        end
        e2 = strain(i);
        e1 = max(exey)-e2;
        sf = 1/(0.8-0.34*e1/s0);
        end
        if sf>0.85
            sf=0.85;
        end
        sf_bottle(i)=sf;
    end

end

end
 %% -------------------------------------------------------------------------
```

```
%% -------------------------------------------------------------------------
function [theta, Nodalzone, Area, Length] = Geometry(e,n,conn, nodes,...
    nodes_defined,defined_dimensions,h_C,nodes_C,Rstrut_C,h_T,nodes_T,...
    Rstrut_T,e_b_flex,e_b_stirrup,e_s_pris,Area_flex,Area_stirrup,z)
theta = zeros(1,e);
for i = 1:e
    conn_e = conn(i,:);
    delta_x = nodes(1, conn_e(2))- nodes(1, conn_e(1));
    delta_y = nodes(2, conn_e(2))- nodes(2, conn_e(1));
    theta(i) = atand(delta_y/delta_x);
end

% nodal zones mm
Nodalzone = zeros(n,2);
for i = 1:n
    if ismember(i,nodes_defined)==1
        Nodalzone(i,:)=defined_dimensions(find(nodes_defined==i),:);
    elseif ismember(i,nodes_C)==1
        Nodalzone(i,1)=h_C*tand(theta(Rstrut_C(find(nodes_C==i))));
        Nodalzone(i,2)=h_C;
    elseif ismember(i,nodes_T)==1
        Nodalzone(i,1)=h_T*tand(theta(Rstrut_T(find(nodes_T==i))));
        Nodalzone(i,2)=h_T;
    else
        Nodalzone(i,:)=0;
    end
end

% Area of elements mm^2
Area = zeros(1,e);
for i = 1:e
    if ismember(i,e_b_flex)==1
        Area(i) = Area_flex;
    elseif ismember(i,e_b_stirrup)==1
        Area(i) = Area_stirrup;
```

```
    elseif ismember(i,e_s_pris)==1
        Area(i) = z*h_C;
    else
        s_conn = conn(i,:);
        s_width1 = Nodalzone(s_conn(1),1)*sind(theta(i))...
                   +Nodalzone(s_conn(1),2)*cosd(theta(i));
        s_width2 = Nodalzone(s_conn(2),1)*sind(theta(i))...
                   +Nodalzone(s_conn(2),2)*cosd(theta(i));
        Area(i) = z*min(s_width1, s_width2);
    end
end

% Length of elements mm
Length = zeros(1,e);
for i = 1:e
    l_conn = conn(i,:);
    Length(i) = sqrt((nodes(1,l_conn(1))-nodes(1,l_conn(2)))^2+...
                (nodes(2,l_conn(1))-nodes(2,l_conn(2)))^2);
end

end
%% -------------------------------------------------------------------------
```

```
%% -------------------------------------------------------------------------
function [d,r,stress,strain,f_internal,E_end,Ebs,strain0_end,sfb,P_fail,h_C]...
    =ISTAnalysis(P_max,P_in,P_inc,h_Ci,nodes_nocheck,E_origi,E_flex,...
    E_stirrup,model,f_cc,E_check,lim_CCC,lim_CCT,lim_CTT,lim_FRP,INF,...
    Model_num,bar_c,bearing_s,bearing_P,Unstable_check,z,P_exp,L_full,...
    d_eff,sfModel,lim,a,fflex,s_stirrup,Area_flex,Area_stirrup,gamma_c,aaa,h_full)

fail_location = []; exclude = nodes_nocheck; out = []; P_fail = 0;

for i = 1:(P_max/P_inc+1)

P = (P_in+P_inc*(i-1))/2;

fail_location_prev = fail_location;


%% Truss Model
% h_C
if i<2
    h_C = h_Ci;
else
    if aaa==1
    % Compute N.A. location (c)
    nn = E_flex/Ec;
    dd=d_eff-h_C;
    s_cTlim = 0.33*sqrt(f_cc)/Ec;
    s_FRP = -P*L_full/(dd*Area_flex*E_flex);
    if s_FRP < s_cTlim
        % Uncracked concrete
        Aconc = h_full*z; yconc=h_full/2;
        Afrp = (nn-1)*Area_flex;
```

```
        c = (Aconc*yconc+Afrp*d_eff)/(Aconc+Afrp);
    else
        % Cracked concrete
        rouflex=Area_flex/(d_eff*z);
        rounn=rouflex*nn;
        c = (sqrt(2*rounn+rounn^2)-rounn)*d_eff;
    end
    % Compute top fibre strain and beta1
    f_c1=f_cc;
    strain00 = 2*f_c1/Ec;
    AA=-1; BB=3*strain00;
    CC=-3*strain00^2*(-P)*L_full/dd/z/f_c1/c;
    DD=BB^2-4*AA*CC;
    if DD<0
    DD=0;
    %P_fail=P;
    %fprintf('\nFlexural Failure\n')
    end
    strain_ctop=(-BB+sqrt(DD))/2/AA;
    b1 = (4*strain00-strain_ctop)/(6*strain00-2*strain_ctop);
    % Actual hc under this load.
    h_C = b1*c;
    end
end
% Geometries
[e,n,nodes,conn,e_s_pris,e_s_bottle,e_s,e_b_flex,e_b_stirrup,e_b,...
    nodes_defined,defined_dimensions,nodes_nocheck,nodes_C,Rstrut_C,nodes_T,...
    Rstrut_T,nodes_load,ndof,fixed_dofs,fixed_u,free_dofs,dof_load,h_T,a]...
    = Model(Model_num,h_C,bar_c,L_full,s_stirrup,bearing_s,bearing_P,d_eff);

[theta, Nodalzone, Area, Length] = Geometry(e,n,conn,nodes,...
    nodes_defined,defined_dimensions,h_C,nodes_C,Rstrut_C,h_T,nodes_T,...
    Rstrut_T,e_b_flex,e_b_stirrup,e_s_pris,Area_flex,Area_stirrup,z);

%% Analysis
% Elasticity MPa (softened Hognestad Parabola)
if i == 1
    E = E_origi;
else
    E = E_loop;
end

% Solving system (FEA)
[d,r,strain,stress,f_internal]=FEASystem(ndof,e,conn,theta,Area,E,Length,...
    dof_load,fixed_dofs,free_dofs,fixed_u,P);

% Check new Elasticity MPa
strain_c = -strain;
[E_loop,strain0,ccc,Ec] = Elasticity(e,e_b_flex,E_flex,e_b_stirrup,E_stirrup,...
    e_s_bottle,strain_c,e_s_pris,model,f_cc,L_full,d_eff,theta,sfModel,lim,...
    a,conn,fflex,s_stirrup,gamma_c);
fl_a = find(E_loop<=E_check);
if size(fl_a,2) > size(fail_location,2)
    fail_location = fl_a;
end
E_loop(fail_location) = E_check(fail_location);

if isempty(fail_location) == 1
    fail_location_prev = 0;
end

ssf(i,:)=ccc;
Esf(i,:)= E_loop;
```

```
%% Checks-----------------------------------------------------------------
% Check FRP Rupture
for ib = setdiff(e_b,out)
    s_b(ib) = stress(ib);

    if s_b(ib) >= lim_FRP
        P_fail = P;
        fprintf('Bar %d failed @ P = %f kN\n',ib, -2*P/1000)
        out = union(out,ib);
    end

end

% Check Node Strengths
for in = setdiff(1:n,exclude)
    [sc_node, direc] = find(conn==in);
    Anodex = Nodalzone(in,1)*z;
    Anodey = Nodalzone(in,2)*z;
    Anodexy = sqrt((Anodex/z)^2+(Anodey/z)^2)*z;

    if sum(ismember(sc_node, e_b))>=2
        Nodecheck = lim_CTT;
    elseif sum(ismember(sc_node, e_b))==1
        Nodecheck = lim_CCT;
    else
        Nodecheck = lim_CCC;
    end
    if in==nodes_load
        Nodecheck = lim_CCC;
    end

    direc(ismember(sc_node,e_b))=[];
    sc_node = setdiff(sc_node,e_b);

    f_x1 = sum(f_internal(sc_node(direc==1))'.*cosd(theta(sc_node(direc==1))));
    f_y1 = sum(f_internal(sc_node(direc==1))'.*sind(theta(sc_node(direc==1))));
    f_xy1 = sqrt(f_x1^2 + f_y1^2);
    f_x2 = sum(f_internal(sc_node(direc==2))'.*cosd(theta(sc_node(direc==2))));
    f_y2 = sum(f_internal(sc_node(direc==2))'.*sind(theta(sc_node(direc==2))));
    f_xy2 = sqrt(f_x2^2 + f_y2^2);
    s_xy1(in) = f_xy1/Anodexy; s_xy2(in) = f_xy2/Anodexy;

    if sum([s_xy1(in), s_xy2(in)]>=Nodecheck)>=1
        P_fail = P;
        fprintf('\nNode %d failed @ P = %.2f kN\n',in, -2*P/1000)
        exclude = union(exclude,in);
    end
end

% Check the crushing of struts

%if aaa==1
%fail_location1 = fail_location;
%for ifl=1:numel(fail_location)
    %if ismember(fail_location(ifl), e_s_pris)==1
        %fail_location1(ifl)=[];
    %end
%end
%fail_location = fail_location1;
%end
```

```
if fail_location~=0
    if size(fail_location,2) ~= size(fail_location_prev,2)
        if size(fail_location,2)<=Unstable_check
        fprintf('\n#%d element failed', fail_location)
        fprintf('\n@ P = %.4f kN\n', -P*2/1000)
        end
        if size(fail_location,2)==Unstable_check
        P_fail = P;
        elseif size(fail_location,2)<Unstable_check
        fprintf('System not yet failed\n')
        end
    end
end

if P_fail ~= 0
        fprintf('System Failed\n\n')
    if INF ==1
        P = f_internal(end)*(sind(theta(end)));
    end
        P_predict = -P*2/1000; % kN
        ratio = P_predict/P_exp;
        fprintf('Predicted Applied load is %.2f kN\n', P_predict)
        fprintf('P_predict/P_exp = %.4f\n', ratio)
        break
           if exclude == nodes_nocheck
              fprintf('\nNo Nodal section is failed\n')
           end
           if isempty(out) == 1
               fprintf('\nNo FRP bar is failed\n')
           end
elseif i == (P_max/P_inc+1)
P_fail = P;
if size(fail_location,2)==0
    disp('No element has failed, increase P_max')
elseif size(fail_location,2)<Unstable_check
    disp('\nIncrease P_max')
end
end

end

E_end = E_loop;
strain0_end = strain0;
sfb=ssf(:,e_s_bottle);
Ebs = Esf(:,e_s_bottle);

end
%% ------------------------------------------------------------------------
```

B: General Results for Concrete Model Comparison on Beams with Stirrups

ISTM Type	Beam	sfModel	model	StrengthV	over H1
Kr Model	BM12-220	ACI	H1	359.43	1.131956
Kr Model	BM12-220	ACI	H2	317.53	1
Kr Model	BM12-220	ACI	T1	384.22	1.210027
Kr Model	BM12-220	ACI	T2	322.85	1.016754
Kr Model	BM12-220	Nehdi	H1	274.8	1.147774
Kr Model	BM12-220	Nehdi	H2	239.42	1
Kr Model	BM12-220	Nehdi	T1	290.91	1.215061
Kr Model	BM12-220	Nehdi	T2	285.2	1.191212
Kr Model	BM12-220	CSA	H1	249.64	1.042861
Kr Model	BM12-220	CSA	H2	239.38	1
Kr Model	BM12-220	CSA	T1	295.55	1.234648
Kr Model	BM12-220	CSA	T2	285.19	1.191369
Kr Model	BM12-220	Proposed	H1	284.15	1.143369
Kr Model	BM12-220	Proposed	H2	248.52	1
Kr Model	BM12-220	Proposed	T1	295.7	1.189844
Kr Model	BM12-220	Proposed	T2	249.41	1.003581
Kr Model	BM12-150	ACI	H1	260.12	1.118844
Kr Model	BM12-150	ACI	H2	232.49	1
Kr Model	BM12-150	ACI	T1	285.43	1.227709
Kr Model	BM12-150	ACI	T2	254.09	1.092907
Kr Model	BM12-150	Nehdi	H1	205.36	0.962866
Kr Model	BM12-150	Nehdi	H2	213.28	1
Kr Model	BM12-150	Nehdi	T1	254.38	1.192704
Kr Model	BM12-150	Nehdi	T2	254.1	1.191392
Kr Model	BM12-150	CSA	H1	211.76	0.992966
Kr Model	BM12-150	CSA	H2	213.26	1
Kr Model	BM12-150	CSA	T1	262.14	1.229204
Kr Model	BM12-150	CSA	T2	254.09	1.191456
Kr Model	BM12-150	Proposed	H1	224.24	1.051388
Kr Model	BM12-150	Proposed	H2	213.28	1
Kr Model	BM12-150	Proposed	T1	262.49	1.23073
Kr Model	BM12-150	Proposed	T2	254.12	1.191485
Kr Model	BM12-s230	ACI	H1	379.3	0.994181
Kr Model	BM12-s230	ACI	H2	381.52	1
Kr Model	BM12-s230	ACI	T1	460.97	1.208246
Kr Model	BM12-s230	ACI	T2	446.25	1.169663
Kr Model	BM12-s230	Nehdi	H1	337.06	0.98426
Kr Model	BM12-s230	Nehdi	H2	342.45	1
Kr Model	BM12-s230	Nehdi	T1	418.4	1.221784

Kr Model	BM12-s230	Nehdi	T2	363.02	1.060067
Kr Model	BM12-s230	CSA	H1	306.54	1.108483
Kr Model	BM12-s230	CSA	H2	276.54	1
Kr Model	BM12-s230	CSA	T1	358.5	1.296377
Kr Model	BM12-s230	CSA	T2	308.37	1.115101
Kr Model	BM12-s230	Proposed	H1	371.12	0.979105
Kr Model	BM12-s230	Proposed	H2	379.04	1
Kr Model	BM12-s230	Proposed	T1	452.12	1.192803
Kr Model	BM12-s230	Proposed	T2	424.2	1.119143
Kr Model	BM16-220	ACI	H1	363.07	1.123569
Kr Model	BM16-220	ACI	H2	323.14	1
Kr Model	BM16-220	ACI	T1	391.34	1.211054
Kr Model	BM16-220	ACI	T2	329.42	1.019434
Kr Model	BM16-220	Nehdi	H1	277.4	1.159021
Kr Model	BM16-220	Nehdi	H2	239.34	1
Kr Model	BM16-220	Nehdi	T1	290.88	1.215342
Kr Model	BM16-220	Nehdi	T2	285.09	1.191151
Kr Model	BM16-220	CSA	H1	249.63	1.043168
Kr Model	BM16-220	CSA	H2	239.3	1
Kr Model	BM16-220	CSA	T1	295.49	1.23481
Kr Model	BM16-220	CSA	T2	285.12	1.191475
Kr Model	BM16-220	Proposed	H1	284.99	1.143941
Kr Model	BM16-220	Proposed	H2	249.13	1
Kr Model	BM16-220	Proposed	T1	297.09	1.19251
Kr Model	BM16-220	Proposed	T2	249.63	1.002007
Kr Model	BM16-150	ACI	H1	262.96	1.117457
Kr Model	BM16-150	ACI	H2	235.32	1
Kr Model	BM16-150	ACI	T1	288.88	1.227605
Kr Model	BM16-150	ACI	T2	254	1.079381
Kr Model	BM16-150	Nehdi	H1	205.34	0.963133
Kr Model	BM16-150	Nehdi	H2	213.2	1
Kr Model	BM16-150	Nehdi	T1	254.35	1.193011
Kr Model	BM16-150	Nehdi	T2	254	1.19137
Kr Model	BM16-150	CSA	H1	211.7	0.993058
Kr Model	BM16-150	CSA	H2	213.18	1
Kr Model	BM16-150	CSA	T1	262.06	1.22929
Kr Model	BM16-150	CSA	T2	253.99	1.191434
Kr Model	BM16-150	Proposed	H1	224.42	1.052627
Kr Model	BM16-150	Proposed	H2	213.2	1
Kr Model	BM16-150	Proposed	T1	262.41	1.230816
Kr Model	BM16-150	Proposed	T2	254.03	1.19151
Kr Model	BM16-s230	ACI	H1	374.66	0.99755
Kr Model	BM16-s230	ACI	H2	375.58	1
Kr Model	BM16-s230	ACI	T1	453.87	1.208451

Kr Model	BM16-s230	ACI	T2	438.28	1.166942
Kr Model	BM16-s230	Nehdi	H1	335.32	0.964422
Kr Model	BM16-s230	Nehdi	H2	347.69	1
Kr Model	BM16-s230	Nehdi	T1	415.08	1.193822
Kr Model	BM16-s230	Nehdi	T2	374.86	1.078144
Kr Model	BM16-s230	CSA	H1	304.26	1.100637
Kr Model	BM16-s230	CSA	H2	276.44	1
Kr Model	BM16-s230	CSA	T1	350.88	1.269281
Kr Model	BM16-s230	CSA	T2	302.58	1.094559
Kr Model	BM16-s230	Proposed	H1	367.64	0.983415
Kr Model	BM16-s230	Proposed	H2	373.84	1
Kr Model	BM16-s230	Proposed	T1	447.25	1.196367
Kr Model	BM16-s230	Proposed	T2	415.03	1.110181
Kr Model	BM25-220	ACI	H1	370.67	1.035738
Kr Model	BM25-220	ACI	H2	357.88	1
Kr Model	BM25-220	ACI	T1	400.89	1.12018
Kr Model	BM25-220	ACI	T2	372.68	1.041355
Kr Model	BM25-220	Nehdi	H1	290.73	1.217411
Kr Model	BM25-220	Nehdi	H2	238.81	1
Kr Model	BM25-220	Nehdi	T1	290.69	1.217244
Kr Model	BM25-220	Nehdi	T2	284.46	1.191156
Kr Model	BM25-220	CSA	H1	248.87	1.042082
Kr Model	BM25-220	CSA	H2	238.82	1
Kr Model	BM25-220	CSA	T1	283.83	1.188468
Kr Model	BM25-220	CSA	T2	256.65	1.074659
Kr Model	BM25-220	Proposed	H1	288.08	1.13079
Kr Model	BM25-220	Proposed	H2	254.76	1
Kr Model	BM25-220	Proposed	T1	306.25	0
Kr Model	BM25-220	Proposed	T2	252.65	0.991718
Kr Model	BM25-150	ACI	H1	280.76	1.109153
Kr Model	BM25-150	ACI	H2	253.13	1
Kr Model	BM25-150	ACI	T1	310.74	0
Kr Model	BM25-150	ACI	T2	265.14	1.047446
Kr Model	BM25-150	Nehdi	H1	205.2	0.964739
Kr Model	BM25-150	Nehdi	H2	212.7	1
Kr Model	BM25-150	Nehdi	T1	254.18	1.195016
Kr Model	BM25-150	Nehdi	T2	253.41	1.191396
Kr Model	BM25-150	CSA	H1	211.33	0.993606
Kr Model	BM25-150	CSA	H2	212.69	1
Kr Model	BM25-150	CSA	T1	261.61	1.230006
Kr Model	BM25-150	CSA	T2	253.41	0
Kr Model	BM25-150	Proposed	H1	226.17	1.063279
Kr Model	BM25-150	Proposed	H2	212.71	1
Kr Model	BM25-150	Proposed	T1	261.95	1.231489

Kr Model	BM25-150	Proposed	T2	253.45	1.191528
Kr Model	BM25-s230	ACI	H1	348.69	1.015021
Kr Model	BM25-s230	ACI	H2	343.53	1
Kr Model	BM25-s230	ACI	T1	417.2	1.21445
Kr Model	BM25-s230	ACI	T2	397.49	1.157075
Kr Model	BM25-s230	Nehdi	H1	309.36	1.053356
Kr Model	BM25-s230	Nehdi	H2	293.69	1
Kr Model	BM25-s230	Nehdi	T1	380.97	1.297184
Kr Model	BM25-s230	Nehdi	T2	341.81	1.163846
Kr Model	BM25-s230	CSA	H1	272.76	1.031697
Kr Model	BM25-s230	CSA	H2	264.38	1
Kr Model	BM25-s230	CSA	T1	312.22	1.180952
Kr Model	BM25-s230	CSA	T2	274.74	1.039186
Kr Model	BM25-s230	Proposed	H1	349.18	1.012644
Kr Model	BM25-s230	Proposed	H2	344.82	1
Kr Model	BM25-s230	Proposed	T1	408.51	1.184705
Kr Model	BM25-s230	Proposed	T2	366.84	1.063859
WSF	BM12-220	ACI	H1	400.89	1.003203
WSF	BM12-220	ACI	H2	399.61	1
WSF	BM12-220	ACI	T1	400.89	1.003203
WSF	BM12-220	ACI	T2	400.89	1.003203
WSF	BM12-220	Nehdi	H1	371.94	1.002993
WSF	BM12-220	Nehdi	H2	370.83	1
WSF	BM12-220	Nehdi	T1	400.89	1.081061
WSF	BM12-220	Nehdi	T2	375.19	1.011757
WSF	BM12-220	CSA	H1	223.39	0.929591
WSF	BM12-220	CSA	H2	240.31	1
WSF	BM12-220	CSA	T1	256.26	1.066373
WSF	BM12-220	CSA	T2	229.9	0.956681
WSF	BM12-220	Proposed	H1	353.16	1.009836
WSF	BM12-220	Proposed	H2	349.72	1
WSF	BM12-220	Proposed	T1	387.1	1.106886
WSF	BM12-220	Proposed	T2	346.54	0.990907
WSF	BM12-150	ACI	H1	400.89	1.044093
WSF	BM12-150	ACI	H2	383.96	1
WSF	BM12-150	ACI	T1	400.89	1.044093
WSF	BM12-150	ACI	T2	395.09	1.028987
WSF	BM12-150	Nehdi	H1	348.23	1.005138
WSF	BM12-150	Nehdi	H2	346.45	1
WSF	BM12-150	Nehdi	T1	400.89	1.157137
WSF	BM12-150	Nehdi	T2	397.81	1.148247
WSF	BM12-150	CSA	H1	307.01	1.030131
WSF	BM12-150	CSA	H2	298.03	1
WSF	BM12-150	CSA	T1	347.53	1.166091

WSF	BM12-150	CSA	T2	278.15	0.933295
WSF	BM12-150	Proposed	H1	363.9	1.048945
WSF	BM12-150	Proposed	H2	346.92	1
WSF	BM12-150	Proposed	T1	400.89	1.155569
WSF	BM12-150	Proposed	T2	399.34	1.151101
WSF	BM12-s230	ACI	H1	416.57	1.063492
WSF	BM12-s230	ACI	H2	391.7	1
WSF	BM12-s230	ACI	T1	437.19	1.116135
WSF	BM12-s230	ACI	T2	418.5	1.06842
WSF	BM12-s230	Nehdi	H1	402.96	1.055118
WSF	BM12-s230	Nehdi	H2	381.91	1
WSF	BM12-s230	Nehdi	T1	452.24	1.184153
WSF	BM12-s230	Nehdi	T2	368.57	0.96507
WSF	BM12-s230	CSA	H1	235.93	0.964712
WSF	BM12-s230	CSA	H2	244.56	1
WSF	BM12-s230	CSA	T1	267.06	1.092002
WSF	BM12-s230	CSA	T2	234.13	0.957352
WSF	BM12-s230	Proposed	H1	410.02	1.068512
WSF	BM12-s230	Proposed	H2	383.73	1
WSF	BM12-s230	Proposed	T1	435.52	1.134965
WSF	BM12-s230	Proposed	T2	373.96	0.974539
WSF	BM16-220	ACI	H1	397.24	1.008479
WSF	BM16-220	ACI	H2	393.9	1
WSF	BM16-220	ACI	T1	400.89	1.017746
WSF	BM16-220	ACI	T2	400.89	1.017746
WSF	BM16-220	Nehdi	H1	370.63	0.995782
WSF	BM16-220	Nehdi	H2	372.2	1
WSF	BM16-220	Nehdi	T1	400.89	1.077082
WSF	BM16-220	Nehdi	T2	374.55	1.006314
WSF	BM16-220	CSA	H1	218.73	0.928908
WSF	BM16-220	CSA	H2	235.47	1
WSF	BM16-220	CSA	T1	250.41	1.063448
WSF	BM16-220	CSA	T2	224.43	0.953115
WSF	BM16-220	Proposed	H1	348.03	1.016413
WSF	BM16-220	Proposed	H2	342.41	1
WSF	BM16-220	Proposed	T1	379.98	1.109722
WSF	BM16-220	Proposed	T2	338.21	0.987734
WSF	BM16-150	ACI	H1	400.89	1.033408
WSF	BM16-150	ACI	H2	387.93	1
WSF	BM16-150	ACI	T1	400.89	1.033408
WSF	BM16-150	ACI	T2	387.51	0.998917
WSF	BM16-150	Nehdi	H1	345.03	1.013989
WSF	BM16-150	Nehdi	H2	340.27	1
WSF	BM16-150	Nehdi	T1	400.89	1.178153

WSF	BM16-150	Nehdi	T2	390.41	1.147354
WSF	BM16-150	CSA	H1	300.17	1.037753
WSF	BM16-150	CSA	H2	289.25	1
WSF	BM16-150	CSA	T1	339.57	1.173967
WSF	BM16-150	CSA	T2	271.52	0.938704
WSF	BM16-150	Proposed	H1	359.7	1.056202
WSF	BM16-150	Proposed	H2	340.56	1
WSF	BM16-150	Proposed	T1	400.89	1.177149
WSF	BM16-150	Proposed	T2	391.97	1.150957
WSF	BM16-s230	ACI	H1	410.74	1.067994
WSF	BM16-s230	ACI	H2	384.59	1
WSF	BM16-s230	ACI	T1	429.65	1.117164
WSF	BM16-s230	ACI	T2	410.02	1.066122
WSF	BM16-s230	Nehdi	H1	399.5	1.067982
WSF	BM16-s230	Nehdi	H2	374.07	1
WSF	BM16-s230	Nehdi	T1	446.1	1.192558
WSF	BM16-s230	Nehdi	T2	360.18	0.962868
WSF	BM16-s230	CSA	H1	230.82	0.973595
WSF	BM16-s230	CSA	H2	237.08	1
WSF	BM16-s230	CSA	T1	260.76	1.099882
WSF	BM16-s230	CSA	T2	226.62	0.95588
WSF	BM16-s230	Proposed	H1	401.49	1.076727
WSF	BM16-s230	Proposed	H2	372.88	1
WSF	BM16-s230	Proposed	T1	425.32	1.140635
WSF	BM16-s230	Proposed	T2	363.16	0.973933
WSF	BM25-220	ACI	H1	372.2	1.03034
WSF	BM25-220	ACI	H2	361.24	1
WSF	BM25-220	ACI	T1	400.89	1.109761
WSF	BM25-220	ACI	T2	400.89	1.109761
WSF	BM25-220	Nehdi	H1	362.4	1.018492
WSF	BM25-220	Nehdi	H2	355.82	1
WSF	BM25-220	Nehdi	T1	400.89	1.126665
WSF	BM25-220	Nehdi	T2	352.03	0.989349
WSF	BM25-220	CSA	H1	195.66	0.951006
WSF	BM25-220	CSA	H2	205.74	1
WSF	BM25-220	CSA	T1	221.61	1.077136
WSF	BM25-220	CSA	T2	194.61	0.945903
WSF	BM25-220	Proposed	H1	319.46	1.056485
WSF	BM25-220	Proposed	H2	302.38	1
WSF	BM25-220	Proposed	T1	342.42	1.132416
WSF	BM25-220	Proposed	T2	299.52	0.990542
WSF	BM25-150	ACI	H1	400.89	1
WSF	BM25-150	ACI	H2	400.89	1
WSF	BM25-150	ACI	T1	400.89	1

WSF	BM25-150	ACI	T2	400.89	1
WSF	BM25-150	Nehdi	H1	326.55	1.064617
WSF	BM25-150	Nehdi	H2	306.73	1
WSF	BM25-150	Nehdi	T1	388.99	1.268184
WSF	BM25-150	Nehdi	T2	359.33	1.171486
WSF	BM25-150	CSA	H1	266.34	1.059722
WSF	BM25-150	CSA	H2	251.33	1
WSF	BM25-150	CSA	T1	300.49	1.195599
WSF	BM25-150	CSA	T2	236.31	0.940238
WSF	BM25-150	Proposed	H1	338.58	1.082486
WSF	BM25-150	Proposed	H2	312.78	1
WSF	BM25-150	Proposed	T1	400.89	1.2817
WSF	BM25-150	Proposed	T2	354.68	1.13396
WSF	BM25-s230	ACI	H1	378.89	1.089641
WSF	BM25-s230	ACI	H2	347.72	1
WSF	BM25-s230	ACI	T1	390.39	1.122714
WSF	BM25-s230	ACI	T2	367.59	1.057144
WSF	BM25-s230	Nehdi	H1	320.22	1.144992
WSF	BM25-s230	Nehdi	H2	279.67	1
WSF	BM25-s230	Nehdi	T1	359.08	1.283942
WSF	BM25-s230	Nehdi	T2	275.24	0.98416
WSF	BM25-s230	CSA	H1	205.61	1.025077
WSF	BM25-s230	CSA	H2	200.58	1
WSF	BM25-s230	CSA	T1	229.99	1.146625
WSF	BM25-s230	CSA	T2	192.09	0.957673
WSF	BM25-s230	Proposed	H1	357.38	1.119086
WSF	BM25-s230	Proposed	H2	319.35	1
WSF	BM25-s230	Proposed	T1	374.39	1.17235
WSF	BM25-s230	Proposed	T2	310.94	0.973665
HSF	BM12-220	ACI	H1	309.92	1.005711
HSF	BM12-220	ACI	H2	308.16	1
HSF	BM12-220	ACI	T1	360.2	1.168873
HSF	BM12-220	ACI	T2	359.17	1.165531
HSF	BM12-220	Nehdi	H1	313.88	1.024413
HSF	BM12-220	Nehdi	H2	306.4	1
HSF	BM12-220	Nehdi	T1	366.2	1.19517
HSF	BM12-220	Nehdi	T2	314.71	1.027121
HSF	BM12-220	CSA	H1	202.68	0.942391
HSF	BM12-220	CSA	H2	215.07	1
HSF	BM12-220	CSA	T1	234.97	1.092528
HSF	BM12-220	CSA	T2	211.38	0.982843
HSF	BM12-220	Proposed	H1	282.04	1.002381
HSF	BM12-220	Proposed	H2	281.37	1
HSF	BM12-220	Proposed	T1	316.28	1.124072

HSF	BM12-220	Proposed	T2	283.52	1.007641
HSF	BM12-150	ACI	H1	296.39	0.99872
HSF	BM12-150	ACI	H2	296.77	1
HSF	BM12-150	ACI	T1	366.11	1.233649
HSF	BM12-150	ACI	T2	352.79	1.188766
HSF	BM12-150	Nehdi	H1	295.6	0.996628
HSF	BM12-150	Nehdi	H2	296.6	1
HSF	BM12-150	Nehdi	T1	365.5	1.232299
HSF	BM12-150	Nehdi	T2	352.6	1.188806
HSF	BM12-150	CSA	H1	283.88	1.001588
HSF	BM12-150	CSA	H2	283.43	1
HSF	BM12-150	CSA	T1	323.48	1.141305
HSF	BM12-150	CSA	T2	273.3	0.964259
HSF	BM12-150	Proposed	H1	295.44	0.996055
HSF	BM12-150	Proposed	H2	296.61	1
HSF	BM12-150	Proposed	T1	364.95	1.230404
HSF	BM12-150	Proposed	T2	352.48	1.188362
HSF	BM12-s230	ACI	H1	367.67	1.009417
HSF	BM12-s230	ACI	H2	364.24	1
HSF	BM12-s230	ACI	T1	413.4	1.134966
HSF	BM12-s230	ACI	T2	411.98	1.131067
HSF	BM12-s230	Nehdi	H1	358.92	1.030432
HSF	BM12-s230	Nehdi	H2	348.32	1
HSF	BM12-s230	Nehdi	T1	423.93	1.217071
HSF	BM12-s230	Nehdi	T2	355.43	1.020412
HSF	BM12-s230	CSA	H1	219.03	0.935466
HSF	BM12-s230	CSA	H2	234.14	1
HSF	BM12-s230	CSA	T1	253.73	1.083668
HSF	BM12-s230	CSA	T2	228.41	0.975527
HSF	BM12-s230	Proposed	H1	359.22	1.001561
HSF	BM12-s230	Proposed	H2	358.66	1
HSF	BM12-s230	Proposed	T1	403.82	1.125913
HSF	BM12-s230	Proposed	T2	364.77	1.017036
HSF	BM16-220	ACI	H1	309.68	1.005846
HSF	BM16-220	ACI	H2	307.88	1
HSF	BM16-220	ACI	T1	359.56	1.167858
HSF	BM16-220	ACI	T2	358.49	1.164382
HSF	BM16-220	Nehdi	H1	313.81	1.027134
HSF	BM16-220	Nehdi	H2	305.52	1
HSF	BM16-220	Nehdi	T1	365.69	1.196943
HSF	BM16-220	Nehdi	T2	313.74	1.026905
HSF	BM16-220	CSA	H1	198.9	0.943996
HSF	BM16-220	CSA	H2	210.7	1
HSF	BM16-220	CSA	T1	230.3	1.093023

HSF	BM16-220	CSA	T2	206.46	0.979877
HSF	BM16-220	Proposed	H1	279.64	1.003841
HSF	BM16-220	Proposed	H2	278.57	1
HSF	BM16-220	Proposed	T1	313.34	1.124816
HSF	BM16-220	Proposed	T2	280.39	1.006533
HSF	BM16-150	ACI	H1	296	0.99892
HSF	BM16-150	ACI	H2	296.32	1
HSF	BM16-150	ACI	T1	365.58	1.233734
HSF	BM16-150	ACI	T2	352.23	1.188681
HSF	BM16-150	Nehdi	H1	295.24	0.996927
HSF	BM16-150	Nehdi	H2	296.15	1
HSF	BM16-150	Nehdi	T1	365.01	1.232517
HSF	BM16-150	Nehdi	T2	352.06	1.188789
HSF	BM16-150	CSA	H1	278.77	0.999857
HSF	BM16-150	CSA	H2	278.81	1
HSF	BM16-150	CSA	T1	317.8	1.139844
HSF	BM16-150	CSA	T2	267.81	0.960547
HSF	BM16-150	Proposed	H1	295.06	0.996286
HSF	BM16-150	Proposed	H2	296.16	1
HSF	BM16-150	Proposed	T1	364.47	1.230652
HSF	BM16-150	Proposed	T2	351.94	1.188344
HSF	BM16-s230	ACI	H1	367.09	1.009848
HSF	BM16-s230	ACI	H2	363.51	1
HSF	BM16-s230	ACI	T1	411.78	1.132789
HSF	BM16-s230	ACI	T2	410.31	1.128745
HSF	BM16-s230	Nehdi	H1	358.09	1.033419
HSF	BM16-s230	Nehdi	H2	346.51	1
HSF	BM16-s230	Nehdi	T1	421.69	1.216963
HSF	BM16-s230	Nehdi	T2	353.12	1.019076
HSF	BM16-s230	CSA	H1	214.83	0.937713
HSF	BM16-s230	CSA	H2	229.1	1
HSF	BM16-s230	CSA	T1	248.48	1.084592
HSF	BM16-s230	CSA	T2	222.85	0.972719
HSF	BM16-s230	Proposed	H1	354.59	1.00459
HSF	BM16-s230	Proposed	H2	352.97	1
HSF	BM16-s230	Proposed	T1	397.91	1.12732
HSF	BM16-s230	Proposed	T2	358.45	1.015525
HSF	BM25-220	ACI	H1	308.29	1.006628
HSF	BM25-220	ACI	H2	306.26	1
HSF	BM25-220	ACI	T1	355.85	1.161921
HSF	BM25-220	ACI	T2	354.59	1.157807
HSF	BM25-220	Nehdi	H1	313.97	1.045382
HSF	BM25-220	Nehdi	H2	300.34	1
HSF	BM25-220	Nehdi	T1	362.82	1.208031

HSF	BM25-220	Nehdi	T2	308.08	1.025771
HSF	BM25-220	CSA	H1	180.1	0.953415
HSF	BM25-220	CSA	H2	188.9	1
HSF	BM25-220	CSA	T1	207.19	1.096824
HSF	BM25-220	CSA	T2	182.35	0.965326
HSF	BM25-220	Proposed	H1	266.3	1.011893
HSF	BM25-220	Proposed	H2	263.17	1
HSF	BM25-220	Proposed	T1	297.15	1.129118
HSF	BM25-220	Proposed	T2	263.35	1.000684
HSF	BM25-150	ACI	H1	293.68	0.999966
HSF	BM25-150	ACI	H2	293.69	1
HSF	BM25-150	ACI	T1	362.5	1.234295
HSF	BM25-150	ACI	T2	348.97	1.188226
HSF	BM25-150	Nehdi	H1	293.12	0.998467
HSF	BM25-150	Nehdi	H2	293.57	1
HSF	BM25-150	Nehdi	T1	362.08	1.233369
HSF	BM25-150	Nehdi	T2	348.86	1.188337
HSF	BM25-150	CSA	H1	252.53	0.98795
HSF	BM25-150	CSA	H2	255.61	1
HSF	BM25-150	CSA	T1	289.18	1.131333
HSF	BM25-150	CSA	T2	241.34	0.944173
HSF	BM25-150	Proposed	H1	292.89	0.997718
HSF	BM25-150	Proposed	H2	293.56	1
HSF	BM25-150	Proposed	T1	361.76	1.23232
HSF	BM25-150	Proposed	T2	347.22	1.182791
HSF	BM25-s230	ACI	H1	363.7	1.01219
HSF	BM25-s230	ACI	H2	359.32	1
HSF	BM25-s230	ACI	T1	402.6	1.12045
HSF	BM25-s230	ACI	T2	401.15	1.116414
HSF	BM25-s230	Nehdi	H1	301.6	1.057837
HSF	BM25-s230	Nehdi	H2	285.11	1
HSF	BM25-s230	Nehdi	T1	352.78	1.237347
HSF	BM25-s230	Nehdi	T2	280.5	0.983831
HSF	BM25-s230	CSA	H1	193.98	0.951582
HSF	BM25-s230	CSA	H2	203.85	1
HSF	BM25-s230	CSA	T1	222.57	1.091832
HSF	BM25-s230	CSA	T2	195.58	0.959431
HSF	BM25-s230	Proposed	H1	329.9	1.020257
HSF	BM25-s230	Proposed	H2	323.35	1
HSF	BM25-s230	Proposed	T1	366.83	1.134467
HSF	BM25-s230	Proposed	T2	325.65	1.007113
Design	BM12-220	ACI	H1	342.02	1.015951
Design	BM12-220	ACI	H2	336.65	1
Design	BM12-220	ACI	T1	400.89	1.190821

Design	BM12-220	ACI	T2	361.97	1.075212
Design	BM12-220	Nehdi	H1	276.43	0.972797
Design	BM12-220	Nehdi	H2	284.16	1
Design	BM12-220	Nehdi	T1	338.59	1.191547
Design	BM12-220	Nehdi	T2	297.75	1.047825
Design	BM12-220	CSA	H1	209.55	0.961591
Design	BM12-220	CSA	H2	217.92	1
Design	BM12-220	CSA	T1	242.56	1.113069
Design	BM12-220	CSA	T2	220.55	1.012069
Design	BM12-220	Proposed	H1	287.07	0.982141
Design	BM12-220	Proposed	H2	292.29	1
Design	BM12-220	Proposed	T1	324.78	1.111157
Design	BM12-220	Proposed	T2	301.46	1.031373
Design	BM12-150	ACI	H1	320.29	1.049512
Design	BM12-150	ACI	H2	305.18	1
Design	BM12-150	ACI	T1	368.17	1.206403
Design	BM12-150	ACI	T2	318.57	1.043876
Design	BM12-150	Nehdi	H1	266.78	0.964602
Design	BM12-150	Nehdi	H2	276.57	1
Design	BM12-150	Nehdi	T1	318.19	1.150486
Design	BM12-150	Nehdi	T2	286.84	1.037133
Design	BM12-150	CSA	H1	206.39	0.92229
Design	BM12-150	CSA	H2	223.78	1
Design	BM12-150	CSA	T1	236.58	1.057199
Design	BM12-150	CSA	T2	221.09	0.987979
Design	BM12-150	Proposed	H1	306.76	1.012175
Design	BM12-150	Proposed	H2	303.07	1
Design	BM12-150	Proposed	T1	343.18	1.132346
Design	BM12-150	Proposed	T2	314.52	1.03778
Design	BM12-s230	ACI	H1	353.08	1.067804
Design	BM12-s230	ACI	H2	330.66	1
Design	BM12-s230	ACI	T1	401.09	1.212998
Design	BM12-s230	ACI	T2	342.37	1.035414
Design	BM12-s230	Nehdi	H1	300.21	0.987111
Design	BM12-s230	Nehdi	H2	304.13	1
Design	BM12-s230	Nehdi	T1	354.2	1.164634
Design	BM12-s230	Nehdi	T2	312.69	1.028146
Design	BM12-s230	CSA	H1	223.81	0.938682
Design	BM12-s230	CSA	H2	238.43	1
Design	BM12-s230	CSA	T1	255.08	1.069832
Design	BM12-s230	CSA	T2	233.96	0.981252
Design	BM12-s230	Proposed	H1	342.76	1.024694
Design	BM12-s230	Proposed	H2	334.5	1
Design	BM12-s230	Proposed	T1	381.77	1.141315

Design	BM12-s230	Proposed	T2	347.32	1.038326
Design	BM16-220	ACI	H1	338.97	1.019857
Design	BM16-220	ACI	H2	332.37	1
Design	BM16-220	ACI	T1	400.89	1.206156
Design	BM16-220	ACI	T2	356.15	1.071547
Design	BM16-220	Nehdi	H1	275.42	0.965234
Design	BM16-220	Nehdi	H2	285.34	1
Design	BM16-220	Nehdi	T1	336.38	1.178874
Design	BM16-220	Nehdi	T2	298.89	1.047487
Design	BM16-220	CSA	H1	205.34	0.950208
Design	BM16-220	CSA	H2	216.1	1
Design	BM16-220	CSA	T1	237.24	1.097825
Design	BM16-220	CSA	T2	216.52	1.001944
Design	BM16-220	Proposed	H1	283.25	0.986109
Design	BM16-220	Proposed	H2	287.24	1
Design	BM16-220	Proposed	T1	319.7	1.113007
Design	BM16-220	Proposed	T2	295.43	1.028513
Design	BM16-150	ACI	H1	316.99	1.053788
Design	BM16-150	ACI	H2	300.81	1
Design	BM16-150	ACI	T1	363.37	1.207972
Design	BM16-150	ACI	T2	313.47	1.042086
Design	BM16-150	Nehdi	H1	265.49	0.96926
Design	BM16-150	Nehdi	H2	273.91	1
Design	BM16-150	Nehdi	T1	315.84	1.153079
Design	BM16-150	Nehdi	T2	283.58	1.035304
Design	BM16-150	CSA	H1	202.18	0.925436
Design	BM16-150	CSA	H2	218.47	1
Design	BM16-150	CSA	T1	231.38	1.059093
Design	BM16-150	CSA	T2	215.26	0.985307
Design	BM16-150	Proposed	H1	302.09	1.015599
Design	BM16-150	Proposed	H2	297.45	1
Design	BM16-150	Proposed	T1	337.44	1.134443
Design	BM16-150	Proposed	T2	308.23	1.036241
Design	BM16-s230	ACI	H1	348.9	1.071922
Design	BM16-s230	ACI	H2	325.49	1
Design	BM16-s230	ACI	T1	395.59	1.215368
Design	BM16-s230	ACI	T2	336.74	1.034563
Design	BM16-s230	Nehdi	H1	298.42	0.994269
Design	BM16-s230	Nehdi	H2	300.14	1
Design	BM16-s230	Nehdi	T1	351.29	1.17042
Design	BM16-s230	Nehdi	T2	308.12	1.026588
Design	BM16-s230	CSA	H1	219.11	0.944399
Design	BM16-s230	CSA	H2	232.01	1
Design	BM16-s230	CSA	T1	249.37	1.074824

Design	BM16-s230	CSA	T2	227.14	0.97901
Design	BM16-s230	Proposed	H1	336.89	1.027135
Design	BM16-s230	Proposed	H2	327.99	1
Design	BM16-s230	Proposed	T1	374.93	1.143114
Design	BM16-s230	Proposed	T2	340.37	1.037745
Design	BM25-220	ACI	H1	320.6	1.041653
Design	BM25-220	ACI	H2	307.78	1
Design	BM25-220	ACI	T1	372.66	1.2108
Design	BM25-220	ACI	T2	325.31	1.056956
Design	BM25-220	Nehdi	H1	268.68	0.963114
Design	BM25-220	Nehdi	H2	278.97	1
Design	BM25-220	Nehdi	T1	322.91	1.157508
Design	BM25-220	Nehdi	T2	291.56	1.04513
Design	BM25-220	CSA	H1	184.35	0.924616
Design	BM25-220	CSA	H2	199.38	1
Design	BM25-220	CSA	T1	210.98	1.05818
Design	BM25-220	CSA	T2	193.4	0.970007
Design	BM25-220	Proposed	H1	262.59	1.008604
Design	BM25-220	Proposed	H2	260.35	1
Design	BM25-220	Proposed	T1	293.29	1.126522
Design	BM25-220	Proposed	T2	264.86	1.017323
Design	BM25-150	ACI	H1	298.12	1.075081
Design	BM25-150	ACI	H2	277.3	1
Design	BM25-150	ACI	T1	338.11	1.219293
Design	BM25-150	ACI	T2	287.5	1.036783
Design	BM25-150	Nehdi	H1	257.47	1.003938
Design	BM25-150	Nehdi	H2	256.46	1
Design	BM25-150	Nehdi	T1	302.58	1.179833
Design	BM25-150	Nehdi	T2	263.45	1.027256
Design	BM25-150	CSA	H1	181.29	0.952654
Design	BM25-150	CSA	H2	190.3	1
Design	BM25-150	CSA	T1	205.88	1.081871
Design	BM25-150	CSA	T2	185.38	0.974146
Design	BM25-150	Proposed	H1	277.5	1.032251
Design	BM25-150	Proposed	H2	268.83	1
Design	BM25-150	Proposed	T1	308.23	1.146561
Design	BM25-150	Proposed	T2	277.43	1.03199
Design	BM25-s230	ACI	H1	325.72	1.091409
Design	BM25-s230	ACI	H2	298.44	1
Design	BM25-s230	ACI	T1	367.13	1.230164
Design	BM25-s230	ACI	T2	308.64	1.034178
Design	BM25-s230	Nehdi	H1	247.6	1.01243
Design	BM25-s230	Nehdi	H2	244.56	1
Design	BM25-s230	Nehdi	T1	294.28	1.203304

Design	BM25-s230	Nehdi	T2	244.24	0.998692
Design	BM25-s230	CSA	H1	195.86	0.980526
Design	BM25-s230	CSA	H2	199.75	1
Design	BM25-s230	CSA	T1	221.46	1.108686
Design	BM25-s230	CSA	T2	193.62	0.969312
Design	BM25-s230	Proposed	H1	307.81	1.039899
Design	BM25-s230	Proposed	H2	296	1
Design	BM25-s230	Proposed	T1	341.87	1.154966
Design	BM25-s230	Proposed	T2	307.64	1.039324

C: Spreadsheets and Plots of Detailed Analyses

Most of the data here are with the H2 concrete model, except the ones to verify the proposed method with different concrete models.

For deep beams with stirrups analyzed with h_C based on strain compatibility:

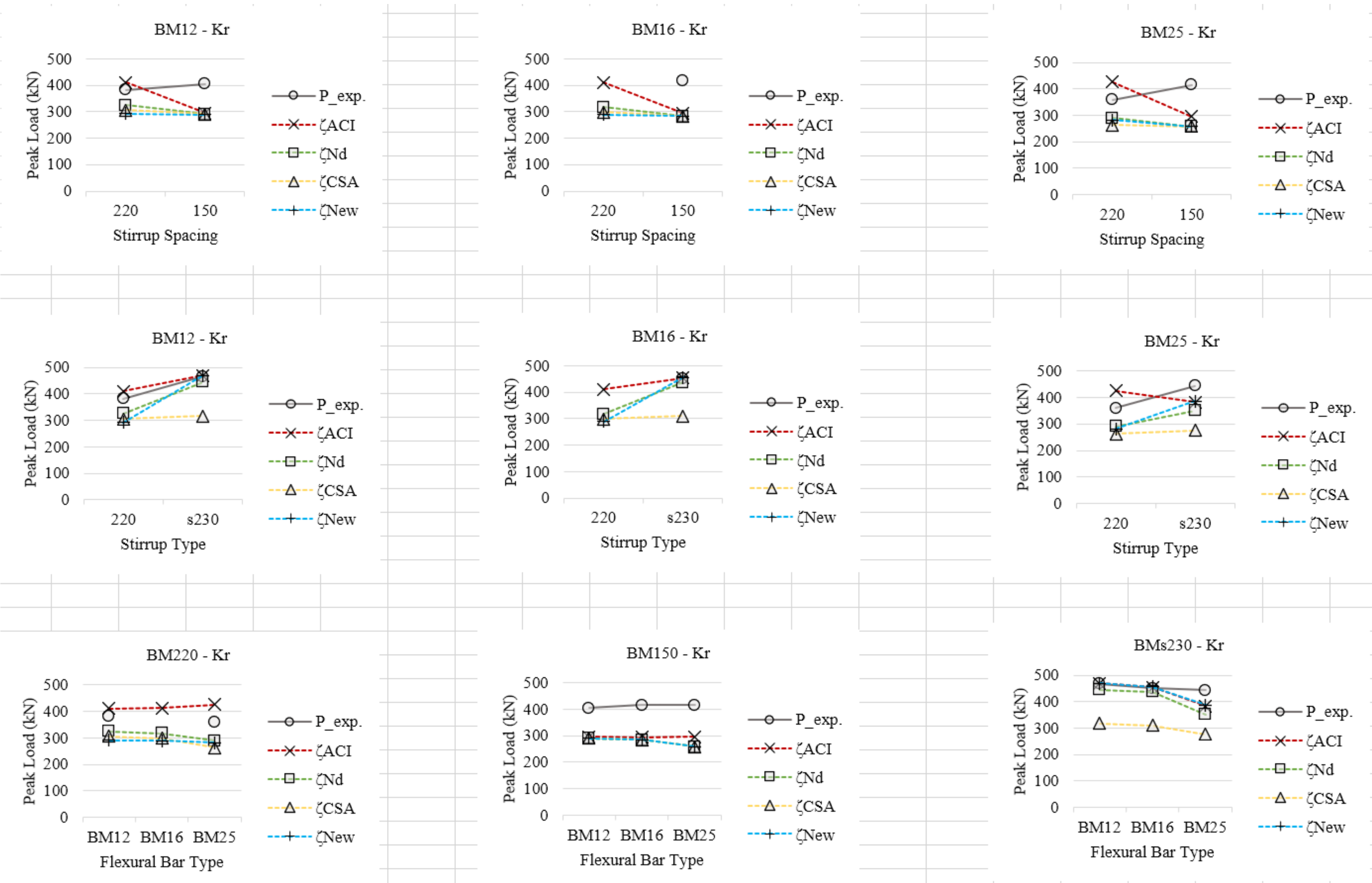
BM12 - Kr
BM16 - Kr
BM25 - Kr
Peak Load (kN)
Stirrup Spacing
220
150
Stirrup Type
s230
BM220 - Kr
BM150 - Kr
BMs230 - Kr
Flexural Bar Type
BM12
BM16
BM25
P_exp.
ζACI
ζNd
ζCSA
ζNew

M. Krall		P_exp.	P_predict with							
			ζACI	Fail.Elem	ζNd	Fail.Elem	ζCSA	Fail.Elem	ζNew	Fail.Elem
BM12	220	382.4	411.07	S12	199.73	S12	155.34	S12	290.76	S12
	76.89		411.11	S5	325.26	S5	305.98	S11	292.48	S10
			411.11	**Combine**	**325.26**	**Combine**	**305.98**	**Shear**	**292.48**	**Shear**
	150	405.2	295.48	S20	142.00	S20	126.32	S20	247.45	S20
			295.69	S9	290.88	S9	290.87	S9	290.91	S9
			295.69	**Combine**	**290.88**	**Combine**	**290.87**	**Combine**	**290.91**	**Combine**
	s230	466.9	469.31	S5	445.88	S5	273.90	S12	469.38	S5
	72.68		469.33	S12	445.89	S12	317.17	S11	469.39	S12
			469.33	**Combine**	**445.89**	**Combine**	**317.17**	**Shear**	**469.39**	**Combine**
BM16	220	309.3	411.97	S12	200.45	S12	153.23	S12	288.66	S12
	75.03		412.01	S5	318.51	S5	298.54	S11	288.94	S10
			412.01	**Combine**	**318.51**	**Combine**	**298.54**	**Shear**	**288.94**	**Shear**
	150	416.5	294.44	S20	141.52	S20	124.16	S20	244.29	S20
			294.58	S9	284.76	S9	284.75	S9	284.79	S9
			294.58	**Combine**	**284.76**	**Combine**	**284.75**	**Combine**	**284.79**	**Combine**
	s230	450.8	454.76	S5	438.12	S5	273.65	S12	456.20	S5
	71.15		454.78	S12	438.13	S12	309.64	S11	456.22	S12
			454.78	**Combine**	**438.13**	**Combine**	**309.64**	**Shear**	**456.22**	**Combine**
BM25	220	360.1	426.61	S12	210.64	S12	144.44	S12	282.43	S12
	67.424		426.62	S5	290.06	S5	263.82	S11	282.50	S10
			426.62	**Combine**	**290.06**	**Combine**	**263.82**	**Shear**	**282.50**	**Shear**
	150	415.8	295.91	S20	142.35	S20	114.46	S20	231.41	S20
			295.97	S9	258.99	S9	258.98	S9	259.02	S9
			295.97	**Combine**	**258.99**	**Combine**	**258.98**	**Combine**	**259.02**	**Combine**
	s230	444	382.89	S5	351.70	S12	275.62	S12	387.35	S5
	63.28		382.92	S12	351.75	S5	275.80	S11	387.37	S12
			382.92	**Combine**	**351.75**	**Combine**	**275.80**	**Shear**	**387.37**	**Combine**

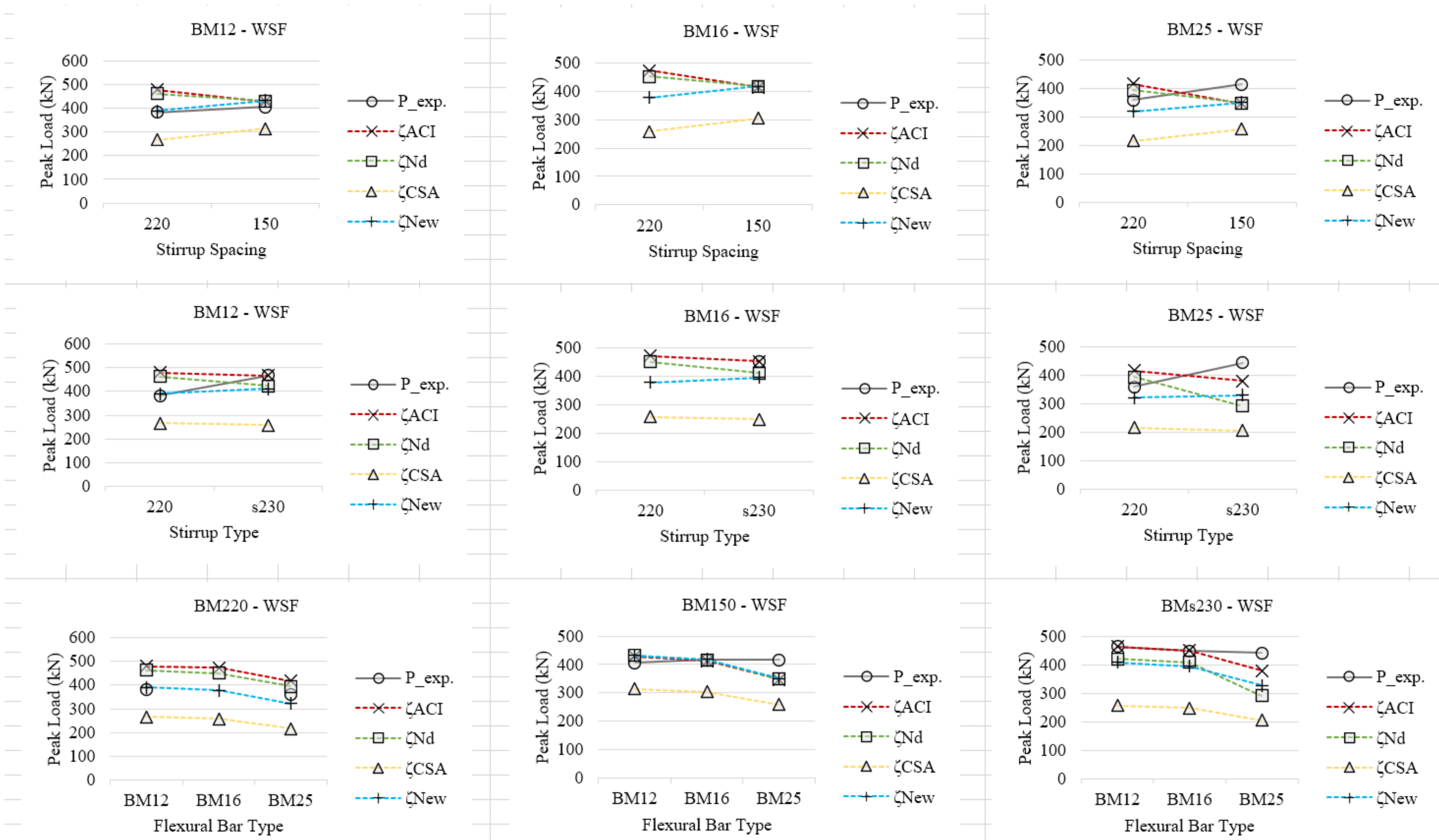

BM12 - WSF
Peak Load (kN)
Stirrup Spacing
BM16 - WSF
BM25 - WSF
Stirrup Type
BM220 - WSF
BM150 - WSF
BMs230 - WSF
Flexural Bar Type
220
150
s230
BM12
BM16
BM25
P_exp.
ζACI
ζNd
ζCSA
ζNew

Whole Section Fanning		P_exp.	P_predict with							
			ζACI	Fail.Elem	ζNd	Fail.Elem	ζCSA	Fail.Elem	ζNew	Fail.Elem
BM12	220	382.4	478.61	N7	462.02	S10	266.75	S10	389.42	S10
					462.03	S11	266.76	S11	389.46	S11
					462.04	S12	266.77	S12	389.48	S12
			478.61	**Node Crush**	**462.04**	**Shear**	**266.77**	**Shear**	**389.48**	**Shear**
	150	405.2	427.94	S9	431.35	S9	310.88	S18	432.49	S9
			478.61	N11	431.37	S19	314.09	S21	432.53	S19
					431.38	S20	314.12	S19	432.55	S20
					431.40	S21	314.12	S20	432.56	S21
					431.41	N9	314.14	S17	432.57	S17/N9
			427.94	**Flexure**	**431.37**	**Combine**	**314.14**	**Shear**	**432.53**	**Combine**
	s230	466.9	466.46	S5	423.19	S10	258.26	S10	410.18	S10
			466.51	S11	423.22	S11	258.28	S12	410.24	S12
			466.52	S12	423.22	S12	258.29	S11	410.25	S11
			466.51	**Combine**	**423.22**	**Shear**	**258.29**	**Shear**	**410.25**	**Shear**
BM16	220	309.3	472.20	N7	451.32	S10	258.35	S10	377.57	S10
					451.33	S11	258.36	S11	377.62	S11
					451.34	S12	258.36	S12	377.63	S12
			472.20	**Shear**	**451.34**	**Shear**	**258.36**	**Shear**	**377.63**	**Shear**
	150	416.5	413.27	S9	416.52	S9	299.71	S18	417.67	S9
			472.20	N11	416.54	S19	304.48	S21	417.72	S19
					416.55	S20	304.51	S19	417.74	S20
					416.58	S21	304.52	S20	417.75	S21
					416.61	S17	304.53	S17	417.76	S17/N9
			413.27	**Flexure**	**416.54**	**Combine**	**304.53**	**Shear**	**417.72**	**Combine**
	s230	450.8	451.87	S5	410.60	S10	249.20	S10	396.39	S10
			451.92	S11	410.63	S11	249.22	S12	396.45	S12
			451.93	S12	410.63	S12	249.23	S11	396.46	S11
			451.92	**Combine**	**410.63**	**Shear**	**249.23**	**Shear**	**396.46**	**Shear**
BM25	220	360.1	416.68	S5	394.18	S10	216.62	S10	320.56	S10
			416.71	S11	394.20	S11	216.64	S11	321.11	S11
			416.73	S12	394.20	S12	216.65	S12	321.11	S12
			416.71	**Combine**	**394.20**	**Shear**	**216.65**	**Shear**	**321.11**	**Shear**
	150	415.8	347.33	S9	349.59	S9	246.92	S18	350.99	S9
			446.02	N11	349.62	S19	258.32	S21	351.26	S19
					349.64	S20	258.37	S20	351.29	S20
					349.66	S21	258.38	S19	351.30	S21
					349.70	S17	258.38	S17	351.32	S17
			347.33	**Flexure**	**349.62**	**Combine**	**258.38**	**Shear**	**351.26**	**Combine**
	s230	444	380.72	S5	292.53	S10	206.21	S10	330.30	S10
			380.82	S11	292.56	S12	206.23	S12	330.37	S12
			380.83	S12	292.57	S11	206.24	S11	330.39	S11
			380.82	**Combine**	**292.57**	**Shear**	**206.24**	**Shear**	**330.39**	**Shear**

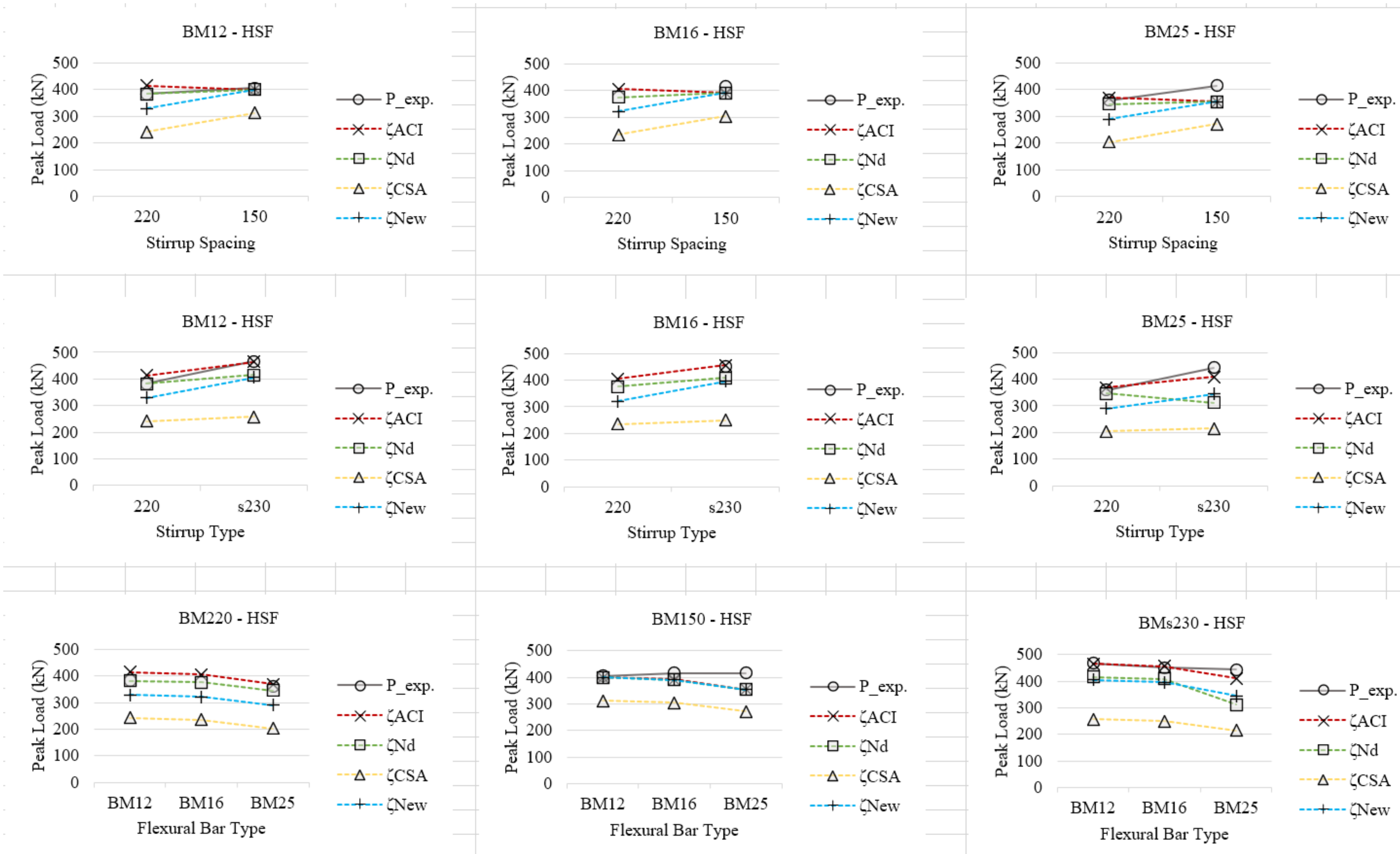
BM12 - HSF
BM16 - HSF
BM25 - HSF
Peak Load (kN)
0
100
200
300
400
500
220
150
Stirrup Spacing
P_exp.
ζACI
ζNd
ζCSA
ζNew
BM12 - HSF
BM16 - HSF
BM25 - HSF
220
s230
Stirrup Type
BM220 - HSF
BM150 - HSF
BMs230 - HSF
BM12
BM16
BM25
Flexural Bar Type

Half Section Fanning		P_exp.	P_predict with							
			ζACI	Fail.Elem	ζNd	Fail.Elem	ζCSA	Fail.Elem	ζNew	Fail.Elem
BM12	220	382.4	414.00	S5	382.18	S10	242.23	S10	328.27	S10
			414.01	B6	382.20	S11	242.24	S11	328.30	S11
			414.00	**Flexure+Bar**	**382.20**	**Shear**	**242.24**	**Shear**	**328.30**	**Shear**
	150	405.2	399.54	S9	399.24	S9	311.63	S19	398.95	S9
			399.58	S19	399.27	S19	311.71	S18	398.97	S19
			399.59	N9	399.28	N9	311.72	S17	398.98	S17/N9
			399.58	**Combine**	**399.27**	**Combine**	**311.72**	**Shear**	**398.97**	**Combine**
	s230	466.9	464.36	S5	415.22	S10	257.39	S10	405.52	S10
			464.37	S11	415.24	S11	257.39	S11	405.54	S11
			464.37	**Combine**	**415.24**	**Shear**	**257.39**	**Shear**	**405.54**	**Shear**
BM16	220	309.3	405.46	S5	375.70	S10	235.39	S10	321.54	S10
			405.48	S11	375.72	S11	235.40	S11	321.56	S11
			405.48	**Combine**	**375.72**	**Shear**	**235.40**	**Shear**	**321.56**	**Shear**
	150	416.5	390.99	S9	390.73	S9	304.53	S19	390.47	S9
			391.03	S19	390.76	S19	304.60	S18	390.49	S19
			391.04	N9	390.77	N9	304.61	S17	390.50	S17/N9
			391.03	**Combine**	**390.76**	**Combine**	**304.61**	**Shear**	**390.49**	**Combine**
	s230	450.8	455.54	S5	407.94	S10	250.09	S10	395.55	S10
			455.56	S11	407.95	S11	250.10	S11	395.56	S11
			455.56	**Combine**	**407.95**	**Shear**	**250.10**	**Shear**	**395.56**	**Shear**
BM25	220	360.1	369.27	S5	346.23	S10	203.53	S10	289.75	S10
			369.29	S11	346.25	S11	203.54	S11	289.78	S11
			369.29	**Combine**	**346.25**	**Shear**	**203.54**	**Shear**	**289.78**	**Shear**
	150	415.8	354.50	S9	354.37	S9	271.67	S19	354.27	S9
			354.55	S19	354.40	S19	271.72	S18	354.29	S19
			354.56	N9	354.41	N9	271.73	S17	354.30	N9
			354.55	**Combine**	**354.40**	**Combine**	**271.73**	**Shear**	**354.29**	**Combine**
	s230	444	409.42	S5	311.73	S10	214.29	S10	344.97	S10
			409.44	S11	311.75	S11	214.30	S11	344.99	S11
			409.44	**Combine**	**311.75**	**Shear**	**214.30**	**Shear**	**344.99**	**Shear**

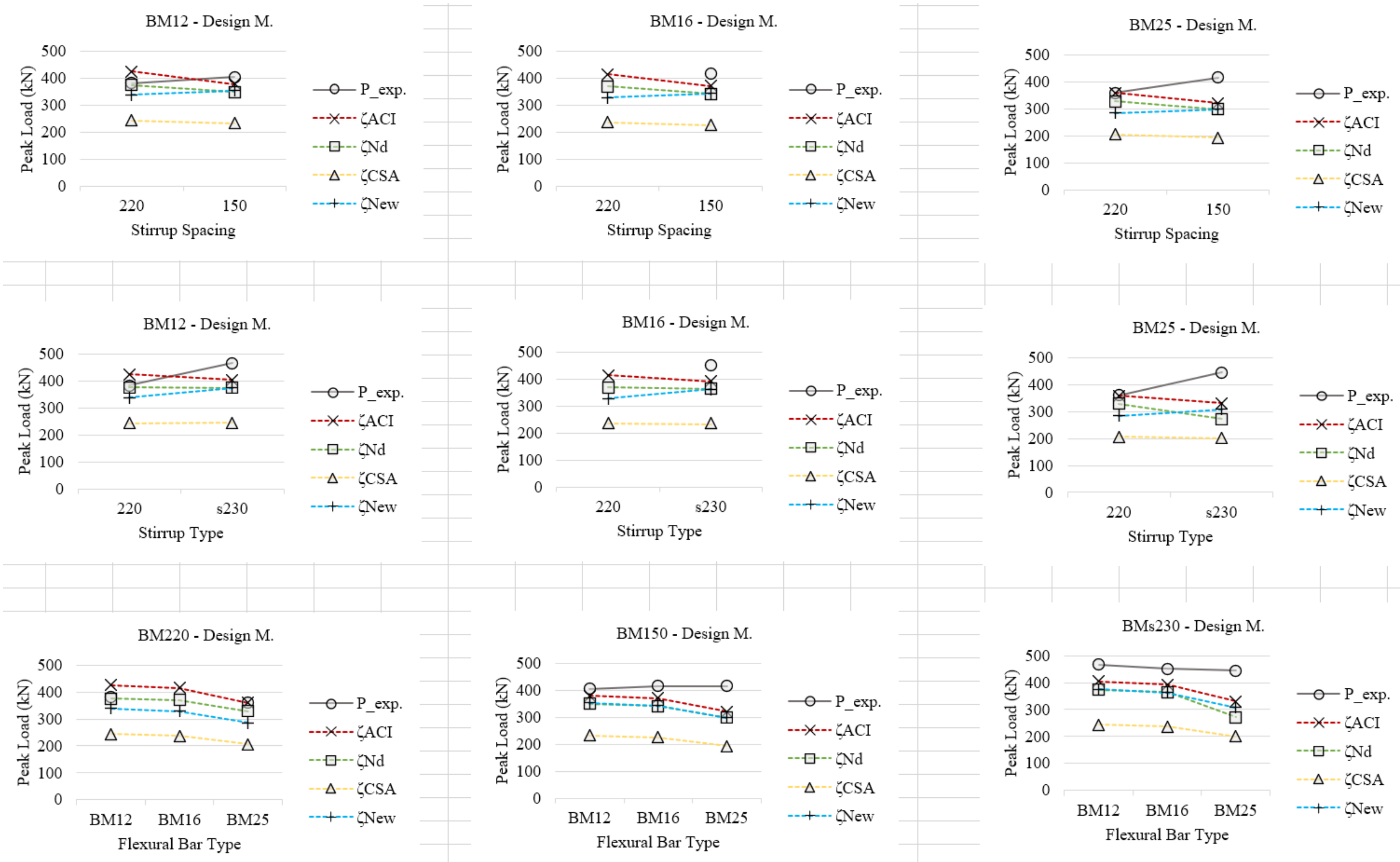
BM12 - Design M.
Peak Load (kN)
500
400
300
200
100
0
220
150
Stirrup Spacing
P_exp.
ζACI
ζNd
ζCSA
ζNew
BM16 - Design M.
Peak Load (kN)
500
400
300
200
100
0
220
150
Stirrup Spacing
P_exp.
ζACI
ζNd
ζCSA
ζNew
BM25 - Design M.
Peak Load (kN)
500
400
300
200
100
0
220
150
Stirrup Spacing
P_exp.
ζACI
ζNd
ζCSA
ζNew
BM12 - Design M.
Peak Load (kN)
500
400
300
200
100
0
220
s230
Stirrup Type
P_exp.
ζACI
ζNd
ζCSA
ζNew
BM16 - Design M.
Peak Load (kN)
500
400
300
200
100
0
220
s230
Stirrup Type
P_exp.
ζACI
ζNd
ζCSA
ζNew
BM25 - Design M.
Peak Load (kN)
500
400
300
200
100
0
220
s230
Stirrup Type
P_exp.
ζACI
ζNd
ζCSA
ζNew
BM220 - Design M.
Peak Load (kN)
500
400
300
200
100
0
BM12
BM16
BM25
Flexural Bar Type
P_exp.
ζACI
ζNd
ζCSA
ζNew
BM150 - Design M.
Peak Load (kN)
500
400
300
200
100
0
BM12
BM16
BM25
Flexural Bar Type
P_exp.
ζACI
ζNd
ζCSA
ζNew
BMs230 - Design M.
Peak Load (kN)
500
400
300
200
100
0
BM12
BM16
BM25
Flexural Bar Type
P_exp.
ζACI
ζNd
ζCSA
ζNew

Design Model		P_exp.	P_predict with							
			ζACI	Fail.Elem	ζNd	Fail.Elem	ζCSA	Fail.Elem	ζNew	Fail.Elem
BM12	220	382.4	425.37	S7	375.66	S7	243.75	S7	338.63	S6
	76.89		425.39	S8	375.67	S8	243.75	S8	338.65	S8
			425.39	**Shear**	**375.67**	**Shear**	**243.75**	**Shear**	**338.65**	**Shear**
	150	405.2	379.59	S7	349.74	S7	233.53	S7	354.12	S6
			379.61	S8	349.74	S8	233.53	S8	354.14	S8
			379.61	**Shear**	**349.74**	**Shear**	**233.53**	**Shear**	**354.14**	**Shear**
	s230	466.9	404.09	S7	374.37	S7	244.40	S7	375.11	S7
	72.68		404.12	S8	374.38	S8	244.41	S8	375.13	S8
			404.12	**Shear**	**374.38**	**Shear**	**244.41**	**Shear**	**375.13**	**Shear**
BM16	220	309.3	415.69	S7	369.63	S7	237.75	S7	329.15	S6
	75.03		415.71	S8	369.64	S8	237.76	S8	329.17	S8
			415.71	**Shear**	**369.64**	**Shear**	**237.76**	**Shear**	**329.17**	**Shear**
	150	416.5	371.23	S7	342.49	S7	226.57	S7	343.99	S6
			371.25	S8	342.50	S8	226.58	S8	344.01	S8
									347.10	S7
			371.25	**Shear**	**342.50**	**Shear**	**226.58**	**Shear**	**344.01**	**Shear**
	s230	450.8	392.52	S6	364.05	S6	236.95	S7	363.25	S7
	71.148		392.55	S8	364.06	S8	236.96	S8	363.27	S8
			392.55	**Shear**	**364.06**	**Shear**	**236.96**	**Shear**	**363.27**	**Shear**
BM25	220	360.1	359.23	S6	329.09	S6	205.88	S7	284.80	S6
	67.424		359.25	S8	329.10	S8	205.89	S8	284.83	S8
			359.25	**Shear**	**329.10**	**Shear**	**205.89**	**Shear**	**284.83**	**Shear**
	150	415.8	321.46	S6	298.48	S6	193.30	S7	298.27	S6
			321.49	S8	298.49	S8	193.31	S8	298.29	S8
			321.49	**Shear**	**298.49**	**Shear**	**193.31**	**Shear**	**298.29**	**Shear**
	s230	444	330.88	S6	271.91	S6	201.42	S7	307.46	S7
	63.279		330.90	S8	271.92	S8	201.43	S8	307.49	S8
			330.90	**Shear**	**271.92**	**Shear**	**201.43**	**Shear**	**307.49**	**Shear**

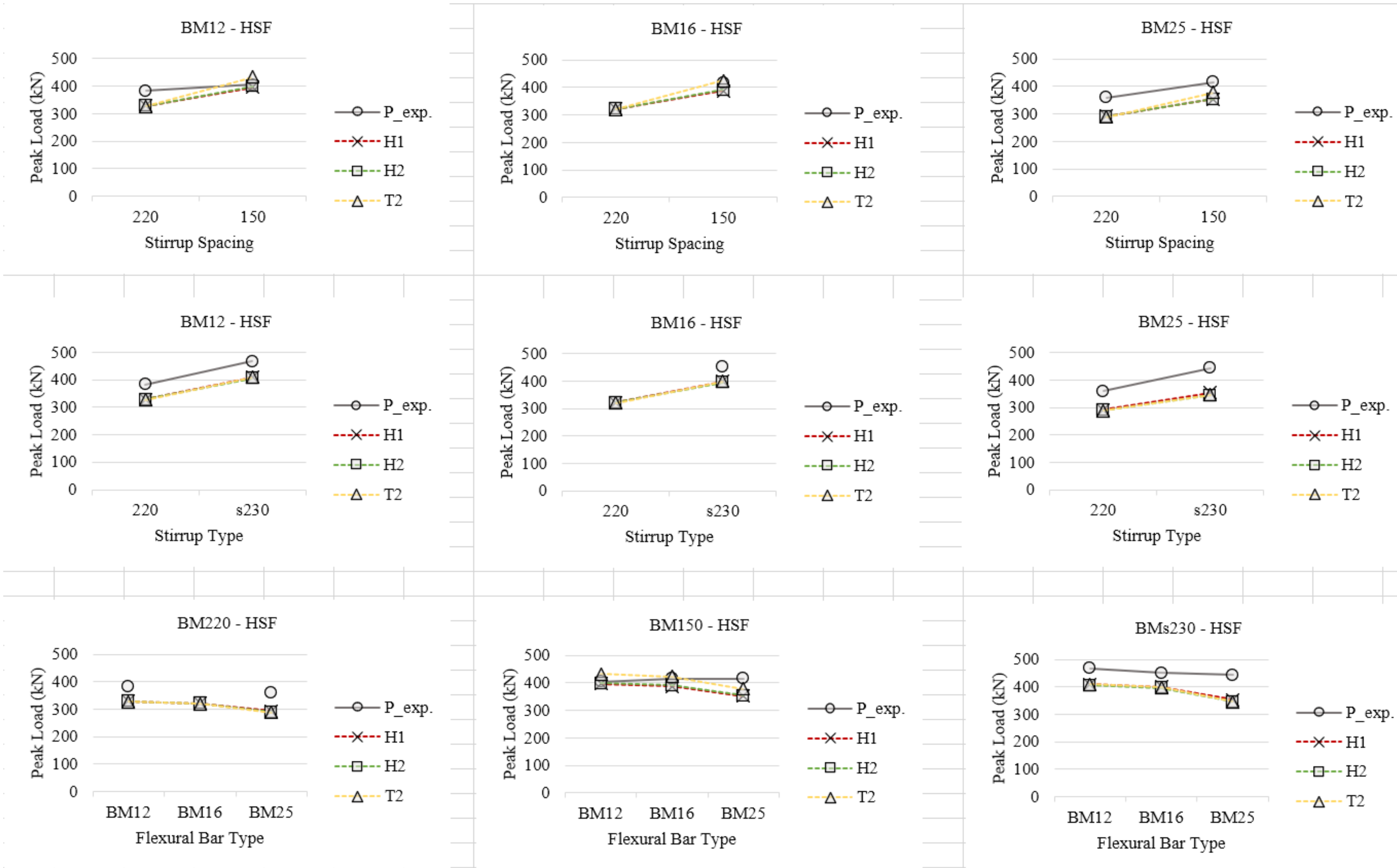
BM12 - HSF
BM16 - HSF
BM25 - HSF
Peak Load (kN)
0
100
200
300
400
500
220
150
Stirrup Spacing
s230
Stirrup Type
BM220 - HSF
BM150 - HSF
BMs230 - HSF
BM12
BM16
BM25
Flexural Bar Type
P_exp.
H1
H2
T2

Half Section Fanning		P_exp.	P_predict with					
			H1	Fail.Elem	H2	Fail.Elem	T2	Fail.Elem
BM12	220	382.4	328.04	S10	328.27	S10	327.03	S10
			328.05	S11	328.30	S11	327.07	S11
			328.05	**Shear**	**328.30**	**Shear**	**327.07**	**Shear**
	150	405.2	396.42	S9	398.95	S9	433.37	S17
			396.44	S19	398.97	S19	433.40	S19
			396.46	S17	399.28	N9/17	433.40	N10
			396.44	**Combine**	**398.97**	**Combine**	**433.40**	**Combine**
	s230	466.9	408.88	S10	405.52	S10	409.35	S10
			408.89	S11	405.54	S11	409.38	S11
			408.89	**Shear**	**405.54**	**Shear**	**409.38**	**Shear**
BM16	220	309.3	321.86	S10	321.54	S10	320.22	S10
			321.87	S11	321.56	S11	320.26	S11
			321.87	**Shear**	**321.56**	**Shear**	**320.26**	**Shear**
	150	416.5	388.17	S9	390.47	S9	423.97	S17
			388.19	S19	390.49	S19	423.99	S19
			388.20	S17	390.50	N9/17	424.00	S18/N10
			388.19	**Combine**	**390.49**	**Combine**	**424.00**	**Combine**
	s230	450.8	399.77	S10	395.55	S10	398.84	S10
			399.78	S11	395.56	S11	398.86	S11
			399.78	**Shear**	**395.56**	**Shear**	**398.86**	**Shear**
BM25	220	360.1	292.73	S10	289.75	S10	287.82	S10
			292.74	S11	289.78	S11	287.86	S11
			292.74	**Shear**	**289.78**	**Shear**	**287.86**	**Shear**
	150	415.8	353.05	S9	354.27	S9	379.02	S17
			353.07	S19	354.29	S19	379.04	S19
			353.09	S17	354.30	N9	379.05	S18/N10
			353.07	**Combine**	**354.29**	**Combine**	**379.05**	**Combine**
	s230	444	353.13	S10	344.97	S10	346.03	S10
			353.14	S11	344.99	S11	346.05	S11
			353.14	**Shear**	**344.99**	**Shear**	**346.05**	**Shear**

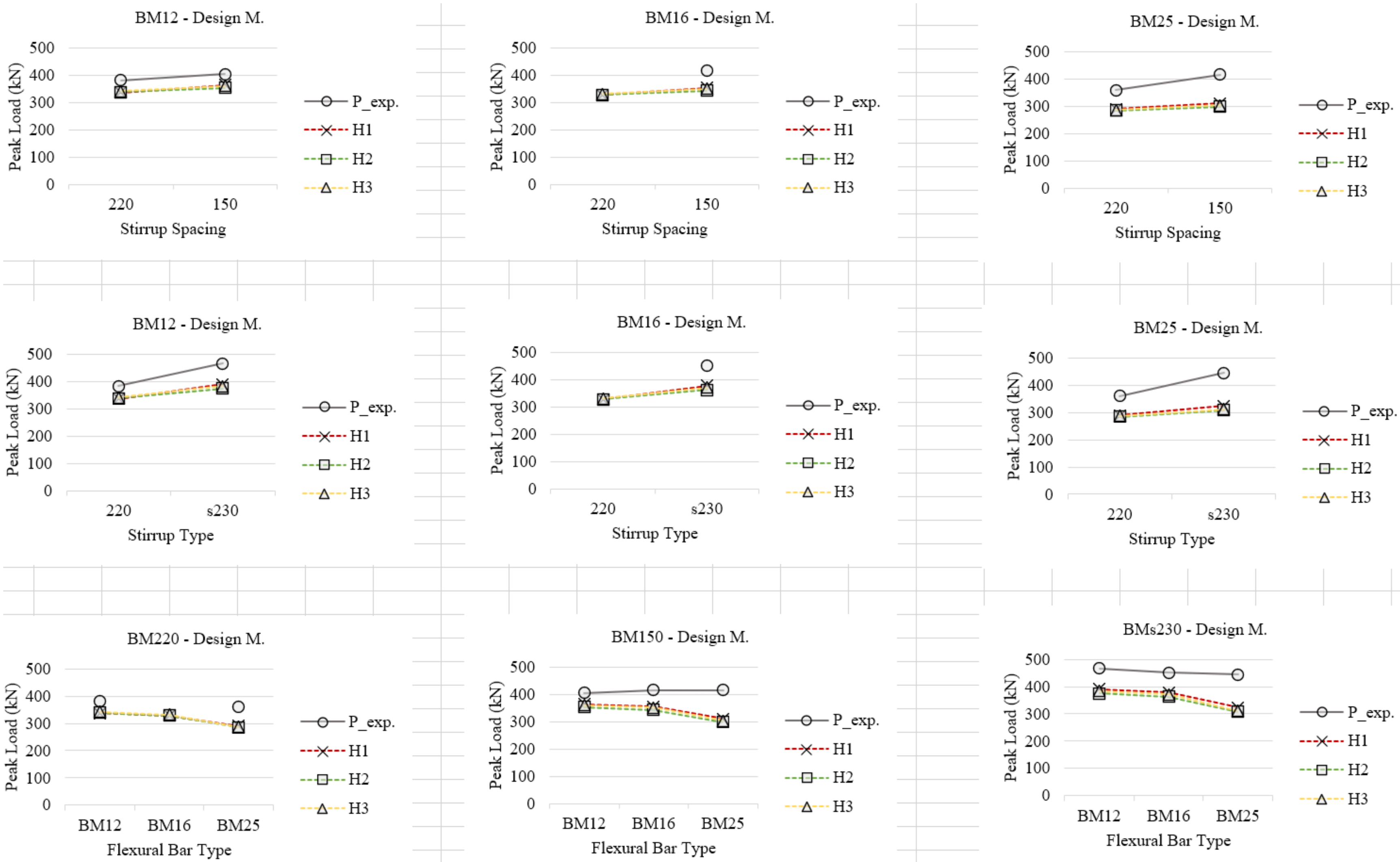
BM12 - Design M.
BM16 - Design M.
BM25 - Design M.
Peak Load (kN)
0
100
200
300
400
500
220
150
Stirrup Spacing
220
s230
Stirrup Type
BM220 - Design M.
BM150 - Design M.
BMs230 - Design M.
BM12
BM16
BM25
Flexural Bar Type
P_exp.
H1
H2
H3

Design Model		P_exp.	P_predict with					
			H1	Fail.Elem	H2	Fail.Elem	H3	Fail.Elem
BM12	220	382.4	336.91	S6	338.63	S6	342.06	S6
	76.89		336.93	S8	338.65	S8	342.08	S8
			336.93	**Shear**	**338.65**	**Shear**	**342.08**	**Shear**
	150	405.2	364.39	S6	354.12	S6	361.21	S6
			364.41	S8	354.14	S8	361.23	S8
			364.41	**Shear**	**354.14**	**Shear**	**361.23**	**Shear**
	s230	466.9	389.93	S7	375.11	S7	383.76	S7
	72.68		389.95	S8	375.13	S8	383.79	S8
			389.95	**Shear**	**375.13**	**Shear**	**383.79**	**Shear**
BM16	220	309.3	328.73	S6	329.15	S6	332.26	S6
	75.03		328.75	S8	329.17	S8	332.28	S8
			328.75	**Shear**	**329.17**	**Shear**	**332.28**	**Shear**
	150	416.5	354.89	S6	343.99	S6	350.99	S6
			354.91	S8	344.01	S8	351.01	S8
			354.91	**Shear**	**344.01**	**Shear**	**351.01**	**Shear**
	s230	450.8	378.34	S7	363.25	S7	371.06	S7
	71.148		378.36	S8	363.27	S8	371.09	S8
			378.36	**Shear**	**363.27**	**Shear**	**371.09**	**Shear**
BM25	220	360.1	290.16	S6	284.80	S6	286.77	S6
	67.424		290.18	S8	284.83	S8	286.80	S8
			290.18	**Shear**	**284.83**	**Shear**	**286.80**	**Shear**
	150	415.8	311.27	S6	298.27	S6	303.26	S6
			311.29	S8	298.29	S8	303.29	S8
			311.29	**Shear**	**298.29**	**Shear**	**303.29**	**Shear**
	s230	444	323.45	S7	307.46	S7	311.94	S7
	63.279		323.47	S8	307.49	S8	311.97	S8
			323.47	**Shear**	**307.49**	**Shear**	**311.97**	**Shear**

For deep beams with stirrups analyzed with h_c based on force equilibrium:

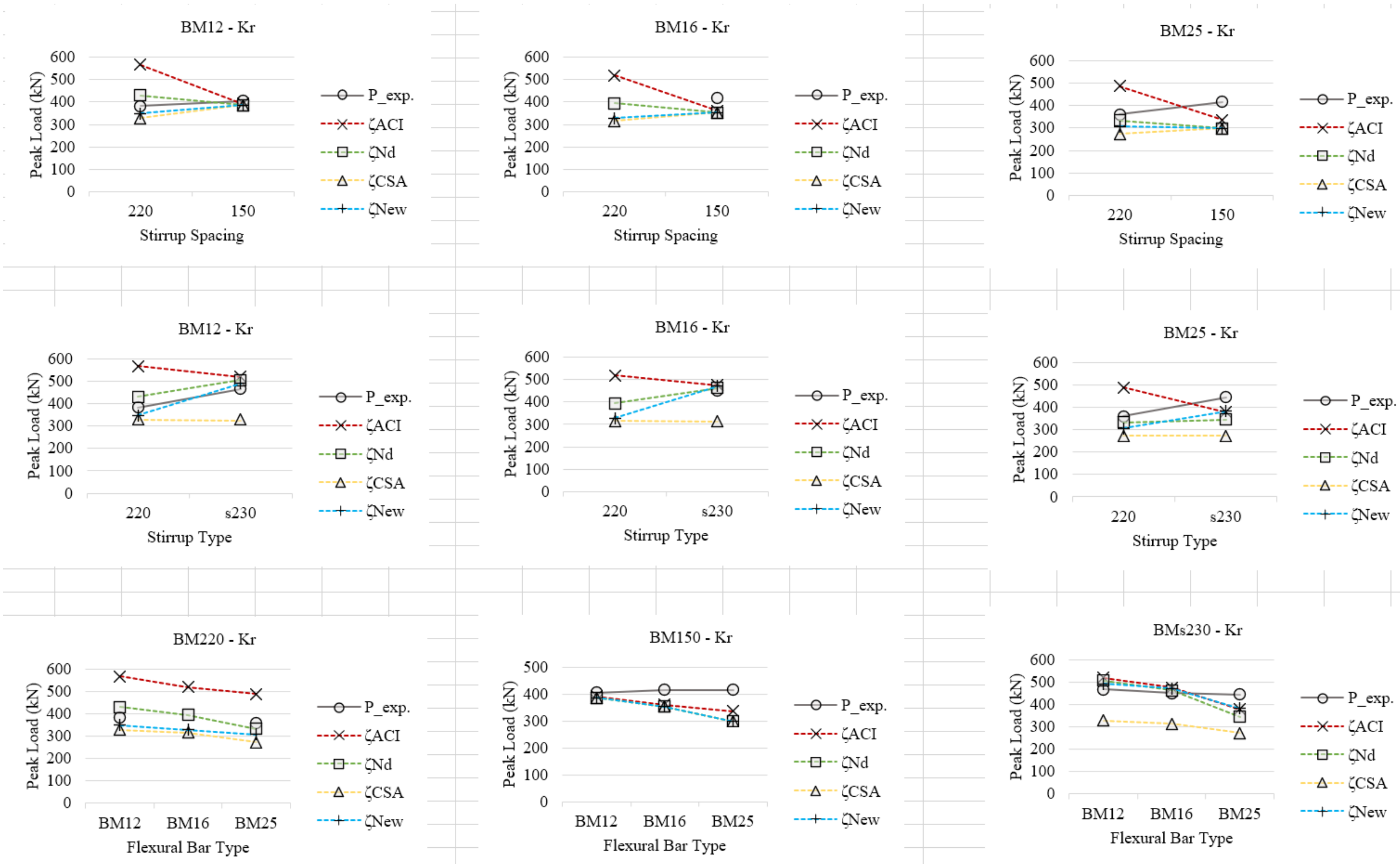

Kr Model		P_exp.	P_predict with							
			ζACI	Fail.Elem	ζNd	Fail.Elem	ζCSA	Fail.Elem	ζNew	Fail.Elem
BM12	220	382.4	566.59	S12	276.20	S12	172.18	S12	347.93	S12
			566.59	B6/B7	430.65	S5	328.51	S11	348.09	S10
			566.59	**Bar Failure**	**430.65**	**Combine**	**328.51**	**Shear**	**348.09**	**Shear**
	150	405.2	391.85	S20	188.29	S20	137.55	S20	290.93	S20
			392.07	S9	386.23	S9	386.27	S9	386.34	S9
			392.07	**Combine**	**386.23**	**Combine**	**386.27**	**Combine**	**386.34**	**Combine**
	s230	466.9	519.43	S5	506.15	S5	299.81	S12	491.68	S11
			519.45	S12	506.16	S12	328.26	S11	491.70	S12
			519.45	**Combine**	**506.16**	**Combine**	**328.26**	**Shear**	**491.70**	**Shear**
BM16	220	309.3	518.34	S12	252.64	S12	165.55	S12	328.80	S12
			518.34	B6/B7	393.80	S5	315.21	S11	328.97	S10
			518.34	**Bar Failure**	**393.80**	**Combine**	**315.21**	**Shear**	**328.97**	**Shear**
	150	416.5	360.98	S20	173.48	S20	132.63	S20	275.17	S20
			361.16	S9	352.91	S9	352.93	S9	352.99	S9
			361.16	**Combine**	**352.91**	**Combine**	**352.93**	**Combine**	**352.99**	**Combine**
	s230	450.8	475.40	S5	461.88	S5	284.22	S12	470.08	S11
			475.42	S12	461.88	S12	314.19	S11	470.10	S12
			475.42	**Combine**	**461.88**	**Combine**	**314.19**	**Shear**	**470.10**	**Shear**
BM25	220	360.1	487.21	N7	243.61	S12	152.33	S12	306.63	S12
					332.85	S5	272.81	S11	306.70	S10
			487.21	**Node Crush**	**332.85**	**Combine**	**272.81**	**Shear**	**306.70**	**Shear**
	150	415.8	335.64	S20	161.44	S20	119.70	S20	249.16	S20
			335.70	S9	297.70	S9	297.71	S9	297.75	S9
			335.70	**Combine**	**297.70**	**Combine**	**297.71**	**Combine**	**297.75**	**Combine**
	s230	444	378.22	S5	344.41	S12	272.50	S12	382.01	S5
			378.25	S12	344.45	S5	272.81	S11	382.02	S12
			378.25	**Combine**	**344.45**	**Combine**	**272.81**	**Shear**	**382.02**	**Combine**

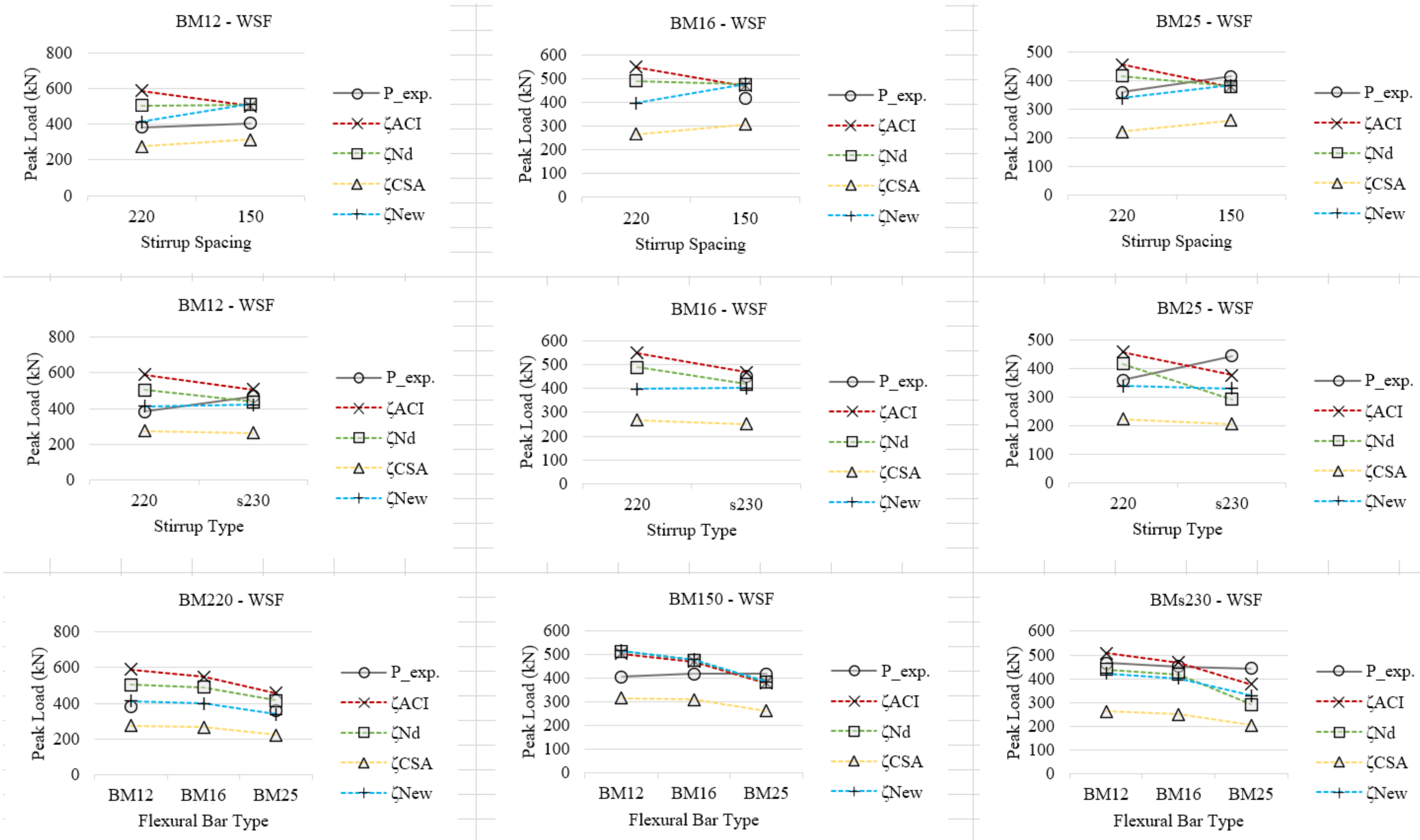
BM12 - WSF
BM16 - WSF
BM25 - WSF
Peak Load (kN)
Stirrup Spacing
220
150
Stirrup Type
s230
BM220 - WSF
BM150 - WSF
BMs230 - WSF
Flexural Bar Type
BM12
BM16
BM25
P_exp.
ζACI
ζNd
ζCSA
ζNew

Whole Section Fanning		P_exp.	P_predict with							
			ζACI	Fail.Elem	ζNd	Fail.Elem	ζCSA	Fail.Elem	ζNew	Fail.Elem
BM12	220	382.4	588.52	N7	504.20	S10	275.66	S10	413.61	S10
					504.23	S11	275.68	S11	413.86	S11
					504.23	S12	275.68	S12	413.86	S12
			588.52	**Node Crush**	**504.23**	**Shear**	**275.68**	**Shear**	**413.86**	**Shear**
	150	405.2	502.59	S9	511.33	S9	304.91	S18	513.59	S9
			588.52	N11	511.36	S19	315.34	S21	513.64	S19
					511.37	S20	315.42	S19	513.66	S20
					511.39	S21	315.42	S20	513.66	S21
					511.44	S17	315.45	S17	513.67	S17
			502.59	**Flexure**	**511.36**	**Combine**	**315.45**	**Shear**	**513.64**	**Combine**
	s230	466.9	507.60	S5	438.48	S10	262.38	S10	421.90	S10
			507.66	S11	438.51	S12	262.39	S12	421.97	S12
			507.67	S12	438.52	S11	262.40	S11	421.99	S11
			507.66	**Combine**	**438.52**	**Shear**	**262.40**	**Shear**	**421.99**	**Shear**
BM16	220	309.3	548.83	N7	489.68	S10	267.06	S10	397.29	S10
					489.70	S11	267.07	S11	397.42	S11
					489.71	S12	267.07	S12	397.43	S12
			548.83	**Node Crush**	**489.71**	**Shear**	**267.07**	**Shear**	**397.43**	**Shear**
	150	416.5	469.25	S9	474.89	S9	298.23	S18	477.56	S9
			548.83	N11	474.92	S19	307.60	S21	477.61	S19
					474.93	S20	307.66	S20	477.63	S20
					474.95	S21	307.67	S19	477.64	S21
					475.00	S17	307.69	S17	477.65	S17
			469.25	**Flexure**	**474.92**	**Combine**	**307.69**	**Shear**	**477.61**	**Combine**
	s230	450.8	468.92	S5	417.85	S10	251.30	S10	401.56	S10
			468.97	S11	417.88	S12	251.32	S12	401.61	S12
			468.99	S12	417.89	S11	251.33	S11	401.63	S11
			468.97	**Combine**	**417.89**	**Shear**	**251.33**	**Shear**	**401.63**	**Shear**
BM25	220	360.1	457.49	S5	416.73	S10	222.06	S10	331.74	S10
			457.52	S11	416.76	S11	222.08	S11	339.16	S11
			457.53	B6	416.76	S12	222.08	S12	339.16	S12
			457.52	**Combine+Bar**	**416.76**	**Shear**	**222.08**	**Shear**	**339.16**	**Shear**
	150	415.8	378.32	S9	381.06	S9	247.74	S18	383.61	S9
			487.21	N11	381.10	S19	261.22	S21	383.77	S19
					381.11	S20	261.32	S20	383.80	S20
					381.14	S21	261.33	S19	383.81	S21
					381.19	S17	261.34	S17	383.83	S17
			378.32	**Flexure**	**381.10**	**Combine**	**261.34**	**Shear**	**383.77**	**Combine**
	s230	444	376.84	S5	291.17	S10	205.62	S10	329.07	S10
			376.94	S11	291.21	S11	205.64	S12	329.14	S12
			376.95	S12	291.21	S12	205.65	S11	329.16	S11
			376.94	**Combine**	**291.21**	**Shear**	**205.65**	**Shear**	**329.16**	**Shear**

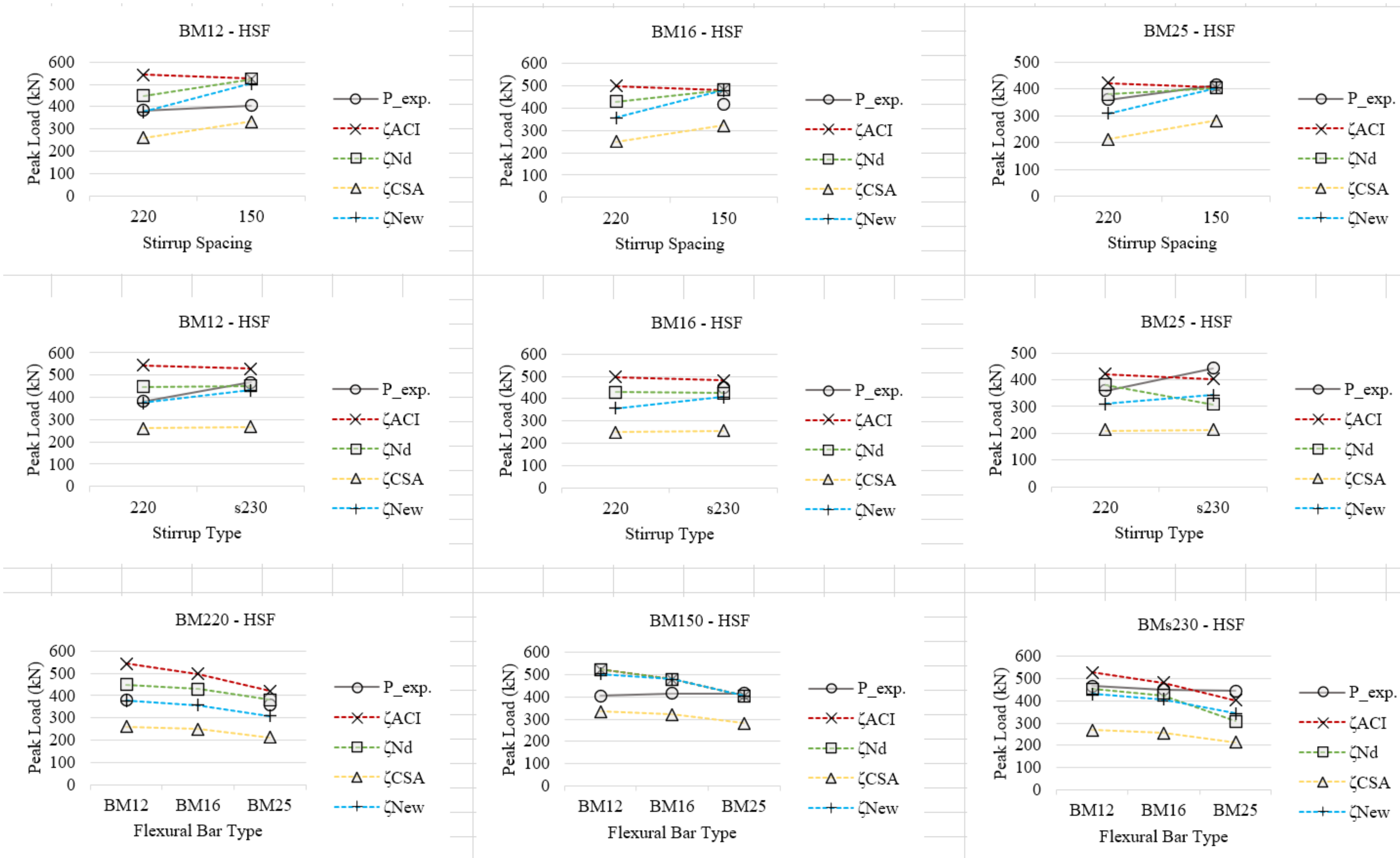
BM12 - HSF
Peak Load (kN)
600
500
400
300
200
100
0
220
150
Stirrup Spacing
P_exp.
ζACI
ζNd
ζCSA
ζNew
BM16 - HSF
Peak Load (kN)
220
150
Stirrup Spacing
BM25 - HSF
Peak Load (kN)
220
150
Stirrup Spacing
BM12 - HSF
220
s230
Stirrup Type
BM16 - HSF
220
s230
Stirrup Type
BM25 - HSF
220
s230
Stirrup Type
BM220 - HSF
BM12
BM16
BM25
Flexural Bar Type
BM150 - HSF
BM12
BM16
BM25
Flexural Bar Type
BMs230 - HSF
BM12
BM16
BM25
Flexural Bar Type

Half Section Fanning		P_exp.	P_predict with							
			ζACI	Fail.Elem	ζNd	Fail.Elem	ζCSA	Fail.Elem	ζNew	Fail.Elem
BM12	220	382.4	543.50	S5	448.57	S10	260.43	S10	376.16	S10
			543.51	B6	448.59	S11	260.44	S11	376.19	S11
			543.50	**Flexure+Bar**	**448.59**	**Shear**	**260.44**	**Shear**	**376.19**	**Shear**
	150	405.2	524.13	S9	523.62	S9	333.70	S19	504.15	S9
			524.17	S19	523.64	S19	333.80	S18	504.17	S19
			524.18	B12	523.65	B12	333.82	S17	504.18	S18/N10
			524.17	**Combine+Bar**	**523.64**	**Combine+Bar**	**333.82**	**Shear**	**504.17**	**Combine**
	s230	466.9	528.42	S5	451.80	S10	268.15	S10	432.06	S10
			528.44	S11	451.82	S11	268.16	S11	432.07	S11
			528.44	**Combine**	**451.82**	**Shear**	**268.16**	**Shear**	**432.07**	**Shear**
BM16	220	309.3	497.95	S5	428.85	S10	250.31	S10	356.69	S10
			497.96	B6	428.87	S11	250.32	S11	356.72	S11
			497.96	**Flexure+Bar**	**428.87**	**Shear**	**250.32**	**Shear**	**356.72**	**Shear**
	150	416.5	480.11	S9	479.72	S9	321.84	S19	478.32	S17
			480.15	S19	479.75	S19	321.93	S18	478.34	S19
			480.20	S17	479.78	S17	321.95	S17	390.50	S18/N10
			480.15	**Combine**	**479.75**	**Combine**	**321.95**	**Shear**	**478.34**	**Combine**
	s230	450.8	481.46	S5	423.58	S10	254.82	S10	406.53	S10
			481.48	S11	423.59	S11	254.83	S11	406.54	S11
			481.48	**Combine**	**423.59**	**Shear**	**254.83**	**Shear**	**406.54**	**Shear**
BM25	220	360.1	421.74	S5	380.68	S10	213.01	S10	309.84	S10
			421.75	B6	380.70	S11	213.03	S11	309.87	S11
			421.75	**Flexure+Bar**	**380.70**	**Shear**	**213.03**	**Shear**	**309.87**	**Shear**
	150	415.8	404.96	S9	404.79	S9	282.80	S19	404.64	S9
			405.01	S19	404.82	S19	282.86	S17	404.66	S19
			405.06	S17	404.86	S17	282.86	S18	404.67	S17
			405.01	**Combine**	**404.82**	**Combine**	**282.86**	**Shear**	**404.66**	**Combine**
	s230	444	403.32	S5	308.64	S10	213.11	S10	342.43	S10
			403.34	S11	308.66	S11	213.12	S11	342.45	S11
			403.34	**Combine**	**308.66**	**Shear**	**213.12**	**Shear**	**342.45**	**Shear**

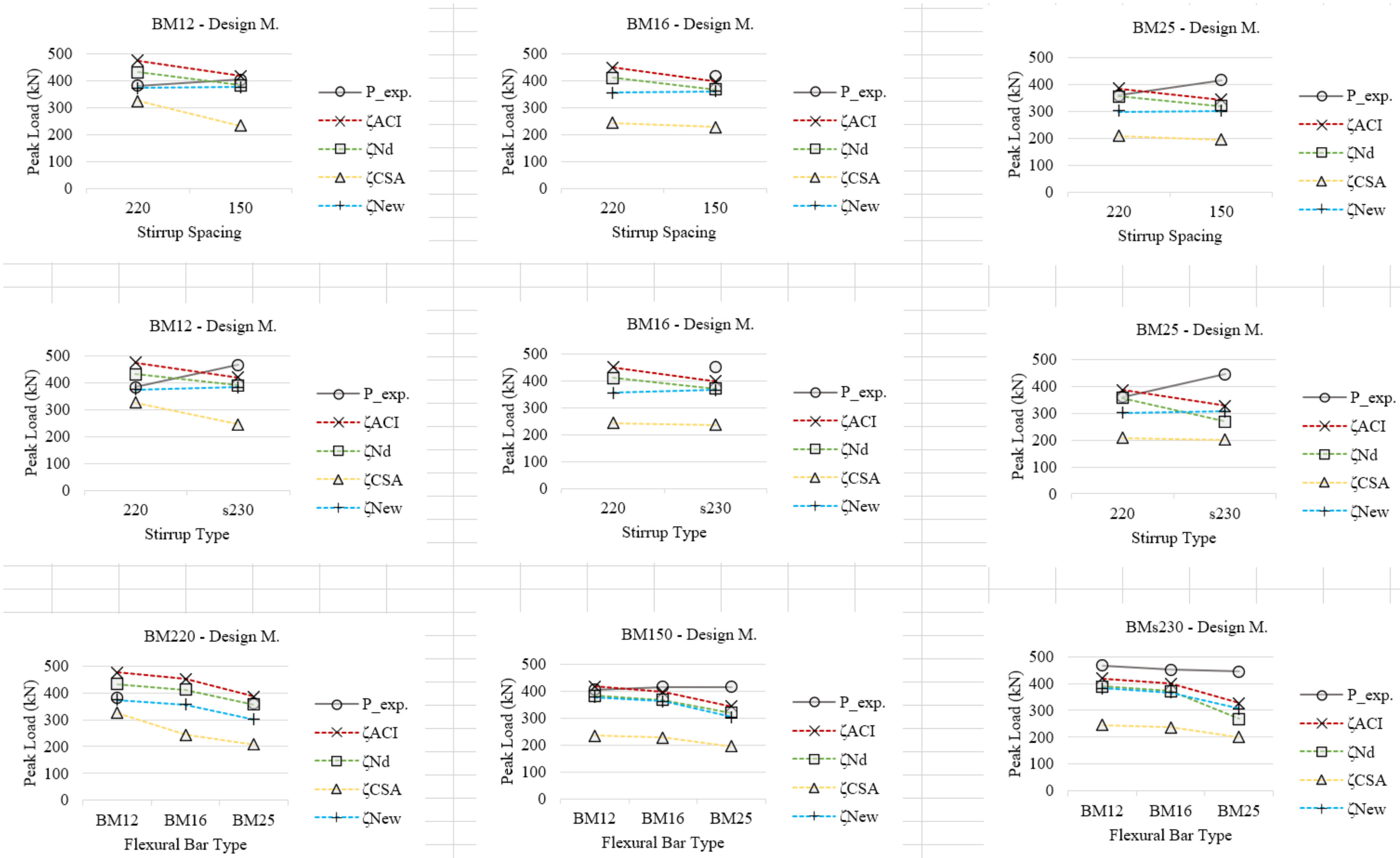
BM12 - Design M.
BM16 - Design M.
BM25 - Design M.
Peak Load (kN)
500
400
300
200
100
0
220
150
Stirrup Spacing
P_exp.
ζACI
ζNd
ζCSA
ζNew
s230
Stirrup Type
BM220 - Design M.
BM150 - Design M.
BMs230 - Design M.
BM12
BM16
BM25
Flexural Bar Type

Design Model		P_exp.	P_predict with							
			ζACI	Fail.Elem	ζNd	Fail.Elem	ζCSA	Fail.Elem	ζNew	Fail.Elem
BM12	220	382.4	474.87	S7	431.70	S7	251.75	S7	374.47	S6
	76.89		474.89	S8	431.71	S8	325.60	S8	374.50	S8
			474.89	**Shear**	**431.71**	**Shear**	**325.60**	**Shear**	**374.50**	**Shear**
	150	405.2	417.94	S7	383.40	S7	233.90	S7	377.88	S7
			417.97	S8	383.41	S8	233.91	S8	377.91	S8
			417.97	**Shear**	**383.41**	**Shear**	**233.91**	**Shear**	**377.91**	**Shear**
	s230	466.9	418.76	S7	389.48	S7	245.73	S7	382.71	S7
	72.68		418.79	S8	389.49	S8	245.74	S8	382.74	S8
			418.79	**Shear**	**389.49**	**Shear**	**245.74**	**Shear**	**382.74**	**Shear**
BM16	220	309.3	450.55	S7	411.78	S7	244.66	S7	357.04	S6
	75.03		450.57	S8	411.79	S8	244.67	S8	357.06	S8
			450.57	**Shear**	**411.79**	**Shear**	**244.67**	**Shear**	**357.06**	**Shear**
	150	416.5	397.63	S7	367.85	S7	228.07	S7	362.24	S7
			397.66	S8	367.86	S8	228.08	S8	362.26	S8
			397.66	**Shear**	**367.86**	**Shear**	**228.08**	**Shear**	**362.26**	**Shear**
	s230	450.8	400.00	S6	371.60	S6	237.68	S7	366.16	S7
	71.148		400.03	S8	371.61	S8	237.69	S8	366.19	S8
			400.03	**Shear**	**371.61**	**Shear**	**237.69**	**Shear**	**366.19**	**Shear**
BM25	220	360.1	385.37	S7	355.95	S7	208.59	S7	301.51	S6
	67.424		385.40	S8	355.96	S8	208.59	S8	301.54	S8
			385.40	**Shear**	**355.96**	**Shear**	**208.59**	**Shear**	**301.54**	**Shear**
	150	415.8	343.03	S7	319.21	S7	194.48	S7	302.81	S7
			343.06	S8	319.22	S8	194.49	S8	302.84	S8
			343.06	**Shear**	**319.22**	**Shear**	**194.49**	**Shear**	**302.84**	**Shear**
	s230	444	326.96	S6	268.63	S6	201.25	S7	306.94	S7
	63.279		326.99	S8	268.64	S8	201.26	S8	306.97	S8
			326.99	**Shear**	**268.64**	**Shear**	**201.26**	**Shear**	**306.97**	**Shear**

For deep beams with stirrups analyzed with h_C equal to 0.2d:

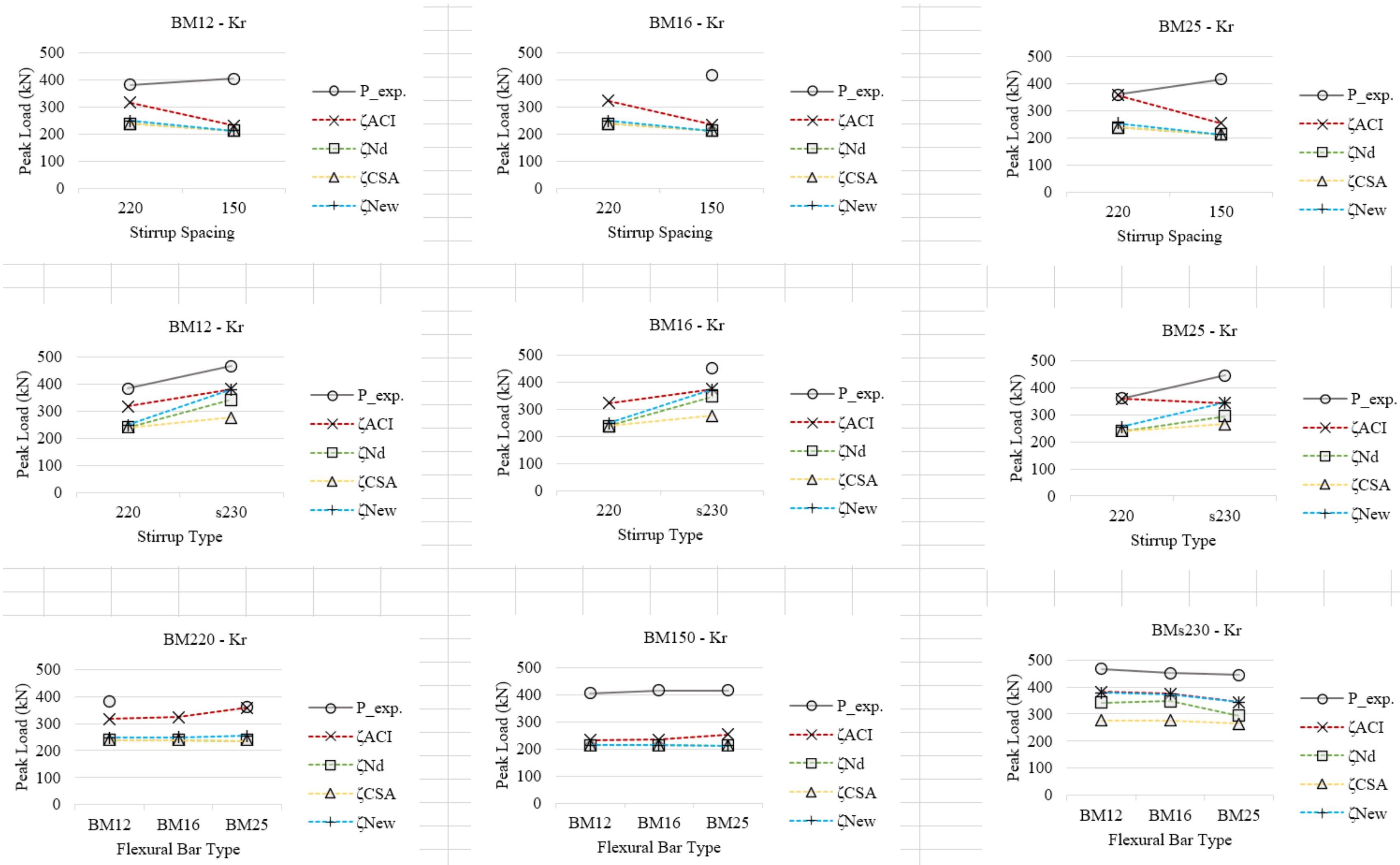

Kr Model		P_exp.	P_predict with							
			ζACI	Fail.Elem	ζNd	Fail.Elem	ζCSA	Fail.Elem	ζNew	Fail.Elem
BM12	220	382.4	317.50	S12	154.62	S12	140.21	S12	248.39	S12
			317.53	S5	239.42	S5	239.38	S5	248.52	S5
			317.53	**Combine**	**239.42**	**Combine**	**239.38**	**Combine**	**248.52**	**Combine**
	150	405.2	232.41	S20	111.75	S20	114.45	S20	212.00	S20
			232.49	S9	213.28	S9	213.26	S9	213.28	S9
			232.49	**Combine**	**213.28**	**Combine**	**213.26**	**Combine**	**213.28**	**Combine**
	s230	466.9	381.51	S5	342.44	S12	238.38	S12	379.02	S5
			381.52	S12	342.45	S5	276.54	S5	379.04	S12
			381.52	**Combine**	**342.45**	**Combine**	**276.54**	**Combine**	**379.04**	**Combine**
BM16	220	309.3	323.11	S12	157.57	S12	139.16	S12	249.13	S12
			323.14	S5	239.34	S5	239.30	S5	400.89	N7
			323.14	**Combine**	**239.34**	**Combine**	**239.30**	**Combine**	**249.13**	**Shear**
	150	416.5	235.24	S20	113.13	S20	113.26	S20	211.60	S20
			235.32	S9	213.20	S9	213.18	S9	213.20	S9
			235.32	**Combine**	**213.20**	**Combine**	**213.18**	**Combine**	**213.20**	**Combine**
	s230	450.8	375.56	S5	347.69	S5	239.30	S12	373.82	S5
			375.58	S12	347.69	S12	276.44	S5	373.84	S12
			375.58	**Combine**	**347.69**	**Combine**	**276.44**	**Combine**	**373.84**	**Combine**
BM25	220	360.1	357.86	S12	176.98	S12	134.74	S12	254.70	S12
			357.88	S5	238.81	S5	238.82	S5	254.76	S10
			357.88	**Combine**	**238.81**	**Combine**	**238.82**	**Combine**	**254.76**	**Shear**
	150	415.8	253.08	S20	121.80	S20	107.50	S20	210.11	S20
			253.13	S9	212.70	S9	212.69	S9	212.71	S9
			253.13	**Combine**	**212.70**	**Combine**	**212.69**	**Combine**	**212.71**	**Combine**
	s230	444	343.51	S5	293.61	S12	250.66	S12	344.80	S5
			343.53	S12	293.69	S5	264.38	S11	344.82	S12
			343.53	**Combine**	**293.69**	**Combine**	**264.38**	**Shear**	**344.82**	**Combine**

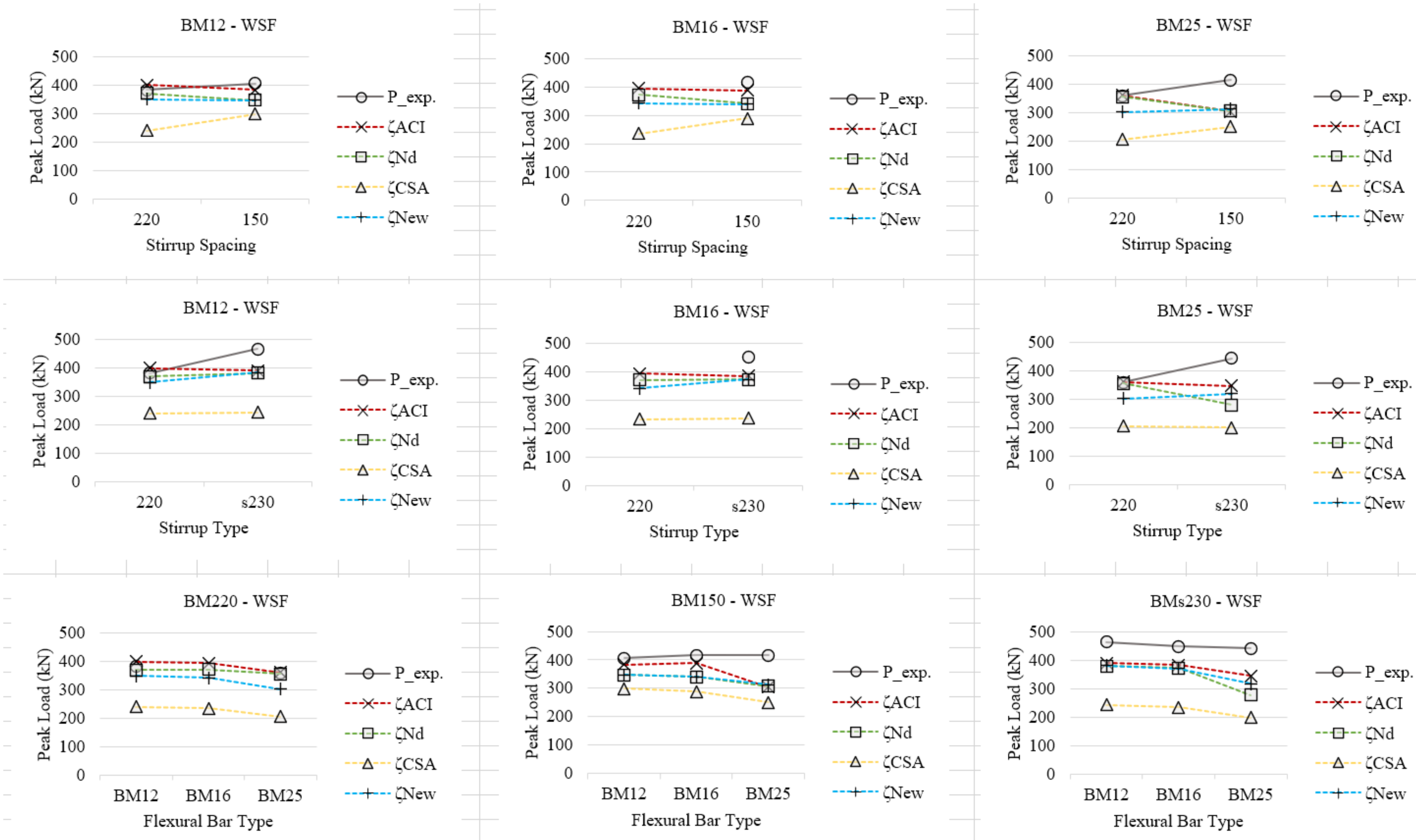
BM12 - WSF
BM16 - WSF
BM25 - WSF
Peak Load (kN)
500
400
300
200
100
0
220
150
s230
Stirrup Spacing
Stirrup Type
BM220 - WSF
BM150 - WSF
BMs230 - WSF
BM12
BM16
BM25
Flexural Bar Type
P_exp.
ζACI
ζNd
ζCSA
ζNew

Whole Section Fanning		P_exp.	P_predict with							
			ζACI	Fail.Elem	ζNd	Fail.Elem	ζCSA	Fail.Elem	ζNew	Fail.Elem
BM12	220	382.4	399.57	S5	370.81	S10	240.30	S10	349.68	S10
			399.59	S11	370.82	S11	240.30	S11	349.71	S11
			399.61	S12	370.83	S12	240.31	S12	349.72	S12
			399.59	**Combine**	**370.83**	**Shear**	**240.31**	**Shear**	**349.72**	**Shear**
	150	405.2	345.34	S9	346.39	S9	297.79	S18	346.82	S9
			383.90	S19	346.41	S19	298.00	S21	346.88	S19
			383.93	S20	346.42	S20	298.01	S19	346.90	S20
			383.95	S21	346.44	S21	298.02	S20	346.91	S21
			383.96	N9	346.45	N9	298.03	S17	346.92	S17/N9
			383.90	**Combine**	**346.41**	**Combine**	**298.03**	**Shear**	**346.88**	**Combine**
	s230	466.9	391.65	S5	381.89	S10	244.54	S10	383.67	S10
			391.69	S11	381.91	S11	244.55	S12	383.71	S12
			391.70	S12	381.91	S12	244.56	S11	383.73	S11
			391.69	**Combine**	**381.91**	**Shear**	**244.56**	**Shear**	**383.73**	**Shear**
BM16	220	309.3	393.86	S5	372.18	S10	235.46	S10	342.38	S10
			393.88	S11	372.19	S11	235.46	S11	342.41	S11
			393.90	S12	372.20	S12	235.47	S12	400.89	N7
			393.88	**Combine**	**372.20**	**Shear**	**235.47**	**Shear**	**342.41**	**Shear**
	150	416.5	338.83	S9	340.21	S9	288.50	S18	340.45	S9
			387.87	S19	340.23	S19	289.22	S21	340.51	S19
			387.90	S20	340.24	S20	289.24	S19	340.53	S20
			387.92	S21	340.26	S21	289.24	S20	340.55	S21
			387.93	N9	340.27	N9	289.25	S17	340.56	S17/N9
			387.87	**Combine**	**340.23**	**Combine**	**289.25**	**Shear**	**340.51**	**Combine**
	s230	450.8	384.54	S5	374.04	S10	237.05	S10	372.82	S10
			384.58	S11	374.06	S12	237.07	S12	372.86	S12
			384.59	S12	374.07	S11	237.08	S11	372.88	S11
			384.58	**Combine**	**374.07**	**Shear**	**237.08**	**Shear**	**372.88**	**Shear**
BM25	220	360.1	361.19	S5	355.80	S10	205.72	S10	302.26	S10
			361.22	S11	355.81	S11	205.73	S11	302.38	S11
			361.24	S12	355.82	S12	205.74	S12	302.38	S12
			361.22	**Combine**	**355.82**	**Shear**	**205.74**	**Shear**	**302.38**	**Shear**
	150	415.8	304.84	S9	306.65	S9	242.03	S18	306.93	S9
			400.89	N11	306.68	S19	251.29	S21	312.73	S19
					306.69	S20	251.33	S17	312.76	S20
					306.72	S21	251.33	S19	312.77	S21
					306.73	N9	251.33	S20	312.78	N9
			304.84	**Flexure**	**306.68**	**Combine**	**251.33**	**Shear**	**312.73**	**Combine**
	s230	444	347.63	S5	279.64	S10	200.55	S10	319.26	S10
			347.71	S11	279.67	S11	200.57	S12	319.33	S12
			347.72	S12	279.67	S12	200.58	S11	319.35	S11
			347.71	**Combine**	**279.67**	**Shear**	**200.58**	**Shear**	**319.35**	**Shear**

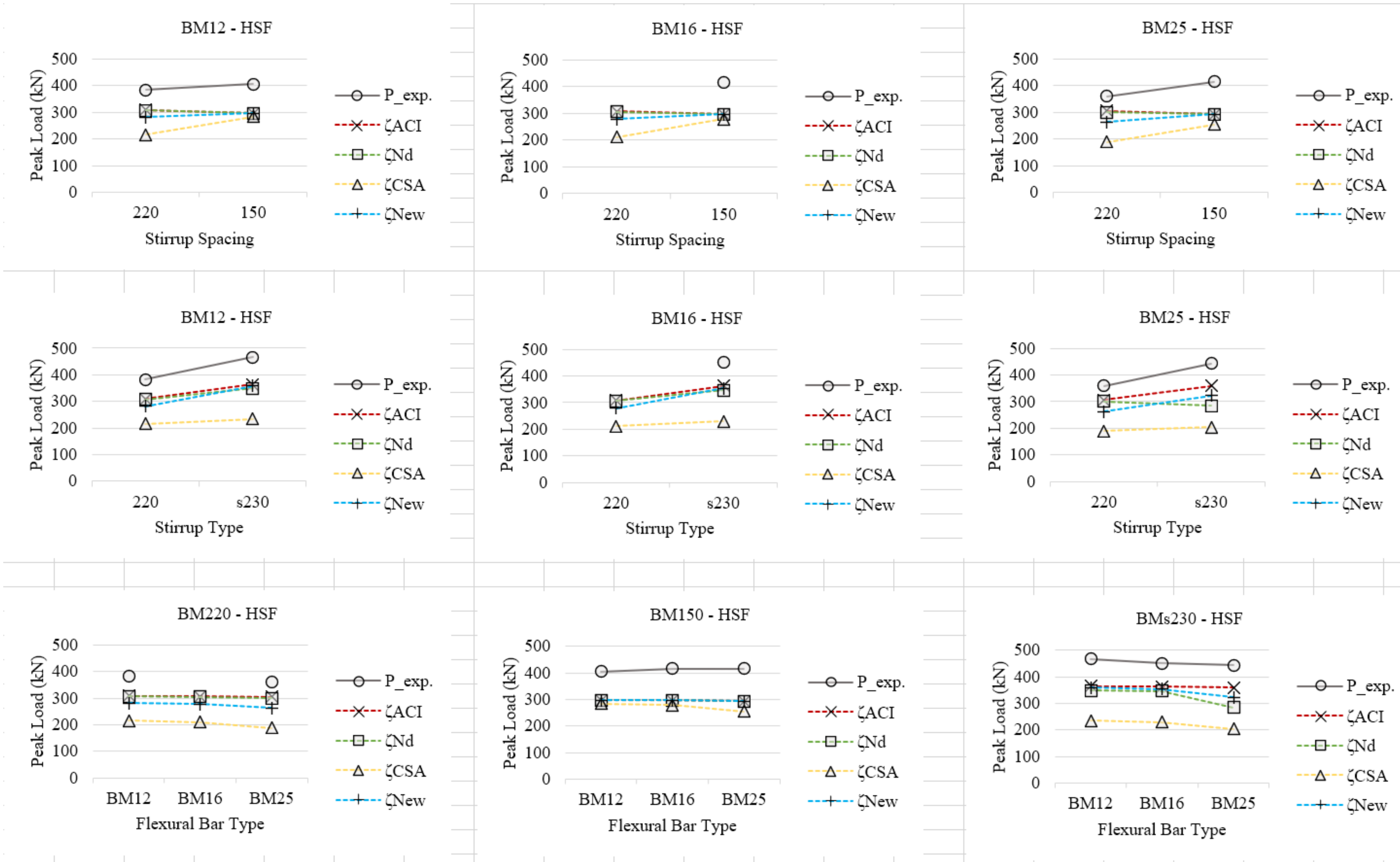
BM12 - HSF
Peak Load (kN)
500
400
300
200
100
0
220
150
Stirrup Spacing
P_exp.
ζACI
ζNd
ζCSA
ζNew
BM16 - HSF
Peak Load (kN)
500
400
300
200
100
0
220
150
Stirrup Spacing
P_exp.
ζACI
ζNd
ζCSA
ζNew
BM25 - HSF
Peak Load (kN)
500
400
300
200
100
0
220
150
Stirrup Spacing
P_exp.
ζACI
ζNd
ζCSA
ζNew
BM12 - HSF
Peak Load (kN)
500
400
300
200
100
0
220
s230
Stirrup Type
P_exp.
ζACI
ζNd
ζCSA
ζNew
BM16 - HSF
Peak Load (kN)
500
400
300
200
100
0
220
s230
Stirrup Type
P_exp.
ζACI
ζNd
ζCSA
ζNew
BM25 - HSF
Peak Load (kN)
500
400
300
200
100
0
220
s230
Stirrup Type
P_exp.
ζACI
ζNd
ζCSA
ζNew
BM220 - HSF
Peak Load (kN)
500
400
300
200
100
0
BM12
BM16
BM25
Flexural Bar Type
P_exp.
ζACI
ζNd
ζCSA
ζNew
BM150 - HSF
Peak Load (kN)
500
400
300
200
100
0
BM12
BM16
BM25
Flexural Bar Type
P_exp.
ζACI
ζNd
ζCSA
ζNew
BMs230 - HSF
Peak Load (kN)
500
400
300
200
100
0
BM12
BM16
BM25
Flexural Bar Type
P_exp.
ζACI
ζNd
ζCSA
ζNew

Half Section Fanning		P_exp.	P_predict with							
			ζACI	Fail.Elem	ζNd	Fail.Elem	ζCSA	Fail.Elem	ζNew	Fail.Elem
BM12	220	382.4	308.14	S5	306.38	S10	215.06	S10	281.34	S10
			308.16	S11	306.40	S11	215.07	S11	281.37	S11
			308.16	**Combine**	**306.40**	**Shear**	**215.07**	**Shear**	**281.37**	**Shear**
	150	405.2	296.72	S9	296.56	S9	283.43	S19	296.57	S9
			296.76	S19	296.59	S19	400.89	N11	296.60	S19
			296.77	N9	296.60	N9			296.61	N9
			296.76	**Combine**	**296.59**	**Combine**	**283.43**	**Shear**	**296.60**	**Combine**
	s230	466.9	364.22	S5	348.31	S10	234.13	S10	358.64	S10
			364.24	S11	348.32	S11	234.14	S11	358.66	S11
			364.24	**Combine**	**348.32**	**Shear**	**234.14**	**Shear**	**358.66**	**Shear**
BM16	220	309.3	307.86	S5	305.50	S10	210.68	S10	278.54	S10
			307.88	S11	305.52	S11	210.70	S11	278.57	S11
			307.88	**Combine**	**305.52**	**Shear**	**210.70**	**Shear**	**278.57**	**Shear**
	150	416.5	296.26	S9	296.12	S9	278.76	S19	296.12	S9
			296.31	S19	296.14	S19	278.81	S18	296.15	S19
			296.32	N9	296.15	N9	278.81	S17	296.16	N9
			296.31	**Combine**	**296.14**	**Combine**	**278.81**	**Shear**	**296.15**	**Combine**
	s230	450.8	363.49	S5	346.49	S10	229.09	S10	352.95	S10
			363.51	S11	346.51	S11	229.10	S11	352.97	S11
			363.51	**Combine**	**346.51**	**Shear**	**229.10**	**Shear**	**352.97**	**Shear**
BM25	220	360.1	306.24	S5	300.32	S10	188.88	S10	263.13	S10
			306.26	S11	300.34	S11	188.90	S11	263.17	S11
			306.26	**Combine**	**300.34**	**Shear**	**188.90**	**Shear**	**263.17**	**Shear**
	150	415.8	293.63	S9	293.53	S9	255.57	S19	293.52	S9
			293.68	S19	293.56	S19	255.61	S17	293.55	S19
			293.69	N9	293.57	N9	255.61	S18	293.56	S17/N9
			293.68	**Combine**	**293.56**	**Combine**	**255.61**	**Shear**	**293.55**	**Combine**
	s230	444	359.30	S5	285.10	S10	203.84	S10	323.33	S10
			359.32	S11	285.11	S11	203.85	S11	323.35	S11
			359.32	**Combine**	**285.11**	**Shear**	**203.85**	**Shear**	**323.35**	**Shear**

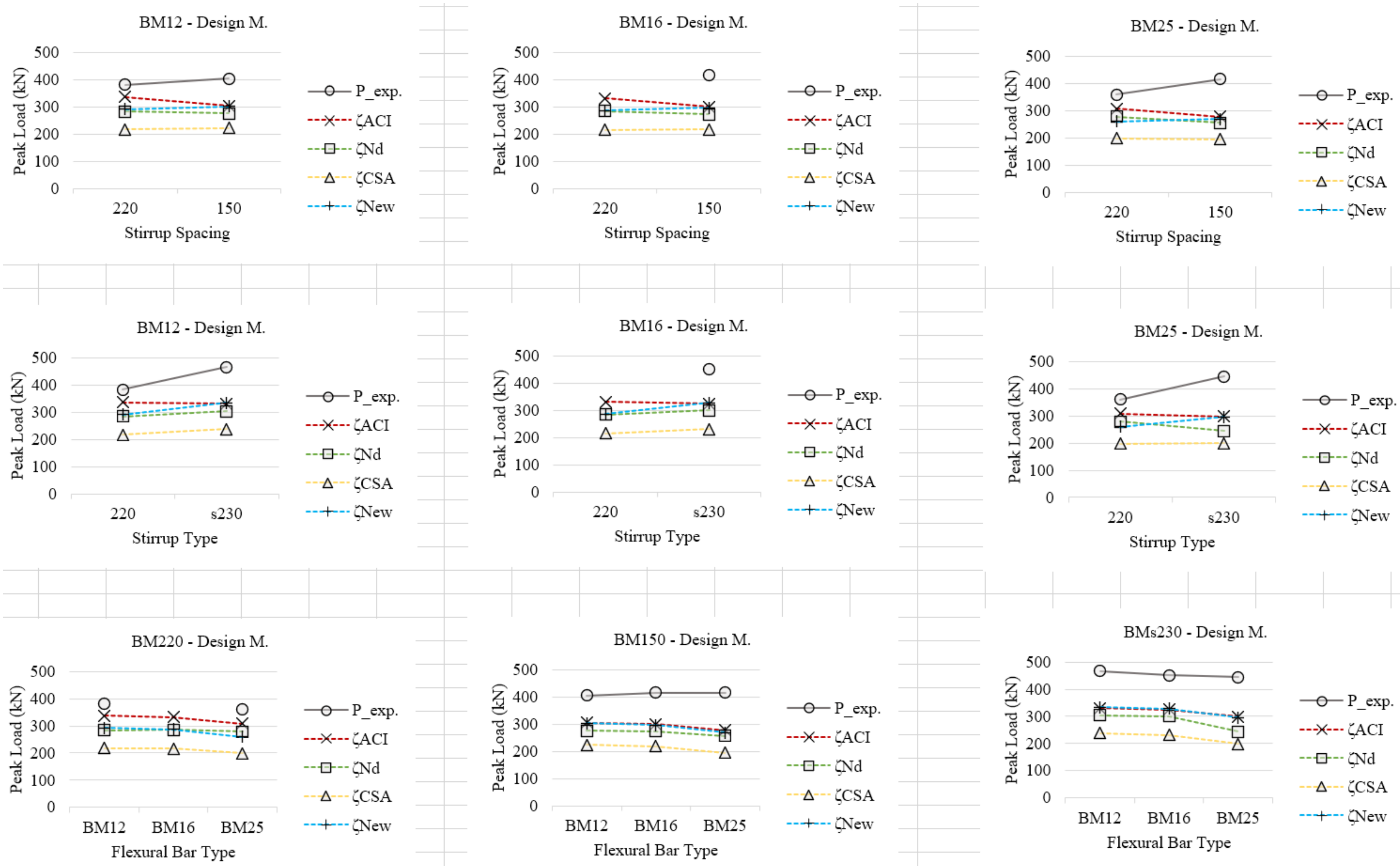
BM12 - Design M.
BM16 - Design M.
BM25 - Design M.
Peak Load (kN)
0
100
200
300
400
500
220
150
Stirrup Spacing
P_exp.
ζACI
ζNd
ζCSA
ζNew
s230
Stirrup Type
BM220 - Design M.
BM150 - Design M.
BMs230 - Design M.
BM12
BM16
BM25
Flexural Bar Type

Design Model		P_exp.	P_predict with							
			ζACI	Fail.Elem	ζNd	Fail.Elem	ζCSA	Fail.Elem	ζNew	Fail.Elem
BM12	220	382.4	336.64	S6	284.16	S6	217.89	S8	292.27	S6
	76.89		336.65	S8	284.16	S8	217.92	S7	292.29	S8
			336.65	**Shear**	**284.16**	**Shear**	**217.92**	**Shear**	**292.29**	**Shear**
	150	405.2	305.16	S6	276.56	S6	223.78	S7	303.05	S6
			305.18	S8	276.57	S8	223.78	S8	303.07	S8
			305.18	**Shear**	**276.57**	**Shear**	**223.78**	**Shear**	**303.07**	**Shear**
	s230	466.9	330.64	S6	304.12	S6	238.42	S7	334.48	S6
	72.68		330.66	S8	304.13	S8	238.43	S8	334.50	S8
			330.66	**Shear**	**304.13**	**Shear**	**238.43**	**Shear**	**334.50**	**Shear**
BM16	220	309.3	332.36	S6	285.33	S6	216.08	S8	287.22	S6
	75.03		332.37	S8	285.34	S8	216.10	S7	287.24	S8
			332.37	**Shear**	**285.34**	**Shear**	**216.10**	**Shear**	**287.24**	**Shear**
	150	416.5	300.79	S6	273.90	S6	218.47	S7	297.43	S6
			300.81	S8	273.91	S8	218.47	S8	297.45	S8
			300.81	**Shear**	**273.91**	**Shear**	**218.47**	**Shear**	**297.45**	**Shear**
	s230	450.8	325.46	S6	300.13	S6	232.00	S7	327.97	S6
	71.148		325.49	S8	300.14	S8	232.01	S8	327.99	S8
			325.49	**Shear**	**300.14**	**Shear**	**232.01**	**Shear**	**327.99**	**Shear**
BM25	220	360.1	307.76	S6	278.96	S6	199.37	S7	260.32	S6
	67.424		307.78	S8	278.97	S8	199.38	S8	260.35	S8
			307.78	**Shear**	**278.97**	**Shear**	**199.38**	**Shear**	**260.35**	**Shear**
	150	415.8	277.27	S6	256.45	S6	194.48	S7	268.81	S6
			277.30	S8	256.46	S8	194.49	S8	268.83	S8
			277.30	**Shear**	**256.46**	**Shear**	**194.49**	**Shear**	**268.83**	**Shear**
	s230	444	298.41	S6	244.56	S6	199.74	S7	295.97	S6
	63.279		298.44	S8	244.56	S8	199.75	S8	296.00	S8
			298.44	**Shear**	**244.56**	**Shear**	**199.75**	**Shear**	**296.00**	**Shear**

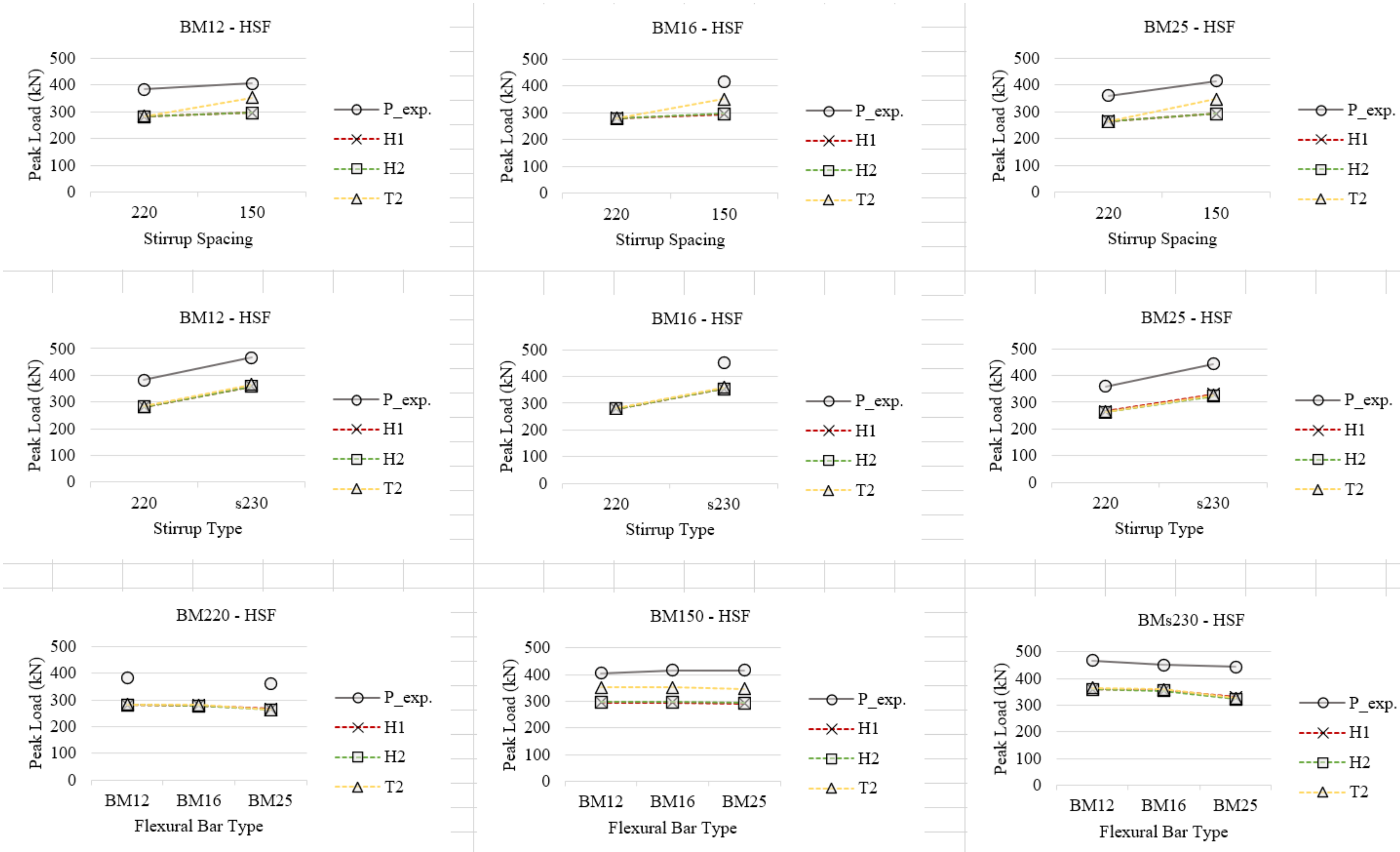
BM12 - HSF
BM16 - HSF
BM25 - HSF
Peak Load (kN)
0
100
200
300
400
500
220
150
Stirrup Spacing
P_exp.
H1
H2
T2
BM12 - HSF
BM16 - HSF
BM25 - HSF
220
s230
Stirrup Type
BM220 - HSF
BM150 - HSF
BMs230 - HSF
BM12
BM16
BM25
Flexural Bar Type

Half Section Fanning		P_exp.	P_predict with					
			H1	Fail.Elem	H2	Fail.Elem	T2	Fail.Elem
BM12	220	382.4	282.03	S10	281.34	S10	283.52	S10
			282.04	S11	281.37	S11	358.96	N6
			282.04	**Shear**	**281.37**	**Shear**	**283.52**	**Shear**
	150	405.2	295.40	S9	296.57	S9	352.45	S9
			295.43	S19	296.60	S19	352.47	S19
			295.44	N9	296.61	N9	352.48	S17/N9
			295.43	**Combine**	**296.60**	**Combine**	**352.47**	**Combine**
	s230	466.9	359.22	S10	358.64	S10	364.75	S10
			359.22	S11	358.66	S11	364.77	S11
			359.22	**Shear**	**358.66**	**Shear**	**364.77**	**Shear**
BM16	220	309.3	279.62	S10	278.54	S10	280.39	S10
			279.64	S11	278.57	S11	358.92	N6
			279.64	**Shear**	**278.57**	**Shear**	**280.39**	**Shear**
	150	416.5	295.02	S9	296.12	S9	351.91	S9
			295.05	S19	296.15	S19	351.93	S19
			295.06	N9	296.16	N9	351.94	S17/N9
			295.05	**Combine**	**296.15**	**Combine**	**351.93**	**Combine**
	s230	450.8	354.58	S10	352.95	S10	358.43	S10
			354.59	S11	352.97	S11	358.45	S11
			354.59	**Shear**	**352.97**	**Shear**	**358.45**	**Shear**
BM25	220	360.1	266.29	S10	263.13	S10	263.30	S10
			266.30	S11	263.17	S11	263.35	S11
			266.30	**Shear**	**263.17**	**Shear**	**263.35**	**Shear**
	150	415.8	292.85	S9	293.52	S9	347.18	S17
			292.88	S19	293.55	S19	347.21	S19
			292.89	S17	293.56	S17/N9	347.22	S18/N10
			292.88	**Combine**	**293.55**	**Combine**	**347.21**	**Shear**
	s230	444	329.89	S10	323.33	S10	325.62	S10
			329.90	S11	323.35	S11	325.65	S11
			329.90	**Shear**	**323.35**	**Shear**	**325.65**	**Shear**

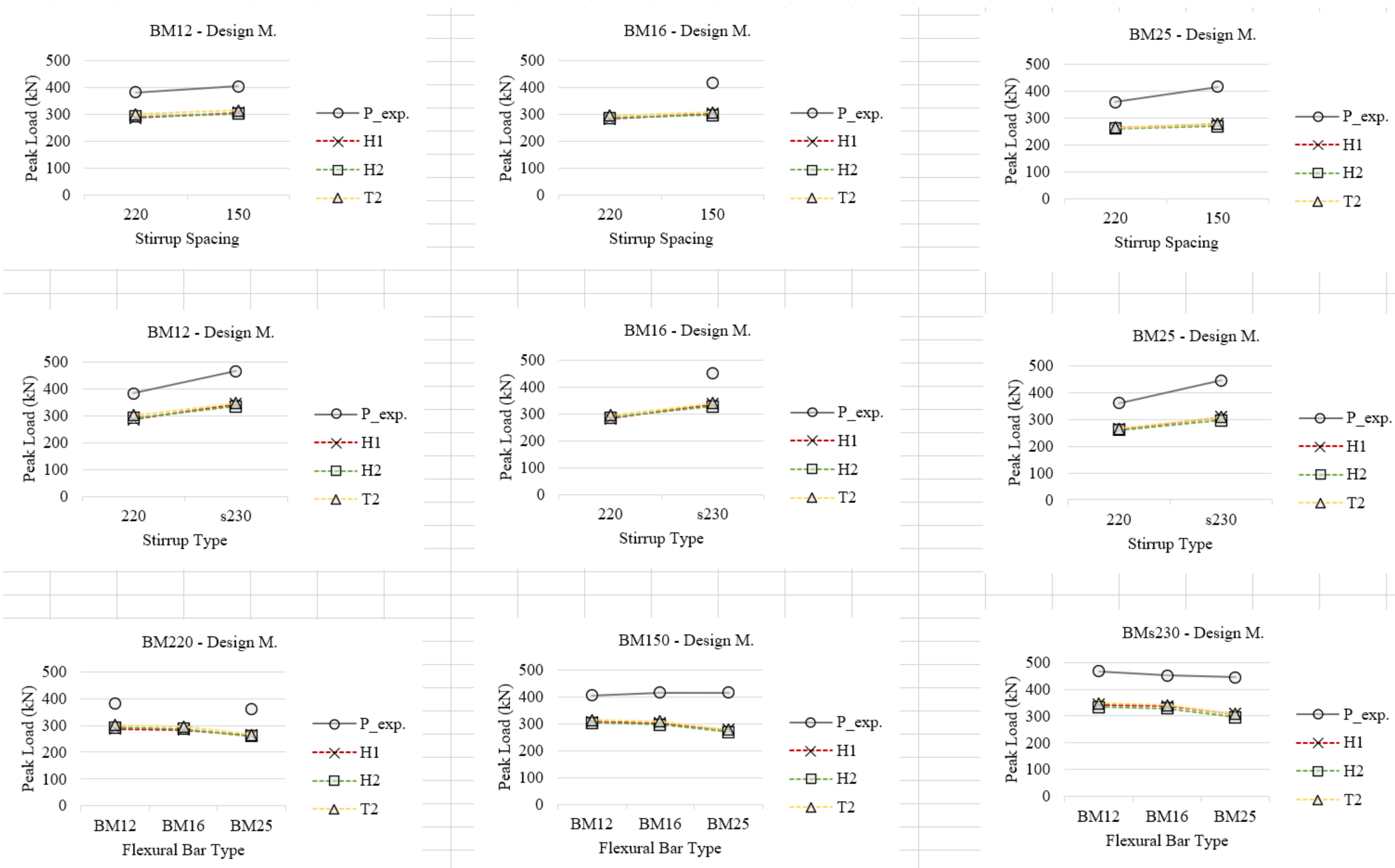
BM12 - Design M.
BM16 - Design M.
BM25 - Design M.
Peak Load (kN)
500
400
300
200
100
0
220
150
s230
Stirrup Spacing
Stirrup Type
P_exp.
H1
H2
T2
BM220 - Design M.
BM150 - Design M.
BMs230 - Design M.
BM12
BM16
BM25
Flexural Bar Type

Design Model		P_exp.	P_predict with					
			H1	Fail.Elem	H2	Fail.Elem	T2	Fail.Elem
BM12	220	382.4	287.05	S6	292.27	S6	301.44	S6
	76.89		287.07	S8	292.29	S8	301.46	S8
			287.07	**Shear**	**292.29**	**Shear**	**301.46**	**Shear**
	150	405.2	306.74	S6	303.05	S6	314.50	S6
			306.76	S8	303.07	S8	314.52	S8
			306.76	**Shear**	**303.07**	**Shear**	**314.52**	**Shear**
	s230	466.9	342.74	S6	334.48	S6	347.30	S6
	72.68		342.76	S8	334.50	S8	347.32	S8
			342.76	**Shear**	**334.50**	**Shear**	**347.32**	**Shear**
BM16	220	309.3	283.24	S6	287.22	S6	295.41	S6
	75.03		283.25	S8	287.24	S8	295.43	S8
			283.25	**Shear**	**287.24**	**Shear**	**295.43**	**Shear**
	150	416.5	302.07	S6	297.43	S6	308.21	S6
			302.09	S8	297.45	S8	308.23	S8
			302.09	**Shear**	**297.45**	**Shear**	**308.23**	**Shear**
	s230	450.8	336.87	S6	327.97	S6	340.35	S6
	71.148		336.89	S8	327.99	S8	340.37	S8
			336.89	**Shear**	**327.99**	**Shear**	**340.37**	**Shear**
BM25	220	360.1	262.57	S6	260.32	S6	264.83	S6
	67.424		262.59	S8	260.35	S8	264.86	S8
			262.59	**Shear**	**260.35**	**Shear**	**264.86**	**Shear**
	150	415.8	277.48	S6	268.81	S6	277.41	S6
			277.50	S8	268.83	S8	277.43	S8
			277.50	**Shear**	**268.83**	**Shear**	**277.43**	**Shear**
	s230	444	307.79	S6	295.97	S6	307.61	S6
	63.279		307.81	S8	296.00	S8	307.64	S8
			307.81	**Shear**	**296.00**	**Shear**	**307.64**	**Shear**

For deep beams with stirrups analyzed with h_c based on new approach:

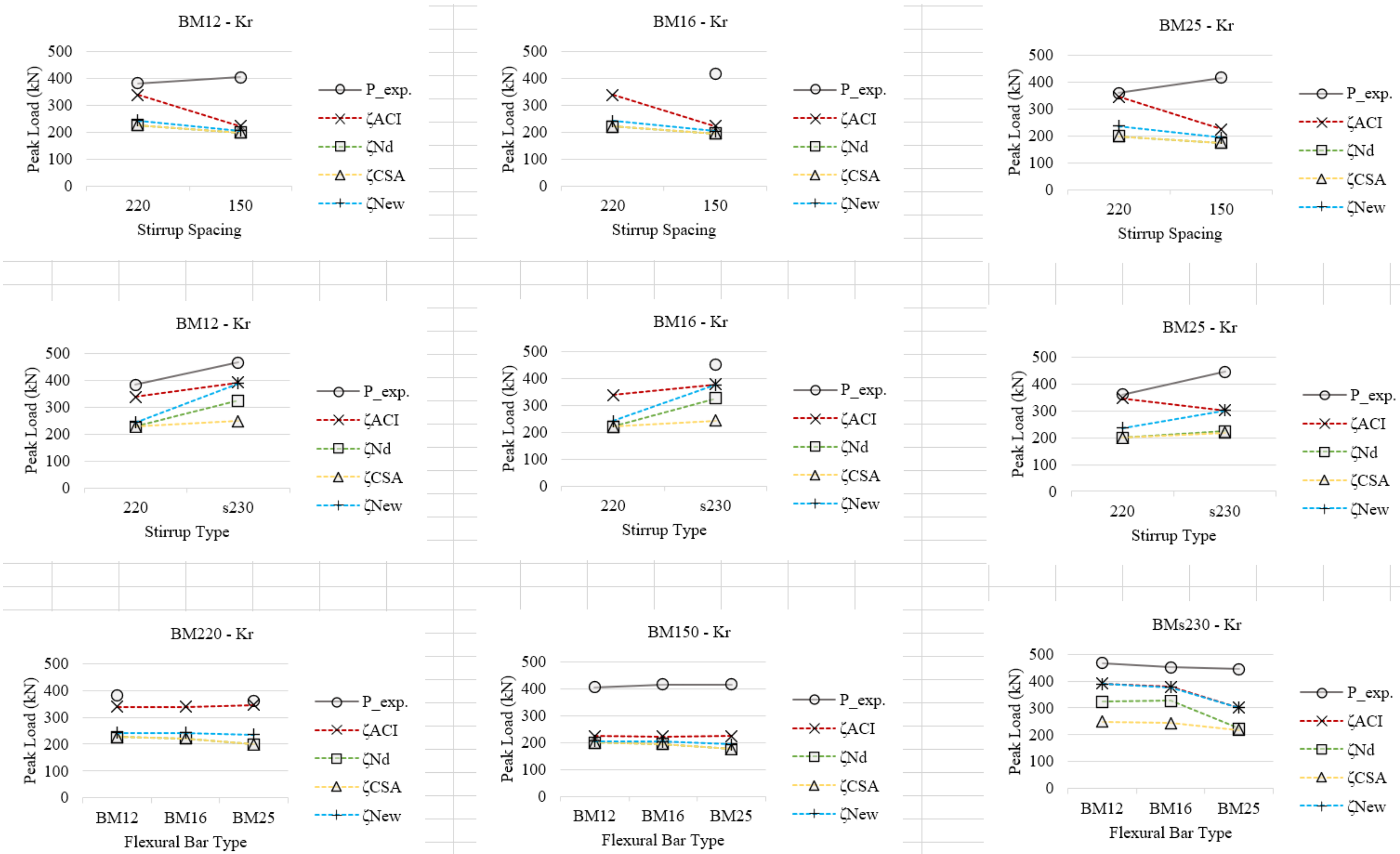

Kr Model		P_exp.	P_predict with							
			ζACI	Fail.Elem	ζNd	Fail.Elem	ζCSA	Fail.Elem	ζNew	Fail.Elem
BM12	220	382.4	338.75	S12	145.64	S12	136.36	S12	243.20	S12
			338.78	S5	226.94	S5	226.89	S5	243.30	S5
			338.78	**Combine**	**226.94**	**Combine**	**226.89**	**Combine**	**243.30**	**Combine**
	150	405.2	223.68	S20	104.75	S20	111.07	S20	205.81	S20
			223.75	S9	199.58	S9	199.56	S9	205.96	S9
			223.75	**Combine**	**199.58**	**Combine**	**199.56**	**Combine**	**205.96**	**Combine**
	s230	466.9	391.45	S5	324.06	S12	225.33	S12	388.92	S5
			391.47	S12	324.07	S5	248.48	S5	388.93	S12
			391.47	**Combine**	**324.07**	**Combine**	**248.48**	**Combine**	**388.93**	**Combine**
BM16	220	309.3	339.68	S12	146.28	S12	134.44	S12	241.79	S12
			339.71	S5	222.23	S5	222.18	S5	241.88	S5
			339.71	**Combine**	**222.23**	**Combine**	**222.18**	**Combine**	**241.79**	**Combine**
	150	416.5	223.50	S20	104.59	S20	109.22	S20	203.57	S20
			223.56	S9	195.41	S9	195.39	S9	203.70	S9
			223.56	**Combine**	**195.41**	**Combine**	**195.39**	**Combine**	**203.70**	**Combine**
	s230	450.8	378.96	S5	326.25	S5	223.60	S12	377.24	S5
			378.98	S12	326.25	S12	243.29	S5	377.26	S12
			378.98	**Combine**	**326.25**	**Combine**	**243.29**	**Combine**	**377.26**	**Combine**
BM25	220	360.1	346.28	S12	151.59	S12	125.52	S12	236.01	S12
			346.29	S5	199.18	S5	199.15	S5	393.34	N7
			346.29	**Combine**	**199.18**	**Combine**	**199.15**	**Combine**	**236.01**	**Shear**
	150	415.8	224.86	S20	104.64	S20	100.33	S20	193.07	S20
			224.90	S9	174.95	S9	174.94	S9	193.15	S9
			224.90	**Combine**	**174.95**	**Combine**	**174.94**	**Combine**	**193.15**	**Combine**
	s230	444	300.80	S5	222.85	S12	217.18	S12	301.03	S5
			300.83	S12	223.02	S5	217.95	S5	301.05	S12
			300.83	**Combine**	**223.02**	**Combine**	**217.95**	**Combine**	**301.05**	**Combine**

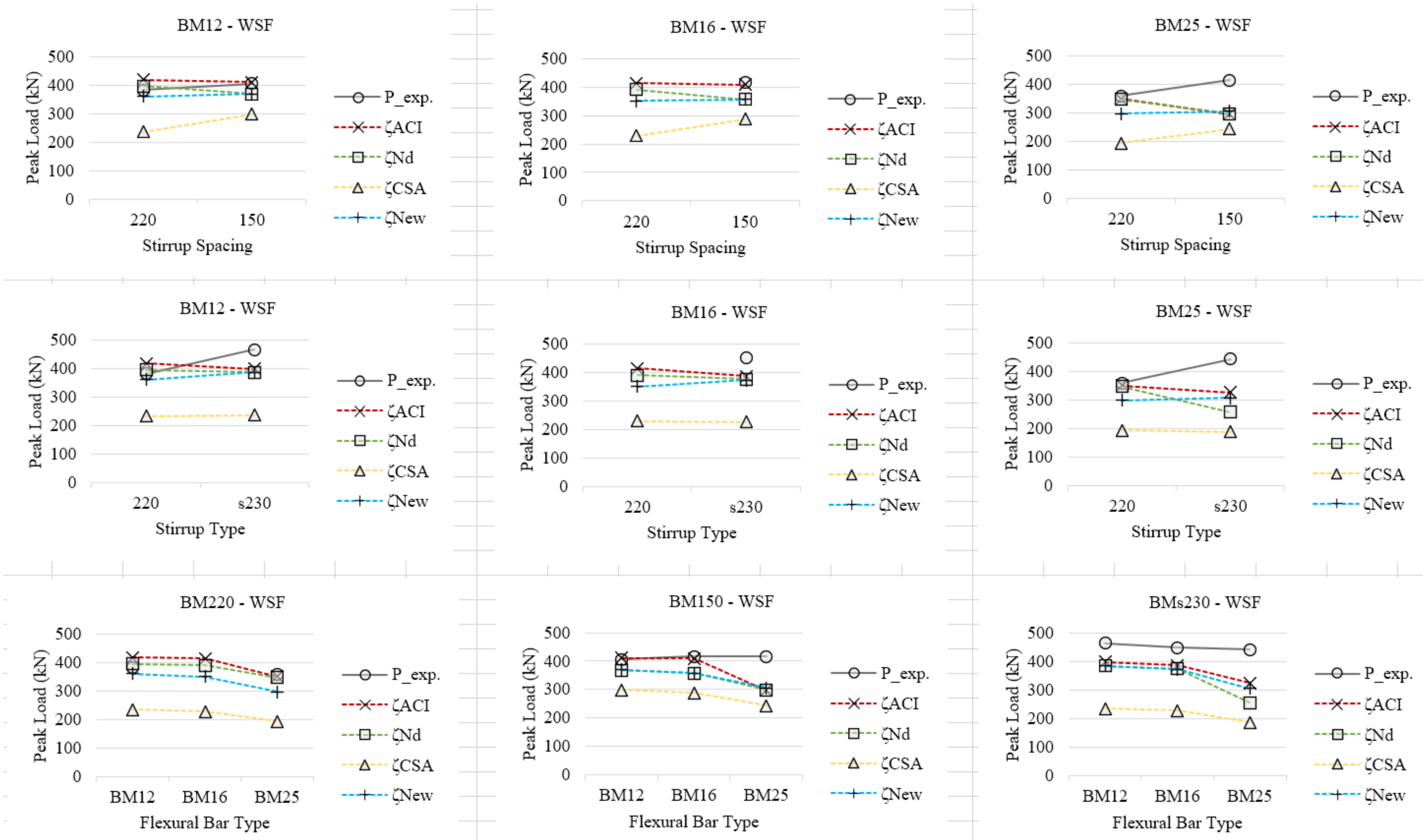
BM12 - WSF
BM16 - WSF
BM25 - WSF
Peak Load (kN)
Stirrup Spacing
220
150
P_exp.
ζACI
ζNd
ζCSA
ζNew
BM12 - WSF
BM16 - WSF
BM25 - WSF
Stirrup Type
220
s230
BM220 - WSF
BM150 - WSF
BMs230 - WSF
Flexural Bar Type
BM12
BM16
BM25
0
100
200
300
400
500

Whole Section Fanning		P_exp.	P_predict with							
			ζACI	Fail.Elem	ζNd	Fail.Elem	ζCSA	Fail.Elem	ζNew	Fail.Elem
BM12	220	382.4	418.64	N7	396.75	S10	235.60	S10	360.98	S10
					396.75	S11	235.61	S11	361.01	S11
					396.76	S12	235.61	S12	361.02	S12
			418.64	**Node Crush**	**396.76**	**Shear**	**235.61**	**Shear**	**361.02**	**Shear**
	150	405.2	367.17	S9	368.78	S9	297.92	S18	369.26	S9
			410.76	S19	368.79	S19	298.14	S21	369.30	S19
			410.80	S20	368.80	S20	298.15	S19	369.32	S20
			410.82	S21	368.82	S21	298.16	S20	369.34	S21
			410.83	N9	368.83	N9	298.17	S17	369.35	S17/N9
			410.76	**Combine**	**368.79**	**Combine**	**298.17**	**Shear**	**369.30**	**Combine**
	s230	466.9	400.32	S5	387.28	S10	237.16	S10	386.97	S10
			400.36	S11	387.31	S11	237.18	S12	387.02	S12
			400.37	S12	387.31	S12	237.18	S11	387.03	S11
			400.36	**Combine**	**387.31**	**Shear**	**237.18**	**Shear**	**387.03**	**Shear**
BM16	220	309.3	414.25	N7	390.69	S10	229.07	S10	350.59	S10
					390.70	S11	229.08	S11	350.63	S11
					390.71	S12	229.09	S12	350.64	S12
			414.25	**Node Crush**	**390.71**	**Shear**	**229.09**	**Shear**	**350.64**	**Shear**
	150	416.5	354.95	S9	356.69	S9	287.07	S18	357.03	S9
			408.60	S19	356.71	S19	287.60	S21	357.09	S19
			408.64	S20	356.72	S20	287.61	S19	357.11	S20
			408.66	S21	356.74	S21	287.62	S20	357.12	S21
			408.67	N9	356.75	N9	287.63	S17	357.13	S17/N9
			408.60	**Combine**	**356.71**	**Combine**	**287.63**	**Shear**	**357.09**	**Combine**
	s230	450.8	387.50	S5	375.85	S10	228.68	S10	373.93	S10
			387.54	S11	375.87	S12	228.70	S11	373.98	S12
			387.55	S12	375.88	S11	228.70	S12	373.99	S11
			387.54	**Combine**	**375.88**	**Shear**	**228.70**	**Shear**	**373.99**	**Shear**
BM25	220	360.1	350.49	S5	347.74	S10	193.52	S10	298.38	S10
			350.52	S11	347.75	S11	193.53	S11	298.49	S11
			350.54	S12	347.76	S12	193.54	S12	298.49	S12
			350.52	**Combine**	**347.76**	**Shear**	**193.54**	**Shear**	**298.49**	**Shear**
	150	415.8	296.58	S9	298.30	S9	236.09	S18	298.42	S9
			393.34	N11	298.33	S19	244.04	S21	306.10	S19
					298.34	S20	244.07	S17	306.12	S20
					298.37	S21	244.07	S19	306.14	S21
					298.38	N9	244.07	S20	306.15	N9
			296.58	**Flexure**	**298.33**	**Combine**	**244.07**	**Shear**	**306.10**	**Combine**
	s230	444	326.24	S5	256.85	S10	188.54	S10	307.17	S10
			326.31	S11	256.87	S11	188.56	S12	307.23	S12
			326.32	S12	256.88	S12	188.57	S11	307.25	S11
			326.31	**Combine**	**256.88**	**Shear**	**188.57**	**Shear**	**307.25**	**Shear**

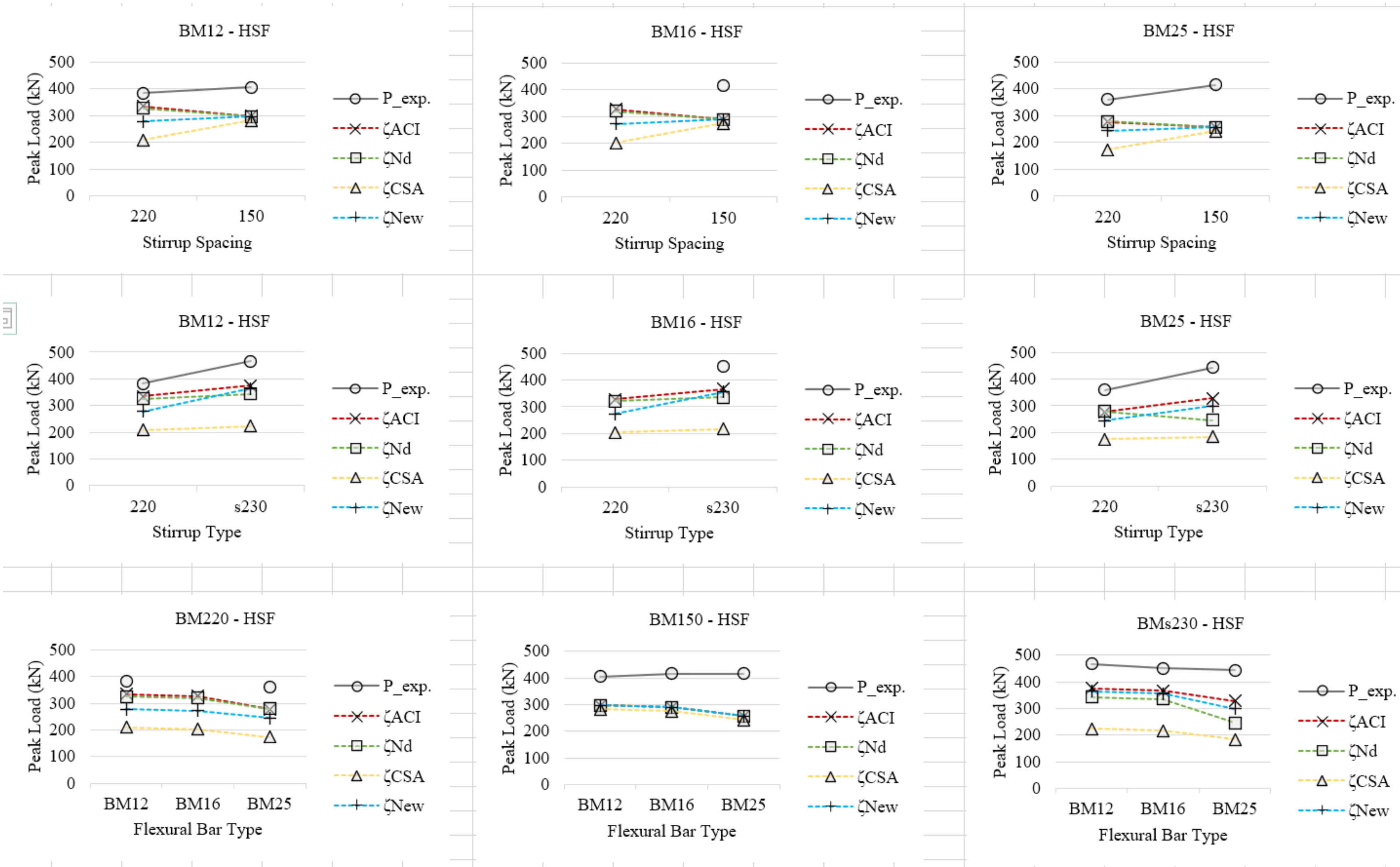
BM12 - HSF
Peak Load (kN)
500
400
300
200
100
0
220
150
Stirrup Spacing
P_exp.
ζACI
ζNd
ζCSA
ζNew
BM16 - HSF
Peak Load (kN)
500
400
300
200
100
0
220
150
Stirrup Spacing
P_exp.
ζACI
ζNd
ζCSA
ζNew
BM25 - HSF
Peak Load (kN)
500
400
300
200
100
0
220
150
Stirrup Spacing
P_exp.
ζACI
ζNd
ζCSA
ζNew
BM12 - HSF
Peak Load (kN)
500
400
300
200
100
0
220
s230
Stirrup Type
P_exp.
ζACI
ζNd
ζCSA
ζNew
BM16 - HSF
Peak Load (kN)
500
400
300
200
100
0
220
s230
Stirrup Type
P_exp.
ζACI
ζNd
ζCSA
ζNew
BM25 - HSF
Peak Load (kN)
500
400
300
200
100
0
220
s230
Stirrup Type
P_exp.
ζACI
ζNd
ζCSA
ζNew
BM220 - HSF
Peak Load (kN)
500
400
300
200
100
0
BM12
BM16
BM25
Flexural Bar Type
P_exp.
ζACI
ζNd
ζCSA
ζNew
BM150 - HSF
Peak Load (kN)
500
400
300
200
100
0
BM12
BM16
BM25
Flexural Bar Type
P_exp.
ζACI
ζNd
ζCSA
ζNew
BMs230 - HSF
Peak Load (kN)
500
400
300
200
100
0
BM12
BM16
BM25
Flexural Bar Type
P_exp.
ζACI
ζNd
ζCSA
ζNew

Half Section Fanning		P_exp.	P_predict with							
			ζACI	Fail.Elem	ζNd	Fail.Elem	ζCSA	Fail.Elem	ζNew	Fail.Elem
BM12	220	382.4	334.06	S5	325.98	S10	209.38	S10	278.55	S10
			334.08	S11	326.00	S11	209.39	S11	278.58	S11
			334.08	**Combine**	**326.00**	**Shear**	**209.39**	**Shear**	**278.58**	**Shear**
	150	405.2	296.88	S9	296.61	S9	281.74	S19	296.63	S9
			296.93	S19	296.64	S19	281.78	S9	296.66	S19
			296.93	N9	296.65	N9	281.79	S17	296.67	N9
			296.93	**Combine**	**296.64**	**Combine**	**281.78**	**Combine**	**296.66**	**Combine**
	s230	466.9	375.02	S5	342.84	S10	223.19	S10	363.93	S10
			375.04	S11	342.86	S11	223.20	S11	363.95	S11
			375.04	**Combine**	**342.86**	**Shear**	**223.20**	**Shear**	**363.95**	**Shear**
BM16	220	309.3	327.46	S5	320.34	S10	203.26	S10	272.90	S10
			327.48	S11	320.36	S11	203.27	S11	272.93	S11
			327.48	**Combine**	**320.36**	**Shear**	**203.27**	**Shear**	**272.93**	**Shear**
	150	416.5	289.94	S9	289.71	S9	274.99	S19	289.74	S9
			289.99	S19	289.74	S19	275.03	S9	289.77	S19
			290.00	N9	289.75	N9	275.04	S17	289.78	N9
			289.99	**Combine**	**289.74**	**Combine**	**275.03**	**Combine**	**289.77**	**Combine**
	s230	450.8	367.26	S5	335.09	S10	216.54	S10	354.79	S10
			367.28	S11	335.11	S11	216.55	S11	354.81	S11
			367.28	**Combine**	**335.11**	**Shear**	**216.55**	**Shear**	**354.81**	**Shear**
BM25	220	360.1	277.10	S5	279.33	S10	173.96	S10	244.18	S10
			277.13	S11	279.35	S11	173.98	S11	244.21	S11
			277.13	**Combine**	**279.35**	**Shear**	**173.98**	**Shear**	**244.21**	**Shear**
	150	415.8	256.96	S9	256.85	S9	242.60	S19	256.89	S9
			257.01	S19	256.88	S19	242.63	S17	256.92	S19
			257.02	N9	256.89	N9	242.63	S18	256.93	N9
			257.01	**Combine**	**256.88**	**Combine**	**242.63**	**Shear**	**256.92**	**Combine**
	s230	444	328.98	S5	245.66	S10	184.61	S10	298.97	S10
			329.00	S11	245.68	S11	184.62	S11	298.99	S11
			329.00	**Combine**	**245.68**	**Shear**	**184.62**	**Shear**	**298.99**	**Shear**

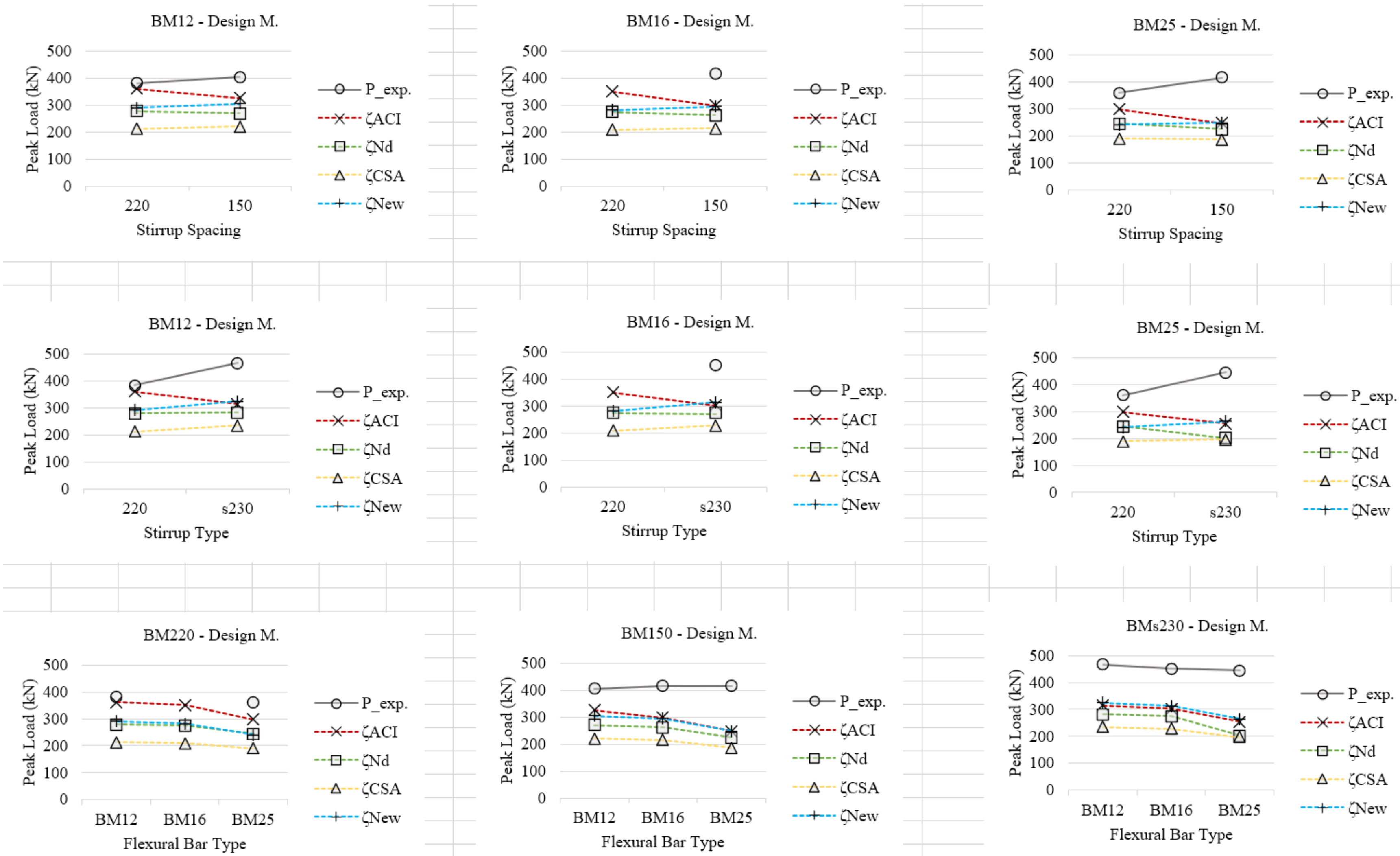
BM12 - Design M.
BM16 - Design M.
BM25 - Design M.
Peak Load (kN)
0
100
200
300
400
500
220
150
Stirrup Spacing
P_exp.
ζACI
ζNd
ζCSA
ζNew
BM12 - Design M.
BM16 - Design M.
BM25 - Design M.
220
s230
Stirrup Type
BM220 - Design M.
BM150 - Design M.
BMs230 - Design M.
BM12
BM16
BM25
Flexural Bar Type

Design Model		P_exp.	P_predict with							
			ζACI	Fail.Elem	ζNd	Fail.Elem	ζCSA	Fail.Elem	ζNew	Fail.Elem
BM12	220	382.4	361.41	S6	278.98	S6	212.29	S8	291.27	S6
	76.89		361.43	S8	278.98	S8	212.32	S7	291.29	S8
			361.43	**Shear**	**278.98**	**Shear**	**212.32**	**Shear**	**291.29**	**Shear**
	150	405.2	326.29	S6	270.24	S6	221.34	S7	305.50	S6
			326.31	S8	270.25	S8	221.35	S8	305.52	S8
			326.31	**Shear**	**270.25**	**Shear**	**221.35**	**Shear**	**305.52**	**Shear**
	s230	466.9	314.11	S6	282.67	S6	234.94	S7	324.72	S6
	72.68		314.13	S8	282.68	S8	234.94	S8	324.74	S8
			314.13	**Shear**	**282.68**	**Shear**	**234.94**	**Shear**	**324.74**	**Shear**
BM16	220	309.3	350.72	S6	275.16	S6	208.83	S8	282.65	S6
	75.03		350.74	S8	275.16	S8	208.86	S7	282.67	S8
			350.74	**Shear**	**275.16**	**Shear**	**208.86**	**Shear**	**282.67**	**Shear**
	150	416.5	298.85	S6	262.69	S6	215.49	S7	295.15	S6
			298.87	S8	262.69	S8	215.50	S8	295.17	S8
			298.87	**Shear**	**262.69**	**Shear**	**215.50**	**Shear**	**295.17**	**Shear**
	s230	450.8	303.34	S6	274.17	S6	228.35	S7	313.87	S6
	71.148		303.36	S8	274.18	S8	228.36	S8	313.89	S8
			303.36	**Shear**	**274.18**	**Shear**	**228.36**	**Shear**	**313.89**	**Shear**
BM25	220	360.1	298.19	S6	244.86	S6	189.80	S8	241.09	S6
	67.424		298.21	S8	244.86	S8	189.81	S7	241.11	S8
			298.21	**Shear**	**244.86**	**Shear**	**189.81**	**Shear**	**241.11**	**Shear**
	150	415.8	247.73	S6	224.79	S6	186.59	S7	248.85	S6
			247.76	S8	224.80	S8	186.59	S8	248.87	S8
			247.76	**Shear**	**224.80**	**Shear**	**186.59**	**Shear**	**248.87**	**Shear**
	s230	444	253.90	S6	201.86	S6	196.44	S7	263.98	S6
	63.279		253.93	S8	201.87	S8	196.45	S8	264.01	S8
			253.93	**Shear**	**201.87**	**Shear**	**196.45**	**Shear**	**264.01**	**Shear**

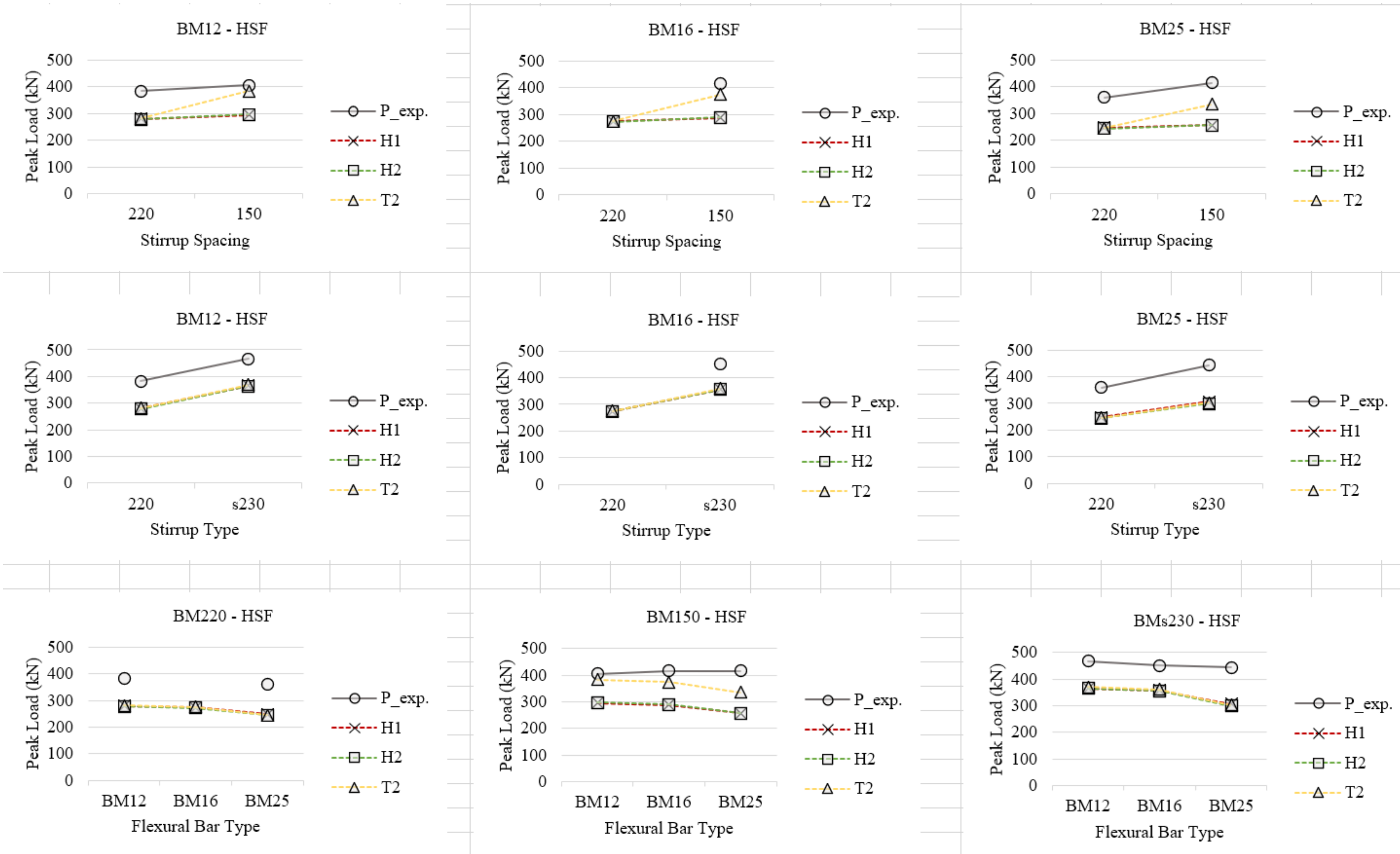
BM12 - HSF
Peak Load (kN)
500
400
300
200
100
0
220
150
Stirrup Spacing
P_exp.
H1
H2
T2
BM16 - HSF
Peak Load (kN)
220
150
Stirrup Spacing
P_exp.
H1
H2
T2
BM25 - HSF
Peak Load (kN)
220
150
Stirrup Spacing
P_exp.
H1
H2
T2
BM12 - HSF
Peak Load (kN)
220
s230
Stirrup Type
P_exp.
H1
H2
T2
BM16 - HSF
Peak Load (kN)
220
s230
Stirrup Type
P_exp.
H1
H2
T2
BM25 - HSF
Peak Load (kN)
220
s230
Stirrup Type
P_exp.
H1
H2
T2
BM220 - HSF
Peak Load (kN)
BM12
BM16
BM25
Flexural Bar Type
P_exp.
H1
H2
T2
BM150 - HSF
Peak Load (kN)
BM12
BM16
BM25
Flexural Bar Type
P_exp.
H1
H2
T2
BMs230 - HSF
Peak Load (kN)
BM12
BM16
BM25
Flexural Bar Type
P_exp.
H1
H2
T2

Half Section Fanning		P_exp.	P_predict with					
			H1	Fail.Elem	H2	Fail.Elem	T2	Fail.Elem
BM12	220	382.4	279.42	S10	278.55	S10	281.18	S10
			279.43	S11	278.58	S11	387.00	N6
			279.43	**Shear**	**278.58**	**Shear**	**281.18**	**Shear**
	150	405.2	294.74	S9	296.63	S9	382.34	S9
			294.77	S19	296.66	S19	382.36	S19
			294.78	N9	296.67	N9	382.37	S17/N9
			294.77	**Combine**	**296.66**	**Combine**	**382.36**	**Combine**
	s230	466.9	364.83	S10	363.93	S10	369.98	S10
			364.84	S11	363.95	S11	370.00	S11
			364.84	**Shear**	**363.95**	**Shear**	**370.00**	**Shear**
BM16	220	309.3	274.29	S10	272.90	S10	275.30	S10
			274.30	S11	272.93	S11	380.16	N6
			274.30	**Shear**	**272.93**	**Shear**	**275.30**	**Shear**
	150	416.5	288.12	S9	289.74	S9	374.52	S9
			288.15	S19	289.77	S19	374.54	S19
			288.16	N9	289.78	N9	374.55	S17/N9
			288.15	**Combine**	**289.77**	**Combine**	**374.54**	**Combine**
	s230	450.8	356.52	S10	354.79	S10	360.23	S10
			356.53	S11	354.81	S11	360.25	S11
			356.53	**Shear**	**354.81**	**Shear**	**360.25**	**Shear**
BM25	220	360.1	248.04	S10	244.18	S10	245.47	S10
			248.05	S11	244.21	S11	245.52	S11
			248.05	**Shear**	**244.21**	**Shear**	**245.52**	**Shear**
	150	415.8	256.36	S9	256.89	S9	335.82	S9
			256.39	S19	256.92	S19	335.84	S19
			256.40	N9	256.93	N9	335.85	S17/N9
			256.39	**Combine**	**256.92**	**Combine**	**335.85**	**Combine**
	s230	444	306.47	S10	298.97	S10	303.03	S10
			306.48	S11	298.99	S11	303.05	S11
			306.48	**Shear**	**298.99**	**Shear**	**303.05**	**Shear**

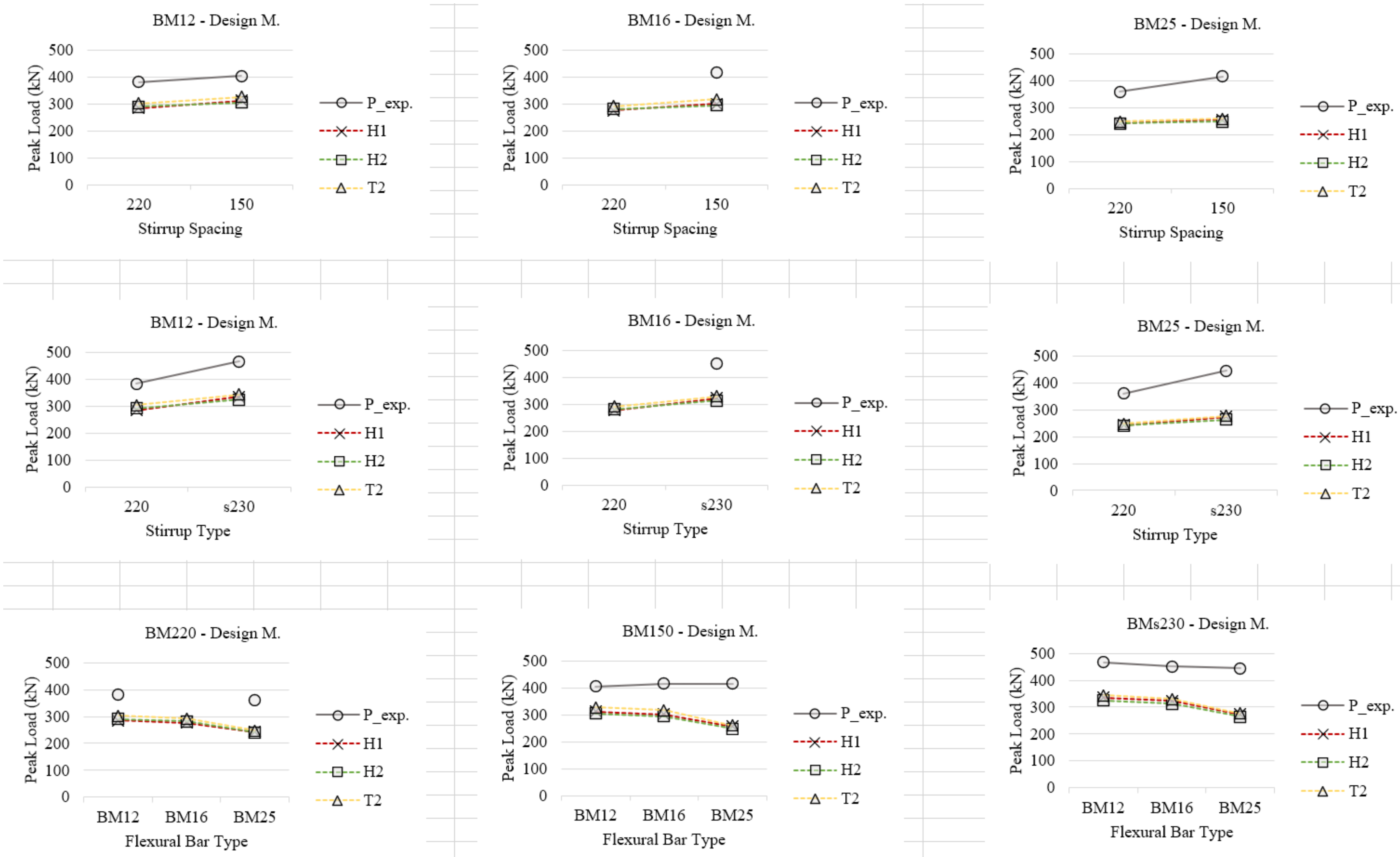
BM12 - Design M.
Peak Load (kN)
500
400
300
200
100
0
220
150
Stirrup Spacing
P_exp.
H1
H2
T2
BM16 - Design M.
BM25 - Design M.
Stirrup Type
s230
BM220 - Design M.
BM150 - Design M.
BMs230 - Design M.
BM12
BM16
BM25
Flexural Bar Type

Design Model		P_exp.	P_predict with					
			H1	Fail.Elem	H2	Fail.Elem	T2	Fail.Elem
BM12	220	382.4	284.90	S6	291.27	S6	302.83	S6
	76.89		284.92	S8	291.29	S8	302.85	S8
			284.92	**Shear**	**291.29**	**Shear**	**302.85**	**Shear**
	150	405.2	312.85	S6	305.50	S6	327.26	S6
			312.87	S8	305.52	S8	327.28	S8
			312.87	**Shear**	**305.52**	**Shear**	**327.28**	**Shear**
	s230	466.9	334.79	S6	324.72	S6	344.23	S6
	72.68		334.81	S8	324.74	S8	344.25	S8
			334.81	**Shear**	**324.74**	**Shear**	**344.25**	**Shear**
BM16	220	309.3	277.68	S6	282.65	S6	293.07	S6
	75.03		277.70	S8	282.67	S8	293.09	S8
			277.70	**Shear**	**282.67**	**Shear**	**293.09**	**Shear**
	150	416.5	301.67	S6	295.15	S6	317.73	S6
			301.69	S8	295.17	S8	317.75	S8
			301.69	**Shear**	**295.17**	**Shear**	**317.75**	**Shear**
	s230	450.8	323.50	S6	313.87	S6	330.76	S6
	71.148		323.52	S8	313.89	S8	330.78	S8
			323.52	**Shear**	**313.89**	**Shear**	**330.78**	**Shear**
BM25	220	360.1	241.86	S6	241.09	S6	248.01	S6
	67.424		241.88	S8	241.11	S8	248.03	S8
			241.88	**Shear**	**241.11**	**Shear**	**248.03**	**Shear**
	150	415.8	256.47	S6	248.85	S6	259.86	S6
			256.49	S8	248.87	S8	259.88	S8
			256.49	**Shear**	**248.87**	**Shear**	**259.88**	**Shear**
	s230	444	273.15	S6	263.98	S6	277.22	S6
	63.279		273.17	S8	264.01	S8	277.25	S8
			273.17	**Shear**	**264.01**	**Shear**	**277.25**	**Shear**

For deep beams without stirrups:

Strain Compatibility		P_exp.	P_Predict				Sften. Factor @ Failure								
			ζACI	ζNd	ζCSA	ζNew	ζACI	ζNd	ζCSA	ζNew	ζACI	ζNd	ζCSA	ζNew	h_C
BM12	INF	163.1	93.3	83.9	90.7	159.1	0.34	0.3055	0.3288	0.5772	0.57	0.51	0.56	0.98	76.89
BM16	INF	150.2	91.8	82.5	88.6	155.6	0.34	0.3055	0.3259	0.5735	0.61	0.55	0.59	1.04	75.03
BM25	INF	125.1	85.7	77.0	78.5	139.6	0.34	0.3055	0.3098	0.5521	0.68	0.62	0.63	1.12	67.42
										Error	0.38	0.44	0.41	0.06	
										STDV	0.06	0.05	0.04	0.07	

0.2d		P_exp.	P_Predict				Sften. Factor @ Failure								
			ζACI	ζNd	ζCSA	ζNew	ζACI	ζNd	ζCSA	ζNew	ζACI	ζNd	ζCSA	ζNew	h_C
BM12	INF	163.1	74.3	66.7	81.9	136.6	0.34	0.3055	0.3734	0.6228	0.46	0.41	0.50	0.84	54.00
BM16	INF	150.2	74.3	66.7	80.6	135.1	0.34	0.3055	0.3672	0.6168	0.49	0.44	0.54	0.90	54.00
BM25	INF	125.1	74.3	66.7	73.8	127.4	0.34	0.3055	0.3363	0.5811	0.59	0.53	0.59	1.02	54.00
										Error	0.49	0.54	0.46	0.09	
										STDV	0.07	0.06	0.04	0.09	

New		P_exp.	P_Predict				Sften. Factor @ Failure								
			ζACI	ζNd	ζCSA	ζNew	ζACI	ζNd	ζCSA	ζNew	ζACI	ζNd	ζCSA	ζNew	h_C
BM12	INF	163.1	74.3	66.7	81.9	130.6	0.34	0.3055	0.3734	0.6336	0.46	0.41	0.50	0.80	48.97
BM16	INF	150.2	74.3	66.7	80.6	128.0	0.34	0.3055	0.3672	0.6297	0.49	0.44	0.54	0.85	47.88
BM25	INF	125.1	74.3	66.7	73.8	115.1	0.34	0.3055	0.3363	0.6087	0.59	0.53	0.59	0.92	42.60
										Error	0.49	0.54	0.46	0.14	
										STDV	0.07	0.06	0.04	0.06	

Proposed		P_exp.	P_Predict				Sften. Factor @ Failure								
			H1	H2	T2		H1	H2	T2		H1	H2	T2		h_C
BM12	INF	163.1	120.4	130.6	146.0		0.5848	0.6336	0.6366		0.74	0.80	0.90		48.97
BM16	INF	150.2	118.0	128.0	142.8		0.5815	0.6297	0.6329		0.79	0.85	0.95		47.88
BM25	INF	125.1	106.1	115.1	126.8		0.562	0.6087	0.6096		0.85	0.92	1.01		42.60
										Error	0.21	0.14	0.06		
										STDV	0.06	0.06	0.06		

Strain Compatibility		P_exp.	P_predict				Sften. Factor @ Failure								
			ζACI	ζNd	ζCSA	ζNew	ζACI	ζNd	ζCSA	ζNew	ζACI	ζNd	ζCSA	ζNew	h_C
A3D9M-1.4	INF	136.05	94.4	143.3	86.8	128.5	0.34	0.5168	0.3115	0.4612	0.69	1.05	0.64	0.94	52.7
A3D9M-1.7	INF	98.98	77.5	101.3	62.8	101.8	0.34	0.445	0.2743	0.445	0.78	1.02	0.63	1.03	52.7
A3D9M-2.1	INF	88	61.4	48.5	43.1	77.0	0.34	0.2683	0.237	0.4244	0.70	0.55	0.49	0.87	52.7
A4D9M-1.7	INF	121	81.3	104.2	71.4	114.8	0.34	0.4363	0.297	0.4782	0.67	0.86	0.59	0.95	59.76
A5D9M-1.7	INF	133.97	84.5	106.3	78.6	125.6	0.34	0.4283	0.3148	0.5033	0.63	0.79	0.59	0.94	65.75
A3D9S-1.7	INF	109.58	70.8	90.8	58.6	95.1	0.34	0.4367	0.2798	0.4553	0.65	0.83	0.53	0.87	45.15
A5D9L-1.7	INF	134.27	91.9	117.7	83.9	134.0	0.34	0.436	0.3089	0.4936	0.68	0.88	0.62	1.00	74.35
C3D9M-1.4	INF	169.26	100.3	150.6	103.1	151.1	0.34	0.511	0.3478	0.5101	0.59	0.89	0.61	0.89	62.68
C3D9M-1.7	INF	106.54	82.9	105.3	74.9	120.1	0.34	0.4324	0.3058	0.4906	0.78	0.99	0.70	1.13	62.68
C3D9M-2.1	INF	52.64	66.2	46.6	51.6	91.1	0.34	0.239	0.2636	0.4664	1.26	0.88	0.98	1.73	62.68
C4D9M-1.7	INF	96.09	87.1	107.8	84.6	134.6	0.34	0.4211	0.3287	0.523	0.91	1.12	0.88	1.40	70.79
C5D9M-1.7	INF	151.39	90.5	109.3	92.7	146.5	0.34	0.4107	0.3462	0.5477	0.60	0.72	0.61	0.97	77.62
C3D9S-1.7	INF	104.84	74.8	92.7	69.0	110.9	0.34	0.4217	0.3123	0.5024	0.71	0.88	0.66	1.06	53.5
C5D9L-1.7	INF	145.39	99.4	122.9	99.9	157.8	0.34	0.4208	0.3401	0.5375	0.68	0.85	0.69	1.09	88.07
										Error	**0.32**	**0.15**	**0.39**	**0.07**	
										St D	**0.06**	**0.14**	**0.06**	**0.08**	

0.2d		P_exp.	P_predict				Sften. Factor @ Failure								
			ζACI	ζNd	ζCSA	ζNew	ζACI	ζNd	ζCSA	ζNew	ζACI	ζNd	ζCSA	ζNew	h_C
A3D9M-1.4	INF	136.05	92.7	141.2	86.4	127.4	0.34	0.5183	0.3155	0.4655	0.68	1.04	0.64	0.94	50
A3D9M-1.7	INF	98.98	76.0	100.1	62.5	100.8	0.34	0.4482	0.2783	0.4495	0.77	1.01	0.63	1.02	50
A3D9M-2.1	INF	88	60.1	48.8	42.8	76.2	0.34	0.2757	0.2409	0.4294	0.68	0.55	0.49	0.87	50
A4D9M-1.7	INF	121	76.0	100.1	70.2	111.0	0.34	0.4482	0.3124	0.4944	0.63	0.83	0.58	0.92	50
A5D9M-1.7	INF	133.97	76.0	100.1	76.5	118.9	0.34	0.4482	0.3406	0.5301	0.57	0.75	0.57	0.89	50
A3D9S-1.7	INF	109.58	67.2	88.5	58.1	93.0	0.34	0.4482	0.2928	0.4687	0.61	0.81	0.53	0.85	38
A5D9L-1.7	INF	134.27	84.8	111.7	81.8	128.4	0.34	0.4482	0.3264	0.5126	0.63	0.83	0.61	0.96	62
C3D9M-1.4	INF	169.26	92.7	141.2	101.0	145.1	0.34	0.5183	0.3689	0.5297	0.55	0.83	0.60	0.86	50
C3D9M-1.7	INF	106.54	76.0	100.1	73.3	114.9	0.34	0.4482	0.3263	0.5122	0.71	0.94	0.69	1.08	50
C3D9M-2.1	INF	52.64	60.1	48.8	50.3	86.9	0.34	0.2757	0.2832	0.4895	1.14	0.93	0.96	1.65	50
C4D9M-1.7	INF	96.09	76.0	100.1	81.7	125.2	0.34	0.4482	0.3637	0.5581	0.79	1.04	0.85	1.30	50
C5D9M-1.7	INF	151.39	76.0	100.1	88.5	133.0	0.34	0.4482	0.394	0.5929	0.50	0.66	0.58	0.88	50
C3D9S-1.7	INF	104.84	67.2	88.5	67.9	105.5	0.34	0.4482	0.3422	0.5319	0.64	0.84	0.65	1.01	38
C5D9L-1.7	INF	145.39	84.8	111.7	95.0	144.2	0.34	0.4482	0.379	0.9919	0.58	0.77	0.65	0.99	62
										Error	0.37	0.19	0.40	0.08	
										St D	0.07	0.14	0.06	0.07	

New		P_exp.	P_predict				Sften. Factor @ Failure								h_C			
			ζACI	ζNd	ζCSA	ζNew	ζACI	ζNd	ζCSA	ζNew	ζACI	ζNd	ζCSA	ζNew	ζACI	ζNd	ζCSA	ζNew
A3D9M-1.4	INF	136.05	77.7	120.8	81.8	116.4	0.34	0.5264	0.3566	0.5051	0.57	0.89	0.60	0.86	25.968	26.718	26.027	26.624
A3D9M-1.7	INF	98.98	62.1	86.5	58.6	91.0	0.34	0.4722	0.3195	0.4937	0.63	0.87	0.59	0.92	25.937	26.403	25.88	26.504
A3D9M-2.1	INF	88	47.7	46.6	39.6	67.6	0.34	0.3327	0.2817	0.4784	0.54	0.53	0.45	0.77	25.885	25.864	25.732	26.338
A4D9M-1.7	INF	121	64.2	88.8	66.3	101.5	0.34	0.469	0.3497	0.5321	0.53	0.73	0.55	0.84	29.485	29.93	29.519	30.209
A5D9M-1.7	INF	133.97	66.0	90.7	72.9	110.2	0.34	0.4661	0.3731	0.561	0.49	0.68	0.54	0.82	32.537	32.971	32.648	33.393
A3D9S-1.7	INF	109.58	58.9	81.5	56.3	87.4	0.34	0.4687	0.3236	0.4998	0.54	0.74	0.51	0.80	22.451	22.939	22.405	23.101
A5D9L-1.7	INF	134.27	69.5	96.2	75.8	114.7	0.34	0.4691	0.3686	0.5547	0.52	0.72	0.56	0.85	36.533	36.973	36.629	37.336
C3D9M-1.4	INF	169.26	80.9	125.7	96.6	134.9	0.34	0.5264	0.4037	0.5608	0.48	0.74	0.57	0.80	30.992	31.704	31.212	31.888
C3D9M-1.7	INF	106.54	65.1	89.8	69.5	105.8	0.34	0.4676	0.3614	0.5465	0.61	0.84	0.65	0.99	30.967	31.407	31.039	31.756
C3D9M-2.1	INF	52.64	50.4	47.7	47.3	79.0	0.34	0.322	0.3179	0.5277	0.96	0.91	0.90	1.50	30.922	30.871	30.863	31.568
C4D9M-1.7	INF	96.09	67.5	92.3	78.3	117.3	0.34	0.4636	0.3919	0.5835	0.70	0.96	0.82	1.22	35.132	35.56	35.308	36.097
C5D9M-1.7	INF	151.39	69.6	94.4	85.7	126.8	0.34	0.46	0.4156	0.6114	0.46	0.62	0.57	0.84	38.694	39.115	38.959	39.805
C3D9S-1.7	INF	104.84	61.2	83.7	66.3	100.8	0.34	0.4634	0.3663	0.5538	0.58	0.80	0.63	0.96	26.711	27.155	26.801	27.596
C5D9L-1.7	INF	145.39	73.9	101.0	89.8	132.9	0.34	0.4636	0.4106	0.6043	0.51	0.69	0.62	0.91	43.564	43.999	43.811	44.62
										Error	**0.46**	**0.26**	**0.43**	**0.14**				
										St D	**0.05**	**0.10**	**0.05**	**0.07**				

Proposed		P_exp.	P_predict			Sften. Factor @ Failure						h_C		
			H1	H2	M2	H1	H2	M2	H1	H2	M2	H1	H2	M2
A3D9M-1.4	INF	136.05	111.1	116.4	108.7	0.4807	0.5051	0.5275	0.82	0.86	0.80	25.968	26.624	26.47
A3D9M-1.7	INF	98.98	86.2	91.0	84.6	0.4667	0.4937	0.5163	0.87	0.92	0.85	26.397	26.504	26.361
A3D9M-2.1	INF	88	63.5	67.6	62.6	0.4477	0.4784	0.5018	0.72	0.77	0.71	26.233	26.338	26.212
A4D9M-1.7	INF	121	96.1	101.5	95.7	0.5021	0.5321	0.5526	0.79	0.84	0.79	30.085	30.209	30.077
A5D9M-1.7	INF	133.97	104.3	110.2	105.0	0.5301	0.561	0.5812	0.78	0.82	0.78	33.255	33.393	33.271
A3D9S-1.7	INF	109.58	82.8	87.4	81.5	0.4721	0.4998	0.5222	0.76	0.80	0.74	22.974	23.101	22.939
A5D9L-1.7	INF	134.27	108.6	114.7	109.1	0.5235	0.5547	0.5747	0.81	0.85	0.81	37.209	37.336	37.219
C3D9M-1.4	INF	169.26	128.5	134.9	128.4	0.5329	0.5608	0.5802	0.76	0.80	0.76	31.758	31.888	31.755
C3D9M-1.7	INF	106.54	100.1	105.8	100.3	0.5162	0.5465	0.5668	0.94	0.99	0.94	31.625	31.756	31.629
C3D9M-2.1	INF	52.64	73.9	79.0	74.4	0.4929	0.5277	0.5488	1.40	1.50	1.41	31.438	31.568	31.451
C4D9M-1.7	INF	96.09	111.0	117.3	112.7	0.5512	0.5835	0.6021	1.15	1.22	1.17	35.948	36.097	35.987
C5D9M-1.7	INF	151.39	119.9	126.8	123.0	0.5775	0.6114	0.6292	0.79	0.84	0.81	39.642	39.805	39.714
C3D9S-1.7	INF	104.84	95.4	100.8	95.8	0.523	0.5538	0.5736	0.91	0.96	0.91	27.443	27.596	27.455
C5D9L-1.7	INF	145.39	125.8	132.9	132.9	0.5713	0.6043	0.6043	0.87	0.91	0.91	44.468	44.62	44.62
								Error	**0.18**	**0.14**	**0.18**			
								St D	**0.07**	**0.07**	**0.07**			